Robust Control of Industrial Hydraulic Cylinder Drives - with Special Reference to Sliding Mode- & Finite-Time Control

Schmidt, Lasse

Publication date:
2014

Document Version
Publisher's PDF, also known as Version of record

Robust Control of Industrial Hydraulic Cylinder Drives

- with Special Reference to Sliding Mode- & Finite-Time Control

By

Lasse Schmidt

Department of Energy Technology

AALBORG UNIVERSITY
DENMARK

A Dissertation Submitted to
The Faculty of Engineering and Science, Aalborg University
in Partial Fulfilment for the Degree of Doctor of Philosophy

November 2013
Aalborg, Denmark

Robust Control of Industrial Hydraulic Cylinder Drives
- with Special Reference to Sliding Mode- & Finite-Time Control

Department of Energy Technology
Pontoppidanstraede 101
DK-9220 Aalborg
Denmark

Printed in Denmark by UniPrint, 2014

ISBN 978-87-92846-33-4

Preface

This dissertation has been submitted to the Faculty of Engineering and Science at Aalborg University in partial fulfilment of the requirements for the Ph.D. degree in Engineering. The work has been carried out at Bosch Rexroth A/S and at the Department of Energy Technology at Aalborg University. The work has been partially funded by the Danish Ministry of Science, Technology and Innovation under the Industrial Ph.D. initiative.

The work could not have been initiated without the help and support from Bosch Rexroth A/S. In this regard I would like to direct great thanks to Morten H. Brask, who was my company supervisor, and Thomas Jansen, for their support in making this work possible. Especially, I would like to thank Morten H. Brask who has supported me throughout the project, and whom I have bothered both day and night whenever I needed to discuss theoretical topics or practical test bench issues.

Special acknowledgements go to my supervisor, Prof. Torben O. Andersen, for many inspiring discussions, enthusiastic support and many ideas throughout my work. Likewise, I would like to thank Assoc. Prof. Henrik C. Pedersen and Assoc. Prof. Michael M. Bech, for always being ready for providing insights, feedback on- and ideas to my work.

Also I would like to thank my office mates, Daniel B. Rømer, Per Johansen, Rico H. Hansen and Anders H. Hansen for many enthusiastic discussions and enjoyable and fun hours. Furthermore, I would like to thank a group of students, Thomas Schmidt, Claus Vad, Niels Haldrup, Christian Jeppesen, Mathias Friis and Kasper Bitch, whom I supervised during their master theses, where they did an outstanding job in the preliminary implementation of several algorithms developed during my work.

Finally, very special gratitude goes to my daughter Liva and girlfriend Tania for standing by me and supporting me in my work, and for demonstrating great patience with me during this long period.

Aalborg, Denmark, November 2013

Lasse Schmidt

Contents

Abstract

In industry, performance requirements regarding machinery, applications etc., are constantly increasing, and with the development of reliable proportional flow control components to reasonable prices, the market is increasingly turning its attention toward controllable fluid power solutions. For series produced systems such as presses etc., dedicated controls are often developed. However, the great majority of the hydraulic systems developed, are produced in limited numbers for specialized applications, and here *stand alone* economically feasible digital controllers with *ease-of-use* interfaces are widely used. Such controllers typically provide the possibility to employ traditional linear controls such as PID schemes, and variants of this, with parameters tunable via graphical user interfaces. However, due to the intrinsic nonlinearities of hydraulic systems as well as the often limited knowledge of system parameters and control theory, hydraulic control systems are often implemented with poor results and with no indications on stability margins, robustness toward parameter perturbations, disturbances etc. Hence commissioning of such control systems is often an iterative and hence expensive process, making it difficult to comply with tight budgets and delivery deadlines.

The objective of this project is to overcome these issues, and develop controls aiming at robustness, consistent performance, simple parameter design and applicability under industrial conditions, i.e. with only pressure- piston- and spool position sensors, standard proportional valves- and control electronic hardware. The project is limited to consider only position control systems. To achieve the project objective, the possibility of online tracking of system parameters has been investigated, targeting compensations of nonlinearities and online controller adjustment. In regard to this, methods for compensation of the system gain have been developed - one based on the recursive least squares approach, and a model based type using a generalized system gain model and sensors.

In order to achieve consistent position control performance, simple parameter design and robustness in the presence of uncertain parameters- and disturbances, the field of sliding mode control has been investigated. Especially high order sliding mode control methods have been studied, due the intriguing possibility of maintaining the main properties of sliding mode control but with continuous control inputs. The applicability of second order modes has been investigated, and modifications of such controls have been developed based on homogeneity principles in order to provide more suitable controllers for hydraulic systems, than conventional second order sliding mode types. Also, an extension of the second order sliding algorithm known as the twisting algorithm has been developed, with compensation of local equilibria, and even an arbitrary order sliding mode design has been considered in a future perspective.

Experimental results reveal that the model based gain compensator may significantly improve performance of even control systems with linear controllers. The results of compensator-plus-control designs demonstrate improved tracking performance compared to common linear control methods based on *best industrial practice*. In particular homogeneous extensions / modifications of first- and second order sliding controls show to be especially suitable for hydraulic cylinder drives operating under industrial conditions. These controllers demonstrate superior performance compared with conventional methods, and may be commissioned with limited tuning effort. Combined with the proposed gain compensator, the resulting control structures are considered the main results in regard to the overall objective of the project.

Resumé

I industrien er kravene til maskiners og applikationers ydeevne konstant stigende, og med udviklingen af proportionale flow-styringskomponenter til rimelige priser, har markedet i stigende grad fokus på styrede hydrauliske løsninger. Til serieproducerede systemer såsom presser osv. udvikles der ofte dedikerede regulatorer og styringer, men det store flertal af de hydrauliske systemer der udvikles, produceres i begrænset antal og til specielle applikationer, og her anvendes ofte *stand alone* regulatorer. Sådanne regulatorstrukturer giver typisk mulighed for at anvende traditionelle lineære regulatorer såsom PID regulatorer og varianter af disse, hvor parametre kan justeres via grafiske brugerflader. På grund af ulineariteterne i hydrauliske systemer samt den ofte begrænsede viden om systemparametre og reguleringsteori, idriftsættes hydrauliske reguleringssystemer ofte med dårlige resultater til følge, og uden indikatorer på stabilitetsmarginer, robusthed mod parametervariationer, forstyrrelser osv. Idriftsættelse af denne type systemer er derfor ofte en iterativ og dermed kostbar proces, hvilket gør det vanskeligt at overholde stramme budgetter og leveringsdeadlines.

Formålet med dette projekt er at overvinde disse problemer, og at udvikle regulatorer med fokus på robusthed, ensartet ydeevne, enkle parameterdesigns og anvendelighed under industrielle betingelser, dvs. med kun tryk-, stempel- og gliderpositionssensorer, standard- proportionalventiler og elektronisk regulerings-hardware. Projektet er begrænset til positionsregulering. For at opfylde projektets mål, er muligheden for at monitorere systemets parametre online blevet undersøgt med det formål at kompensere for ulineariteter samt online regulatortuning. I denne forbindelse er metoder til kompensering af systemets forstærking blevet udviklet - en metode baseret på rekursive *mindste kvadraters* metode, og en modelbaseret type ved brug af sensorer.

For at opnå en konsistent regulatorydeevne, et simpelt parameter design og robusthed på trods af usikre parametre og forstyrrelser, er *sliding mode* reguleringsmetoder blevet undersøgt. Særligt er højere ordens *sliding mode* reguleringsmetoder blevet undersøgt, hvilket skyldes muligheden for at opretholde de vigtigste egenskaber ved *sliding mode* regulering, men med kontinuerte indgangssignaler. Anvendeligheden af anden ordens *sliding mode* regulatorer er blevet undersøgt, og videreudviklet baseret på homogenitetsprincipper, med henblik på mere egnede regulatorer til hydrauliske systemer, end konventionelle anden orderns *sliding mode* regulatorer. Desuden er en udvidelse af anden ordens *sliding* algoritmen kendt som *twisting* algoritmen blevet udviklet, med kompensering for lokale ligevægtspunkter, og selv en vilkårlig ordens *sliding mode* regulator er blevet undersøgt i et fremtidigt perspektiv.

Eksperimentelle resultater viser at den modelbaserede systemforstærkningskompensator forbedrer ydeevnen, selv i reguleringssystemer med lineære regulatorer. Resultaterne af de forskellige reguleringsdesigns demonstrerer forbedret evne til at følge tidsvariende referencesignaler sammenlignet med konventionelle lineære reguleringsmetoder baseret på den bedste industrielle praksis. Særligt videreudviklingerne af anden ordens *sliding mode* regulatorerne baseret på homogenitetsprincipper findes specielt egnede til hydrauliske cylinderdrev, der opererer under industrielle betingelser. Disse regulatorer demonstrerer en overlegen ydeevne sammenlignet med konventionelle metoder, og kan idriftsættes med en begrænset tuningsindsats. Kombineret med den nævnte systemforstærkningskompensator, anses de resulterende reguleringsstrukturer for at være de vigtigste resultater i forhold til det overordnede mål for projektet.

List of Publications

Scientific Papers

[A] Lasse Schmidt, Torben O. Andersen & Henrik C. Pedersen, 2013, "Finite-Time Convergent Continuous Control Design Based on Sliding Mode Algorithms with Application to A Hydraulic Drive", Accepted for publication, International Journal of Mechatronics and Automation, 2014.

[B] Lasse Schmidt, Torben O. Andersen & Henrik C. Pedersen, 2013, "An Approach for Second Order Control with Finite Time Convergence for Electro-Hydraulic Drives", in Proceedings of the ASME/Bath Symposium on Fluid Power and Motion Control (FPMC 2013).

[C] Lasse Schmidt, Torben O. Andersen & Henrik C. Pedersen, 2013, "Second Order Sliding Control with State Dependent Gain and its Application to a Hydraulic Drive", in Proceedings of the ASME/Bath Symposium on Fluid Power and Motion Control (FPMC 2013).

[D] Lasse Schmidt, Torben O. Andersen & Henrik C. Pedersen, 2013, "A Novel Control Approach Based on Second Order Sliding Modes and Its Application to Hydraulic Drives", in Proceedings of the IEEE International Conference on Mechatronics and Automation (ICMA 2013).

[E] Lasse Schmidt, Torben O. Andersen & Henrik C. Pedersen, 2013, "An Approach for State Observation in Dynamical Systems Based on the Twisting Algorithm", in Proceedings of the IEEE International Conference on Mechatronics and Automation (ICMA 2013).

[F] Michael M. Bech, Torben O. Andersen, Henrik C. Pedersen & Lasse Schmidt, 2013, "Experimental Evaluation of Control Strategies for Hydraulic Servo Robot", in Proceedings of the IEEE International Conference on Mechatronics and Automation (ICMA 2013).

[G] Lasse Schmidt, Torben O. Andersen & Henrik C. Pedersen, 2013, "Robust Non-Chattering Observer Based Sliding Control Concept for Electro-Hydraulic Drives", in Proceedings of the 6^{th} IFAC Symposium on Mechatronic Systems (IFAC MECH'13).

[H] Lasse Schmidt, Torben O. Andersen, Henrik C. Pedersen & Michael M. Bech, 2013, "Adaptive Sliding Mode Control for Hydraulic Drives - A New Approach", in Proceedings of the 8^{th} International Conference on Fluid Power Transmission and Control (ICFP 2013).

[I] Lasse Schmidt, Torben O. Andersen, Henrik C. Pedersen & Michael M. Bech, 2013, "Super Twisting Second Order Sliding Mode Control for Position Tracking Control of Hydraulic Drives", in Proceedings of the 8^{th} International Conference on Fluid Power Transmission and Control (ICFP 2013).

[J] Lasse Schmidt, Torben O. Andersen, Henrik C. Pedersen & Michael M. Bech, 2013, "Second Order Sliding Mode Control with Prescribed Convergence Law for Electro-Hydraulic Drives", in Proceedings of the 8^{th} International Conference on Fluid Power Transmission and Control (ICFP 2013).

[K] Lasse Schmidt, Torben O. Andersen, Henrik C. Pedersen & Michael M. Bech, 2012, "2-SMC of Electro-Hydraulic Drives Using the Twisting Algorithm", Applied Mechanics and Materials, vol 233, pp. 131-134.

[L] Lasse Schmidt, Torben O. Andersen, Henrik C. Pedersen & Michael M. Bech, 2012, "Sliding Control with Chattering Elimination for Hydraulic Drives", Applied Mechanics and Materials, vol 233, pp. 168-171.

[M] Lasse Schmidt, Torben O. Andersen, Henrik C. Pedersen & Michael M. Bech, 2012, "Robust Position Tracking for Electro-Hydraulic Drives Based on Generalized Feedforward Compensation Approach", Applied Mechanics and Materials, vol 233, pp. 100-103.

Abbreviations

1SMC	First order sliding mode controller
1SMC-e	First order sliding output feedback controller
1SMC-S	First order sliding surface controller
3TA	Third order twisting-like algorithm
AGC	Active gain compensator
CCT-RLS	Recursive least squares algorithm with controlled covariance trace
HOSM	High order sliding mode
HPU	Hydraulic power unit
M-P	Modified relay controller
M-TA	Modified twisting algorithm
M-STA	Modified super twisting algorithm
PI	Proportional plus integral (controller)
PI-AGC	Proportional plus integral (controller) with active gain compensator
PI_{sw}	Proportional plus integral (controller) with switching integral term
RLS	Recursive least squares
STA	Super twisting algorithm
STA-B	Super twisting algorithm with boundary layer
TA	Twisting algorithm
TC1	Test case number 1
TC2	Test case number 2
TC3	Test case number 3
SOSM	Second order sliding mode
SR	Slew rate
VFF-RLS	Recursive least squares algorithm with variable forgetting factor

Nomenclature

α_1	Controller parameter	[-]
α_2	Controller parameter	[-]
α_3	Controller parameter	[-]
α_{vff}	Adaption gain control variable	[-]
β_{Air}	Bulk modulus for air	[Pa]
β_{Ae}	Effective bulk modulus for A-chamber	[Pa]
β_{Be}	Effective bulk modulus for B-chamber	[Pa]
β_e	Effective bulk modulus	[Pa]
β_F	Fluid bulk modulus	[Pa]
β_{PS}	Effective bulk modulus in pressure supply line	[Pa]
γ_1	Controller parameter	[-]
γ_2	Controller parameter	[-]
$\bar{\gamma}$	Controller parameter	[-]
ε_{Air0}	Volumetric constant for undissolved air at atmospheric pressure	[-]
ε_{cs}	Boundary layer coefficient	[-]
ε_{ht}	Boundary layer coefficient	[-]
ζ_{ps}	Damping ratio of swivel mechanism	[-]
ζ_s	System damping ratio	[-]

ζ_{v}	Valve damping ratio	[-]
θ	Angle	[rad]
λ_{cct}	Constant forgetting factor	[-]
λ_{vff}	Variable forgetting factor	[-]
$\bar{\lambda}$	Parameter related to Filippov solution	[-]
ξ	Homogeneity degree	[-]
ρ	Chamber volume ratio	[-]
σ	Static flow gain ratio	[-]
τ_{c}	Controller time constant	[s]
τ_{d}	Time delay	[s]
τ_{s1}	Oscillation time constant	[s]
τ_{vd}	Valve time delay	[s]
φ_{01}	Angle related to manipulator kinematics	[rad]
φ_{03}	Angle related to manipulator kinematics	[rad]
φ_{33}	Angle related to manipulator kinematics	[rad]
φ_{b}	Boundary layer width / thickness	[-]
φ_{H1}	Angle related to manipulator kinematics	[rad]
ψ_{s}	Swivel / swash plate angle	[-]
ψ_{sR}	Swivel angle reference	[-]
$\omega_{1\mathrm{v}}$	Frequency related to valve dynamics	[rad/s]
$\omega_{2\mathrm{v}}$	Frequency related to valve dynamics	[rad/s]
ω_{m}	Motor speed (supply)	[rad/s]
ω_{n}	System natural frequency	[rad/s]
ω_{s}	Natural frequency of swivel mechanism	[rad/s]
ω_{v}	Valve band width	[rad/s]
a_{sr}	Oscillation amplitude	[1]
A_{A}	Piston area on A-side	[m^2]
A_{B}	Piston area on B-side	[m^2]
B_{h}	Hydraulic viscous friction coefficient	[Ns/m]
B_{m}	Viscous friction coefficient for joint	[Ns/rad]
B_{V}	Combined viscous friction coefficient	[Ns/m]
B_{v}	Total (equivalent) viscous friction coefficient	[Ns/m]
C	Parameter bound	[-]/[m/s]
$\bar{C}$	Parameter bound	[-]/[$\mathrm{m/s}^2$]
C_{ad}	Adiabatic constant	[-]
C_{L}	Leakage coefficient	[m^3/s/Pa]
C_{Lp}	Pump leakage coefficient	[m^3/s/Pa]
C_{LAex}	External leakage coefficient	[m^3/s/Pa]
C_{LBex}	External leakage coefficient	[m^3/s/Pa]
C_{Ll}	Leakage coefficient	[m^3/s/Pa]
C_{f1}	Stribeck velocity	[m/s]
C_{f2}	Inclination for continuous approximation of sign function	[-]
D_{P}	Pump displacement coefficient	[m^3/rad]
d_{τ}	Torque-force relation (torque arm)	[m]
d_{κ}	Dilation	[-]

F_{ext}	External disturbance force	[N]
F_{C}	Forces resulting from coriolis- and centripetal impacts	[N]
F_{f}	Total forces due to friction	[N]
F_{fC}	Coulomb friction force	[Nm]
F_{fS}	Friction force resulting from Stribeck effects	[Nm]
F_{g}	Force due to gravity	[N]
F_{ext}	External forces	[N]
G_{M}	Parameter bound	[-]
G_{Mh}	Parameter bound	[-]
H_{max}	Parameter bound	[-]
I_{zz1}	Moment of inertia related to Link 1	[kgm^2]
I_{yy2}	Moment of inertia related to Link 2	[kgm^2]
I_{zz3}	Moment of inertia related to Link 3	[kgm^2]
I_{zz4}	Moment of inertia related to Link 4	[kgm^2]
K_{M}	Parameter bound	[-]/[m/s]
$\bar{K}_{\text{M}}$	Parameter bound	[-]/[m/s^2]
K_{m}	Parameter bound	[-]/[m/s]
$\bar{K}_{\text{m}}$	Parameter bound	[-]/[m/s^2]
K_{vA}	Valve flow gain of flow port A	[m^3/(s$\sqrt{\text{Pa}}$V)]
K_{vB}	Valve flow gain of flow port B	[m^3/(s$\sqrt{\text{Pa}}$V))]
K_{s}	Linear system gain	[m/V]
K_{i}	Gain for liner integral term	[V/m]
K_{isw}	Logic limit for activation of controller integral term	[-]
$K_{\text{f+}}$	System gain for positive motion	[-]
$K_{\text{f-}}$	System gain for negative motion	[-]
K_{p}	Proportional gain	[V/m]
L_{ABmin}	Length	[m]
L_{AO0}	Length	[m]
L_{BO0}	Length	[m]
L_{BC}	Length	[m]
L_{CDmin}	Length	[m]
L_{CM1x}	Length	[m]
L_{CM1y}	Length	[m]
L_{CM2x}	Length	[m]
L_{CM2z}	Length	[m]
L_{CM3x}	Length	[m]
L_{CM3y}	Length	[m]
L_{CO0}	Length	[m]
L_{CO1}	Length	[m]
L_{DO1}	Length	[m]
L_{EFmin}	Length	[m]
L_{EG}	Length	[m]
L_{EH}	Length	[m]
L_{FH}	Length	[m]
L_{FI}	Length	[m]
L_{GH}	Length	[m]

L_{HO3}	Length	[m]
L_{IO3}	Length	[m]
L_{IO4}	Length	[m]
L_{O3O4}	Length	[m]
L_{O0O1}	Length	[m]
$L_{O2O3min}$	Length	[m]
m_1	Mass of manipulator Link 1	[kg]
m_2	Mass of manipulator Link 2	[kg]
m_3	Mass of manipulator Link 3	[kg]
m_4	Mass of manipulator Link 4	[kg]
M_{eq}	Equivalent inertia load	[kg]
P_{Atm}	Atmospheric pressure	[Pa]
P_A	Pressure in A-chamber	[Pa]
P_B	Pressure in B-chamber	[Pa]
P_L	Load pressure (virtual)	[Pa]
P_S	Supply pressure	[Pa]
P_T	Tank pressure	[Pa]
Q_A	Flow through flow port A	[m^3/s]
Q_B	Flow through flow port B	[m^3/s]
Q_V	Total valve flow (consumption from supply)	[m^3/s]
Q_S	Supply pump flow	[m^3/s]
sat()	Saturation function	[-]
sgn()	Sign function	[-]
u_v	Valve control input	[V]
V_{0A}	Initial volume of A-chamber	[m^3]
V_{0B}	Initial volume of B-chamber	[m^3]
V_A	Total volume of A-chamber	[m^3]
V_B	Total volume of B-chamber	[m^3]
V_{A0}	Volume of A-chamber at operating point	[m^3]
V_{B0}	Volume of B-chamber at operating point	[m^3]
V_S	Volume of supply line	[m^3]
x_P	Piston position	[m]
x_{P1}	Piston position of cylinder 1	[m]
x_{P2}	Piston position of cylinder 2	[m]
x_{P3}	Piston position of cylinder 3	[m]
x_{P4}	Piston position of cylinder 4	[m]
x_R	Piston position reference	[m]
x_v	Valve spool position	[m]
$\lvert\dot{x}_v\rvert_{max}$	Valve slew rate	[m/s]

Redundant Nomenclature

α	In control design chapters, denotes a tuning parameter	[-]
γ	Forgetting factor / controller parameter	[-]
δ	Maximum covariance trace / controller parameter	[-]
λ	Forgetting factor / controller parameter	[-]
μ	Piston area ratio / Lebesgue measure	[-]
φ	Angle / controller parameter	[-]
B	Boundary layer function / Region related to Filippov solution	[-]
$\mathbf{R}$	Rotation matrix / Information matrix	

1 Introduction

In the following, the motivation for the initiation of this research project is presented. Furthermore, specific aims of the research are introduced in terms of a research hypothesis and the primary activities of the project. Finally, the main contribution of the project as well as a dissertation outline is presented.

1.1 Motivation for the Research Project

With the development of reliable proportional flow control components with *medium* transient performance characteristics to acceptable prices, the market has turned its attention to controllable fluid power solutions. As a result, trends and demands are increasingly to develop and deliver high performance *turn-key* solutions, meaning complete electro-hydraulic systems with integrated control systems, motion control of individual hydraulic axes and so forth, installed and commissioned. The key parameters of competition in this market may be outlined as; Performance, Reliability, Price, and Delivery time.

This has provided basis for the development of commercially available *stand alone* hydraulic axis controllers. For series produced systems such as presses etc., dedicated axis control systems are often developed. However, the great majority of the hydraulic systems developed are *one off a kind* systems, or systems produced in limited numbers for specialized applications, where budgets are too limited to design professionally engineered model based control systems. In these cases, *stand alone* economically feasible digital controllers dedicated to control electro-hydraulic components with *ease-of-use* configuration interfaces, are widely used. These controllers typically provide the possibility to employ closed loop control in terms of traditional linear control schemes such as the widely known PID controller approach, and variants of this, tunable via graphical user interfaces. The reason for this control approach is that parameters are somewhat comprehensible by many operators in the fluid power industry, and that parameters may be designed from tests on the physical system and the use of well-known tuning rules. In general the limited engineering effort in the field of hydraulic control systems (servo systems) is a problem of both educational and technical nature, and has not evolved on a level with classical disciplines in electrical engineering. The field of modern control theory traditionally concerns model based control and analysis of linear systems, however as hydraulic systems are inherently nonlinear, this makes the applicability of linear control theory somewhat limited / restricted. This together with limited budgets for model based control design, and the limited knowledge on control theory, often cause engineers to employ PID controllers which are experimentally tuned on site, often with poor results in terms tracking effort, response time etc. and with no indications on stability margins, robustness toward perturbations in

system parameters due to viscosity-temperature relations, friction factors, air content and so forth. Due to this, commissioning of fluid power control systems are often an iterative and hence expensive process making it difficult to comply with tight delivery deadlines.

These facts and the considerations above outline the issues that are the motivation for this research project.

1.2 Aims of Research

The difficulties described in the motivation call for new controller types that adapt to / are robust toward the intrinsic nonlinearities of hydraulic drives, such that consistent performance is guaranteed even under varying operating conditions. Furthermore, such controls should be easily implemented and commissioned from simple guide lines and without knowledge of advanced control theory. In order for such control methods to be appealing to the industry, these must not require additional economic efforts compared to those of a conventional system design. This means that, in order to work properly, the developed controllers must not require advanced- and / or specialized hydraulic components, sensors, electronic control hardware etc.

1.2.1 Research Hypothesis

Typical states to be controlled in hydraulic systems are the position, velocity or force output of hydraulic cylinders- or motors, flow outputs of flow components or the pressure of hydraulic transmission lines, chambers etc. In order to focus research efforts, the control methods under consideration in this project are restricted to position control methods, as such controllers are found to be most profound in industry [1].

The research hypothesis for the project is given by:

It is possible to develop control methods / structures for a class of hydraulic cylinder drives with simple commissioning routines, that adapt to / are robust toward varying operating conditions and the inherent nonlinearities of hydraulic cylinder drives, and provide for improved tracking performance compared to conventional linear methods, without any or limited predefined system information.

This hypothesis will be answered through the following sub-hypotheses:

- *It is possible to adapt / track key system parameters online based on commonly available sensors, in a reliable way, such that these can be applied for online controller adjustment- and / or compensation of nonlinearities.*

- *It is possible to develop advanced control schemes that provide global stability, improved tracking performance and disturbance rejection compared to conventional methods, despite nonlinearities and varying operating conditions.*

The work carried out in order to answer this research hypothesis, is divided into several project activities, which are presented in the following.

[1] Bosch Rexroth A/S, Denmark

1.2.2 Project Activities

From the above, the objective is to develop adaptive / robust controllers that utilize only commonly available sensors (piston- and spool position- and pressure sensors), that are commissioned with few- and easily tuned parameters, and provides for improved *and* consistent performance, compared to conventional linear methods that can be considered *best industrial practice*. The project activities are chosen as described below.

Activity 1 - Classification of Applications, Test Bench & Modeling Common application types are classified in terms of their hydraulic systems- and load structures. Based on this, a test bench is established, modeled and verified, and a control design model framework is established.

Activity 2 - Online parameter estimation Online parameter estimation using the Recursive Least Squares (RLS) method is investigated. This method is chosen due to its proven mathematical properties, and the applicability of state-of-the-art will be investigated and modified in order to suit the purpose of this project. Furthermore the possibility for online parameter estimation using a model based approach is considered. The target is to utilize estimated parameters for compensation of system nonlinearities- and / or for online controller adjustment.

Activity 3 - Design of Control Structures Based on the findings of Activity 2, a suitable control strategy is chosen, investigated, and based on this new control structures are developed to suit the purpose of the project.

Activity 4 - Implementation, Validation & Testing The results are implemented in the test bench and compared with *best industrial practice* linear control methods commonly applied in industry.

1.3 Main Contribution of the Research Project

This dissertation presents the study and implementation of different methods for online tracking of system parameters, both adaptive- and model based methods, considering valve driven hydraulic cylinder drives. The applicability of first- and second order sliding mode methods- as well as homogeneous methods is investigated in regard to output feedback control for position tracking of hydraulic cylinders. Furthermore, third and arbitrary order sliding algorithms are considered in a future perspective.

The main contribution of the research presented, is the *Active Gain Compensator* (AGC) that allows to compensate the system gain of arbitrary valve driven cylinder drives, combined with the *modified twisting algorithm* (M-TA) or the *modified super twisting algorithm* (M-STA) that are homogeneous finite-time continuous output feedback controllers. The combined compensator-controller structures utilize pressure-, piston- and spool position measurements and are highly versatile, allowing for application in a broad range of applications. Furthermore, these structures allow for accurate and robust position tracking control of hydraulic cylinder drives, with little and simple tuning efforts. This contribution provides for significant improvement of performance compared to controllers that can be considered *best industrial practice*.

Furthermore, another relevant contribution is the *third order twisting-like algorithm* (3TA), being a contribution of a more theoretical nature. The extension of the simple twisting algorithm to the third order is investigated and thoroughly elaborated through geometrical considerations, and local equilibria are compensated by simple efforts. In systems with *high performance* components, this controller will expectedly provide for accurate tracking performance combined with the proposed compensator, with the most simple tuning effort.

1.4 Dissertation Outline

In Chapter 2 the framework for the project regarding test facilities, models, experimental conditions and evaluation criteria is established. Furthermore, benchmark controllers are established based on *best industrial practice*. In Chapter 3 the possibility for online tracking of system parameters is investigated, focusing on the recursive least squares method, and a model based approach. Furthermore, *compensated* drive models for use in position control designs are established, and a control strategy to be investigated, is outlined. In Chapter 4 the fundamentals and most important features in regard to first order sliding mode controls (1SMC) and sliding mode controls of higher orders (HOSMC), are discussed in their ideal cases. Furthermore, chattering issues are addressed in regard to their application in especially hydraulic systems, and state-of-the-art for application of sliding controls to hydraulic systems is outlined. In Chapter 5 different conventional sliding mode controllers are designed for hydraulic cylinder drives and evaluated experimentally. In Chapter 6, different controllers utilizing second order sliding algorithms are proposed, mainly focused on output feedback control for hydraulic drives, and results are experimentally verified and the results discussed. In Chapter 7, several homogeneous extensions / modifications of first- and second order sliding controllers are proposed, based on the findings of Chapter 6. In Chapter 8 an extension of the twisting algorithm to the third order is proposed, and furthermore a partial framework for a controller based on a homogeneous surface design is established. In Chapter 9 the results for the controllers considered in the project are compared quantitatively, and a final control structure is proposed. Finally, in Chapter 10, the project work and results are discussed and summarized.

2 Drive Classification, Modeling & Benchmark Controllers

This chapter outlines the framework for the project in regard to test facilities and models used throughout the project. Based on a classification of application types that can be expected in the industry, a test bench is chosen representing the main load characteristics. Nonlinear models are developed and experimentally verified. Based on this, a generalized compact model description is established in order to facilitate control design, and linear models and transfer functions are derived. Finally, experimental conditions and evaluation criteria are defined, and benchmark controllers are established based on *best industrial practice*.

2.1 Classification of Applications

In the industry hydraulic systems are usually applied in systems where large forces / torques-, high power-weight ratios etc. are necessary. Furthermore, applications where hydraulics are applied varies strongly, and often differ significantly in regard to dominating characteristics. In the following, different load systems recently delivered by Bosch Rexroth A/S, are considered in order to classify expected loads, hence the characteristics of the systems target for the work of the project. In all, six different applications are chosen, which also emphasizes the diversity of applications where hydraulic drives are applied. The chosen application types are depicted in figure 2.1.

Application # 1 In this application a horizontally mounted differential cylinder is actuating a mass, with the mass guided by a slide. The load is dominated by inertia forces resulting from a constant mass, and friction primarily arising between the slider components. The pump supplying the valve is attached to multiple consumers and supply lines are long, resulting in a fluctuating supply pressure. Furthermore, the valve is pilot operated, and the valve flow gains are asymmetric and are not matched with the cylinder asymmetry.

Application # 2 In this application a rotary symmetric actuator / *cylinder* is driven by a symmetric proportional valve, with the static flow characteristic being progressive. The motion of the load is characterized by strong accelerations, resulting in large inertia forces. Furthermore, the load is characterized by gravitation forces.

Application # 3 Here several differential cylinders are parallel coupled to the valve, driving a sledge which accumulates bulk material, i.e. the mass is changing. Furthermore, the load exhibits strong impact from friction phenomena, where nonlinear elements are significant. Also, the valve is pilot operated, and the static flow gain is nonlinear.

Application # 4 The load of this application is somewhat similar to that of Application # 3, however the actuation system is different. Here the load is actuated by multiple differential cylinders coupled in *opposite* parallel, forming an *equivalent* double rod / symmetric cylinder. The cylinders are driven by a unidirectional pump, operating in closed circuit, and as such the system resembles a hydrostatic transmission.

Application # 5 In this application a vertically mounted cylinder is applied to push / force a hub into an impeller for a (central) heating pump. Hence, the cylinder is operated in a way similar to a conventional press, and meets an *abrupt* contact load, that subsequently changes due to deformation of the hub. The static flow gains are nonlinear.

Application # 6 This application differs significantly from the remaining applications in the sense that several (four) cylinders control the position of a large axle bearing. Hence, the cylinders exhibit coupled loads. Furthermore, gravitational forces are present. The flow gains of the valves applied, are in all cases nonlinear.

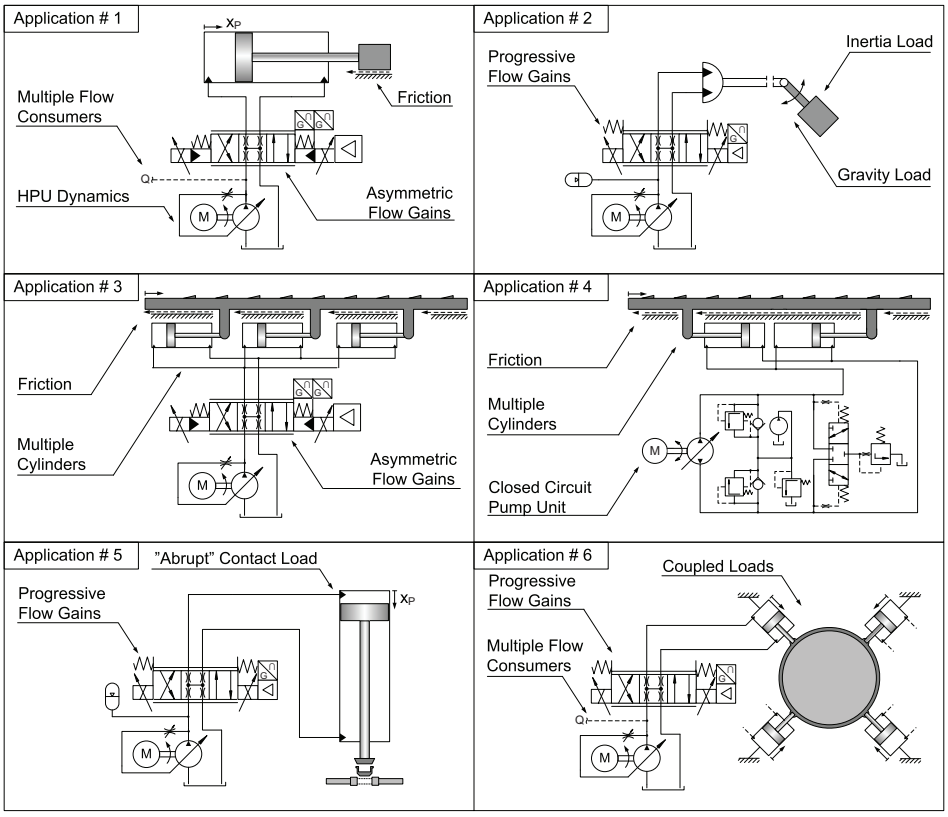

Figure 2.1: *Chosen applications depicting load characterizations and actuation systems.*

The applications under consideration differ significantly from each other in regard to load characteristics, output power range, and flow components. In general for these applications, the most undesirable characteristics in regard to control are:

- Varying inertia load (influences system natural frequency and damping)
- Nonlinear friction phenomena (causes strong load variations at low velocities and may cause limit cycles when the system is in closed loop control)
- Nonlinear static flow gains (asserts an additional nonlinearity to the system gain)
- Valve- and cylinder asymmetries (causes the system gain to change abruptly at valve spool zero crossing)
- Load variations resulting from gravitational impact, abrupt contact loads and disturbances (Causes variation in the load pressure, hence the system gain etc.)
- Supply pressure variations (causes system gain variations and an *unsteady* power inlet)

Hence, in order for a successful outcome of the project, the developed control methods / structures should provide a consistent and accurate performance, despite such undesirable system properties.

2.2 Laboratory Test Bench

Based on the classification of dominant system characteristics which can be expected in hydraulic drive applications, the load system chosen for the project is the rear crane of a backhoe loader. This produces most of the dominant load characteristics discussed in Section 2.1, in terms of friction phenomena, gravitational forces as well as varying inertia. **Note;** This load application is therefore chosen in its capacity of producing the desired load characteristics, and *NOT* in its capacity of being a mobile crane. Throughout this dissertation, the crane is referred *manipulator*.
A sketch of the manipulator is depicted in figure 2.2, with the notation used in the following sections. In general a hydraulic cylinder plus load (the manipulator link it actuates) is referred as a hydraulic axis. The hydraulic system applied for actuation of the manipulator is designed based on common industrial standards in order to meet the purpose of the project, and component types are chosen based on the applications considered in the previous section. This means that all components, from valves, supply pump etc. to electronic control hardware are common industrial standard components. A list of main components utilized in the system can be found in the Appendix.

The cylinders are controlled by proportional flow control valves commonly seen in industry. Specifically, Link 1 is actuated by a 4WRKE 10 E1-100L two-stage overlapped valve [Rexroth, 2004], Link 2 by a 4WRTE 10 V1-100L two-stage zero lapped valve [Rexroth, 2006] and links 3 and 4 by 4WREE 10 V50 and 4WREE 6 V32 valves [Rexroth, 2005], respectively (both single stage and zero lapped). The control electronics applied is an industrial grade *PLC*, more specifically the Bosch Rexroth MLC L65 [Rexroth, 2008], with a control cycle time (scan time, sample time) of 1 [ms]. In the following sections the system is modeled in detail.

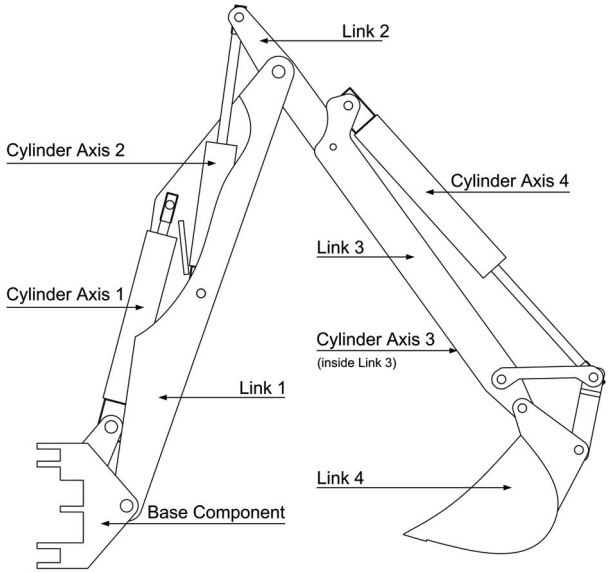

Figure 2.2: *Sketch depicting the manipulator used as load system in the test bench.*

2.3 Nonlinear Load Model

The nonlinear manipulator model is developed using conventional systematic methods to the extend this is possible. The forward kinematics is derived using the Denavit-Hartenberg (D-H) convention, and the dynamic model is derived using the iterative Newton-Euler dynamic formulation ([Craig, 2005], [Andersen, 1993], [Spong et al., 2004], among others). These methods provide a model expressed in the manipulator joint space. The relation between joint- and actuator (cylinder) space in terms of relations between joint- and actuator variables and torque-force relations are derived using standard trigonometric approaches. The following derivations are based on figure 2.3, depicting the local reference frame related to each link following the D-H convention, as well as the joint variables. In the following, e.g. L_{AB} denotes the length between points A and B, and so fourth. All dimensions, masses etc. used in the following can be found in the Appendix.

2.3.1 Joint Kinematics

Based on figure 2.4, depicting the manipulator in zero state configuration, the D-H parameters are as given in table 2.1.

Link	θ_i	d_i	a_i	α_i
1	θ_1	0	L_{O0O1}	0
2	θ_2	0	0	$\pi/2$
3	0	$L_{\mathrm{O2O3min}} + d_3$	0	$-\pi/2$
4	θ_3	0	$-L_{\mathrm{O3O4}}$	0

Table 2.1: *DH-parameters for the manipulator.*

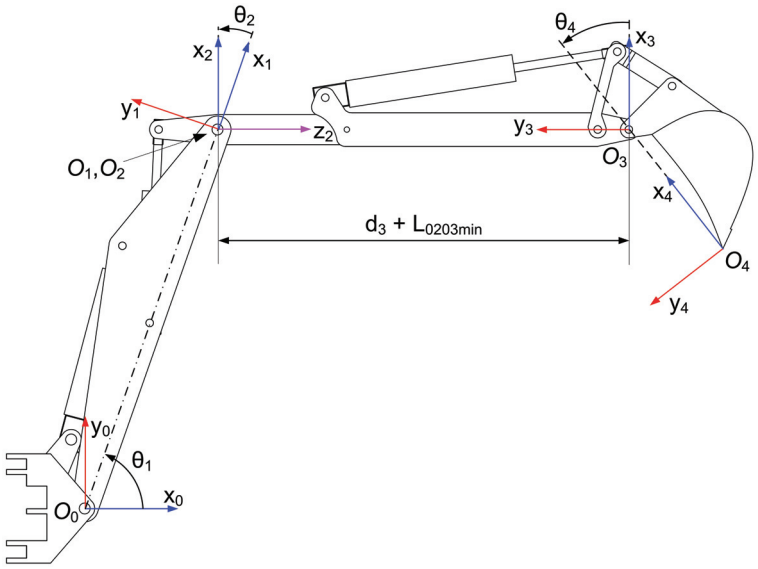

Figure 2.3: *Sketch of manipulator with reference frame assigned according to the D-H convention, and joint variables.*

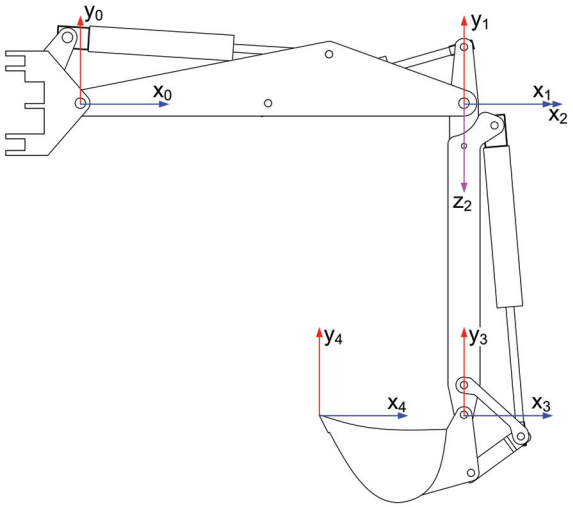

Figure 2.4: *Sketch of manipulator in* zero state *configuration.*

The position and orientation of each coordinate frame may be described by a transformation matrix (2.1), where the subscript i denotes the i^{th} reference frame. The upper left 3×3 submatrix of (2.1) is the rotation matrix expressing the orientation of the i^{th} reference frame with respect to the $i-1$ reference frame, i.e. with respect to its base coordinate frame, and the upper right 3×1 vector expresses the distance from the origin of the $i-1$ reference frame to the i^{th} reference frame.

$$ {}^{i}_{i-1}\mathbf{T} = \begin{bmatrix} \cos(\theta_i) & -\sin(\theta_i)\cos(\alpha_i) & \sin(\theta_i)\sin(\alpha_i) & a_i\cos(\theta_i) \\ \sin(\theta_i) & \cos(\theta_i)\cos(\alpha_i) & -\cos(\theta_i)\sin(\alpha_i) & a_i\sin(\theta_i) \\ 0 & \sin(\alpha_i) & \cos(\alpha_i) & d_i \\ 0 & 0 & 0 & 1 \end{bmatrix} \tag{2.1} $$

Based on (2.1), the rotation matrices for the manipulator links are given by (2.4), (2.3).

$$ {}^{1}_{0}\mathbf{R} = \begin{bmatrix} \cos(\theta_1) & -\sin(\theta_1) & 0 \\ \sin(\theta_1) & \cos(\theta_1) & 0 \\ 0 & 0 & 1 \end{bmatrix}, \; {}^{2}_{1}\mathbf{R} = \begin{bmatrix} \cos(\theta_2) & 0 & \sin(\theta_2) \\ \sin(\theta_2) & 0 & -\cos(\theta_2) \\ 0 & 1 & 0 \end{bmatrix} \tag{2.2} $$

$$ {}^{3}_{2}\mathbf{R} = \begin{bmatrix} 1 & 0 & 0 \\ 0 & 0 & 1 \\ 0 & -1 & 0 \end{bmatrix}, \; {}^{4}_{3}\mathbf{R} = \begin{bmatrix} \cos(\theta_4) & -\sin(\theta_4) & 0 \\ \sin(\theta_4) & \cos(\theta_4) & 0 \\ 0 & 0 & 1 \end{bmatrix} \tag{2.3} $$

Having established the rotation matrices, the remaining relevant quantities that are to be used in the dynamic model formulation, are the vectors ${}^{i}\mathbf{p}_i$, ${}^{i}\mathbf{s}_i$ for each link. The vector ${}^{i}\mathbf{p}_i$ describes the origin of the i^{th} reference frame from the $i-1$ reference frame, however expressed in the i^{th} reference frame, and may be found from ${}^{i}\mathbf{p}_i = \begin{bmatrix} a_i & d_i\sin(\alpha_i) & d_i\cos(\alpha_i) \end{bmatrix}^{\mathsf{T}}$. Hence, from parameters of table 2.1, these vectors are obtained as (2.4).

$$ \begin{aligned} &{}^{1}\mathbf{p}_1 = \begin{bmatrix} L_{\mathrm{O0O1}} & 0 & 0 \end{bmatrix}, \; {}^{2}\mathbf{p}_2 = \begin{bmatrix} 0 & 0 & 0 \end{bmatrix} \\ &, \; {}^{3}\mathbf{p}_3 = \begin{bmatrix} 0 & |L_{\mathrm{O2O3}}|_{\min} + d_3 & 0 \end{bmatrix}, \; {}^{4}\mathbf{p}_4 = \begin{bmatrix} -L_{\mathrm{O3O4}} & 0 & 0 \end{bmatrix} \end{aligned} \tag{2.4} $$

Similarly, the vector ${}^{i}\mathbf{s}_i$ expresses the position of the center of mass (CM) for the i^{th} link, with respect to the i^{th} reference frame. Hence, from the assignment of reference frames in figure 2.3, these vectors are given by (2.5).

$$ \begin{aligned} &{}^{1}\mathbf{s}_1 = \begin{bmatrix} L_{\mathrm{CM1x}} & L_{\mathrm{CM1y}} & 0 \end{bmatrix}, \; {}^{2}\mathbf{s}_2 = \begin{bmatrix} L_{\mathrm{CM2x}} & 0 & L_{\mathrm{CM2z}} \end{bmatrix} \\ &{}^{3}\mathbf{s}_3 = \begin{bmatrix} L_{\mathrm{CM3x}} & L_{\mathrm{CM3y}} & 0 \end{bmatrix}, \; {}^{4}\mathbf{s}_4 = \begin{bmatrix} L_{\mathrm{CM4x}} & L_{\mathrm{CM4y}} & 0 \end{bmatrix} \end{aligned} \tag{2.5} $$

Here, e.g. L_{CMix} expresses the x_i-component of the position vector for the i^{th} center of mass, with respect to the i^{th} reference frame. It should be noted that due to the limited mass of Link 4 (the dipper), the masses of adjacent elements are taken into account, and a center of mass is equated by polynomial functions based on CAD model information.

2.3.2 Joint-Actuator Kinematics

In the following the joint kinematics are related to the actuators via their internal kinematic relations. Furthermore, the relations between joint torques and actuator forces are derived. Figure 2.5 outlines necessary quantities in order to derive these relations.

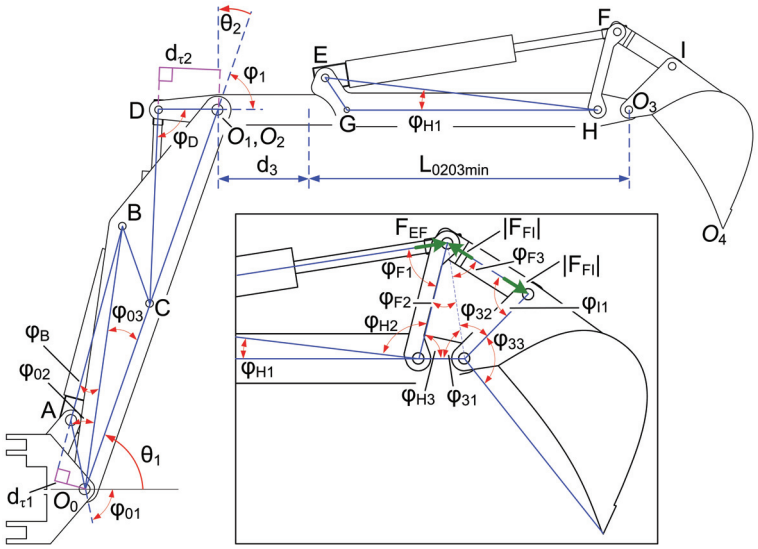

Figure 2.5: *Sketch depicting manipulator with relevant quantities used for derivation of joint-actuator kinematic- and force-torque relations.*

Link 1

The piston position for cylinder 1 expressed in terms of joint angle 1, is given by (2.6), noting that $L_{\mathrm{AB}} = x_{\mathrm{P1}} + L_{\mathrm{ABmin}}$.

$$\theta_1 = \pi - (\varphi_{01} + \varphi_{02} + \varphi_{03}) = \pi - \left(\varphi_{01} + \varphi_{03} + \arccos\left(\frac{L_{\mathrm{AO0}}^2 + L_{\mathrm{BO0}}^2 - L_{\mathrm{AB}}^2}{2 L_{\mathrm{AO0}} L_{\mathrm{BO0}}} \right) \right) \quad \Rightarrow$$

$$x_{\mathrm{P1}} = \sqrt{L_{\mathrm{AO0}}^2 + L_{\mathrm{BO0}}^2 + 2\cos(\theta_1 + \varphi_{01} + \varphi_{03}) L_{\mathrm{AO0}} L_{\mathrm{BO0}}} - L_{\mathrm{ABmin}} \tag{2.6}$$

The piston velocity $\dot{x}_{\mathrm{P1}}$ and torque-force relation are given by (2.7), (2.8), respectively.

$$\dot{x}_{\mathrm{P1}} = -\frac{\sin(\theta_1 + \varphi_{01} + \varphi_{03}) L_{\mathrm{AO0}} L_{\mathrm{BO0}} \dot{\theta}_1}{\sqrt{L_{\mathrm{AO0}}^2 + L_{\mathrm{BO0}}^2 + 2\cos(\theta_1 + \varphi_{01} + \varphi_{03}) L_{\mathrm{AO0}} L_{\mathrm{BO0}}}} \tag{2.7}$$

$$d_{\tau 1} = -L_{\mathrm{BO0}} \sin(\varphi_{\mathrm{B}}) = -L_{\mathrm{BO0}} \sin\left(\arccos\left(\frac{L_{\mathrm{AB}}^2 + L_{\mathrm{BO0}}^2 - L_{\mathrm{AO0}}^2}{2 L_{\mathrm{AB}} L_{\mathrm{BO0}}} \right) \right) \tag{2.8}$$

Link 2

Similarly to Link 1, obtain x_{P2} noting $L_{\mathrm{CD}} = x_{\mathrm{P2}} + L_{\mathrm{CDmin}}$ as (2.9).

$$\theta_2 = \frac{\pi}{2} - \varphi_1 = \pi - \arccos\left(\frac{L_{\mathrm{CO1}}^2 + L_{\mathrm{DO1}}^2 - L_{\mathrm{CD}}^2}{2 L_{\mathrm{CO1}} L_{\mathrm{DO1}}} \right) \quad \Rightarrow$$

$$x_{\mathrm{P1}} = \sqrt{L_{\mathrm{CO1}}^2 + L_{\mathrm{DO1}}^2 - 2\sin(\theta_2) L_{\mathrm{CO1}} L_{\mathrm{DO1}}} - L_{\mathrm{CDmin}} \tag{2.9}$$

Then $\dot{x}_{P2}$ is given by (2.10), and the torque-force relation $d_{\tau 2}$ as (2.11).

$$\dot{x}_{P2} = -\frac{\cos(\theta_2) L_{CO1} L_{DO1} \dot{\theta}_2}{\sqrt{L_{CO1}^2 + L_{DO1}^2 - 2\sin(\theta_2) L_{CO1} L_{DO1}}} \tag{2.10}$$

$$d_{\tau 2} = -L_{DO1}\sin(\varphi_D) = -L_{DO1}\sin\left(\arccos\left(\frac{L_{CD}^2 + L_{CO1}^2 - L_{DO1}^2}{2L_{CD}L_{CO1}}\right)\right) \tag{2.11}$$

Link 3

Due to the translational joint variable of Link 3, the relations are straightforward given by (2.12).

$$x_{P3} = d_3 \quad , \quad \dot{x}_{P3} = \dot{d}_3 \quad , \quad d_{\tau 3} = 1 \tag{2.12}$$

Link 4

Regarding Link 4, the joint angle θ_4 is obtained as (2.13).

$$\begin{aligned}\theta_4 &= \frac{3\pi}{2} - (\varphi_{31} + \varphi_{32} + \varphi_{33}) \\ &= \frac{3\pi}{2} - \varphi_{33} - \arccos\left(\frac{L_{FO3}^2 + L_{HO3}^2 - L_{FH}^2}{2L_{FO3}L_{HO3}}\right) - \arccos\left(\frac{L_{FO3}^2 + L_{IO3}^2 - L_{FI}^2}{2L_{FO3}L_{IO3}}\right)\end{aligned} \tag{2.13}$$

The length L_{FO3} is variable and given by (2.14).

$$\begin{aligned}L_{FO3} &= \sqrt{L_{FH}^2 + L_{HO3}^2 - 2\cos(\pi + \varphi_{H1} + \varphi_{H2}) L_{FH} L_{HO3}} \\ &= \sqrt{L_{FH}^2 + L_{HO3}^2 - 2\cos\left(\pi + \varphi_{H1} + \arccos\left(\frac{L_{EH}^2 + L_{FH}^2 - L_{EF}^2}{2L_{EH}L_{FH}}\right)\right) L_{FH} L_{HO3}}\end{aligned} \tag{2.14}$$

Hence to torque-force relation for Link 4 is derived by virtue of $L_{EF} = x_{P4} + L_{EFmin}$. The time derivative of $\dot{\theta}_4$ is omitted here, due to its comprehensive expression. Note; In the simulation model also the mapping $\theta_4 \rightarrow x_{P4}$ is utilized in the joint space implementation. Using the above relations for this purpose leads to rather extensive terms, and has instead been derived opposite to the above but in a similar way, using L_{HI} instead of L_{FO3}. The torque equilibrium around point H leads to (2.15).

$$L_{FH}\sin(\varphi_{F2} + \varphi_{F3}) F_{FI} - L_{FH}\sin(\varphi_{F1}) F_{EF} = 0 \quad \Rightarrow \quad F_{FI} = \frac{\sin(\varphi_{F1})}{\sin(\varphi_{F2} + \varphi_{F3})} F_{EF} \tag{2.15}$$

In a similar way, obtain τ_4 around point O_3 as (2.16).

$$\tau_4 = -L_{IO3}\sin(\varphi_{I1}) F_{FI} = -L_{IO3}\frac{\sin(\varphi_{I1})\sin(\varphi_{F1})}{\sin(\varphi_{F2} + \varphi_{F3})} F_{EF} \tag{2.16}$$

Hence, the torque-force relation for Link 4 is given by (2.17), (2.18).

$$d_{\tau 4} = -L_{IO3}\frac{\sin(\varphi_{I1})\sin(\varphi_{F1})}{\sin(\varphi_{F2} + \varphi_{F3})} \quad , \quad \varphi_{F1} = \arccos\left(\frac{L_{EF}^2 + L_{FH}^2 - L_{EH}^2}{2L_{EF}L_{FH}}\right) \tag{2.17}$$

$$\varphi_{F2} = \arccos\left(\frac{L_{FO3}^2 + L_{FH}^2 - L_{HO3}^2}{2L_{FO3}L_{FH}}\right) \quad , \quad \varphi_{F3} = \arccos\left(\frac{L_{FO3}^2 + L_{FI}^2 - L_{IO3}^2}{2L_{FO3}L_{FI}}\right) \tag{2.18}$$

2.3.3 Iterative Newton-Euler Dynamic Manipulator Formulation

The iterative Newton-Euler method for dynamic formulation of n-linked manipulators may be outlined as the following (similar to e.g. [Craig, 2005], [Andersen, 1993]).
Let $i \in [1,...,n]$ where n is the number of links, and let initial conditions be given by (2.19).

$$ {}^0\boldsymbol{\omega}_0 = \begin{bmatrix} 0 & 0 & 0 \end{bmatrix}^\mathsf{T} \ , \ {}^0\dot{\boldsymbol{\omega}}_0 = \begin{bmatrix} 0 & 0 & 0 \end{bmatrix}^\mathsf{T} \ , \ {}^0\dot{\mathbf{v}}_0 = \begin{bmatrix} g_\mathrm{x} & g_\mathrm{y} & g_\mathrm{z} \end{bmatrix}^\mathsf{T} \tag{2.19} $$

The *forward* iteration determines the translational- and rotational acceleration as well as the rotational velocity of the center of mass for every link, approaching the n^{th} link starting with Link 1. The rotational velocity- and acceleration, acceleration of the reference frame and the acceleration of the center of mass are given by (2.20) through (2.21), respectively.

$$ {}^i\boldsymbol{\omega}_i = \begin{cases} {}^i_{i-1}\mathbf{R}({}^{i-1}\boldsymbol{\omega}_{i-1} + \mathbf{z}_0\dot{\theta}_i) & \text{Rotational} \\ {}^i_{i-1}\mathbf{R}\,{}^{i-1}\boldsymbol{\omega}_{i-1} & \text{Translational} \end{cases} \tag{2.20} $$

$$ {}^i\dot{\boldsymbol{\omega}}_i = \begin{cases} {}^i_{i-1}\mathbf{R}({}^{i-1}\dot{\boldsymbol{\omega}}_{i-1} + \mathbf{z}_0\ddot{\theta}_i + {}^{i-1}\boldsymbol{\omega}_{i-1} \times \mathbf{z}_0\dot{\theta}_i) & \text{Rotational} \\ {}^i_{i-1}\mathbf{R}\,{}^{i-1}\dot{\boldsymbol{\omega}}_{i-1} & \text{Translational} \end{cases} $$

$$ {}^i\dot{\mathbf{v}}_i = \begin{cases} {}^i\dot{\boldsymbol{\omega}}_i \times {}^i\mathbf{p}_i + {}^i\boldsymbol{\omega}_i \times ({}^i\boldsymbol{\omega}_i \times {}^i\mathbf{p}_i) + {}^i_{i-1}\mathbf{R}\,{}^{i-1}\dot{\mathbf{v}}_{i-1} & \text{Rot.} \\ {}^i_{i-1}\mathbf{R}(\mathbf{z}_0\ddot{d}_i + {}^{i-1}\dot{\mathbf{v}}_{i-1}) + {}^i\dot{\boldsymbol{\omega}}_i \times {}^i\mathbf{p}_i + 2{}^i\boldsymbol{\omega}_i \times ({}^i_{i-1}\mathbf{R}\mathbf{z}_0\dot{d}_i) + {}^i\boldsymbol{\omega}_i \times ({}^i\boldsymbol{\omega}_i \times {}^i\mathbf{p}_i) & \text{Trans.} \end{cases} $$

$$ {}^i\mathbf{a}_i = {}^i\dot{\boldsymbol{\omega}}_i \times {}^i\mathbf{s}_i + {}^i\boldsymbol{\omega}_i \times ({}^i\boldsymbol{\omega}_i \times {}^i\mathbf{s}_i) + {}^i\dot{\mathbf{v}}_i \tag{2.21} $$

The *backward* iteration is completed by approaching Link 1, starting with the n^{th} link, i.e. for $i = [n,...,1]$. This iteration establishes the forces and torques applied to each link of the manipulator, and through these the joint torques. The forces and torques are given by (2.22), (2.23) and the joint torque of the i^{th} Link by (2.24), respectively.

$$ {}^i\mathbf{f}_i = {}^i_{i+1}\mathbf{R}\,{}^{i+1}\mathbf{f}_{i+1} + m_i\,{}^i\mathbf{a}_i \tag{2.22} $$

$$ {}^i\mathbf{n}_i = {}^i_{i+1}\mathbf{R}\,{}^{i+1}\mathbf{n}_{i+1} + {}^i\mathbf{p}_i \times ({}^i_{i+1}\mathbf{R}\,{}^{i+1}\mathbf{f}_{i+1}) + ({}^i\mathbf{p}_i + {}^i\mathbf{s}_i) \times m_i\,{}^i\mathbf{a}_i + {}^i\mathbf{I}_i\,{}^i\dot{\boldsymbol{\omega}}_i + {}^i\boldsymbol{\omega}_i \times {}^i\mathbf{I}_i\,{}^i\boldsymbol{\omega}_i \tag{2.23} $$

$$ \tau_i = \begin{cases} {}^i\mathbf{n}_i^\mathsf{T}({}^i_{i-1}\mathbf{R}\mathbf{z}_0) & \text{Rotational} \\ {}^i\mathbf{f}_i^\mathsf{T}({}^i_{i-1}\mathbf{R}\mathbf{z}_0) & \text{Translational} \end{cases} \tag{2.24} $$

Forward Iteration for Manipulator

Following the approach described above, obtain the rotational velocity- and acceleration, acceleration of the reference frame- and the center of mass for Link 1 as (2.25) through (2.28).

$$ {}^1\boldsymbol{\omega}_1 = \mathbf{z}_0\dot{\theta}_1 \tag{2.25} $$

$$ {}^1\dot{\boldsymbol{\omega}}_1 = \mathbf{z}_0\ddot{\theta}_1 \tag{2.26} $$

$$ {}^1\dot{\mathbf{v}}_1 = {}^1\dot{\boldsymbol{\omega}}_1 \times {}^1\mathbf{p}_1 + {}^1\boldsymbol{\omega}_1 \times ({}^1\boldsymbol{\omega}_1 \times {}^1\mathbf{p}_1) + {}^1_0\mathbf{R}\,{}^0\dot{\mathbf{v}}_0 \tag{2.27} $$

$$ {}^1\mathbf{a}_1 = {}^1\dot{\boldsymbol{\omega}}_1 \times {}^1\mathbf{s}_1 + {}^1\boldsymbol{\omega}_1 \times ({}^1\boldsymbol{\omega}_1 \times {}^1\mathbf{s}_1) + {}^1\dot{\mathbf{v}}_1 \tag{2.28} $$

For Link 2 as (2.29) trough (2.32).

$$ {}^2\boldsymbol{\omega}_2 = {}^2_1\mathbf{R}({}^1\boldsymbol{\omega}_1 + \mathbf{z}_0\dot{\theta}_2) \tag{2.29} $$

$$ {}^2\dot{\boldsymbol{\omega}}_2 = {}^2_1\mathbf{R}({}^1\dot{\boldsymbol{\omega}}_1 + \mathbf{z}_0\ddot{\theta}_2 + {}^1\boldsymbol{\omega}_1 \times \mathbf{z}_0\dot{\theta}_2) \tag{2.30} $$

$$ {}^2\dot{\mathbf{v}}_2 = {}^2\dot{\boldsymbol{\omega}}_2 \times {}^2\mathbf{p}_2 + {}^2\boldsymbol{\omega}_2 \times ({}^2\boldsymbol{\omega}_2 \times {}^2\mathbf{p}_2) + {}^2_1\mathbf{R}\,{}^1\dot{\mathbf{v}}_1 \tag{2.31} $$

$$ {}^2\mathbf{a}_2 = {}^2\dot{\boldsymbol{\omega}}_2 \times {}^2\mathbf{s}_2 + {}^2\boldsymbol{\omega}_2 \times ({}^2\boldsymbol{\omega}_2 \times {}^2\mathbf{s}_2) + {}^2\dot{\mathbf{v}}_2 \tag{2.32} $$

For Link 3 as (2.33) trough (2.36).

$$
\begin{aligned}
{}^3\boldsymbol{\omega}_3 &= {}^3_2\mathbf{R}\,{}^2\boldsymbol{\omega}_2 && (2.33)\\
{}^3\dot{\boldsymbol{\omega}}_3 &= {}^3_2\mathbf{R}\,{}^2\dot{\boldsymbol{\omega}}_2 && (2.34)\\
{}^3\dot{\mathbf{v}}_3 &= {}^3_2\mathbf{R}(\mathbf{z}_0\ddot{d}_3 + {}^2\dot{\mathbf{v}}_2) + {}^3\dot{\boldsymbol{\omega}}_3 \times {}^3\mathbf{p}_3 + 2\,{}^3\boldsymbol{\omega}_3 \times ({}^3_2\mathbf{R}\mathbf{z}_0\dot{d}_3) + {}^3\boldsymbol{\omega}_3 \times ({}^3\boldsymbol{\omega}_3 \times {}^3\mathbf{p}_3) && (2.35)\\
{}^3\mathbf{a}_3 &= {}^3\dot{\boldsymbol{\omega}}_3 \times {}^3\mathbf{s}_3 + {}^3\boldsymbol{\omega}_3 \times ({}^3\boldsymbol{\omega}_3 \times {}^3\mathbf{s}_3) + {}^3\dot{\mathbf{v}}_3 && (2.36)
\end{aligned}
$$

And for Link 4 as (2.37) trough (2.40).

$$
\begin{aligned}
{}^4\boldsymbol{\omega}_4 &= {}^4_3\mathbf{R}({}^3\boldsymbol{\omega}_3 + \mathbf{z}_0\dot{\theta}_4) && (2.37)\\
{}^4\dot{\boldsymbol{\omega}}_4 &= {}^4_3\mathbf{R}({}^3\dot{\boldsymbol{\omega}}_3 + \mathbf{z}_0\ddot{\theta}_4 + {}^3\boldsymbol{\omega}_3 \times \mathbf{z}_0\dot{\theta}_4) && (2.38)\\
{}^4\dot{\mathbf{v}}_4 &= {}^4\dot{\boldsymbol{\omega}}_4 \times {}^4\mathbf{p}_4 + {}^4\boldsymbol{\omega}_4 \times ({}^4\boldsymbol{\omega}_4 \times {}^4\mathbf{p}_4) + {}^4_3\mathbf{R}\,{}^3\dot{\mathbf{v}}_3 && (2.39)\\
{}^4\mathbf{a}_4 &= {}^4\dot{\boldsymbol{\omega}}_4 \times {}^4\mathbf{s}_4 + {}^4\boldsymbol{\omega}_4 \times ({}^4\boldsymbol{\omega}_4 \times {}^4\mathbf{s}_4) + {}^4\dot{\mathbf{v}}_4 && (2.40)
\end{aligned}
$$

Backward Iteration for Manipulator

From the forward iteration above, the manipulator joint torques are obtained through the backward iteration process (2.22), (2.23), (2.24), resulting in four joint torques, similar to the forward iteration. Due to the extensive expressions describing the joint torques, these are omitted here. The complete manipulator dynamics may be formulated in joint space coordinates as (2.41) with generalized torque- and joint variable vectors given by (2.42).

$$
\begin{aligned}
\boldsymbol{\tau} &= \mathbf{D}_\mathrm{q}(\boldsymbol{q})\ddot{\boldsymbol{q}} + \mathbf{C}_\mathrm{q}(\boldsymbol{q},\dot{\boldsymbol{q}}) + \mathbf{G}_\mathrm{q}(\boldsymbol{q}) && (2.41)\\
\boldsymbol{\tau} &= \begin{bmatrix} \tau_1 & \tau_2 & \tau_3 & \tau_4 \end{bmatrix}^\mathsf{T}\ ,\ \boldsymbol{q} = \begin{bmatrix} \theta_1 & \theta_2 & d_3 & \theta_4 \end{bmatrix}^\mathsf{T} && (2.42)
\end{aligned}
$$

2.3.4 Actuator Space Dynamic Formulation

Define the actuator (cylinder) space variable vector, and its relation the to the joint variables as (2.43), with $\mathbf{J}_\mathrm{S}$ being the Jacobian matrix.

$$
\mathbf{x}_\mathrm{P} = \begin{bmatrix} x_{\mathrm{P}1} & x_{\mathrm{P}2} & x_{\mathrm{P}3} & x_{\mathrm{P}4} \end{bmatrix}^\mathsf{T}\ ,\ \dot{\mathbf{x}}_\mathrm{P} = \mathbf{J}_\mathrm{S}\dot{\mathbf{q}} \qquad (2.43)
$$

From (2.43), obtain (2.44).

$$
\ddot{\mathbf{x}}_\mathrm{P} = \mathbf{J}_\mathrm{S}\ddot{\mathbf{q}} + \dot{\mathbf{J}}_\mathrm{S}\dot{\mathbf{q}} \ \Rightarrow\ \ddot{\mathbf{q}} = \mathbf{J}_\mathrm{S}^{-1}(\ddot{\mathbf{x}}_\mathrm{P} - \dot{\mathbf{J}}_\mathrm{S}\dot{\mathbf{q}}) = \mathbf{J}_\mathrm{S}^{-1}\ddot{\mathbf{x}}_\mathrm{P} - \mathbf{J}_\mathrm{S}^{-1}\dot{\mathbf{J}}_\mathrm{S}\mathbf{J}_\mathrm{S}^{-1}\dot{\mathbf{x}}_\mathrm{P} \qquad (2.44)
$$

The relation between the generalized torque vector (2.41) and the actuator force vector $\mathbf{F}_\mathrm{L}$ is given by (2.45), with the diagonal *Drive Jacobian* matrix $\mathbf{J}_\mathrm{D} = \mathrm{diag}(d_{\tau 1}, d_{\tau 2}, d_{\tau 3}, d_{\tau 4})$.

$$
\boldsymbol{\tau} = \mathbf{J}_\mathrm{D}\mathbf{F}_\mathrm{L} \ \Rightarrow\ \mathbf{F}_\mathrm{L} = \mathbf{J}_\mathrm{D}^{-1}\boldsymbol{\tau} \qquad (2.45)
$$

By substitution of (2.41), (2.44) into (2.45), obtain (2.48).

$$
\begin{aligned}
\mathbf{F}_\mathrm{L} &= \mathbf{J}_\mathrm{D}^{-1}(\mathbf{D}_\mathrm{q}(\boldsymbol{q})\ddot{\boldsymbol{q}} + \mathbf{C}_\mathrm{q}(\boldsymbol{q},\dot{\boldsymbol{q}}) + \mathbf{G}_\mathrm{q}(\boldsymbol{q})) && (2.46)\\
&= \mathbf{J}_\mathrm{D}^{-1}(\mathbf{D}_\mathrm{q}(\boldsymbol{q})(\mathbf{J}_\mathrm{S}^{-1}\ddot{\mathbf{x}}_\mathrm{P} - \mathbf{J}_\mathrm{S}^{-1}\dot{\mathbf{J}}_\mathrm{S}\mathbf{J}_\mathrm{S}^{-1}\dot{\mathbf{x}}_\mathrm{P}) + \mathbf{C}_\mathrm{q}(\boldsymbol{q},\dot{\boldsymbol{q}}) + \mathbf{G}_\mathrm{q}(\boldsymbol{q})) && (2.47)\\
&= \mathbf{J}_\mathrm{D}^{-1}\mathbf{D}_\mathrm{q}(\boldsymbol{q})\mathbf{J}_\mathrm{S}^{-1}\ddot{\mathbf{x}}_\mathrm{P} - \mathbf{J}_\mathrm{D}^{-1}\mathbf{D}_\mathrm{q}(\boldsymbol{q})\mathbf{J}_\mathrm{S}^{-1}\dot{\mathbf{J}}_\mathrm{S}\mathbf{J}_\mathrm{S}^{-1}\dot{\mathbf{x}}_\mathrm{P} + \mathbf{J}_\mathrm{D}^{-1}\mathbf{C}_\mathrm{q}(\boldsymbol{q},\dot{\boldsymbol{q}}) + \mathbf{J}_\mathrm{D}^{-1}\mathbf{G}_\mathrm{q}(\boldsymbol{q}) && (2.48)
\end{aligned}
$$

From (2.48), the manipulator dynamics may be expressed in actuator space as (2.49), noting that $\boldsymbol{q} = \boldsymbol{q}(\mathbf{x}_\mathrm{P})$.

$$\mathbf{F}_\mathrm{L} = \mathbf{M}_\mathrm{x}(\mathbf{x}_\mathrm{P})\ddot{\mathbf{x}}_\mathrm{P} + \mathbf{H}_\mathrm{x}(\mathbf{x}_\mathrm{P}, \dot{\mathbf{x}}_\mathrm{P}) + \mathbf{G}_\mathrm{x}(\mathbf{x}_\mathrm{P}) \tag{2.49}$$

Here $\mathbf{M}_\mathrm{x}, \mathbf{H}_\mathrm{x}, \mathbf{G}_\mathrm{x}$ are given by (2.50), (2.51), (2.52), respectively.

$$\mathbf{M}_\mathrm{x}(\mathbf{x}_\mathrm{P}) = \mathbf{J}_\mathrm{D}^{-1}\mathbf{D}_\mathrm{q}(\boldsymbol{q}(\mathbf{x}_\mathrm{P}))\mathbf{J}_\mathrm{S}^{-1} \tag{2.50}$$

$$\mathbf{H}_\mathrm{x}(\mathbf{x}_\mathrm{P}, \dot{\mathbf{x}}_\mathrm{P}) = \mathbf{J}_\mathrm{D}^{-1}\mathbf{C}_\mathrm{q}(\boldsymbol{q}(\mathbf{x}_\mathrm{P}), \dot{\boldsymbol{q}}(\mathbf{x}_\mathrm{P}, \dot{\mathbf{x}}_\mathrm{P})) - \mathbf{J}_\mathrm{D}^{-1}\mathbf{D}_\mathrm{q}(\boldsymbol{q}(\mathbf{x}_\mathrm{P}))\mathbf{J}_\mathrm{S}^{-1}\dot{\mathbf{J}}_\mathrm{S}\mathbf{J}_\mathrm{S}^{-1}\dot{\mathbf{x}}_\mathrm{P} \tag{2.51}$$

$$\mathbf{G}_\mathrm{x}(\mathbf{x}_\mathrm{P}) = \mathbf{J}_\mathrm{D}^{-1}\mathbf{G}_\mathrm{q}(\boldsymbol{q}(\mathbf{x}_\mathrm{P})) \tag{2.52}$$

The diagonal elements of the mass matrix $\mathbf{M}_\mathrm{x}(\mathbf{x}_\mathrm{P})$ are depicted in figure 2.6 for different manipulator configurations (noting that $M_{\mathrm{x}33}$ is constant due the translational joint).

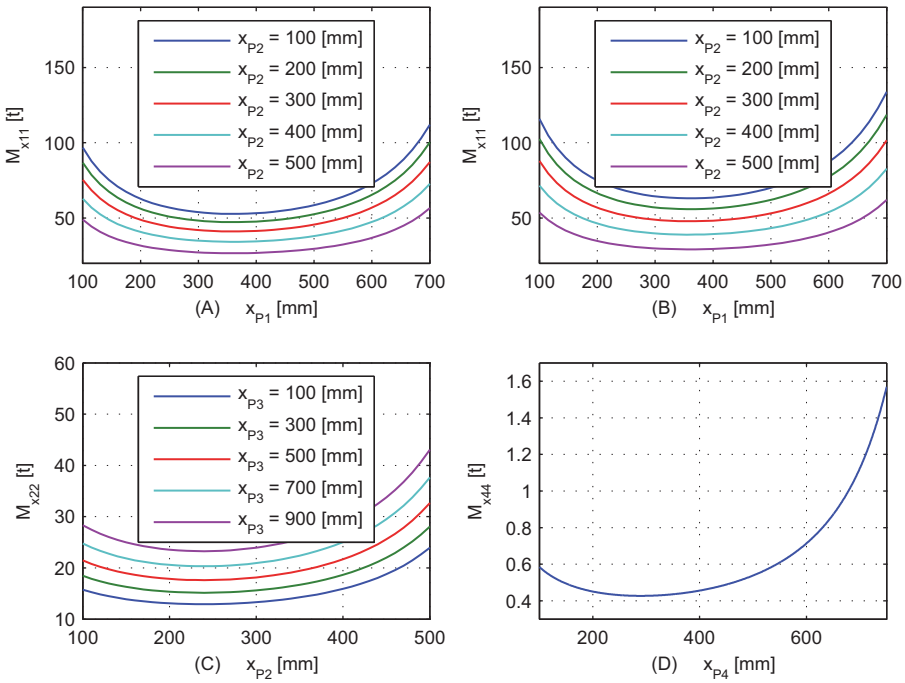

Figure 2.6: *Elements (diagonal) of matrix $\boldsymbol{M}_x(\boldsymbol{x}_P)$. (A) M_{x11} for different x_{P2}, and $x_{P3} = x_{P4} = 100$ [mm]. (B) M_{x11} for different x_{P2}, and $x_{P3} = 800$ [mm], $x_{P4} = 100$ [mm]. (C) M_{x22} for different x_{P3}, and $x_{P1} = x_{P4} = 100$ [mm]. (D) M_{x44} for x_{P4}, with $x_{P1} = x_{P2} = x_{P3} = 100$ [mm]. **Note;** $M_{x33} = m_3 + m_4$ is constant.*

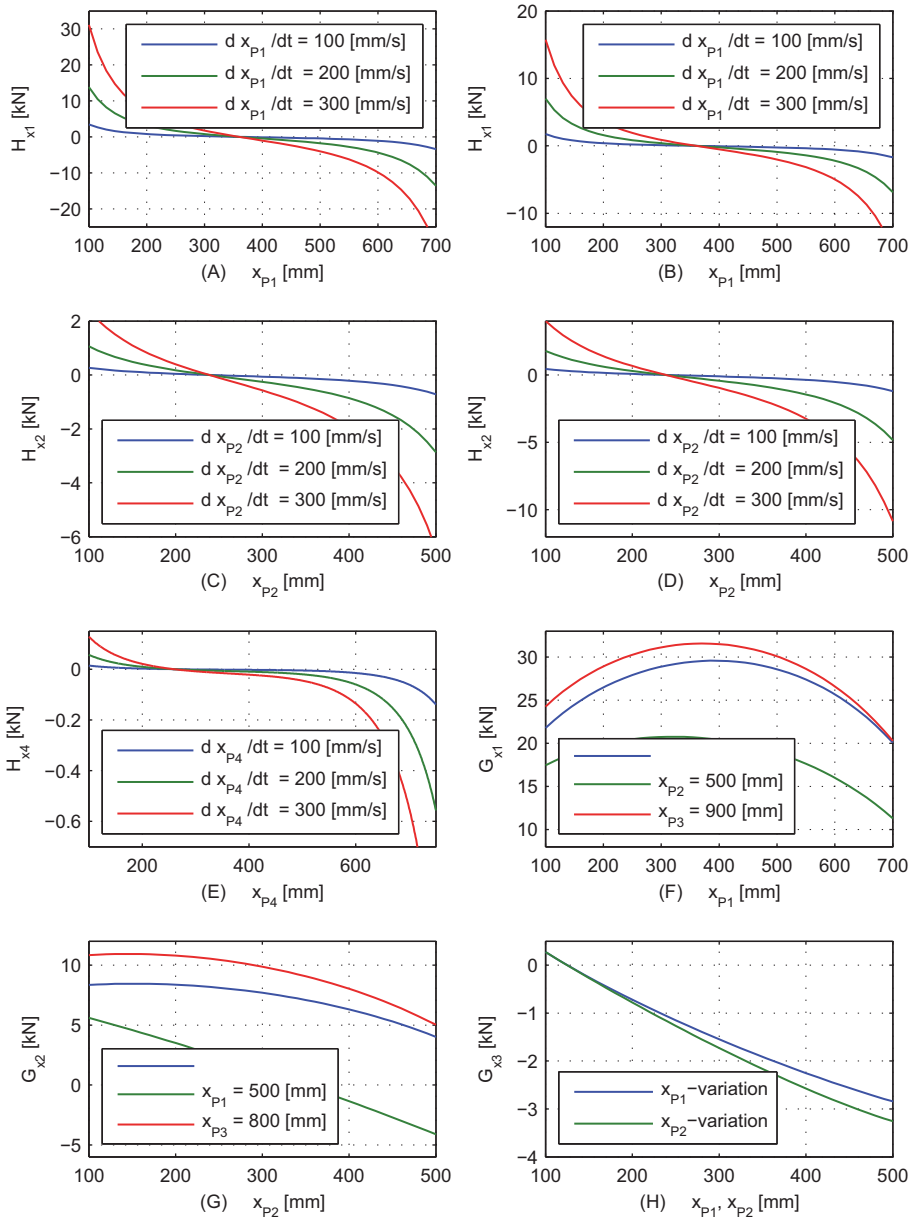

Figure 2.7: *Elements of* $\boldsymbol{H}_x(\boldsymbol{x}_P, \dot{\boldsymbol{x}}_P)$, $\boldsymbol{G}_x(\boldsymbol{x}_P)$. *(A)* H_{x1}. $x_{P2} = x_{P3} = x_{P4} = 100$ *[mm]. (B)* H_{x1}. $x_{P3} = x_{P4} = 100$ *[mm] and* $x_{P2} = 500$ *[mm]. (C)* H_{x2}. $x_{P1} = x_{P3} = x_{P4} = 100$ *[mm]. (D)* H_{x2}. $x_{P1} = x_{P4} = 100$ *[mm] and* $x_{P3} = 800$ *[mm]. (E)* H_{x4}. $x_{P1} = x_{P2} = x_{P3} = 100$ *[mm]. (F)* G_{x1}. $x_{P2} = x_{P3} = x_{P4} = 100$ *[mm],* $x_{P2} = 500$ *[mm],* $x_{P3} = x_{P4} = 100$ *[mm] and* $x_{P3} = 900$ *[mm],* $x_{P2} = x_{P4} = 100$ *[mm], respectively. (G)* G_{x2}. $x_{P1} = x_{P3} = x_{P4} = 100$ *[mm],* $x_{P2} = 100$ *[mm],* $x_{P3} = x_{P4} = 100$ *[mm] and* $x_{P3} = 800$ *[mm],* $x_{P1} = x_{P4} = 100$ *[mm], respectively. (H)* G_{x3}. $x_{P2} = x_{P3} = x_{P4} = 100$ *[mm],* x_{P1}*-var. and* $x_{P1} = x_{P3} = x_{P4} = 100$ *[mm] and* x_{P2}*-var.*

As the project is not concerned with multi axis control, controllers are designed and evaluated in regard to individual axes, while remaining axes are stationary. Hence, $\mathbf{C}_{\mathrm{q}}(\boldsymbol{q}(\mathbf{x}_{\mathrm{P}})) = \mathbf{0}$ (ideally). However, the remaining term of $\mathbf{H}_{\mathrm{x}}(\mathbf{x}_{\mathrm{P}}, \dot{\mathbf{x}}_{\mathrm{P}})$ may provide some impact due to the relative motion between the manipulator links and the cylinders (except for Link 3 due to the translational joint). The resulting forces $\mathbf{H}_{\mathrm{x}}(\mathbf{x}_{\mathrm{P}}, \dot{\mathbf{x}}_{\mathrm{P}})$, for different piston velocities and position-wise manipulator configurations are depicted in figure 2.7 (A), (B), (C), (D) and (E). Furthermore, the impact from gravity (vector $\mathbf{G}_{\mathrm{x}}(\mathbf{x}_{\mathrm{P}})$) is depicted in figure 2.7 (F), (G), (H), for the individual axes. As expected, these figures imply strong variations in the loads acting on the cylinder pistons.

2.4 Hydraulic Drive Models

As discussed previously, all hydraulic axes of the test bench consist of valve controlled differential cylinders, which here is abbreviated *hydraulic valve-cylinder drive*, *hydraulic cylinder drive* or *hydraulic drive*. In general, all hydraulic cylinder drives of the test bench may be represented as the sketch in figure 2.8.

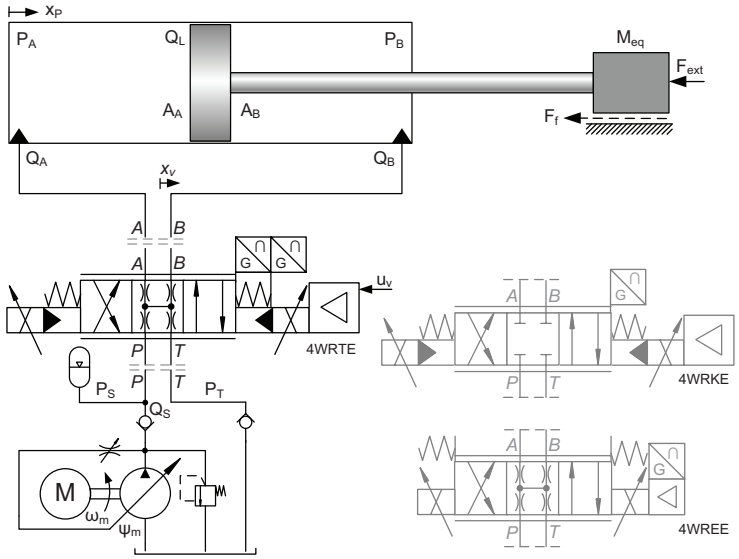

Figure 2.8: *General schematics of hydraulic valve-cylinder drives in test bench.*

In the following, modeling of the cylinder drives are based on figure 2.8.

2.4.1 Cylinder & Hose / Pipe Assembly

The motion equation generally applicable for the cylinder drives of the test bench may be described by (2.53), from Newton's second law.

$$P_{\mathrm{A}}A_{\mathrm{A}} - P_{\mathrm{B}}A_{\mathrm{B}} = M_{\mathrm{eq}}\ddot{x}_{\mathrm{P}} + F_{\mathrm{f}}(\dot{x}_{\mathrm{P}}) + F_{\mathrm{C}}(x_{\mathrm{P}}, \dot{x}_{\mathrm{P}})\dot{x}_{\mathrm{P}} + F_{\mathrm{g}}(x_{\mathrm{P}}) + F_{\mathrm{ext}} \tag{2.53}$$

In (2.53), M_{eq} is the equivalent mass acting on the piston and $F_{\mathrm{C}}(x_{\mathrm{P}},\dot{x}_{\mathrm{P}})\dot{x}_{\mathrm{P}}$, $F_{\mathrm{g}}(x_{\mathrm{P}})$, the forces resulting from possible centripetal- and centrifugal terms and from gravitational impact, respectively. These terms are those of the actuator space load model developed in the previous section (assuming the piston mass negligible). The term $F_{\mathrm{f}}(\dot{x}_{\mathrm{P}})$ represents the combined friction related to the cylinder as well as manipulator joints and contact surfaces, and is described by (2.54), where parameters may be dependent on the motion direction.

$$F_{\mathrm{f}}(\dot{x}_{\mathrm{P}}) = B_{\mathrm{V}}\dot{x}_{\mathrm{P}} + d_{\tau}^{-1}\left(F_{\mathrm{fC}} + F_{\mathrm{fS}}\exp\left(-\frac{|\dot{q}(x_{\mathrm{P}},\dot{x}_{\mathrm{P}})|}{C_{\mathrm{fl}}}\right)\right)\mathrm{sgn}(\dot{q}(x_{\mathrm{P}},\dot{x}_{\mathrm{P}})) \tag{2.54}$$

$$B_{\mathrm{V}} = B_{\mathrm{h}} + d_{\tau}^{-1}B_{\mathrm{m}}(q(x_{\mathrm{P}})) \tag{2.55}$$

Here B_{V} is the combined viscous friction coefficient for the hydraulic system and manipulator joints / contact surfaces, primarily resulting from the shear stress appearing between fluid layers. F_{fC} is the Coulomb friction appearing between manipulator elements with relative motion, and F_{fS} is Stribeck effects, also known as *stick-slip* effects. These effects are related to fluid films between elements with relative motion - it is assumed here that Coulomb friction and Stribeck effects in the cylinders are negligible compared to those of the manipulator joints. Furthermore, C_{fl} denotes the velocity whereafter Stribeck effects do not influence the friction force acting on the cylinder, and the present friction is solely Coulomb- and viscous friction. In order to avoid numerical problems in the simulation model, the function $\mathrm{sgn}(\dot{q}(x_{\mathrm{P}},\dot{x}_{\mathrm{P}}))$ is approximated by the function $\tanh(\dot{q}(x_{\mathrm{P}},\dot{x}_{\mathrm{P}})/C_{\mathrm{f2}})$, where C_{f2} is some large constant.

The pressure dynamics are described by flow continuity equations for the individual cylinder chambers and related pipe / hose assemblies. The flow continuities for the A- and B-chambers are described by (2.56), (2.57), where $V_{\mathrm{A}}(x_{\mathrm{P}}) = V_{0\mathrm{A}} + A_{\mathrm{A}}x_{\mathrm{P}}$, $V_{\mathrm{B}}(x_{\mathrm{P}}) = V_{0\mathrm{B}} - A_{\mathrm{B}}x_{\mathrm{P}}$.

$$Q_{\mathrm{A}} - C_{\mathrm{L}}(P_{\mathrm{A}} - P_{\mathrm{B}}) - C_{\mathrm{LAex}}P_{\mathrm{A}} = \frac{\mathrm{d}V_{\mathrm{A}}(x_{\mathrm{P}})}{\mathrm{d}t} + \frac{V_{\mathrm{A}}(x_{\mathrm{P}})}{\beta_{\mathrm{Ae}}}\frac{\mathrm{d}P_{\mathrm{A}}}{\mathrm{d}t} = A_{\mathrm{A}}\dot{x}_{\mathrm{P}} + \frac{V_{\mathrm{A}}(x_{\mathrm{P}})}{\beta_{\mathrm{Ae}}}\dot{P}_{\mathrm{A}} \tag{2.56}$$

$$C_{\mathrm{L}}(P_{\mathrm{A}} - P_{\mathrm{B}}) - Q_{\mathrm{B}} - C_{\mathrm{LBex}}P_{\mathrm{B}} = -\frac{\mathrm{d}V_{\mathrm{B}}(x_{\mathrm{P}})}{\mathrm{d}t} + \frac{V_{\mathrm{B}}(x_{\mathrm{P}})}{\beta_{\mathrm{Be}}}\frac{\mathrm{d}P_{\mathrm{B}}}{\mathrm{d}t} = -A_{\mathrm{B}}\dot{x}_{\mathrm{P}} + \frac{V_{\mathrm{B}}(x_{\mathrm{P}})}{\beta_{\mathrm{Be}}}\dot{P}_{\mathrm{B}} \tag{2.57}$$

Here C_{L} is the cross-port leakage coefficient, $C_{\mathrm{LAex}}, C_{\mathrm{LBex}}$ external leakage coefficients and $V_{0\mathrm{A}}, V_{0\mathrm{B}}$ initial volumes constituted by dead (or *passive*) volumes in the cylinder chambers, and volumes of the pipe / hose assemblies. The effective bulk modula $\beta_{\mathrm{Ae}}, \beta_{\mathrm{Be}}$ are essentially the effective modula of elasticity related to the hydraulic fluid (a function of temperature), air content of the fluid and the (mechanical) compliance of the pipe / hose assembly. The latter normally may be considered negligible compared to impact from undissolved air in the hydraulic fluid. Taking into account the air content of the hydraulic fluid, the effective bulk modulus β_{e} (for any of the A- and B-chambers, $\beta_{\mathrm{e}} \sim \beta_{\mathrm{Ae}}, \beta_{\mathrm{Be}}$) is described by (2.58) [Andersen and Hansen, 2003] (for constant temperature).

$$\beta_{\mathrm{e}} = \frac{1}{\frac{1}{\beta_{\mathrm{F}}} + \frac{\varepsilon_{\mathrm{Air}}}{\beta_{\mathrm{Air}}}} \quad , \quad \beta_{\mathrm{F}} = C_{\mathrm{ad}}P \quad , \quad \varepsilon_{\mathrm{Air}} \simeq \frac{1}{\frac{1-\varepsilon_{\mathrm{Air0}}}{\varepsilon_{\mathrm{Air0}}}\left(\frac{P_{\mathrm{atm}}}{P}\right)^{-\frac{1}{C_{\mathrm{ad}}}} + 1} \tag{2.58}$$

Here $\varepsilon_{\mathrm{Air0}}$ is the volumetric ratio of undissolved air at atmospheric pressure in the hydraulic fluid, β_{F} is the stiffness of the hydraulic fluid, C_{ad} the adiabatic constant for air and P_{atm} the atmospheric pressure. An example depicting the change in effective bulk modulus as a function of the air content is shown in figure 2.9.

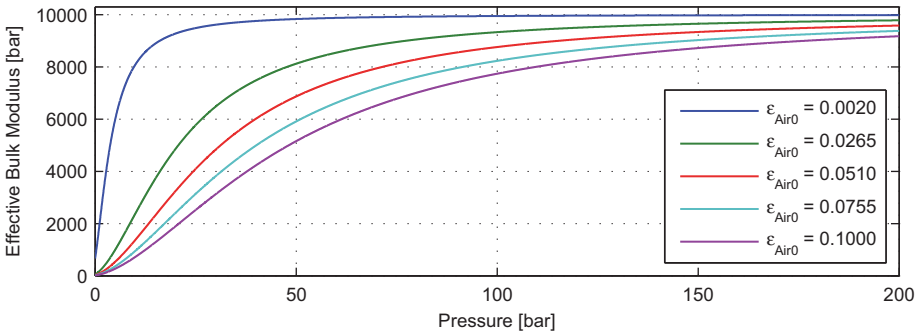

Figure 2.9: *Change in effective bulk modulus, for different ε_{Air0}. Remaining parameters are $C_{ad} = 1.4$, $P_{atm} = 1$ $[bar]$ and $\beta_F = 1e4$ $[bar]$.*

2.4.2 Proportional Flow Control Valves

The proportional flow control valves applied in the test bench are direct operated- (single stage) or pilot operated (two stage) valve types, commonly applied in industry. More specifically Axis 1 is controlled by a 4WRKE 10 E1-100L valve, Axis 2 is controlled by a 4WRTE 10 V1-100L valve, Axis 3 is controlled by a 4WREE 10 V50 valve and Axis 4 is controlled by a 4WREE 6 V32 valve. All valves are configured with integrated amplifier electronic circuits (so-called On Board Electronics (OBE)). The housing etc. of the 4WRKE type valve is similar to that of the 4WRTE type, and the 4WRTE- (pilot operated) and 4WREE (direct operated) type valves are depicted in figure 2.11. The flow characteristics of the valves are modeled by their state dependent flows and dynamic characteristics according to [Merritt, 1967], and the valve port flows are described by (2.59), (2.60).

$$Q_{\mathrm{A}} = K_{\mathrm{vA}}(x_{\mathrm{v}})x_{\mathrm{v}} \begin{cases} \sqrt{|P_{\mathrm{S}} - P_{\mathrm{A}}|}\,\mathrm{sgn}(P_{\mathrm{S}} - P_{\mathrm{A}}) & \text{for } x_{\mathrm{v}} > 0 \\ \sqrt{|P_{\mathrm{A}} - P_{\mathrm{T}}|}\,\mathrm{sgn}(P_{\mathrm{A}} - P_{\mathrm{T}}) & \text{for } x_{\mathrm{v}} < 0 \end{cases} \tag{2.59}$$

$$Q_{\mathrm{B}} = K_{\mathrm{vB}}(x_{\mathrm{v}})x_{\mathrm{v}} \begin{cases} \sqrt{|P_{\mathrm{B}} - P_{\mathrm{T}}|}\,\mathrm{sgn}(P_{\mathrm{B}} - P_{\mathrm{T}}) & \text{for } x_{\mathrm{v}} > 0 \\ \sqrt{|P_{\mathrm{S}} - P_{\mathrm{B}}|}\,\mathrm{sgn}(P_{\mathrm{S}} - P_{\mathrm{B}}) & \text{for } x_{\mathrm{v}} < 0 \end{cases} \tag{2.60}$$

The valve port flow gains $K_{vA}(x_v), K_{vB}(x_v)$ for the different valves differ significantly from each other, as apparent from the data sheets [Rexroth, 2005], [Rexroth, 2006], [Rexroth, 2004]. The flow gains of the 4WRTE 10 V1-100L and 4WRKE 10 E1-100L valves are constant but asymmetric by the relation $2:1$, whereas the flow gains of the 4WREE 10 V50- and 4WREE 6 V32 valves are symmetric. The resulting flow of the 4WREE 10 V50 valve for different pressure drops over the control land(s) are depicted in figure 2.10 (the 4WREE 6 V32 valve feature similar characteristics). Furthermore, the 4WRKE 10 E1-100L valve features a 15 % deadband of the nominal range, whereas the remaining valves are zero lapped.

The dynamic relation between the valve control input and the spool position of a valve is in general highly complex. It is dominated by saturation phenomena in the valve amplification stage imposing slew rate limitations and time delays, resulting from current rise time, flux diffusion in solenoids, mechanical friction between the spool and valve housing etc. Finally, also the nominal input-output (input-spool) dynamic relation has significant impact on performance.

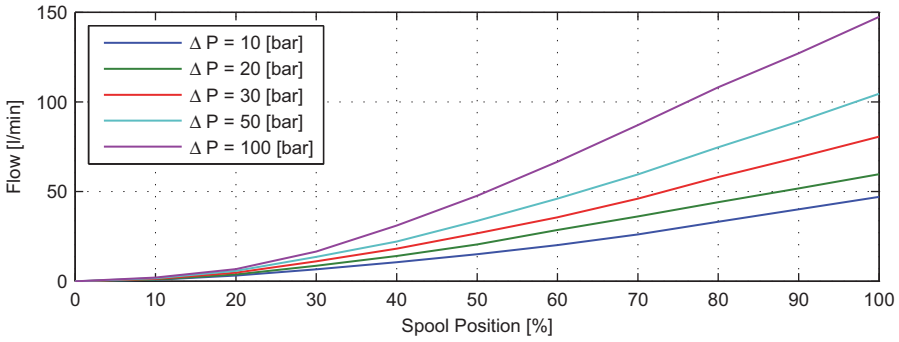

Figure 2.10: *Resulting port flows for the 4WREE 10 V50, for different control land pressure drops (inspired by [Rexroth, 2006]).*

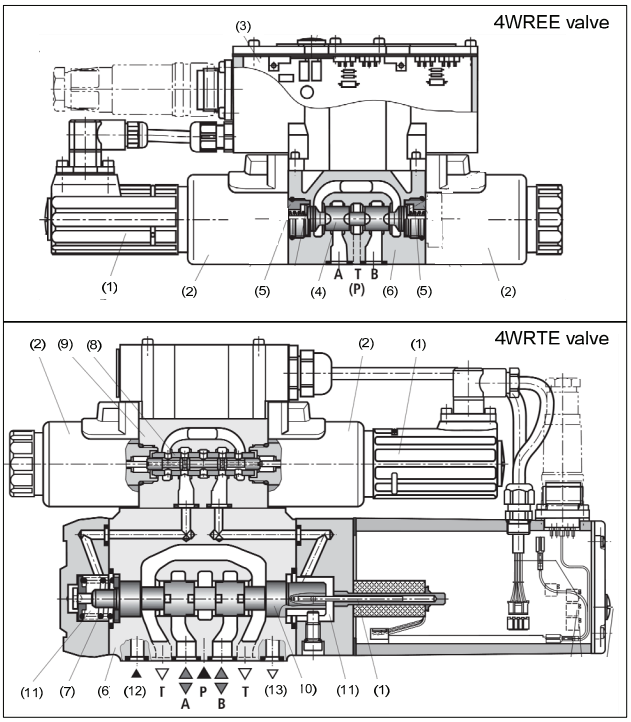

Figure 2.11: *Bosch Rexroth valves, types 4WREE and 4WRTE (inspired by [Rexroth, 2005], [Rexroth, 2006]). (1) Position transducer, (2) Solenoids, (3) Integrated control electronics (amplifier stage), (4) Control spool, (5) Compression springs, (6) Valve housing, (7) Centering spring, (8) Pilot spool, (9) Pilot control valve, (10) Main spool, (11) Control chambers, (12) Pilot oil supply, (13) Pilot oil drain.*

Commonly the nominal input-output dynamics are approximated by a second order dynamic model [Mohieddine Jelali, 2004]. In order to achieve a more accurate representation of the nominal valve dynamics, here, this is represented by third order dynamics (2.61) (standard first- and second order structures).

$$\tau_{v1}^2 \tau_{v2} x_v^{(3)} + (2\tau_{v1}\tau_{v2}\zeta_v + \tau_{v1}^2)\ddot{x}_v + (2\tau_{v1}\zeta_v + \tau_{v2})\dot{x}_v + x_v = u_v \tag{2.61}$$

The nominal input-output dynamics, slew rate limitations and time delays may be estimated from the frequency response and transient time function of data sheets [Rexroth, 2005], [Rexroth, 2006], [Rexroth, 2004].

2.4.3 Hydraulic Power Unit

The hydraulic power unit (HPU) is modeled as depicted in figure 2.8, with the flow continuity of the volume connecting the pump outlet to the valves, given by (2.62).

$$Q_S - Q_V - C_{Lp}P_S = \frac{V_S}{\beta_{PS}}\frac{dP_S}{dt} = \frac{V_S}{\beta_{PS}}\dot{P}_S \tag{2.62}$$

Here Q_S is the pump outlet flow (supply flow), Q_V is the valve flow consumption, C_{Lp} is the pump leakage coefficient and P_S is the pressure in the control volume V_S, i.e. the valve supply pressure. The static pump outlet flow (supply flow) Q_S may be described as (2.63).

$$Q_S = D_P \omega_m \psi_s \tag{2.63}$$

Here D_P is the pump displacement coefficient, ω_m is the pump shaft rotational speed and ψ_s the swivel angle (swash plate angle) of the pump. In the test bench, the pump is driven at constant rotational speed with (ideally) constant pressure output. The pump is configured with power limit control, however as tests should not give reason to power saturation, this is not taken into account in the model. The dynamic properties the pump are modeled by second order dynamics, relating the reference swivel angle ψ_{sR} to the actual swivel angle ψ_s. The pump dynamics applied in the model are given by (2.64) [Cetinkunt, 2006].

$$\tau_s^2 \ddot{\psi}_s + 2\zeta_{ps}\tau_{ps}\dot{\psi}_s + \psi_s = \psi_{sR} \tag{2.64}$$

2.5 Verification of Nonlinear Model

The objective of the model verification is to verify that the dynamic and steady state properties of the individual cylinder axes resembles those of the test bench. As will be discussed in Section 2.8, the hydraulic axes are considered individually in regard to the control development. Hence, the cross coupled dynamics between different axes are of minor interest here, and not verified explicitly. The inputs chosen for the model verification resembles in all cases that of figure 2.12, and are applied for three different initial positions for all cylinders. Such step inputs may be used to evaluate static forces in terms of gravity forces, to some extend the viscous- and Coulomb friction and the equivalent inertia load. The step inputs may also be utilized to verify the static valve flow gains of axes 1 and 2, as these valves have linear flow characteristics. However the static valve gains of axes 3 and 4 are progressive, and several step inputs are necessary in order to verify these. Such procedures have been carried out and the flow gains have been approximated by polynomial functions.

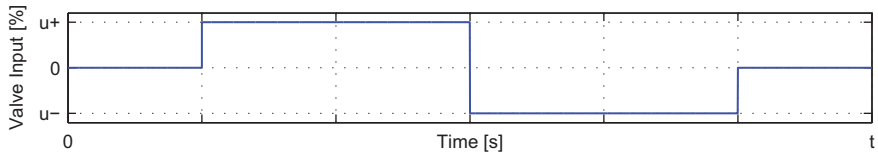

Figure 2.12: *Sketch of step input sequence used for evaluation of the nonlinear model.*

The developed model only takes into account the manipulator and the hydraulic system actuating the four cylinder axes, and assumes that the base component is completely stationary. In reality however, the vehicle on which the manipulator is mounted cannot be considered stationary, primarily due to the tire flexibility. Especially inputs to axes 1 and 2 may result in vehicle oscillations which may be considered disturbances to the hydraulic axes. The verification results are briefly summarized in the following.

Axis 1 The step inputs applied to Axis 1 is 25 % of the nominal signal range, however due to the valve overlap the input is effectively only 10 %. The results for the three test scenarios are depicted in figure 2.13. From this is found that the model captures the main dynamic features of the system in terms of natural frequency, damping, force- and chamber pressure levels and the static flow gain of the valve.

Axis 2 For Axis 2 the magnitude of the step inputs are 20 % of the nominal range. From figure 2.14 depicting the model- and test bench response, it is found that for all three scenarios the dynamic and static properties are captured by the model - however, it is also found that a superposed oscillation with a frequency slightly above 2 $[Hz]$ is present in the measured pressure data. This is assumed to be the result of excitation of resonant modes of Axis 1, as the frequency is coincident.

Axis 3 The verification of Axis 3 is carried out when this is in a horizontal position, and the inputs applied have a magnitude of 60 % of its nominal range, and results are depicted in figure 2.15. As for Axis 2 also a superposed oscillation just above 2 $[Hz]$ is present, which is assumed to be due to the same reasons. The model captures the main transients- as well as the static valve flow gain (for 60 % input) of the test bench. However, the static force- and pressure levels do not match on the level with axes 1 and 2. As no gravity impact is present due to the horizontal positioning of the axis, this is solely ascribed inaccuracies in the friction model, which is rather difficult to model due to the large contact surface of this extender joint, and that friction is most likely position dependent. However, the model is assumed sufficiently accurate for the purpose of the work presented here.

Axis 4 Axis 4 is subjected to step inputs with a magnitude of 75 % of the nominal valve input range. Results are depicted in figure 2.16. It is found that also this axis model captures the main dynamic features of the test bench, however with some deviations in especially force and pressure levels. This is assumed to be due to inaccurate estimation of the variation of the center of mass for the link. However, the results are considered sufficiently accurate for the purpose of the project.

It should be noted that external valve leakage has not been taken into account in order to limit the number of model parameters. Furthermore, in order to achieve matching behavior of the modeled chamber pressures, leakage flows of the model are smaller than those of the test bench. Based on the above results, the model is found to be sufficiently accurate to suit the purpose of this project.

Cylinder Axis 1

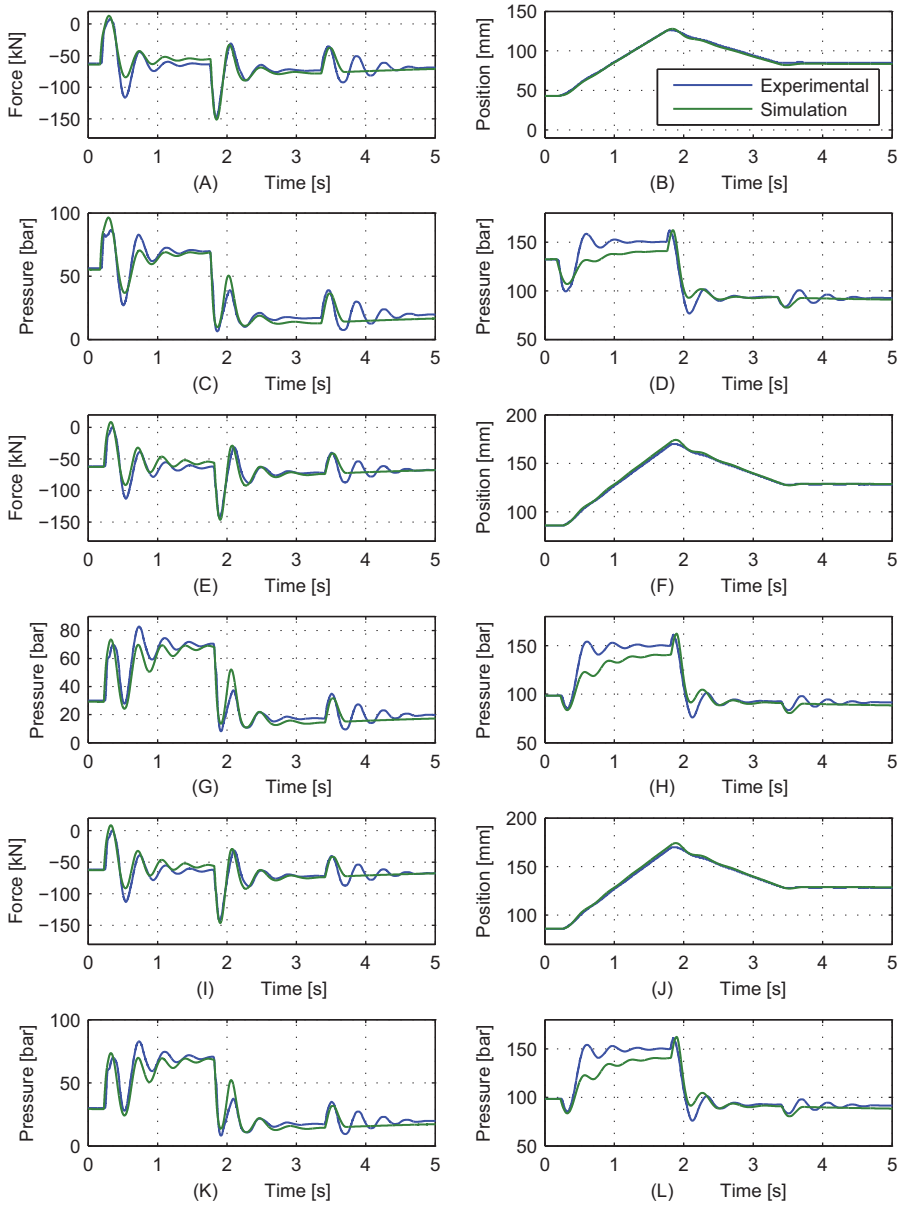

Figure 2.13: *Comparison of measurements and model data for Axis 1, with a step input signal being 25 % of the nominal input range. Cylinder force F_L, cylinder position x_P, chamber pressure P_A and chamber pressure P_B for data set 1, 2 and 3 are depicted in figures (A), (E), (I) and (B), (F), (J) and (C), (G), (K) and in figures (D), (H), (L), respectively.*

Cylinder Axis 2

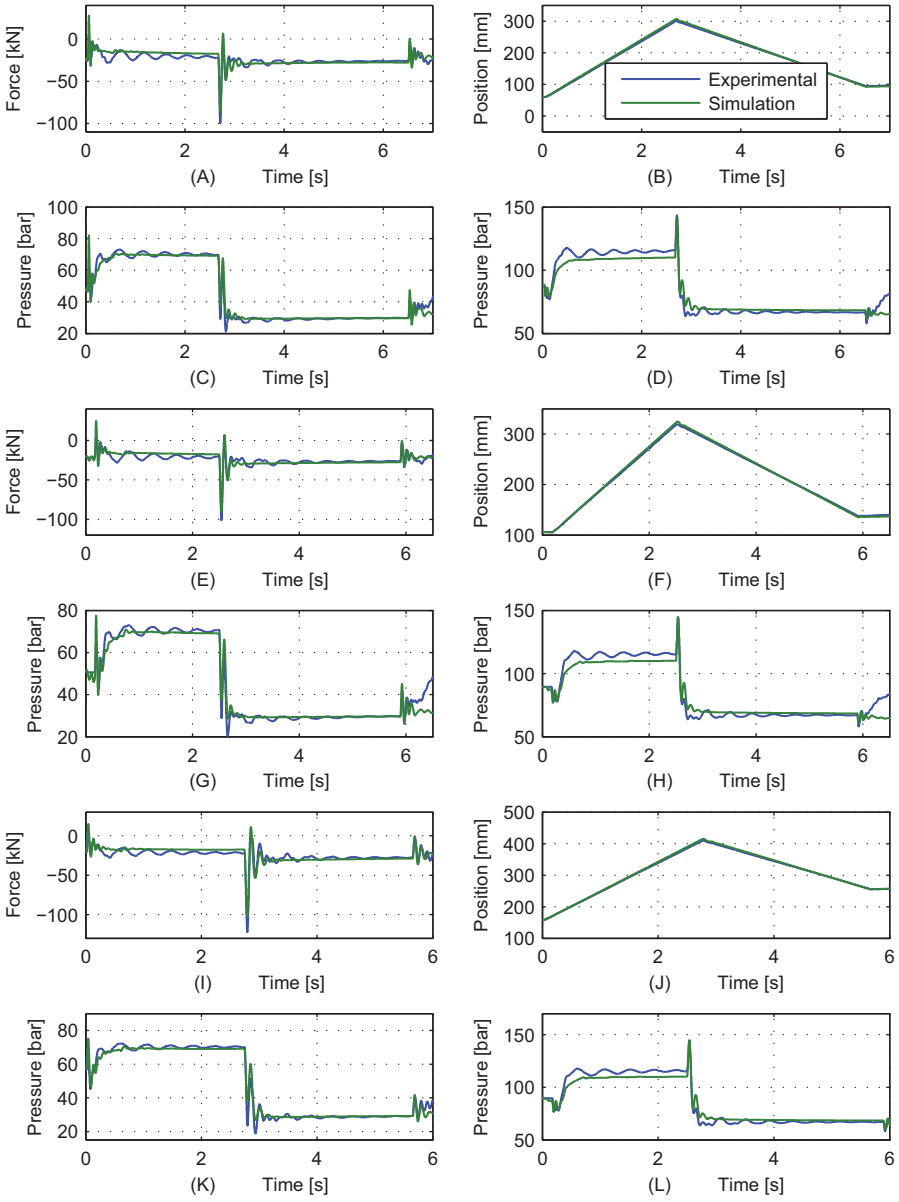

Figure 2.14: *Comparison of measurements and model data for Axis 2, with a step input signal being 20 % of the nominal input range. Cylinder force F_L, cylinder position x_P, chamber pressure P_A and chamber pressure P_B for data set 1, 2 and 3 are depicted in figures (A), (E), (I) and (B), (F), (J) and (C), (G), (K) and in figures (D), (H), (L), respectively.*

Cylinder Axis 3

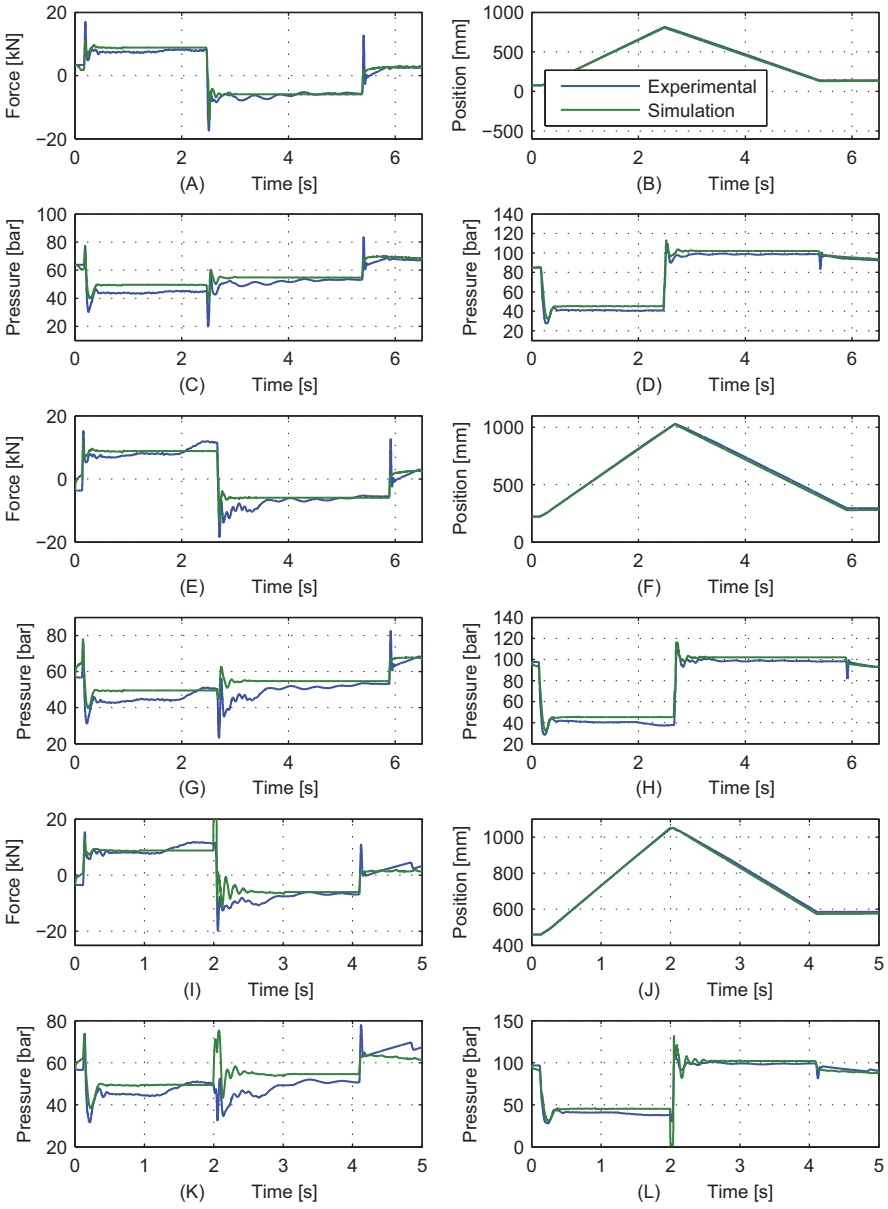

Figure 2.15: *Comparison of measurements and model data for Axis 3, with a step input signal being* 60 *% of the nominal input range. Cylinder force F_L, cylinder position x_P, chamber pressure P_A and chamber pressure P_B for data set 1, 2 and 3 are depicted in figures (A), (E), (I) and (B), (F), (J) and (C), (G), (K) and in figures (D), (H), (L), respectively.*

Cylinder Axis 4

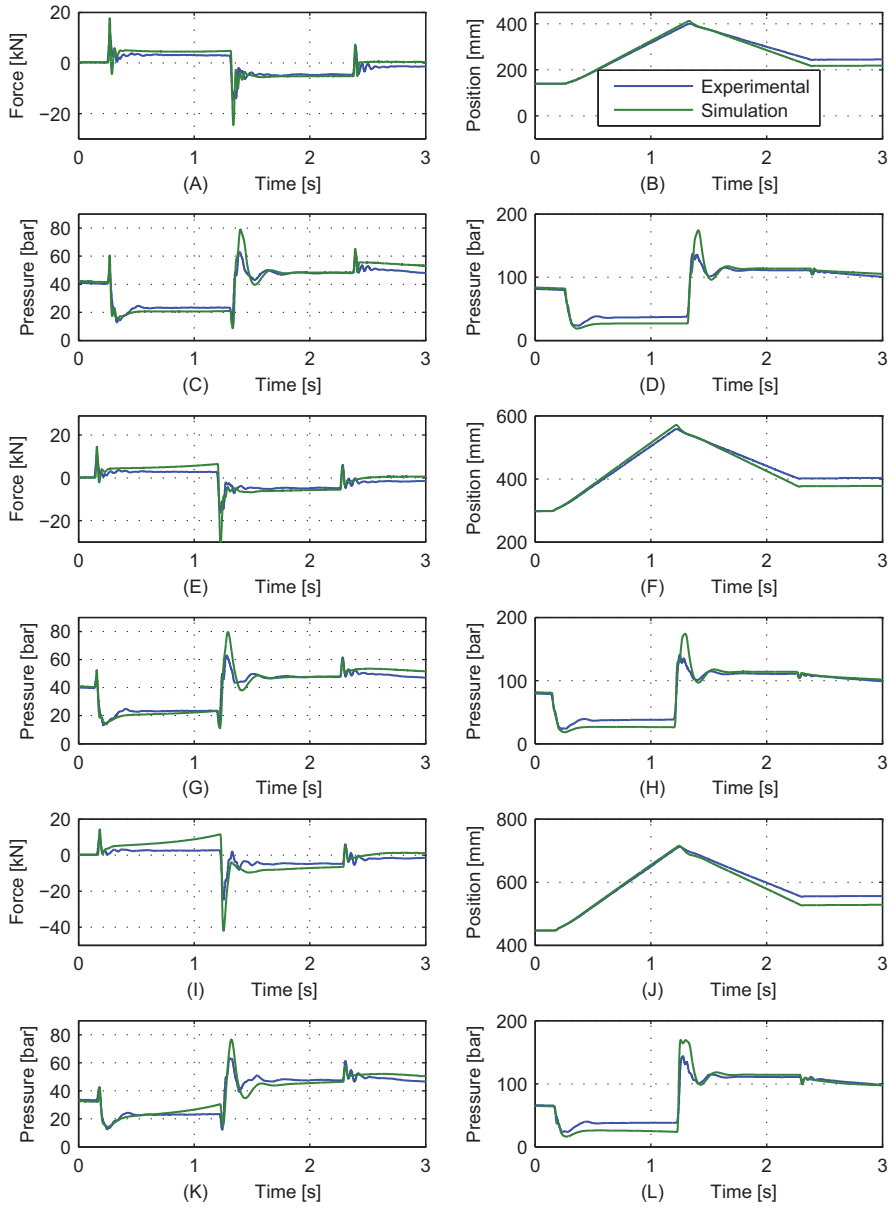

Figure 2.16: *Comparison of measurements and model data for Axis 4, with a step input signal being 75 % of the nominal input range. Cylinder force F_L, cylinder position x_P, chamber pressure P_A and chamber pressure P_B for data set 1, 2 and 3 are depicted in figures (A), (E), (I) and (B), (F), (J) and (C), (G), (K) and in figures (D), (H), (L), respectively.*

2.6 Generalized Model Framework for Control Design

In the following a generalized- and more compact model framework is established. This model framework serves the purpose of reducing the number of describing state equations, in order to facilitate control design processes in following chapters.

2.6.1 Generalized Model Structure

From the modeling sections above, a hydraulic valve-cylinder may be described by (2.67), when assuming $\tau_{v1} >> \tau_{v2}$, $\tau_{v1}^{-1} = \omega_v$, defining the state vector $\mathbf{x} = (x_P, \dot{x}_P, P_A, P_B, x_v, \dot{x}_v)$ and functions (2.65), (2.66) (recall the valve flows (2.59), (2.60) and that $V_A(x_P) = V_{0A} + A_A x_P$, $V_B(x_P) = V_{0B} - A_B x_P$).

$$F_{ad} = F_{ad}(\mathbf{x}) = F_g(x_P) + F_{ext} + F_f - B_V \dot{x}_P \tag{2.65}$$

$$B_v = B_v(\mathbf{x}) = F_C(x_P, \dot{x}_P) + B_V \tag{2.66}$$

$$\begin{bmatrix} \dot{x}_P \\ \ddot{x}_P \\ \dot{P}_A \\ \dot{P}_B \\ \dot{x}_v \\ \ddot{x}_v \end{bmatrix} = \begin{bmatrix} \dot{x}_P \\ \frac{1}{M_{eq}}(P_A A_A - P_B A_B - B_v \dot{x}_P - F_{ad}) \\ \frac{\beta_{Ae}}{V_A(x_P)}(Q_A - C_L(P_A - P_B) - A_A \dot{x}_P) \\ \frac{\beta_{Be}}{V_B(x_P)}(A_B \dot{x}_P + C_L(P_A - P_B) - Q_B) \\ \dot{x}_v \\ \omega_v^2 u_v - 2\omega_v \zeta_v \dot{x}_v - \omega_v^2 x_v \end{bmatrix} \tag{2.67}$$

The model (2.67) covers all possible valve-cylinder drive configurations, taking into account arbitrary unmatched asymmetries of cylinder areas A_A, A_B and flow port gains K_{vA}, K_{vB}. For control design purposes it is desirable to establish a simplified model description, that captures the dominant dynamic features of the hydraulic drives under consideration, while taking into account asymmetries. For this purpose, relations and a *virtual* load pressure are defined as (2.68) [Merritt, 1967], [Mohieddine Jelali, 2004].

$$\sigma = \frac{K_{vB}}{K_{vA}} \quad , \quad \mu = \frac{A_B}{A_A} \quad , \quad P_L = P_A - \mu P_B \tag{2.68}$$

In the case of positive flow, i.e. $x_v > 0$, the flows Q_A, Q_B of valve ports A and B may be written as (2.69).

$$Q_A = K_{vA} x_v \sqrt{P_S - P_A}, \;\; Q_B = \sigma K_{vA} x_v \sqrt{P_B - P_T} \tag{2.69}$$

Consider the flows (2.59), (2.60) when fluid compression and leakage is absent, satisfying the relation (2.70).

$$\mu Q_A = Q_B \tag{2.70}$$

Substituting (2.59), (2.60) into (2.70), and solving for P_A and P_B, respectively, yield (2.71).

$$P_A = \frac{P_S \mu^2 - \sigma^2 P_B + \sigma^2 P_T}{\mu^2} \quad , \quad P_B = \frac{P_T \sigma^2 + \mu^2 P_S - \mu^2 P_A}{\sigma^2} \tag{2.71}$$

Inserting P_B of (2.71) into (2.68) and solving for P_A and inserting P_A of (2.71) into (2.68) and solving for P_B, respectively, yield (2.72).

$$P_A = \frac{\mu^3 P_S + \sigma^2 P_L + \mu\sigma^2 P_T}{\sigma^2 + \mu^3} \quad , \quad P_B = \frac{\mu^2 P_S - \mu^2 P_L + \sigma^2 P_T}{\sigma^2 + \mu^3} \tag{2.72}$$

Inserting P_A of (2.72) into Q_A (2.69), and P_B (2.72) into Q_B of (2.69), the valve port flow equations expressed in terms of P_L are obtained as (2.73).

$$Q_A = \sigma K_{vA} x_v \sqrt{\frac{P_S - P_L - \mu P_T}{\sigma^2 + \mu^3}} \quad , \quad Q_B = \mu\sigma K_{vA} x_v \sqrt{\frac{P_S - P_L - P_T\mu}{\sigma^2 + \mu^3}} \tag{2.73}$$

In the case of negative flow, i.e. $x_v < 0$, the valve port flows are given by (2.74).

$$Q_A = K_{vA} x_v \sqrt{P_A - P_T} \quad , \quad Q_B = \sigma K_{vA} x_v \sqrt{P_S - P_B} \tag{2.74}$$

Carrying out similar calculations as for $x_v > 0$, the valve port flow equations expressed in terms of P_L are obtained as (2.75).

$$Q_A = \sigma K_{vA} x_v \sqrt{\frac{\mu P_S + P_L - P_T}{\sigma^2 + \mu^3}} \quad , \quad Q_B = \mu\sigma K_{vA} x_v \sqrt{\frac{\mu P_S + P_L - P_T}{\sigma^2 + \mu^3}} \tag{2.75}$$

From (2.73), (2.75), general valve port flow equations may be established as (2.77).

$$Q_A = \mu^{-1} Q_B = x_v \frac{\sigma K_{vA}}{\sqrt{\sigma^2 + \mu^3}} \begin{cases} \sqrt{P_S - P_L - \mu P_T} & \text{for} \quad x_v > 0 \\ \sqrt{\mu P_S + P_L - P_T} & \text{for} \quad x_v < 0 \end{cases} \tag{2.76}$$

$$= x_v \frac{\sigma K_{vA}}{\sqrt{\sigma^2 + \mu^3}} \begin{cases} \sqrt{P_S - \mathrm{sgn}(x_v) P_L - \mu P_T} & \text{for} \quad x_v > 0 \\ \sqrt{\mu P_S - \mathrm{sgn}(x_v) P_L - P_T} & \text{for} \quad x_v < 0 \end{cases} \tag{2.77}$$

The chamber pressure gradients of the model (2.67), may be expressed in terms of the gradient of the virtual load pressure (2.68), as (2.78).

$$\dot{P}_L = \frac{\beta_e}{V_A} \frac{\rho + \mu^2}{\rho} (Q_A - A_A \dot{x}_P - C_L (P_A - P_B)), \quad \rho = \frac{V_B}{V_A} \tag{2.78}$$

The leakage flow does not appear as a function of the *virtual* load pressure, but as a function of the pressure difference $\Delta P_{AB} = P_A - P_B$. Utilizing the relations above, and substituting (2.72) into Q_L assuming P_T negligible compared to P_S, P_L, obtain the leakage flow for positive motion as (2.80).

$$Q_L|_{x_v>0} = C_L (P_A - P_B) = C_L \left(\frac{\mu^3 P_S + \sigma^2 P_L}{\sigma^2 + \mu^3} - \frac{\mu^2 P_S - \mu^2 P_L}{\sigma^2 + \mu^3} \right) \tag{2.79}$$

$$= C_L \left(\frac{\sigma^2 + \mu^2}{\sigma^2 + \mu^3} P_L + \frac{\mu^3 - \mu^2}{\sigma^2 + \mu^3} P_S \right) \tag{2.80}$$

In a similar way, obtain the leakage flow for negative motion as (2.81).

$$Q_L|_{x_v<0} = C_L \left(\frac{\sigma^2 + \mu^2}{\sigma^2 + \mu^3} P_L + \frac{\mu\sigma^2 - \sigma^2}{\sigma^2 + \mu^3} P_S \right) \tag{2.81}$$

Based on (2.80), (2.81), the leakage flow may be described by (2.82).

$$Q_{\mathrm{L}} = C_{\mathrm{L}} P_{\mathrm{L}} \frac{\sigma^2+\mu^2}{\sigma^2+\mu^3} + C_{\mathrm{L}} P_{\mathrm{S}} \begin{cases} \dfrac{\mu^3-\mu^2}{\sigma^2+\mu^3} & \text{for } x_v > 0 \\ \dfrac{\mu^3-\mu^2}{\sigma^2+\mu^3}\dfrac{\sigma^2}{\mu^2} & \text{for } x_v < 0 \end{cases} \tag{2.82}$$

Utilizing (2.84), then (2.78) may be reformulated as (2.83).

$$\dot{P}_{\mathrm{L}} = \frac{\beta_{\mathrm{e}}}{V_{\mathrm{A}}} \frac{\rho+\mu^2}{\rho} (Q_{\mathrm{A}} - A_{\mathrm{A}} \dot{x}_{\mathrm{P}} - C_{\mathrm{Ll}} P_{\mathrm{L}} - C_{\mathrm{Ls}} P_{\mathrm{S}}) \tag{2.83}$$

Here coefficients $C_{\mathrm{Ll}}, C_{\mathrm{Ls}}$ are given by (2.84).

$$C_{\mathrm{Ll}} = C_{\mathrm{L}} \frac{\sigma^2+\mu^2}{\sigma^2+\mu^3} \frac{\rho+\mu}{\rho+\mu^2} \;\;,\;\; C_{\mathrm{Ls}} = C_{\mathrm{L}} \begin{cases} \dfrac{\mu^3-\mu^2}{\sigma^2+\mu^3}\dfrac{\rho+\mu}{\rho+\mu^2} & \text{for } x_v > 0 \\ \dfrac{\mu^3-\mu^2}{\sigma^2+\mu^3}\dfrac{\rho+\mu}{\rho+\mu^2}\dfrac{\sigma^2}{\mu^2} & \text{for } x_v < 0 \end{cases} \tag{2.84}$$

Hence, defining a new state vector $\mathbf{x} = (x_{\mathrm{P}}, \dot{x}_{\mathrm{P}}, P_{\mathrm{L}})$, a compact generalized state space model that may represent valve-cylinder drives with arbitrary unmatched asymmetries, may be established as (2.85).

$$\begin{bmatrix} \dot{x}_{\mathrm{P}} \\ \ddot{x}_{\mathrm{P}} \\ \dot{P}_{\mathrm{L}} \end{bmatrix} = \begin{bmatrix} \dot{x}_{\mathrm{P}} \\ \dfrac{1}{M_{\mathrm{eq}}}(P_{\mathrm{A}} A_{\mathrm{A}} - P_{\mathrm{B}} A_{\mathrm{B}} - B_{\mathrm{v}} \dot{x}_{\mathrm{P}} - F_{\mathrm{ad}}) \\ \dfrac{\beta_{\mathrm{e}}}{V_{\mathrm{A}}} \dfrac{\rho+\mu^2}{\rho} (Q_{\mathrm{A}} - A_{\mathrm{A}} \dot{x}_{\mathrm{P}} - C_{\mathrm{Ll}} P_{\mathrm{L}} - C_{\mathrm{Ls}} P_{\mathrm{S}}) \end{bmatrix} \tag{2.85}$$

This finalizes the derivation of the compact nonlinear generalized drive model.

2.7 Generalized Linear Drive Model & Transfer functions

In the following a linear model is derived based on the generalized nonlinear drive model developed in the previous section. The linearization is established around an operating point, and is concerned with the dynamics in a small vicinity of this operating point, hence concerned with *change variables*. By Taylor expansion the valve model (2.77) may be established as (2.86) with linearization coefficients (2.87), (2.88) where x_{v0}, P_{L0} are related to the linearization point.

$$q_{\mathrm{A}} = \mu^{-1} q_{\mathrm{B}} = K_{\mathrm{q}} x_{\mathrm{v}} - K_{\mathrm{qp}} p_{\mathrm{L}} \tag{2.86}$$

$$K_{\mathrm{q}} = \left.\frac{\partial Q_{\mathrm{A}}}{\partial x_{\mathrm{v}}}\right|_{x_{\mathrm{v0}}, P_{\mathrm{L0}}} = \frac{\sigma K_{\mathrm{vA}}}{\sqrt{\sigma^2+\mu^3}} \begin{cases} \sqrt{P_{\mathrm{S}} - P_{\mathrm{L0}} - \mu P_{\mathrm{T}}} & \text{for } x_{\mathrm{v}} > 0 \\ \sqrt{\mu P_S + P_{\mathrm{L0}} - P_{\mathrm{T}}} & \text{for } x_{\mathrm{v}} < 0 \end{cases} \tag{2.87}$$

$$K_{\mathrm{qp}} = \left.\frac{\partial Q_{\mathrm{A}}}{\partial P_{\mathrm{L}}}\right|_{x_{\mathrm{v0}}, P_{\mathrm{L0}}} = \frac{\sigma K_{\mathrm{vA}} x_{\mathrm{v0}}}{\sqrt{\sigma^2+\mu^3}} \begin{cases} \dfrac{1}{2\sqrt{P_{\mathrm{S}} - P_{\mathrm{L0}} - \mu P_{\mathrm{T}}}} & \text{for } x_{\mathrm{v}} > 0 \\ \dfrac{-1}{2\sqrt{\mu P_{\mathrm{S}} + P_{\mathrm{L0}} - P_{\mathrm{T}}}} & \text{for } x_{\mathrm{v}} < 0 \end{cases} \tag{2.88}$$

In regard to the linearization, the operating point is established for a certain piston velocity, hence Stribeck effects (dependent on the piston velocity at the operating point) and Coulomb friction are not included. Furthermore, if the change in piston position is small in a vicinity of the operating point, the gravitational forces can also be left out of the linear model. Bearing in mind (2.65), (2.66), and considering external forces F_{ext} as disturbances, the motion equation of the linear model is given by (2.89).

$$\ddot{x}_{\text{P}} = M_{\text{eq}}^{-1}(p_{\text{L}}A_{\text{A}} - B_{\text{v}}(x_{\text{P0}},\dot{x}_{\text{P0}})\dot{x}_{\text{P}}) \tag{2.89}$$

Assuming P_{S} constant, then in a small vicinity of the operating point, the cross-port leakage flow can be described as $q_{\text{L}} = C_{\text{Ll}}p_{\text{L}}$ with $C_{\text{Ll}} = C_{\text{L}}(\mu^2+\sigma^2)/(\mu^3+\sigma^2)$. Hence, the load pressure dynamics at the linearization point is described by (2.91), with V_{A0}, V_{B0} being linearized volumes.

$$\dot{p}_{\text{L}} = \Lambda(q_{\text{A}} - C_{\text{Ll}}p_{\text{L}} - A_{\text{A}}\dot{x}_{\text{P}}) \tag{2.90}$$

$$= \Lambda(K_{\text{q}}x_{\text{v}} - K_{\text{qp}}p_{\text{L}} - C_{\text{Ll}}p_{\text{L}} - A_{\text{A}}\dot{x}_{\text{P}}),\ \ \Lambda = \frac{\beta_{\text{e}}}{V_{\text{A0}}}\frac{\rho+\mu^2}{\rho} \tag{2.91}$$

The model (2.86), (2.89), (2.91) may be expressed in state space form as (2.92), defining the system state vector as $\mathbf{x} = (x_{\text{P}}, \dot{x}_{\text{P}}, p_{\text{L}})$ and assuming the valve dynamics negligible.

$$\dot{\mathbf{x}} = \mathbf{A}\mathbf{x} + \mathbf{B}x_{\text{v}}\ \ ,\ \ \mathbf{A} = \begin{bmatrix} 0 & 1 & 0 \\ 0 & -M_{\text{eq}}^{-1}B_{\text{v}} & M_{\text{eq}}^{-1}A_{\text{A}} \\ 0 & -\Lambda A_{\text{A}} & -\Lambda(K_{\text{qp}}+C_{\text{Ll}}) \end{bmatrix}\ \ ,\ \ \mathbf{B} = \begin{bmatrix} 0 \\ 0 \\ \Lambda K_{\text{q}} \end{bmatrix} \tag{2.92}$$

From (2.92), transfer functions for all states are readily obtained as (2.93), with $\mathbf{C}$ being the identity matrix, $\mathbf{D} = \mathbf{0}$ and s the Laplace operator.

$$\mathbf{H}(s) = \frac{\mathbf{X}(s)}{X_{\text{v}}(s)} = \begin{bmatrix} H_1(s) \\ H_2(s) \\ H_3(s) \end{bmatrix} = \mathbf{C}(s\mathbf{I}-\mathbf{A})^{-1}\mathbf{B} + \mathbf{D} \tag{2.93}$$

$$= \begin{bmatrix} \frac{1}{s}\frac{\Lambda A_{\text{A}}K_{\text{q}}}{M_{\text{eq}}s^2 + (\Lambda M_{\text{eq}}(K_{\text{qp}}+C_{\text{Ll}}) + B_{\text{v}})s + \Lambda(A_{\text{A}}^2 + B_{\text{v}}(K_{\text{qp}}+C_{\text{Ll}}))} \\ \frac{\Lambda A_{\text{A}}K_{\text{q}}}{M_{\text{eq}}s^2 + (\Lambda M_{\text{eq}}(K_{\text{qp}}+C_{\text{Ll}}) + B_{\text{v}})s + \Lambda(A_{\text{A}}^2 + B_{\text{v}}(K_{\text{qp}}+C_{\text{Ll}}))} \\ \frac{\Lambda K_{\text{q}}(M_{\text{eq}}s + B_{\text{v}})}{M_{\text{eq}}s^2 + (\Lambda M_{\text{eq}}(K_{\text{qp}}+C_{\text{Ll}}) + B_{\text{v}})s + \Lambda(A_{\text{A}}^2 + B_{\text{v}}(K_{\text{qp}}+C_{\text{Ll}}))} \end{bmatrix}$$

As the project is concerned with position control systems, $H_1(s)$ is the transfer function of interest. Considering a *standard* transfer function form, $H_1(s)$ may be written as (2.94).

$$\frac{X_{\text{P}}(s)}{X_{\text{v}}(s)} = \frac{K_{\text{s}}}{\tau_{\text{n}}^2 s^2 + 2\zeta_s\tau_{\text{n}}s + 1}\frac{1}{s}\ \ ,\ \ \tau_{\text{n}} = \frac{1}{\omega_{\text{n}}} \tag{2.94}$$

In (2.94), the system natural frequency ω_{n}, damping ratio ζ_{s} and system gain K_{s} may be found as (2.95), (2.96).

$$\omega_{\text{n}} = \sqrt{\frac{\Lambda(A_{\text{A}}^2 + B_{\text{v}}(K_{\text{qp}}+C_{\text{Ll}}))}{M_{\text{eq}}}}\ \ ,\ \ \zeta_{\text{s}} = \frac{1}{2}\frac{\Lambda M_{\text{eq}}(K_{\text{qp}}+C_{\text{Ll}}) + B_{\text{v}}}{\sqrt{\Lambda M_{\text{eq}}(A_{\text{A}}^2 + B_{\text{v}}(K_{\text{qp}}+C_{\text{Ll}}))}}, \tag{2.95}$$

$$K_{\text{s}} = \frac{A_{\text{A}}K_{\text{q}}}{A_{\text{A}}^2 + B_{\text{v}}(K_{\text{qp}}+C_{\text{Ll}})} \tag{2.96}$$

Characteristics of Linearized Models

As will be discussed in the following section, only Axis 1 and 2 will be used in the following chapters, hence these are considered here. Utilizing ω_n of (2.95), $V_A = V_{0A} + A_A x_P$, $V_B = V_{0B} - A_B x_P$ and relevant diagonal terms of the mass matrix $\mathbf{M}_x$ in (2.49), critical operating points at the lowest possible natural frequencies for Axis 2 and 3, are found as $x_{P2,0} \approx 500$ [mm], $x_{P3,0} \approx 565$ [mm], respectively. The least possible damping occur at small spool openings, hence operating points are chosen according to this. Furthermore, due to the asymmetric piston areas, the dynamic characteristics and especially the system gain change with the direction of motion. The resulting linear models are verified by comparison to their nonlinear counter parts, and results are shown in figure (2.17) (in all cases (and especially for axis 2), slight adjustments of gains (± 5 %) have been necessary to obtain the most adequate response, indicating relatively large gain changes in the vicinity of the operating point).

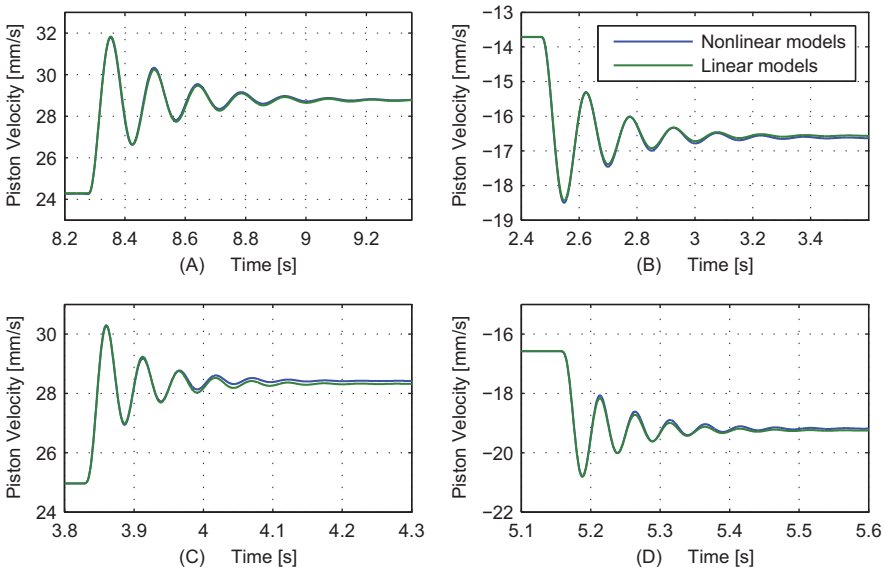

Figure 2.17: *Step responses (± 1 % of nominal input range) from nonlinear- and linear models. (A) Cylinder Axis 2 - positive step. (B) Cylinder Axis 2 - negative step. (C) Cylinder Axis 3 - positive step. (D) Cylinder Axis 3 - negative step.*

The dynamic characteristics at the operating points of Axis 2 and Axis 3, dependent on the direction of motion, are depicted in the frequency responses of figure 2.18. Furthermore, the specific dynamic properties in terms of natural frequency ω_n, damping ratio ζ_s and system gain K_s at the operating points are outlined in table 2.2.

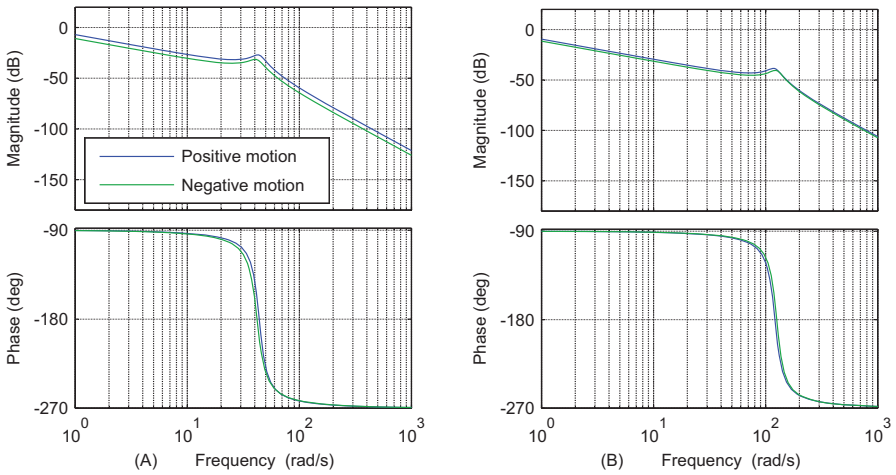

Figure 2.18: *Frequency response for linear models for positive and negative direction of motion. (A) Cylinder axis 2. (B) Cylinder axis 3.*

Dynamic Characteristics at Operating Points	Axis 2	Axis 3
Natural frequency ω_n - positive motion	43.86 [rad/s]	121.01 [rad/s]
Natural frequency ω_n - negative motion	41.91 [rad/s]	125.60 [rad/s]
Damping ratio ζ_s - positive motion	0.12 [-]	0.12 [-]
Damping ratio ζ_s - negative motion	0.13 [-]	0.11 [-]
System gain K_s - positive motion	0.45 [m/%]	0.34 [m/%]
System gain K_s - negative motion	0.29 [m/%]	0.27 [m/%]

Table 2.2: *Dynamic characteristics at operating points for Axis 2 and Axis 3, dependent on the direction of motion.*

2.7.1 Reduced Order Model Considerations

Due to the restrictions in terms of limited sensors and system knowledge (in general), for control design purposes, at may be desirable to reduce the model (2.85) even further. Considering the linear model representation (2.94), then assuming leakage flow is minimal and that the stiffness of the system is sufficiently large, i.e. the stiffness of the load structure and the oil are sufficiently large, then (2.97) hold true.

$$\frac{X_P(s)}{X_v(s)} = \frac{K_s}{\tau_n^2 s^2 + 2\zeta_s \tau_n s + 1} \frac{1}{s} \approx \frac{K_s}{s} \tag{2.97}$$

The nonlinear representation of (2.97), is given by (2.98).

$$\dot{x}_P \approx x_v \frac{\sigma K_{vA}}{A_A \sqrt{\sigma^2 + \mu^3}} \begin{cases} \sqrt{P_S - \text{sgn}(x_v) P_L - \mu P_T} & \text{for} \quad x_v > 0 \\ \sqrt{\mu P_S - \text{sgn}(x_v) P_L - P_T} & \text{for} \quad x_v < 0 \end{cases} \tag{2.98}$$

Hence, under assumptions on stiffness and leakage, it is found reasonable to consider the system as an integrator with a state dependent gain. This reasoning is used to define two levels of reduced order models for a hydraulic valve-cylinder drive.

First Order Model Representation

Covering the entire frequency range, a first order scalar model representation may be established as (2.99).

$$\dot{x}_{\mathrm{P}} \approx F(\mathbf{x}) + G(\mathbf{x})x_{\mathrm{v}} \tag{2.99}$$

In (2.99), $G(\mathbf{x})$ is given by $\dot{x}_{\mathrm{P}}/x_{\mathrm{v}}$ of (2.98) and is essentially the velocity component resulting from the valve flow. The component $F(\mathbf{x})$ is the velocity component resulting from fluid compression and leakage flow, and generally this term may be considered small compared to the valve flow, and it is found reasonable to assume that $|F(\mathbf{x})|_{\max} << |G(\mathbf{x})x_{\mathrm{v}}|_{\max}$. Furthermore, generally for a proper design of the drive then $G(\mathbf{x}) > 0$.

Limited Frequency Range Model Representation

From the above considerations, it is found that for the system being stable, and if leakage flow can be considered negligible, then $F(\mathbf{x}) \to 0$ for $t \to \infty$. Hence, within some frequency range below the system natural frequency, the model representation (2.98) is a reasonable model approximation, and this model is referred as a *limited frequency range* model.

2.8 Experimental Setup & Evaluation Conditions

In order to evaluate the developed controllers, some evaluation criteria are set up. From an *industry* point of view, desirable features of a given control structure are general applicability, few tuning parameters, simple tuning process, robustness toward disturbances and varying operating conditions and ability to track a given reference trajectory as closely- and consistently as possible. Hence the proposed controls should have the following main properties:

Controller Versatility & Tuning The control structure should contain few tuning parameters, and should be easily tuned. Furthermore, it is desirable that the control structure is versatile in the sense, that it should be applicable to a broad range of systems with very different load structures.

Tracking Robustness The controller should provide robustness toward disturbances and uncertainties, meaning the maximum error of the control should be minimized to the extend it is possible. Hence, the reference trajectories as well as the hydraulic axes used for evaluation should provide for significant parametric variations.

Overall Tracking Performance The controller should be able to track a given reference trajectory as closely and consistently as possible throughout the operating range, hence the average error should be as small as possible.

From these desirable properties, Axis 2 and 3 of the test bench are chosen as evaluation targets, with Axis 3 placed in a horizontal position. This produces very different dynamical properties of the load structures. The load of Axis 2 is dominated by inertia- and gravity forces with strong variations, and the load of Axis 3 is dominated by friction, and only exhibits small inertia forces in comparison to Axis 2, and ideally no gravity force impact.

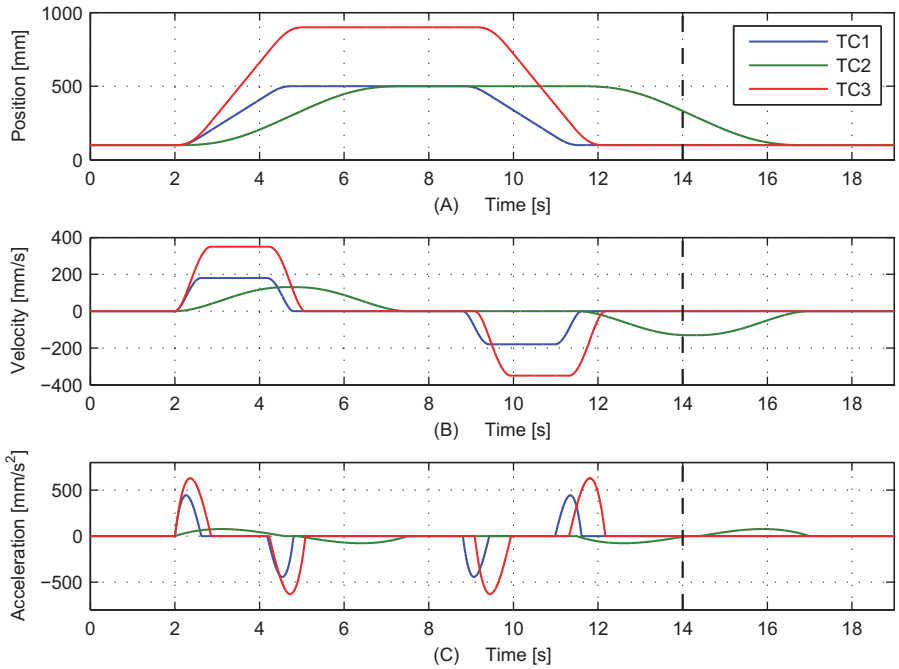

Figure 2.19: *Reference trajectories for test cases TC1, TC2, TC3. The dotted lines indicate the ranges of TC1, TC3, whereas the range of TC2 matches the plot range. (A) Reference position trajectories. (B) Reference velocity trajectories. (C) Reference acceleration trajectories.*

Furthermore, two different reference trajectories are chosen for Axis 2; one reference trajectory requiring large velocities and accelerations, that calls for utilization of nearly the entire input range (henceforward denoted *Test Case 1 (TC1)*), and another trajectory with smaller velocities but nearly always accelerating when in motion (denoted *Test Case 2 (TC2)*). The reference trajectory for Axis 3 is chosen such that large velocities, accelerations and utilization of (nearly) the entire input range is required (denoted *Test Case 3 (TC3)*). These reference trajectories allow to evaluate the high velocity properties of controls together with progressive- or asymmetric valve flow characteristics, and the ability to handle strong friction impact. Furthermore, reference trajectories are in all cases chosen to be *symmetrical*, meaning that the desired velocity and acceleration over positive- and negative stroke equal each other. This provides an idea of how the proposed control structure handle the system asymmetries, present in both axes.

The reference trajectories are in all cases designed as quintic polynomials similar to the approach presented in e.g. [Craig, 2005]. This guarantees that the desired jerk is finite, hence the desired pressure gradients are finite. The reference position-, velocity- and acceleration trajectories are depicted in figure 2.19.

2.9 Benchmark Controllers - *Best Industrial Practice*

In order to evaluate the developed controllers proposed in later chapters, a comparison is drawn to controllers commonly applied in industry, here abbreviated *best industrial practice* controllers. Such controllers are defined as conventional PI controllers with velocity feed forward, taking into account the direction dependent system gain. Furthermore, such a controller is commonly configured with a so-called *switching* integrator with restricted activity, i.e with integral action confined within some boundary δ_{isw} of the control target. The benchmark control structure is given by (2.100).

$$u_{\text{v}} = \frac{1}{K_{\text{f}}}(\dot{x}_{\text{R}} - K_{\text{p}}e - K_{\text{i}}K_{\text{isw}}\int_t e\text{d}e) \ , \tag{2.100}$$

$$K_{\text{f}} = \begin{cases} K_{\text{f+}} & \text{for } x_v > 0 \\ K_{\text{f-}} & \text{for } x_v < 0 \end{cases} \ , \ K_{\text{isw}} = \begin{cases} 1 & \text{for } |e| \leq \delta_{\text{isw}} \\ 0 & \text{for } |e| > \delta_{\text{isw}} \end{cases} \tag{2.101}$$

The benchmark controllers are applied to the three Test Cases discussed in the previous section, and the controllers are designed based on the linear models to have gain margins $GM = 8-9$ $[dB]$ and phase margins $PM = 75-85$ $[degrees]$, in order to limit overshoot. Note that for Test Case 3, the valve gain is progressive, hence $K_{\text{f+}}$, $K_{\text{f-}}$ are designed according to highest flow gain of the valve.

The results are depicted in figure 2.20, and it is found that especially for Test Case 3, the tracking ability is somewhat limited compared to the remaining two test cases. This is due to the conservative choice of $K_{\text{f+}}$, $K_{\text{f-}}$, and might be compensated by just increasing the proportional gain. However, in such a case stability cannot be guaranteed, and local instability modes may occur during operation.

2.10 Summary

A classification of hydraulic (control) applications was carried out in order to outline critical properties commonly seen in industry. Based on this classification, a test bench load system was chosen, and a hydraulic HPU and control valves were applied in order to simulate such applications. A nonlinear model was established, with the load model based on the Iterative Newton-Euler formulation, and the complete model was formulated in actuator space, linked to the hydraulic system model, and verified against experimental measurements from the test bench. Also, reference trajectories to be used for controller evaluation was established.

Hereafter, a generalized model framework was established that may describe any valve-cylinder configuration, regardless of matched / unmatched asymmetries of valve flow gains and piston areas. Linear models, system transfer functions as well as reduced order models were established. Finally, benchmark controllers were designed based on best industrial practice, i.e. PI controllers with switching integral terms combined with velocity feed forward controls with static gains. These controllers were furthermore evaluated experimentally, and serve as references for performance evaluation of the controllers developed in the following chapters.

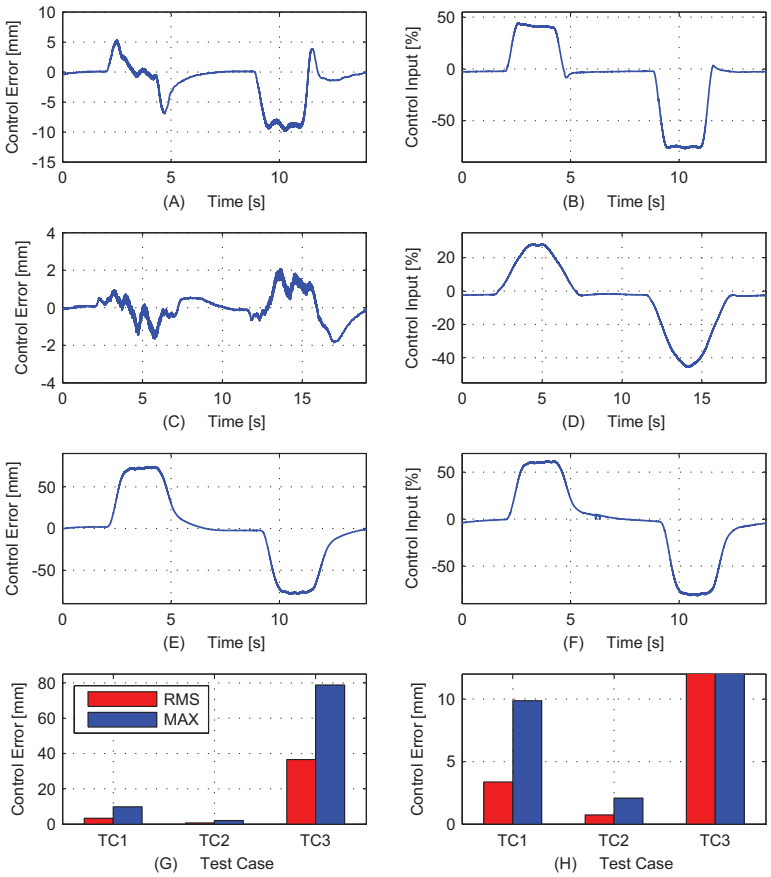

Figure 2.20: *Results with the benchmark control structure 2.100 applied. (A) Error response for Test Case 1. (B) Control input for Test Case 1. (C) Error response for Test Case 2. (D) Control input for Test Case 2. (E) Error response for Test Case 3. (F) Control input for Test Case 3. (G) RMS- and maximum error values for sub figure (A), (C) and (E). (H) Zoom of figure (G).*

3 Preliminary Studies

In order to achieve the best possible control performance in the presence of the intrinsic nonlinearities and varying parameters of hydraulic drives, the possibility for online estimation / tracking of system parameters is considered. If the system parameters can be estimated fully- or partially, in a reliable way, these may be applied for possible controller tuning and / or compensation of nonlinearities / variations. Focus is placed on an adaptive method in terms of the recursive least squares method, and a model based approach. Based on the findings, *compensated* drive models for use in further control designs are established, and finally control strategies to be investigated, are outlined.

3.1 Parameter Adaption Based On Recursive Least Squares Approach

The possibility for online tracking of parameters using the Recursive Least Squares (RLS) approach is investigated, due to its proven mathematical properties and generally few tuning parameters. The RLS algorithm is a recursive version of the least squares (LS) estimation method, and its derivation is briefly summarized below. Consider in the general case a linear system expressed in regression form as (3.1), with y_k being the system output at the k^{th} sample instant, and $\boldsymbol{\theta}_k$, $\boldsymbol{\varphi}_k$ the parameter vector (the vector of system parameters) and the regression vector (the vector of states), respectively.

$$y_k = \boldsymbol{\theta}_k^{\mathsf{T}} \boldsymbol{\varphi}_k \tag{3.1}$$

The elements of the parameter vector may be estimated off-line using the Least Squares (LS) method [Ljung, 1987], [Ljung and Söderström, 1983], [Astrom and Wittenmark, 1989] which may be represented by (3.2) with $\hat{\boldsymbol{\theta}}_k$ being the estimate of $\boldsymbol{\theta}_k$.

$$\hat{\boldsymbol{\theta}}_k = \mathbf{R}_k^{-1}\mathbf{f}_k \;\;,\;\; \mathbf{R}_k = \left[\frac{1}{N}\sum_{k=1}^{N} \boldsymbol{\varphi}_k \boldsymbol{\varphi}_k^{\mathsf{T}}\right] \;\;,\;\; \mathbf{f}_k = \left[\frac{1}{N}\sum_{k=1}^{N} \boldsymbol{\varphi}_k y_k\right] \tag{3.2}$$

In recursive form the terms $\mathbf{R}_k$ and $\mathbf{f}_k$ are given by (3.3), with $\mathbf{R}_k$ being the information matrix.

$$\mathbf{R}_k = \mathbf{R}_{k-1} + \boldsymbol{\varphi}_k \boldsymbol{\varphi}_k^{\mathsf{T}} \;\;,\;\; \mathbf{f}_k = \mathbf{f}_{k-1} + \boldsymbol{\varphi}_k y_k \tag{3.3}$$

Inserting $\mathbf{f}_k$ into (3.2), yield (3.4).

$$\hat{\boldsymbol{\theta}}_k = \mathbf{R}_k^{-1}(\mathbf{f}_{k-1} + \boldsymbol{\varphi}_k y_k) \tag{3.4}$$

Using that $\hat{\boldsymbol{\theta}}_{k-1} = \mathbf{R}_{k-1}^{-1}\mathbf{f}_{k-1}$, i.e. $\mathbf{f}_{k-1} = \mathbf{R}_{k-1}\hat{\boldsymbol{\theta}}_{k-1}$, and substituting into (3.4), leads to (3.5).

$$\hat{\boldsymbol{\theta}}_k = \mathbf{R}_k^{-1}(\mathbf{R}_{k-1}\hat{\boldsymbol{\theta}}_{k-1} + \boldsymbol{\varphi}_k y_k) \tag{3.5}$$

Noting that $\mathbf{R}_k = \mathbf{R}_{k-1} + \boldsymbol{\varphi}_k\boldsymbol{\varphi}_k^\mathsf{T} \;\Rightarrow\; \mathbf{R}_{k-1} = \mathbf{R}_k - \boldsymbol{\varphi}_k\boldsymbol{\varphi}_k^\mathsf{T}$, obtain (3.9).

$$\hat{\boldsymbol{\theta}}_k = \mathbf{R}_k^{-1}((\mathbf{R}_k - \boldsymbol{\varphi}_k\boldsymbol{\varphi}_k^\mathsf{T})\hat{\boldsymbol{\theta}}_{k-1} + \boldsymbol{\varphi}_k y_k) \tag{3.6}$$

$$= \mathbf{R}_k^{-1}(\mathbf{R}_k\hat{\boldsymbol{\theta}}_{k-1} - \boldsymbol{\varphi}_k\boldsymbol{\varphi}_k^\mathsf{T}\hat{\boldsymbol{\theta}}_{k-1} + \boldsymbol{\varphi}_k y_k) \tag{3.7}$$

$$= \hat{\boldsymbol{\theta}}_{k-1} + \mathbf{R}_k^{-1}(\boldsymbol{\varphi}_k y_k - \boldsymbol{\varphi}_k\boldsymbol{\varphi}_k^\mathsf{T}\hat{\boldsymbol{\theta}}_{k-1}) \tag{3.8}$$

$$= \hat{\boldsymbol{\theta}}_{k-1} + \mathbf{R}_k^{-1}\boldsymbol{\varphi}_k(y_k - \boldsymbol{\varphi}_k^\mathsf{T}\hat{\boldsymbol{\theta}}_{k-1}) \tag{3.9}$$

In order to obtain $\mathbf{R}_k$, the matrix inversion Lemma (3.10) is utilized.

$$[\mathbf{A} - \mathbf{BCD}]^{-1} = \mathbf{A}^{-1} - \mathbf{A}^{-1}\mathbf{B}[\mathbf{DA}^{-1}\mathbf{B} + \mathbf{C}^{-1}]^{-1}\mathbf{DA}^{-1} \tag{3.10}$$

It is found that the l.h.s of (3.10) equals $\mathbf{R}_k$ of (3.3) with $\mathbf{A} = \mathbf{R}_{k-1}$, $\mathbf{B} = \boldsymbol{\varphi}_k$, $\mathbf{C} = \mathbf{I}$ and $\mathbf{D} = \boldsymbol{\varphi}_k^\mathsf{T}$, leading to (3.11).

$$\mathbf{R}_k^{-1} = \mathbf{R}_{k-1}^{-1} - \mathbf{R}_{k-1}^{-1}\boldsymbol{\varphi}_k[\boldsymbol{\varphi}_k^\mathsf{T}\mathbf{R}_{k-1}^{-1}\boldsymbol{\varphi}_k + 1]^{-1}\boldsymbol{\varphi}_k^\mathsf{T}\mathbf{R}_{k-1}^{-1} = \mathbf{R}_{k-1}^{-1} - \frac{\mathbf{R}_{k-1}^{-1}\boldsymbol{\varphi}_k\boldsymbol{\varphi}_k^\mathsf{T}\mathbf{R}_{k-1}^{-1}}{1 + \boldsymbol{\varphi}_k^\mathsf{T}\mathbf{R}_{k-1}^{-1}\boldsymbol{\varphi}_k} \tag{3.11}$$

Defining $\mathbf{P}_k = \mathbf{R}_k^{-1}$ the RLS algorithm can be summarized as (3.12), with $y_k - \boldsymbol{\varphi}_k^\mathsf{T}\hat{\boldsymbol{\theta}}_{k-1}$ denoted the *residual* (model estimation error) and $\mathbf{P}_k\boldsymbol{\varphi}_k$ constituting the adaption gain.

$$\hat{\boldsymbol{\theta}}_k = \hat{\boldsymbol{\theta}}_{k-1} + \mathbf{P}_k\boldsymbol{\varphi}_k(y_k - \boldsymbol{\varphi}_k^\mathsf{T}\hat{\boldsymbol{\theta}}_{k-1}) \quad , \quad \mathbf{P}_k = \mathbf{P}_{k-1} - \frac{\mathbf{P}_{k-1}\boldsymbol{\varphi}_k\boldsymbol{\varphi}_k^\mathsf{T}\mathbf{P}_{k-1}}{1 + \boldsymbol{\varphi}_k^\mathsf{T}\mathbf{P}_{k-1}\boldsymbol{\varphi}_k} \tag{3.12}$$

The diagonal elements of $\mathbf{P}_k$ express the variance of the regressor elements (or the covariance with the regressor elements themselves), and the off-diagonal elements express the covariance of the regressor elements. The sum of the diagonal elements of $\mathbf{P}_k$ (or trace$(\mathbf{P}_k)$) equals the total variance of the data set contained in the regression vector.

3.1.1 Stability of the RLS Algorithm

Indeed, the parameter estimate $\hat{\boldsymbol{\theta}}_k$ should tend to the true parameter vector $\boldsymbol{\theta}_k$, i.e $\tilde{\boldsymbol{\theta}}_k = \boldsymbol{\theta}_k - \hat{\boldsymbol{\theta}}_k$ should tend to zero. This property may be evaluated by the Lyapunov candidate function (3.13) [Goodwin and Sin, 2009].

$$V_k(\tilde{\boldsymbol{\theta}}_k, \mathbf{P}_{k-1}) = \tilde{\boldsymbol{\theta}}_k^\mathsf{T}\mathbf{P}_{k-1}\tilde{\boldsymbol{\theta}}_k \tag{3.13}$$

3.1.2 Properties of the RLS Algorithm

In the following some important properties of the RLS algorithm are considered in the context of online parameter tracking. A discrete time version of e.g. the transfer function H_1 of (2.93) may be applied as the regression model used in the identification process. This is given by (3.14) using the Forward Euler transformation.

$$\dot{x}_{\mathrm{P},k} = \boldsymbol{\theta}_k^\mathsf{T}\boldsymbol{\varphi}_k \tag{3.14}$$

$$\boldsymbol{\varphi}_k = \begin{bmatrix} x_{\mathrm{v},k-2} & x_{\mathrm{P},k-1} & x_{\mathrm{P},k-2} \end{bmatrix}^\mathsf{T} \tag{3.15}$$

$$\boldsymbol{\theta}_k = \begin{bmatrix} \dfrac{K_s {T_{rls}}^2}{{\tau_n}^2} & 2\dfrac{T_{rls}\zeta_s - \tau_n}{\tau_n} & \dfrac{-2T_{rls}\zeta_s\tau_n + {T_{rls}}^2 + {\tau_n}^2}{{\tau_n}^2} \end{bmatrix}^\mathsf{T} \tag{3.16}$$

However, parameters contained in the parameter vector are varying due to the nonlinearities of the system. Hence, some considerations on the ability of the algorithm to track parameter variations over time are relevant. Consider again the information matrix (3.17).

$$\mathbf{R}_k = \mathbf{R}_{k-1} + \boldsymbol{\varphi}_k \boldsymbol{\varphi}_k^\mathsf{T} \tag{3.17}$$

The diagonal elements will contain the squared elements of the regression vector and their *history*. Hence, as the number of samples evolves, and the elements of $\boldsymbol{\varphi}_k$ being different from zero, $\text{trace}(\mathbf{R}_k)$ will increase, meaning that $\text{trace}(\mathbf{R}_k^{-1}) = \text{trace}(\mathbf{P}_k)$ will decrease. Hence, $\mathbf{R}_k^{-1}\boldsymbol{\varphi}_k$ (gain of the residual) will tend to zero, causing the parameter update to eventually stop. This suggests a contradiction in regard to online parameter tracking; The repression vector $\boldsymbol{\varphi}_k$ must be *persistently excited* in order for parameter tracking to take place. On the other hand, the same condition causes the adaption gain to tend to zero as the number of samples evolves.

Persistence of Excitation & Parameter Tracking Ability

In order to estimate system parameters online in a reliable way, the mathematical solution of the model must be unique. Otherwise parameters may diverge from their true values, as parameter sets may provide for an output identical to the measured output. Hence, signals must be *persistently exciting*, i.e. must be rich enough, such that the output of the regression model only matches the measured output for a unique set of parameters. A condition for persistence of excitation of signals in the regression vector is stated multiple places in literature (see e.g. [Ljung and Söderström, 1983], [Landau, 1980], [Slotine and Li, 1991], among others). According to the latter, a signal vector $\boldsymbol{\varphi}_k$ is said to be persistently exciting, if (3.18) is satisfied, with λ_{min} denoting the minimum eigenvalue.

$$\lambda_{\min}\left\{\sum_{k=1}^{\infty} \boldsymbol{\varphi}_k \boldsymbol{\varphi}_k^\mathsf{T}\right\} \to \infty \tag{3.18}$$

This merely states that the gradient of the lowest eigenvalue of the information matrix should be positive, in order for the signals to be persistently excited. In its recursive form, this is equivalent to (3.19) (noting that $\mathbf{R}_k = \mathbf{R}_{k-1} + \boldsymbol{\varphi}_k \boldsymbol{\varphi}_k^\mathsf{T}$).

$$\lambda_{\min}\{\mathbf{R}_k\} \to \infty \text{ for } k \to \infty \tag{3.19}$$

A different, and probably more appropriate definition is given in [Astrom and Wittenmark, 1989], from which it follow that signals are persistently exciting leading to a unique estimate, if the information update term $\boldsymbol{\varphi}(k)\boldsymbol{\varphi}^\mathsf{T}(k)$ has full rank. These considerations also lead to the fact that, increasing the order of the regression model, also provides increasing requirements to the richness of signals in order to be persistently exciting. Hence, the repression model should be designed with the least possible number of parameters.

Introduction of Forgetting Factor

A widely known approach to prevent the adaption gain from tending to zero, is the implementation of a so-called exponential forgetting factor (see e.g. [Ljung, 1987], [Ljung and Söderström, 1983], [Astrom and Wittenmark, 1989]). The basic RLS algorithm provides equal weight to all measurements from the initial sample instant. Employing exponential forgetting alters the algorithm to give *old* measurements less weight.

Implementing the forgetting factor proposed in e.g. [Krus and Gunnarsson, 1993], [Ljung, 1987], [Parkum, 1992], the RLS algorithm (3.12) is modified to (3.20).

$$\hat{\boldsymbol{\theta}}_k = \hat{\boldsymbol{\theta}}_{k-1} + \mathbf{P}_k \boldsymbol{\varphi}_k (y_k - \hat{\boldsymbol{\theta}}_{k-1}^T \boldsymbol{\varphi}_k) \quad \text{with} \quad \mathbf{P}_k = \frac{1}{\lambda_k} \left[\mathbf{P}_{k-1} - \frac{\mathbf{P}_{k-1} \boldsymbol{\varphi}_k \boldsymbol{\varphi}_k^T \mathbf{P}_{k-1}}{\lambda_k + \boldsymbol{\varphi}_k^T \mathbf{P}_{k-1} \boldsymbol{\varphi}_k} \right] \tag{3.20}$$

Here λ_k is the forgetting factor at the k^{th} sample instant. It is clear that the forgetting factor imposes a gain on $\mathbf{P}_k$. If $\lambda_k < 1$, the adaption gain is increased, increasing the ability to track parameter variations, but makes the update highly sensitive to noise, which may result in inaccurate parameter estimates. Hence, for $\lambda_k = 1$ the algorithm is equal to the basic RLS algorithm, and for $\lambda_k < 1$ then $\mathbf{P}_k$ will not tend to zero. However, consider the situation where $\boldsymbol{\varphi}_k$ attains zero value, i.e. when the system is non-persistently excited, given by (3.21).

$$\mathbf{P}_k|_{\boldsymbol{\varphi}_k=0} = \frac{1}{\lambda_k} \mathbf{P}_{k-1} \tag{3.21}$$

Here it is found that $\mathbf{P}_k$ will increase exponentially with the number of samples. This phenomenon is known as covariance wind-up (or covariance blow-up), which corresponds to the information matrix becoming singular. This phenomenon is further discussed in e.g. [Parkum, 1992] and [Astrom and Wittenmark, 1989].

In general, the presence of limited noise and sufficient excitation in all of the parameter space, the forgetting factor approach appears to be an appropriate solution to positively influence the tracking properties of the RLS algorithm. The main drawback however, is that the covariance matrix may become unbounded if signals are not persistently excited. In regard to hydraulic drives, situations with persistent excitation of states are undesirable. However, during transients, excitation of signals may be sufficient for online tracking of parameter variations. Hence, a cardinal point in the applicability of the RLS algorithm for the purpose of this project, is the possibility to control the forgetting factor in an appropriate way.

3.1.3 State-of-the-Art for Application to Hydraulic Drives

A state of the art analysis in regard to application of RLS algorithms applied in relation to identification and control of hydraulic systems, has been conducted. Here, special focus has been on methods for control of the update gain, the ability for parameter tracking and the boundedness of the complete algorithm. The complete analysis is found in a *working* paper, which can be found in the Appendix. The main results are outlined in the following. The results of the analysis reveal that approaches reported in literature appear rather fragmented, and it is found that two approaches may be applied in regard to online parameter tracking. These approaches are discussed in the following.

Variable Forgetting Factor

The variable forgetting factor approach (VFF) proposed in [Krus and Gunnarsson, 1993] provides the possibility to avoid the update gain from tending to zero, and at the same time maintain this bounded. Furthermore, the algorithm is robust toward periods when signals are non-persistently exciting. The proposed algorithm is given by (3.22), (3.23).

$$\hat{\boldsymbol{\theta}}_k = \hat{\boldsymbol{\theta}}_{k-1} + \alpha_{\text{vff}} \mathbf{P}_k \boldsymbol{\varphi}_k (y_k - \boldsymbol{\varphi}_k^T \hat{\boldsymbol{\theta}}_{k-1}) \tag{3.22}$$

$$\mathbf{P}_k = \frac{1}{\lambda_{\text{vff}}} \left[\mathbf{P}_{k-1} - \alpha_{\text{vff}} \frac{\mathbf{P}_{k-1} \boldsymbol{\varphi}_k \boldsymbol{\varphi}_k^T \mathbf{P}_{k-1}}{\lambda_{\text{vff}} + \boldsymbol{\varphi}_k^T \mathbf{P}_{k-1} \boldsymbol{\varphi}_k} \right] \tag{3.23}$$

Here $\lambda_{\text{vff}}, \alpha_{\text{vff}}$ are given by (3.24), where $\delta = |\text{trace}(\mathbf{P})|_{\max}$.

$$\lambda_{\text{vff}} = 1 - (1 - \lambda_{\text{vff0}}) \left[1 - \frac{\text{trace}(\mathbf{P}_{k-1})}{\delta} \right] \quad , \quad \alpha_{vff} = 1 - \frac{\text{trace}(\mathbf{P}_{k-1})}{\delta} \lambda_{\text{vff0}} \tag{3.24}$$

Here, it should be noted that λ_{vff} somewhat resembles the *bounded gain forgetting factor* approach in [Slotine and Li, 1991] (here in the discrete time case). From (3.24), it is found that for $\text{trace}(\mathbf{P}_{k-1}) \to \delta$, $\lambda_{\text{vff}} \to 1$, hence tending towards the *basic* RLS algorithm given by (3.12), having the property of $\text{trace}(\mathbf{P}_{k-1})$ tending to zero. Hence the algorithm will stay bounded as the trace of the covariance matrix is not allowed to exceed the predefined maximum level δ.

The variable α_{vff} controls the covariance- and parameter updates. It is found that a large $\text{trace}(\mathbf{P}_{k-1})$ will cause a small α_{vff}, and these are in that sense (linearly) inversely proportional to each other. It is furthermore emphasized in [Krus and Gunnarsson, 1993] that δ should be chosen sufficiently small in order to be able to suppress signals of low amplitude, such that λ_{vff} is increased as soon as the signals tend to diminish.

To improve the identification procedure, it is proposed that in- and output signals are filtered with identical filters [Krus and Gunnarsson, 1993]. When considering the system parameters, these will remain unchanged as the filters cancel each other out (when being identical). Furthermore, dependent of the order of the filter, the input / output derivatives may be obtained, and hence choosing a filter, one order higher than the system order, these can be calculated without numerical problems.

Covariance Trace Control

A different suitable method is based on so-called controlled trace modification (denoted CCT). The algorithm for this purpose proposed in [Plummer and Vaughan, 1996] is given by (3.25).

$$\hat{\theta}_k = \hat{\theta}_{k-1} + \alpha_{\text{cct}} \mathbf{P}_k \varphi_k (y_k - \varphi_k^T \hat{\theta}_{k-1}) \tag{3.25}$$

$$\mathbf{P}_k = \frac{1}{\lambda_{\text{cct}}} \left[\mathbf{P}_{k-1} - \alpha_{\text{cct}} \frac{\mathbf{P}_{k-1} \varphi_k \varphi_k^T \mathbf{P}_{k-1}}{\lambda_{\text{cct}} + \varphi_k^T \mathbf{P}_{k-1} \varphi_k} \right] \tag{3.26}$$

With the CCT modification given by (3.27).

$$\mathbf{P}_k = \frac{\delta}{\text{trace}(\mathbf{P}_{k-1})} \mathbf{P}_{k-1}, \quad \alpha_{\text{cct}} = \begin{cases} 1 & \text{for} \quad \text{trace}(\mathbf{P}_k) \geq \delta \\ 0 & \text{for} \quad \text{trace}(\mathbf{P}_k) < \delta \end{cases} \tag{3.27}$$

It is found that for $\text{trace}(\mathbf{P}_{k-1}) > \delta$, $\mathbf{P}_k$ is reduced, rendering the parameter update gain upper bounded. Furthermore, as $\text{trace}(\mathbf{P}_{k-1}) \geq \delta$ the parameter- and covariance updates are turned of, making the parameter estimates fixed in periods of non-persistently excited signals. Also as $\lambda_{\text{cct}} < 1$ (fixed valued), the ability of increasing parameter tracking is present. Hence, the CCT approach provides an upper bound on the covariance trace, and the ability to turn off the parameter adaption if the upper covariance trace bound is reached.

Results for Online Tracking of Multiple Parameters

The RLS with the VFF- and CCT update gain control approaches have been applied in Test Case 1, with Axis 2 in closed loop control with 2.100. The model applied for parameter estimation is the discrete time transfer function given by (3.14), with filtered signals. All applied signals are filtered with identical fourth order low pass filters, with a filter frequency of 40 $[Hz]$. Furthermore, the

(filtered) velocity is used as model output, reducing the model parameters to three. The velocity is calculated from the filtered position signal. Also, due the identical filters, the results are not distorted by phase shift, but slightly delayed in time.

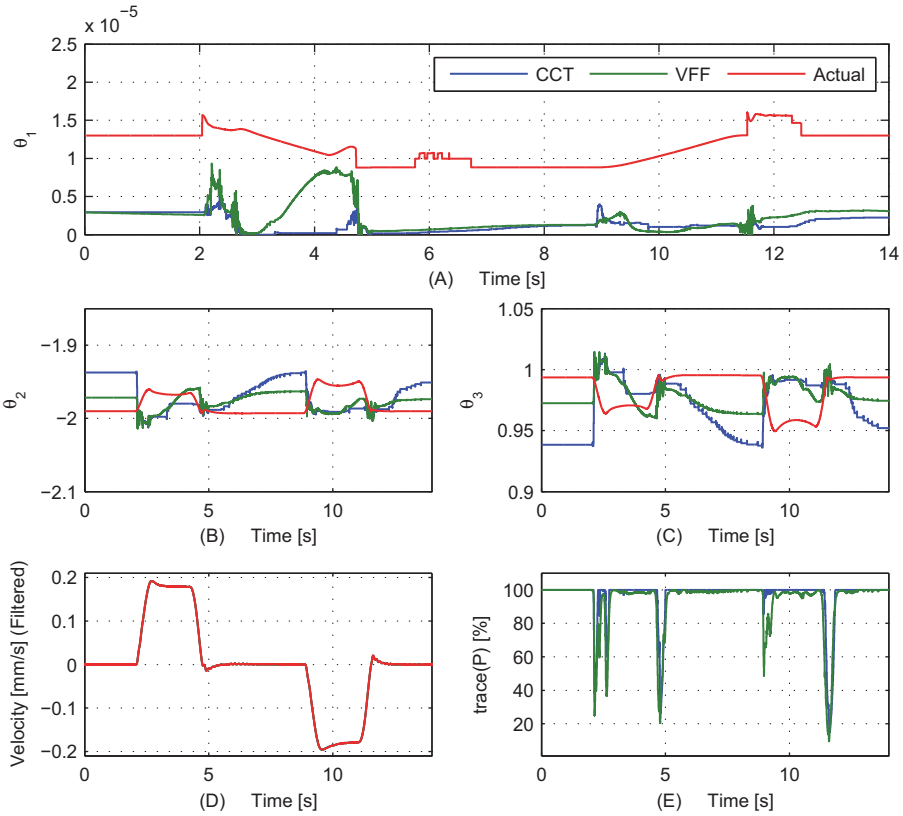

Figure 3.1: *Performance of the RLS algorithm with the VFF- and CCT modifications. (A) Parameter θ_1. (B) Parameter θ_2. (C) Parameter θ_3. (D) Estimated- and actual model outputs. (E) Trace of covariance matrices (in % for comparison).*

The resulting performance for the two methods are depicted in figure 3.1. It is found that the update gains (expressed in the covariance traces) are bounded functions as expected. Furthermore, parameters θ_2, θ_3 are found to be fairly good matches in both cases, whereas both algorithms have difficulties in tracking θ_1 - however, the output of the estimated models depicted in figure (3.1) (D) appears to be accurately estimating the model output. From this it is found that signals are not persistently exciting, meaning that the parametric solution is not unique and causes inaccurate estimates of θ_1. It should be noted that the parameter tracking performance has been sought improved by different scaling of the states, however this did not provide satisfactory results.

Evidently, the estimation results are unreliable, and are found to be too inaccurate for the objective

of this project. Furthermore, issues such as different rates of change in parameters also causes the results to be erroneous, and this issue might be addressed via the so-called *matrix forgetting factor* approach [Parkum, 1992], where a forgetting factor is assigned to the individual parameters. This enables to tune the ability to track parameters taking into account different rates of change in parameters. This approach does however, introduce additional tuning parameters, and as the tuning of the VFF- and CCT gain control methods were found to be somewhat cumbersome, such an approach is found to be unfeasible.

In general, the *smooth* operation of the system, causes signals to be non-persistently exciting, which in turn causes a loss of ability to track parameters accurately online. However, in the event that model parameters can be reduced, this might be a possibility for reasonable parameter tracking.

3.1.4 Online Tracking of System Gain

Based on the results and considerations in the previous section, it is intriguing to consider the possibility of tracking the system gain which strongly influences the performance of a controlled system. Consider the reduced order model representation of Section 2.7.1, given by (3.28).

$$\dot{x}_{\mathrm{P}} = F(\mathbf{x}) + G(\mathbf{x})x_{\mathrm{v}} \tag{3.28}$$

Here the input gain $G(\mathbf{x})$ may be described by (3.29).

$$G(\mathbf{x}) = \frac{\sigma K_{\mathrm{vA}}}{A_{\mathrm{A}}\sqrt{\sigma^2+\mu^3}} \begin{cases} \sqrt{P_{\mathrm{S}} - \mathrm{sgn}(x_{\mathrm{v}})P_{\mathrm{L}} - \mu P_{\mathrm{T}}} & \text{for} \quad x_{\mathrm{v}} > 0 \\ \sqrt{\mu P_{\mathrm{S}} - \mathrm{sgn}(x_{\mathrm{v}})P_{\mathrm{L}} - P_{\mathrm{T}}} & \text{for} \quad x_{\mathrm{v}} < 0 \end{cases} \tag{3.29}$$

It is evident from (3.29), that if the load pressure P_{L} varies due to varying loads, the supply pressure P_{S} varies due to e.g. multiple flow consumers attached to the pump, or the valve flow gain K_{vA} is nonlinear, then the system gain varies. However, for a proper system design, $G(\mathbf{x}) > 0$ can be assumed. Clearly system gain variations give rise to inconsistent control performance, and compensation of this would expectedly enhance consistency of the control performance. Opposite to the above, in the following, a continuous version of the RLS algorithm is considered for analysis purposes. Consider now an algorithm that compensates the system gain, given by (3.30).

$$u_{\mathrm{v}} = \frac{1}{\hat{G}(\mathbf{x})}\bar{u}_{\mathrm{v}} \tag{3.30}$$

When applied to the reduced order model (3.28), the compensated system is obtained as (3.31).

$$\dot{x}_{\mathrm{P}} = F(\mathbf{x}) + \frac{G(\mathbf{x})}{\hat{G}(\mathbf{x})}\bar{u}_{\mathrm{v}} \tag{3.31}$$

From (3.31) it is found that maintaining $G(\mathbf{x})\hat{G}(\mathbf{x})^{-1}$ at some stationary value, or even better, equal to one, would greatly facilitate both control design procedures, but also consistency of control performance. Recalling from Section 2.7.1, that if leakage flow may be considered negligible, then $F(\mathbf{x})$ is a function of the fluid compression i.e. a function of the load dynamics. Furthermore, in general, the flow due to fluid compression may be considered small compared to the valve flow. Hence, by introducing low pass filters of sufficiently high orders to the piston- and spool position signals, then $F(\mathbf{x})$ may be attenuated sufficiently such that (3.32) is a reasonable assumption (here the subscript $_{\mathrm{f}}$ denotes a filtered signal). Here $\dot{x}_{\mathrm{Pf}}$ may be calculated from the filtered position signal, for a filter order above one.

$$\dot{x}_{\mathrm{Pf}} \approx G(\mathbf{x})u_{\mathrm{vf}} \tag{3.32}$$

If the low pass filters are chosen to be identical, then $G(\mathbf{x})$ is not affected, as the filters cancels each other out. In order to estimate $G(\mathbf{x})$, a single parameter version of the RLS algorithm may be applied. An obvious advantage of estimating $G(\mathbf{x})$ based on (3.32) is, that persistent excitation of signals is not a concern, as $G(\mathbf{x})$ is uniquely determined for all $\dot{x}_{\mathrm{Pf}}, x_{\mathrm{vf}} \neq 0$. Consider now the continuous RLS algorithm with forgetting factor given by (3.33) [Slotine and Li, 1991], using $G(\mathbf{x}) = G$.

$$\dot{\hat{G}} = P x_{\mathrm{vf}}^2 (\dot{x}_{\mathrm{Pf}} - \hat{G} x_{\mathrm{vf}}) \;\; , \;\; \frac{\mathrm{d}}{\mathrm{d}t}\left[P^{-1}\right] = -\gamma P^{-1} + x_{\mathrm{vf}}^2 \tag{3.33}$$

In (3.33), $P > 0$ and expresses the variance of x_{vf}, and γ is the forgetting factor. In the case $\gamma = 0$, $x_{\mathrm{vf}} \neq 0$, then $P^{-1} \to \infty$, hence $P \to 0$, meaning that parameter adaption is lost and $\hat{G}$ is stationary. Also, for $\gamma > 0$, $x_{\mathrm{vf}} = 0$, then $P^{-1} \to 0$, i.e. $P \to \infty$, meaning that the adaption gain is unbounded. Using the bounded gain forgetting factor [Slotine and Li, 1991] (3.34), the algorithm is bounded.

$$\gamma = \gamma_0 \left(1 - \frac{|P|}{\delta}\right) \tag{3.34}$$

Consider the Laplace transform of (3.33), given by (3.35), (3.36).

$$s\hat{G} = P x_{\mathrm{vf}}^2 (\dot{x}_{\mathrm{Pf}} - \hat{G} x_{\mathrm{vf}}) \tag{3.35}$$

$$sP^{-1} = -\gamma P^{-1} + x_{\mathrm{vf}}^2 \quad \Rightarrow \quad P x_{\mathrm{vf}}^2 = s + \gamma \tag{3.36}$$

Combining (3.35), (3.36) and using (3.32), obtain (3.37).

$$s\hat{G} = (s+\gamma)(\dot{x}_{\mathrm{Pf}} - \hat{G} x_{\mathrm{vf}}) = (s+\gamma)(G x_{\mathrm{vf}} - \hat{G} x_{\mathrm{vf}}) \quad \Rightarrow \quad \frac{G}{\hat{G}} = \frac{2s+\gamma}{s+\gamma} \tag{3.37}$$

Choosing $\delta > P_{\max}$, then $\gamma > 0$ from (3.34). Hence, the gain $G(\mathbf{x})\hat{G}(\mathbf{x})^{-1}$ of the compensated system (3.31) is bounded as (3.38), in the ideal case.

$$1 \leq \frac{2s+\gamma}{s+\gamma} \leq 2 \tag{3.38}$$

Results for Online Tracking of System Gain

For evaluation, the algorithm is applied to Test Case 1, with control (2.100), similar to the previous section (the estimate is not applied in the control loop). The input-, and output filters are also here fourth order filters, but with a filter frequency of 1 $[Hz]$ in order to sufficiently attenuate the term $F(\mathbf{x})$. Results are depicted in figure 3.2, denoting the proposed single gain RLS algorithm, SG-RLS.

It is found that the proposed algorithm tracks the system gain G fairly good, but with some delay as signal information is delayed due to heavy filtering. Also the estimated model output resembles the filtered piston velocity (calculated), and the covariance term P is maintained bounded and positive. Hence, using this approach provides a simple method for tracking of the system gain. However, even though easily tuned, the algorithm is found to be somewhat sensitive to even small changes in δ, γ_0 (from the tuning process).

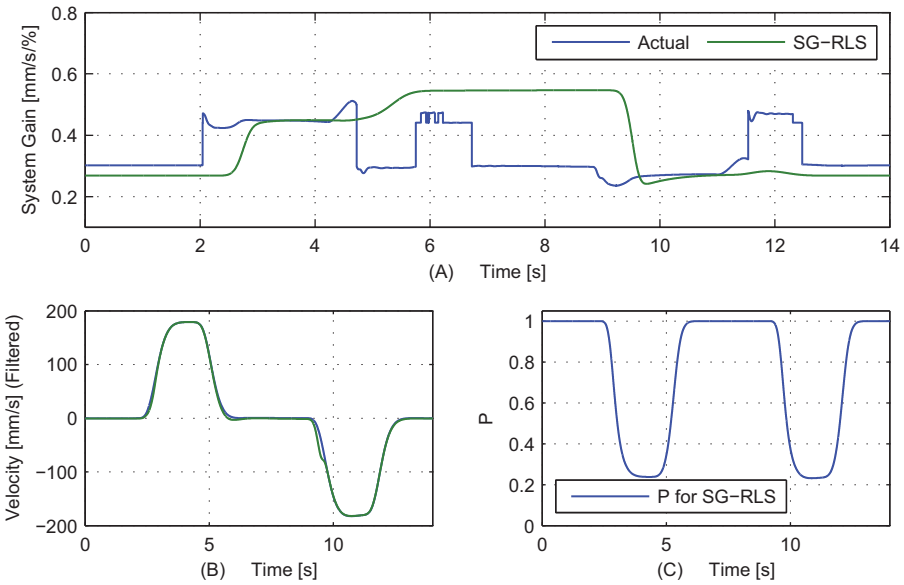

Figure 3.2: *Performance of the single parameter RLS estimation algorithm with bounded gain forgetting factor. (A) System gain G. (B) Estimated- and actual model outputs. (C) Covariance term related to the update gain.*

3.2 Model Based Approach For Online Tracking of System Gain

Having studied the possibilities for online tracking of multiple model parameters, and especially tracking of the system gain via RLS approaches, a completely different approach is considered in this section. Consider again the system gain (3.29) of the reduced order model (3.28), noting that this may be considered a general description of the system gain for arbitrary valve driven cylinder drives, in regard to a first order model representation. In general, the piston areas may be calculated from standard data sheet information. Then in the event that K_{vA} can be estimated fairly accurately, then (3.29) may be estimated by (3.39) using pressure- and spool position sensors, assuming that $P_{\mathrm{T}} << |P_{\mathrm{L}}| + \mu P_{\mathrm{S}}$.

$$\hat{G}(\mathbf{x}) = \frac{\sigma \hat{K}_{\mathrm{vA}}}{A_{\mathrm{A}}\sqrt{\sigma^2+\mu^3}} \begin{cases} \sqrt{P_{\mathrm{S}} - \mathrm{sgn}(x_{\mathrm{v}})P_{\mathrm{L}}} & \text{for} \quad x_{\mathrm{v}} > 0 \\ \sqrt{\mu P_{\mathrm{S}} - \mathrm{sgn}(x_{\mathrm{v}})P_{\mathrm{L}}} & \text{for} \quad x_{\mathrm{v}} < 0 \end{cases} \tag{3.39}$$

Note that the approach of using (3.39) in the compensator (3.30) is particular intriguing, as this *ideally* causes the input gain of the compensated system to be completely stationary and close to one. Furthermore, a valve manufacturer is able to implement accurate estimates $\hat{K}_{\mathrm{vA}}$ in standard controller boards as simple look-up tables.

This ideal compensation however, also introduces a problem which may be deduced from the linear transfer functions of the previous chapter. Note that in the ideal case, i.e. $G(\mathbf{x})\hat{G}(\mathbf{x})^{-1} \equiv 1$, then $K_{\mathrm{q}} = 1$, $K_{\mathrm{qp}} = 0$. In this case the compensated system is characterized by the natural frequency,

damping ratio and system gain given by (3.40).

$$\omega_{\mathrm{n}} = \sqrt{\frac{\Lambda(A_{\mathrm{A}}^2 + B_{\mathrm{v}}C_{\mathrm{Ll}})}{M_{\mathrm{eq}}}} \quad , \quad \zeta_{\mathrm{s}} = \frac{1}{2}\frac{\Lambda M_{\mathrm{eq}}C_{\mathrm{Ll}} + B_{\mathrm{v}}}{\sqrt{\Lambda M_{\mathrm{eq}}(A_{\mathrm{A}}^2 + B_{\mathrm{v}}C_{\mathrm{Ll}})}} \quad , \quad K_{\mathrm{s}} = \frac{A_{\mathrm{A}}^2}{A_{\mathrm{A}}^2 + B_{\mathrm{v}}C_{\mathrm{Ll}}} \tag{3.40}$$

In the event that $K_{\mathrm{qp}} \sim C_{\mathrm{Ll}}$ in the uncompensate system, the compensator (3.40) causes a serious reduction in, most critically, the damping ratio of the system where poor damping already is inherent. However, in case of a certain level of leakage flow, only minor influence can be expected. As an example, this is also found from the frequency response for Axis 2 depicted in figure 3.3.

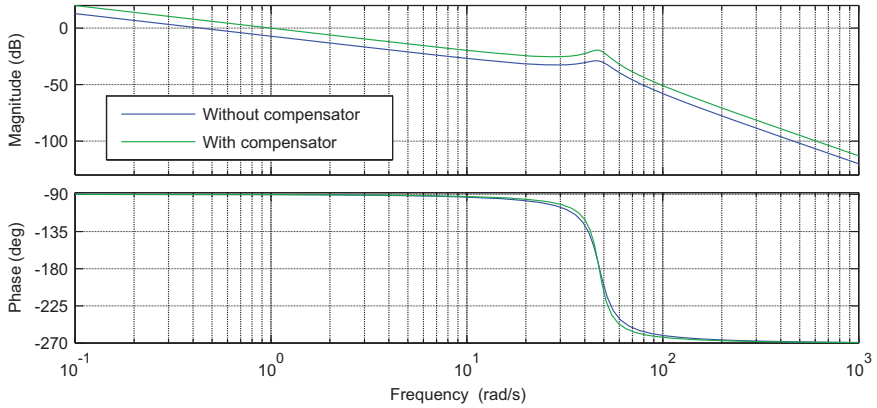

Figure 3.3: *Frequency response for Axis 2, with and without the compensator* (3.30)*,* (3.39)*.*

In figure 3.3, it is worth noting that the system gain for the compensated system is $K_{\mathrm{s}} = 0.997$ [m/%], $\omega_{\mathrm{n}} = 43.67$ [rad/s], $\zeta_{\mathrm{s}} = 0.087$ [-] as opposed to $K_{\mathrm{s}} = 0.446$ [m/%], $\omega_{\mathrm{n}} = 43.79$ [rad/s], $\zeta_{\mathrm{s}} = 0.116$ [-] for the uncompensated system. A compensated reduced order drive model can then be established as (3.41), for a proper estimate $\hat{K}_{\mathrm{vA}}$ and pressure- and spool position sensors available.

$$\dot{x}_{\mathrm{P}} = F(\mathbf{x}) + \rho(\mathbf{x})\bar{x}_{\mathrm{v}} \quad , \quad \rho(\mathbf{x}) = G(\mathbf{x})\hat{G}(\mathbf{x})^{-1} \approx 1 \tag{3.41}$$

The model based approach considered in this section is found to be superior over the RLS based approaches in regard to reliability, ease-of-implementation and tuning parameters.

Results for Online Estimation of System Gain

The proposed compensator is based on the model equations, and may as such best be evaluated when implemented with the compensator (3.30) and applied in the test bench. The compensator is implemented with the controller (3.42), with parameters $K_{\mathrm{p}}, K_{\mathrm{i}}, \delta_{\mathrm{isw}}$ identical to those of (2.100). This will ideally provide the same stability margins at the operating point. However, the compensator will cause the gain to be nearly constant throughout the entire operating range.

$$\bar{u}_{\mathrm{v}} = \dot{x}_{\mathrm{R}} - K_{\mathrm{p}}e - K_{\mathrm{i}}K_{\mathrm{isw}}\int_t e\mathrm{d}e \quad , \quad K_{\mathrm{isw}} = \begin{cases} 1 & \text{for } |e| \leq \delta_{\mathrm{isw}} \\ 0 & \text{for } |e| > \delta_{\mathrm{isw}} \end{cases} \tag{3.42}$$

The resulting performance is depicted in figure 3.4. It is found that performance for the proposed controller is maintained for TC2 when compared to the benchmark controller, which is due to the relative small accelerations and velocities. Hence the load (and thereby the load pressure) does not change with a large rate.

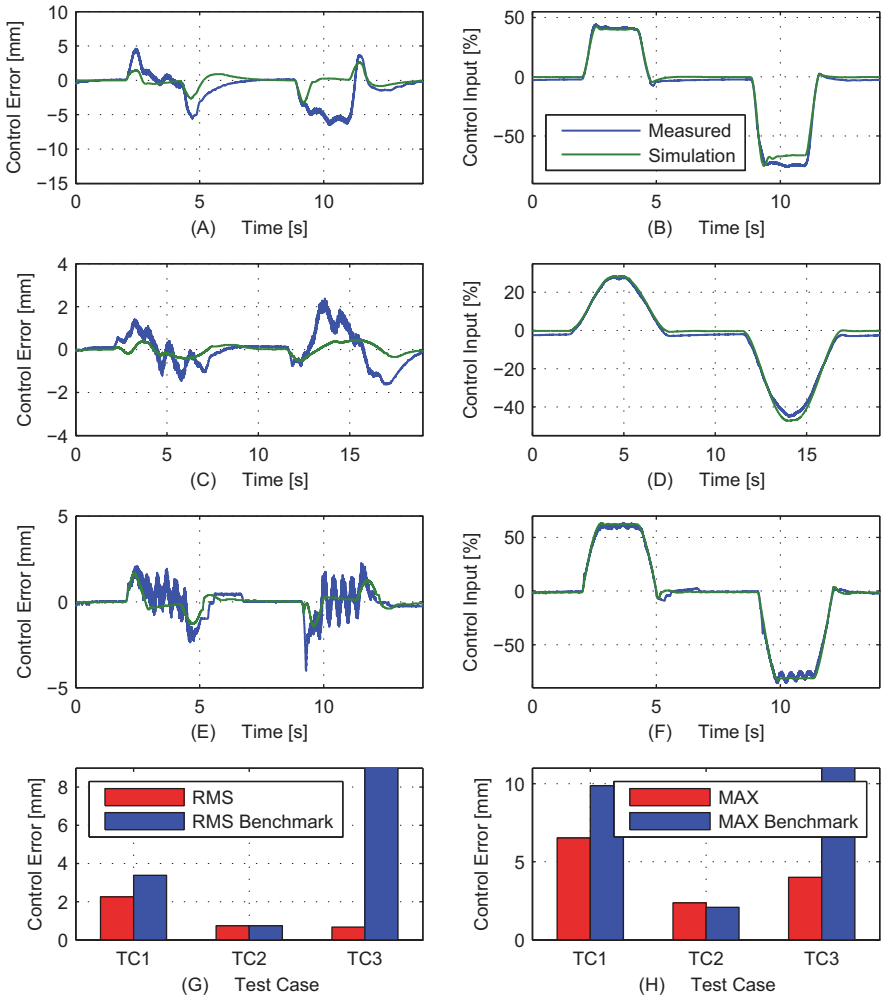

Figure 3.4: *Results with the benchmark control structure* (3.42) *applied. (A) Error response for Test Case 1. (B) Control input for Test Case 1. (C) Error response for Test Case 2. (D) Control input for Test Case 2. (E) Error response for Test Case 3. (F) Control input for Test Case 3. (G) RMS error values for sub figure (A), (C) and (E) compared with the benchmark controller* (2.100)*. (H) Maximum error values for sub figure (A), (C) and (E) compared with the benchmark controller* (2.100)*.*

For TC1 the system gain exhibits larger rates of change, and the proposed compensator effectively compensates these changes, resulting in a more robust performance. In regard to TC3, the compensator eliminates the problem with *static* valve gain variations, and the tracking performance is significantly improved compared to the corresponding benchmark controller. Furthermore, the errors appear somewhat symmetric around the ideal state $e = 0$, meaning that the compensator effectively compensates system asymmetries.

From these results it is found that the proposed gain estimator improves the performance in a satisfactory way when applied for gain compensation. Furthermore, this is achieved with little implementation effort, and in that sense the compensator is highly applicable for the purpose of this project. Hence this is applied throughout the remaining work presented in this dissertation.

3.3 Outline of Control Strategy for Compensated System

Having completed the studies on parameter estimations, and to what extend such methods can be reliably applied for control- and / or compensator structures for hydraulic valve-cylinder drives, a strategy for closed loop control methods to be studied, can be outlined. From the results of the previous sections it is found that the model based gain estimator (3.39) combined with the compensator (3.30) provides for efficient and reliable *active gain compensation* (AGC) of such a system, and closed loop control should then be applied in combination with this compensator.
By application of the AGC, then a velocity feed forward signal directly applied to the compensated system would provide for a nearly ideal steady state flow reference. Hence, the closed loop controller applied should compensate *only* for dynamic effects, i.e. primarily the flow due to fluid compression and leakage. Knowing that the dynamics are nonlinear, it is natural to consider nonlinear control structures able to compensate this. In general, such a control structure should either be able to adapt to- or be robust toward the nonlinear dynamics, and the method should target the following properties:

- Provide for excellent tracking performance
- Contain a minimum of tuning parameters
- Require only position measurements
- Require limited and simple tuning efforts

In regard to the sensor limitation, various types of promising state observers has been considered in literature. This introduces additional algorithms, and thereby additional parameters, and is as such not considered a feasible approach bearing in mind the properties listed above and the general objective of the project. However, in systems implemented with *high end* position sensors, the piston velocity can in some cases be calculated reliably online.

Adaptive control methods for hydraulic control systems have been studied extensively in literature, often with a significant number of parameters in resulting control structures (see [Liu and Yao, 2003], [Bu and Yao, 1999], among others). Some promising methods for adaptive control were proposed in [Hansen, 1997], [Andersen, 1996] and evaluated in [Schmidt and Nielsen, 2008], where several adaptive control algorithms were proposed for hydraulic cylinder drives, using only position feedback and few parameters. Even though promising, the most accurate methods proposed rely on five tuning parameters, and when the AGC discussed above is applied, these methods are considered

infeasible for the problem at hand. Furthermore, as for the RLS algorithms, there is always a risk for the parameter adaption to be inaccurate, possibly resulting in erroneous performance or even instability.

Turning attention to robust controls, methods such as backstepping fail to meet the requirements listed above, especially in regard to tuning parameters, and a method such as H_∞ control is found to be too inadequate in regard to tracking performance. A different approach for robust control is sliding mode control. Sliding mode control algorithms generally have few tuning parameters, are easily tuned, have simple structures and provide for excellent tracking of a desired output. The main drawback of such approaches arises with the possible requirement for full state feedback, and the possible discontinuous control input. However, the general properties of sliding mode control appear intriguing for the objective of this project, provided that focus is placed on output feedback control approaches, in order to maintain the number of tuning parameters at a minimum.

Based on these considerations, the control designs in the following chapters take their offset in sliding mode control methods. Furthermore, the work presented in the following chapters primarily aims at controllers using only position feedback, however due to the possibility for extracting the velocity in some cases, some of the work considered also takes into account velocity feedback.

3.4 Summary

Different approaches to online parameter estimation / tracking were considered. For adaptive parameter tracking the recursive least squares method was considered due to its potential simple parameter design and its proven mathematical features. Based on a study of the algorithm, and state-of-the-art for application in hydraulic systems, the main problem of controlling the algorithm update gain was considered. From simulations, the algorithm was not found to be applicable for online tracking of multiple parameters, primarily due to the lack of excitation of signals in the desired operation of hydraulic drives.

The system gain may be considered the main nonlinearity of the system, and may exhibit strong variations due to e.g. varying loads, hence leading to inconsistent control performance. Motivated by these facts and the possibility for compensation of this, an approach for tracking of the system gain was proposed, using the recursive least squares method and a certain filter technique. The proposed method avoids the strong requirements on signal excitation due to the single parameter estimation algorithm, but the tuning process reveals that the parameter tracking is somewhat sensitive toward even small variations in parameters. Based on this, the algorithm is not found to be feasible for the purpose of this project.

Also a model based parameter tracking approach was proposed, taking its offset in the generalized model developed in the previous chapter. Based on basic data sheet information, pressure- and valve spool position measurements, the system gain may be tracked in a reliable way, without any additional parameters. When implemented for gain compensation, together with benchmark controllers of the previous chapter, the compensator was found to improve closed loop performance significantly compared to the benchmark controllers, which is due to the *nearly* stationary gain of the compensated system. Based on these results, the compensator was found to be applicable for the purpose of this project.

Based on these results and considerations on different control strategies, sliding mode control methodology was found to be the more appealing approach for closed loop (position) control design with focus on output feedback control, taking into account the objective of the project.

In the following chapters, the model based gain compensator combined with the PI controller that was considered in Section 3.2 is denoted **PI-AGC**.

4 Fundamentals of Sliding Mode Control & The Context of Hydraulic Drives

In this chapter the fundamentals and most important features of sliding mode control are discussed. Both conventional so-called first order sliding mode controls (1SMC) and sliding mode controls of higher orders (HOSMC) are discussed in their ideal cases, and chattering issues are addressed in regard to their application in physical applications, with a special attention to hydraulic systems. Here the dynamic properties of valves, and specially the nonlinear dynamics, are considered in relation to the switching terms of sliding controls. Finally, state-of-the-art for application of sliding controls to hydraulic systems is outlined.

4.1 Theoretical Background

Sliding mode control is essentially discontinuous, and causes any closed loop system utilizing such a control approach, to be a discontinuous system, with some dependence on the closed loop system states, and continuous elsewhere, and are as such piece-wise continuous systems. Fundamental mathematical tools for the analysis of discontinuous systems have been presented in literature, however the most frequently applied in regard to sliding mode controlled systems may be considered that of A.F. Filippov, which is considered in the sequel. Furthermore, hydraulic drives are considered autonomous, hence the sequel is restricted to such systems.

4.1.1 Filippov Solution

Consider the ordinary autonomous differential equation (4.1), where $x \in \mathbb{R}^n$ and $f(x(t))$ is piece-wise continuous in some domain D and N is a set of zero measure consisting of points of discontinuity of the function $f(x(t))$.

$$\dot{x} = f(x(t)) \tag{4.1}$$

In systems where the solution approaches a surface of discontinuity S from one side, and travels away on the other side, satisfy the differential equation (4.1) in the usual sense except for the intersection $S = 0$. Here, the change in the state trajectory is abrupt, and the solution does not have a derivative [Filippov, 1988].

However, if the solution approaches the surface S from both sides, it is necessary to define how the trajectory will continue when $S = 0$ is reached. One way to handle this situation is by considering the solution as set-valued, leading to the introduction of a differential *inclusion* (the definition

by A.F. Filippov [Filippov, 1988]). Consider the differential inclusion for an autonomous system (4.2), where $F(x(t))$ is defined as (4.3).

$$\dot{x} \in F(x(t)) \tag{4.2}$$

$$F(x(t)) = \bigcap_{\delta>0} \bigcap_{\mu(N)=0} \overline{\text{conv}} f(B(x(t),\delta) - N) \tag{4.3}$$

In (4.3), $\overline{\text{conv}}$ denotes the closed convex hull, $B(x(t),\delta)$ a ball of radius δ centered at $x(t)$ and μ the Lebesgue measure, which is not given further attention, due to the context of a physical control system. The solution of $F(x(t))$ is an absolutely continuous function satisfying (4.1) almost everywhere. Such a solution is characterized by being differentiable everywhere, except on $x(t) = 0$, being of bounded variation and recoverable from integration of its derivative [al Shammari, 2006]. Note furthermore, that at continuity points $F(x(t)) = f(x(t))$.

4.1.2 Geometric Interpretation

Geometrically the Filippov solution may be interpreted in the following way [Filippov, 1988]. Consider the function (4.1) with $f = f(x(t))$ being discontinuous on a smooth surface $S = S(x)$, that divides its neighborhood in the x-space into domains D_- and D_+ as depicted in figure 4.1.

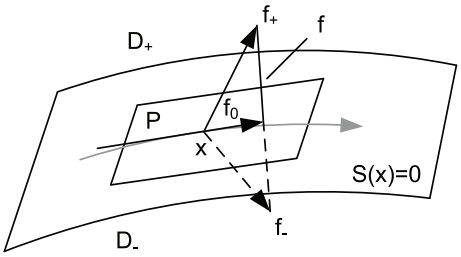

Figure 4.1: *Sketch representing the geometric interpretation of the Filippov solution (inspired by [Filippov, 1988]).*

On the surface S the function f is extended to the set F that is such that the limit points of the domains defined by (4.4), satisfies $f_- \in f$, $f_+ \in f$, where x^* is a continuity point contained in either D_- or D_+.

$$\lim_{x^* \in D_+, x^* \to x} f(x^*(t)) = f_+(x(t)) \;\; , \;\; \lim_{x^* \in D_-, x^* \to x} f(x^*(t)) = f_-(x(t)) \tag{4.4}$$

The smallest set satisfying these properties is the segment joining the endpoints f_- and f_+ given by the inclusion (4.5).

$$\dot{x} \in F = \bar{\lambda} f_+ + (1-\bar{\lambda}) f_-, \;\; \bar{\lambda} \in [0,1] \tag{4.5}$$

If the segment F intersects the tangent plane P, the intersection point is the endpoint of the vector $f_0 \in P$, that represents the velocity of motion along the surface S. Hence a function $x(t)$ satisfying $\dot{x} = f_0$ is a solution to the differential inclusion (4.2), and is assumed to be a solution to the differential equation (4.1) [Filippov, 1988].

From the above considerations, the differential inclusion (4.3) may be defined in a somewhat more *intuitive* form (4.6) with $\bar{\lambda} \in [0,1]$.

$$\dot{x} \in F(x(t)) = \begin{cases} f(x(t)) & \text{for} \quad x \in D_+ \\ \bar{\lambda} f_+ + (1-\bar{\lambda}) f_- & \text{for} \quad x \in S \\ f(x(t)) & \text{for} \quad x \in D_- \end{cases} \tag{4.6}$$

4.1.3 Existence of Sliding Modes

Having considered the basics of discontinuous differential equations and their solutions, it is appropriate to introduce the sliding mode concept. From the above, if $f_0 \neq f_+$, $f_0 \neq f_-$ and the segment F intersects the tangent plane P, then f_0 determines the motion velocity, i.e. $\dot{x} = f_0$, along the surface S. The solution $x(t)$ satisfying $\dot{x} = f_0$, is assumed to be a solution of $\dot{x} = f(x(t))$. A solution satisfying these conditions is called a sliding motion. The abbreviation *sliding mode* is to be understood as a limit of motions on the sliding constraint (Filippov sense trajectories), when switching imperfections vanish and the switching frequency tends to infinity [Filippov, 1960], [Levant, 1993]. The control of physical applications is the main topic of this project, and ideal and infinite switching frequencies are inherently impossible to realize. Hence, in the sequel, *real* sliding denotes the situation when switching imperfections are present and the switching frequency is finite.

4.2 First Order Sliding Modes

Consider for the general case the scalar system (4.7) with $x(t) = x, u \in \mathbb{R}$ and the output function $e \in \mathbb{R}$.

$$\dot{x} = a(x) + b(x)u, \quad e = e(x) \tag{4.7}$$

In (4.7), $a(x), b(x), e$ are considered smooth unknown functions. The output function e is of order one relative to the system, as stated in (4.8).

$$\dot{e}(x) = \frac{\mathrm{d}e(x)}{\mathrm{d}t} = \frac{\partial e(x)}{\partial x}\frac{\mathrm{d}x}{\mathrm{d}t} = \frac{\partial e(x)}{\partial x}\dot{x} \tag{4.8}$$

Substituting the system (4.7) into (4.8), obtain (4.9).

$$\dot{e}(x) = \frac{\partial e(x)}{\partial x}(a(x) + b(x)u) \tag{4.9}$$

Define functions (4.10).

$$h(x) = \dot{e}(x)|_{u=0} = \frac{\partial e(x)}{\partial x}a(x) \quad , \quad g(x) = \frac{\partial e(x)}{\partial u} = \frac{\partial e(x)}{\partial x}b(x) \tag{4.10}$$

Using (4.10), the output function e satisfies (4.11).

$$\dot{e}(x) = h(x) + g(x)u \tag{4.11}$$

As mentioned above, $a(x), b(x), e$ are smooth functions with $a(x), b(x)$ also considered unknown. From (4.10), then also $h(x), g(x)$ are smooth unknown functions, but assumed bounded as (4.12).

$$0 < K_{\mathrm{m}} < g(x) < K_{\mathrm{M}} \quad , \quad |h(x)| \leq C \tag{4.12}$$

With the bounds (4.12), the system (4.9) satisfies the differential inclusion (4.13).

$$\dot{e}(x) \in [-C, C] + [K_{\mathrm{m}}, K_{\mathrm{M}}]u \tag{4.13}$$

The system representation and restrictions presented above are necessary conditions in the following.

4.2.1 Systems With Relative Degree One

The control objective is to achieve and maintain the constraint $e = 0$. In order for this to take place, then $e = 0$ must be attractive, i.e. (4.14) must be satisfied, corresponding to $e\dot{e} < 0$.

$$\lim_{e\to 0^+} \dot{e} < 0 \quad , \quad \lim_{e\to 0^-} \dot{e} > 0 \tag{4.14}$$

For this, consider the system (4.13) with the simple relay control (4.15).

$$u = -\alpha \operatorname{sgn}(e),\ \alpha > C/K_{\mathrm{m}} \tag{4.15}$$

Noting the condition for e to be attractive, obtain (4.16).

$$e\dot{e} = e(h(x) + g(x)u) = eh(x) - \alpha g(x) S \operatorname{sgn}(e) = eh(x) - \alpha g(x)|e| \tag{4.16}$$

From (4.16), (4.12) it is found that the statement (4.17) hold true.

$$\alpha K_{\mathrm{m}} > C \ \Rightarrow \ e\dot{e} \leq 0 \tag{4.17}$$

Furthermore, $e\dot{e} < 0$ by virtue of infinite switching frequency of (4.15). Hence for $e(0) = 0$ a sliding mode (first order) takes place on $e = 0$ from this initial time instant, and for $e(0) \neq 0$ a sliding mode will take place after some convergence period. Furthermore this convergence period will be finite, which is clear from the following consideration. Consider again the control system (4.11), (4.15) with (4.12), in the conservative situation $h(x) = C,\ g(x) = K_{\mathrm{m}}$, and some initial condition $e(0) = e_0 > 0$. Choose $\alpha = (\delta + C)/K_{\mathrm{m}}$ with $\delta > 0$ which satisfies (4.17), and obtain (4.18).

$$\dot{e}(x) = \frac{\mathrm{d}e}{\mathrm{d}t} = C + K_{\mathrm{m}} u = C - K_{\mathrm{m}}\alpha = -\delta \quad \Rightarrow \quad \mathrm{d}t = -\frac{1}{\delta}\mathrm{d}e \tag{4.18}$$

By integration, obtain (4.19) with t_1 being the time of convergence.

$$\int_{t_0}^{t_1} \mathrm{d}t = -\frac{1}{\delta}\int_{e_0}^{0} \mathrm{d}e \quad \Rightarrow \quad t_1 = t_0 + \frac{e_0}{\delta} < \infty \tag{4.19}$$

From (4.19), the convergence period is a bounded function of the control parameter α and initial condition e_0.

On Invariance Properties of Sliding Modes

One of the most profound features of sliding mode control is the so-called invariance property [Utkin et al., 2009]. In the ideal case, i.e. when switching imperfections vanish and the switching frequency tends to infinity, a sliding mode allow for exactly maintaining e.g. the constraint $e(x) = 0$ (in the above example), despite presence of uncertain parameter variations and bounded disturbances, for the switching gain α large enough. Hence the control system is *invariant* with respect uncertainties and disturbances as the control exhibits (ideally) an infinite gain by virtue of (ideally) infinite control bandwidth.

4.2.2 Systems With Higher Relative Degree

If the system under consideration is not a scalar system, but of higher order, the approach of applying a single sgn-function becomes a bit more elaborate. Consider again the system (4.7) with $u \in \mathbb{R}$ but with $\mathbf{e}(x) = \mathbf{e} = (e_1, e_2) \in \mathbb{R}^2$.
Here it is reasonable to construct a *surface* $S(\mathbf{e})$, as proposed in e.g. [Slotine and Li, 1991], by a linear combination of the states of $\mathbf{e}$. Consider the derivative of $S(\mathbf{e})$, given by (4.20).

$$\dot{S}(\mathbf{e}) = \frac{\mathrm{d}S(\mathbf{e})}{\mathrm{d}t} = \frac{\partial S(\mathbf{e})}{\partial e_1 \partial e_2}\frac{\mathrm{d}e_1}{\mathrm{d}t} + \frac{\partial^2 S(\mathbf{e})}{\partial^2 e_1 \partial^2 e_2}\frac{\mathrm{d}e_2}{\mathrm{d}t} = \frac{\partial S(\mathbf{e})}{\partial e_1 \partial e_2}\dot{e}_1 + \frac{\partial^2 S(\mathbf{e})}{\partial^2 e_1 \partial^2 e_2}\dot{e}_2 \tag{4.20}$$

Substituting the system (4.7) (in this case assuming $\mathbf{x} \in \mathbb{R}^2$), obtain (4.21).

$$\dot{S}(\mathbf{e}) = \frac{\partial S(\mathbf{e})}{\partial e_1 \partial e_2}\dot{e}_1 + \frac{\partial^2 S(\mathbf{e})}{\partial^2 e_1 \partial^2 e_2}(h(x) + g(x)u) \tag{4.21}$$

Similar to the previous section, a first order sliding mode on $S = 0$ is achieved by the relay control (and sliding criterion for the control gain) given by (4.22).

$$u = -\alpha \operatorname{sgn}(S(\mathbf{e})), \quad \alpha > \left| \frac{\frac{\partial S(\mathbf{e})}{\partial e_1 \partial e_2}\dot{e}_1 + \frac{\partial^2 S(\mathbf{e})}{\partial^2 e_1 \partial^2 e_2}h(x)}{\frac{\partial^2 S(\mathbf{e})}{\partial^2 e_1 \partial^2 e_2}g(x)} \right|_{max} \tag{4.22}$$

Following the idea of [Slotine and Li, 1991], construct a surface defined as (4.23), with λ being some positive constant.

$$S = S(\mathbf{e}) = e_2 + \lambda e_1 \tag{4.23}$$

Using the particular surface (4.23), then after some possible convergence period, a sliding mode is enforced on $S(\mathbf{e}) = 0$. Indeed, if $\lambda > 0$, then $S(\mathbf{e}) = 0$ provides for stable linear e-dynamics, where λ essentially expresses the time constant of the desired e-dynamics. Hence, after convergence to a sliding mode on $S(\mathbf{e}) = 0$, the states e_1, e_2 will converge to $(e_1, e_2) = (0,0)$ for $t \to \infty$.

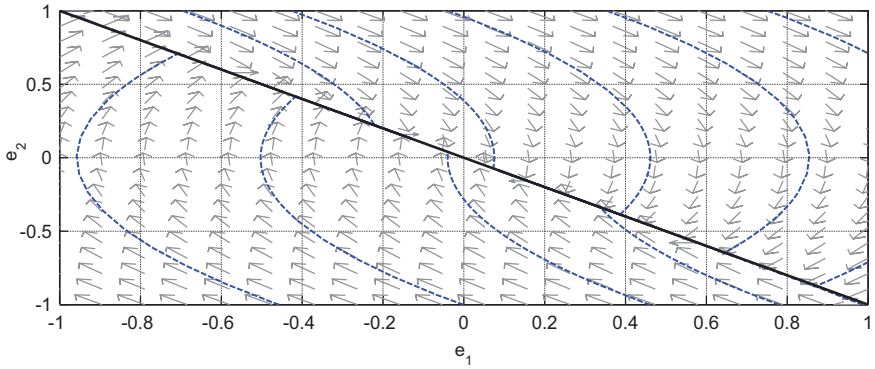

Figure 4.2: *Phase portrait for the states of $S(\mathbf{e})$. The dotted blue graphs depicts state trajectories, and the solid black graph (line) depicts the switching function $e_2 + e_1 = 0$, i.e. for* (4.23) *with $S = 0$ and $\lambda = 1$.*

With $S = 0$, the resulting phase portrait of the trajectory (e_1, e_2) appears as depicted in figure 4.2. From this it is found that the state trajectory is convergent to the switching function $e_2 + \lambda e_1 = 0$, and after intersection with this function, the trajectory *slides* on this function toward the origin. It is furthermore notable, that the time constant λ of the desired *e*-dynamics defines the gradient of the switching line.

4.3 High Order Sliding Modes

With the introduction of the sliding order concept [Levant, 1993], [Levant, 1996], referring to the first total output derivative in which a discontinuity is present, sliding mode control is taken to another level. Based on the sliding order concept, higher order sliding modes have been introduced in order to produce sliding modes on output derivatives in systems with relative degrees above one, or to (possibly) reduce chattering without the introduction of a boundary layer. The first known high order sliding algorithms realizing second order sliding modes were presented in [Levantovsky, 1985], [Emelyanov et al., 1986a, Emelyanov et al., 1986b], [Emelyanov et al., 1990], where the so-called second order sliding algorithm with prescribed convergence as well as the twisting- and super twisting algorithms were presented, with the latter utilizing only the output and not its time derivative, and the first two utilizing the output first derivative, and the sign of the output derivative, respectively. These algorithms were presented for the first time in English in [Levant, 1993]. Arbitrary order sliding controllers with finite time convergence were introduced in [Levant, 1998a], [Levant, 2001a], [Levant, 2001b] among others, and the proofs of these controllers in [Levant, 2003]. These controllers may be realized by usage of full state feedback, or by output differentiation. For differentiation so-called real-time exact robust differentiation techniques may be applied [Levant, 1998b] (first order differentiator), [Levant, 1998a], [Levant, 2003] (arbitrary order differentiators).

High order sliding modes may somewhat resemble the basic ideas presented in the previous section, but with some significant difference. In the example in the previous section with $e \in \mathbb{R}$, a sliding mode on $e = 0$ is guaranteed in finite time for α large enough. However, in the example with $\mathbf{e} \in \mathbb{R}^2$ and the surface (4.23) (or in case of systems with $n > 2$), a sliding mode on S is achieved in finite time, however convergence of the states to $(e_1, e_2) = (0, 0)$ is not. This leads to the main difference between first- and high order sliding modes, i.e. that a high order sliding controller guarantees convergence of all states $e_1, e_2, ..., e_n$ to zero in finite time. For constraint functions and autonomous systems, an r^{th} order sliding mode is here defined by Definition 1 (inspired by [Levant, 2003]), where r denotes the order of the output function e, relative to the system order n.

Definition 1 *Consider a smooth dynamic system $\dot{x} = f(x(t), u)$, $x(t) = x \in \mathbb{R}^n$ with a smooth output function $e = e(x(t)) \in \mathbb{R}$, closed by some discontinuous control u. Then provided that $e, \dot{e}, ..., e^{(r-1)}$ are continuous functions of the closed system state variables, and the r^{th} order sliding point set $e, \dot{e}, ..., e^{(r-1)} = 0$ is non-empty and consists locally of Filippov sense trajectories, then the motion on $e, \dot{e}, ..., e^{(r-1)} = 0$ is called an r^{th} order sliding mode.*

Essentially, Definition 1 states that, for e.g. a second order sliding mode to take place (i.e. the system has order two relative to the constraint e), then motion on $e, \dot{e} = 0$ must consist (locally) of limits of motions on both $e = 0$ and $\dot{e} = 0$. Note that this can only take place if convergence to $e, \dot{e} = 0$ occur in finite time.

Consider now the relation between Definition 1 and the examples of the previous section. For the example of Section 4.2.1 (i.e. for $x \in \mathbb{R}$, the scalar system is of order $r = 1$ relative to e, and a sliding mode is achieved on $e = 0$, and a first order sliding mode takes place, satisfying Definition 1. However, for the example of Section 4.2.2 (i.e. for $S(\mathbf{e})$, $\mathbf{e} \in \mathbb{R}^2$, Definition 1 is not satisfied. Here $e_1, e_2 \to 0$ for $t \to \infty$, i.e. convergence of the states to zero is not guaranteed in finite time, hence limits of motions locally on both $e_1 = 0$ and $e_2 = 0$ cannot take place. In order for this to take place then $e_1, e_2 \to 0$ for $t \to t_s < \infty$. Consider now an example somewhat similar to the example of Section 4.2.2, however, with the surface (4.24) (corresponding to the so-called prescribed convergence algorithm [Levant, 1993]).

$$S = S(\mathbf{e}) = e_2 + \lambda |e_1|^{\gamma} \operatorname{sgn}(e_1), \;\; 0.5 \leq \gamma < 1 \tag{4.24}$$

As in the example of Section 4.2.2, then for α sufficiently large, a sliding mode on $S = 0$ will take place in finite time, and motion on $S = 0$ will consist of Filippov sense trajectories. Using $S = 0$, then by separation of variables obtain (4.25).

$$e_2 = \frac{\mathrm{d}e_1}{\mathrm{d}t} = -\lambda |e_1|^{\gamma} \operatorname{sgn}(e_1) \;\; \Rightarrow \;\; \mathrm{d}t = -\frac{1}{|e_1|^{\gamma} \operatorname{sgn}(e_1)} \mathrm{d}e_1 \tag{4.25}$$

By integration, obtain (4.26), for the initial time instant $t_0 = 0$, and initial condition $e_1|_{t=0} = e_1(0)$.

$$\int_0^{t_s} \mathrm{d}t = -\int_{e_1(0)}^{0} \frac{1}{\lambda |e_1|^{\gamma} \operatorname{sgn}(e_1)} \mathrm{d}e_1 \;\; \Rightarrow \;\; t_s = \frac{1}{\lambda (1-\gamma)} e_1(0)^{1-\gamma} \tag{4.26}$$

From (4.26), then for any $1 > \gamma$ and $\lambda > 0$, a bounded convergence time $t_s < \infty$ is obtained. Hence, e_1, e_2 converges to zero in finite time, by virtue of the (first order) sliding mode on the constraint $S = 0$. Hence, past the time instant t_s, motion on $(e_1, e_2) = (0,0)$ will consist locally of Filippov sense trajectories, and a second order sliding mode takes place. The phase portrait for (4.24) is depicted in figure 4.3.

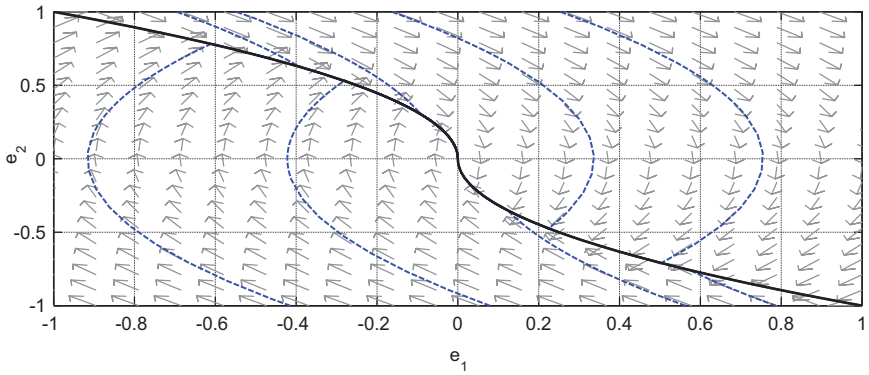

Figure 4.3: *Phase portrait for the states of $S(\boldsymbol{e})$. The dotted blue graphs depicts state trajectories, and the solid black graph depicts the switching function $e_2 + |e_1|^{\frac{1}{2}} \operatorname{sgn}(e_1) = 0$.*

Besides the prescribed convergence algorithm considered in this section, there are several other known second order sliding controllers that are of interest in regard to this project. These are considered in detail in the following chapters.

4.4 Chattering Issues In Physical Applications with Hydraulic Drives

Until this point sliding mode controls have been considered in an *ideal* context, i.e. when the switching frequency is infinite, switching imperfections are absent and the actuator is able to realize the (possibly) discontinues control input ideally. However, turning focus to the applicability in physical applications, a serious obstacle occur in this regard. Due to several dynamic features present in physical actuators, the discontinuous control input cannot be realized, giving rise to control (signal) chattering, which may excite un-modeled high order dynamics, resonant modes of load structures etc. This may in turn lead to increased wear of components or even damage the system. Naturally, the possibility of control chattering in sliding mode controlled systems is well known, as will be clear from the state-of-the-art analysis following this section. In the particular case of a hydraulic drive, the actuator is the proportional flow control valve. Such valves suffer from several dynamic effects that will distort the realization of discontinuous control signals, with the most profound being un-saturated (nominal) dynamics, time delays and slew rate limitations due to saturation phenomena in the electro-mechanical amplification stage, with the latter being (generally) most considerable in pilot operated valves.

4.4.1 Analysis of Hydraulic Valves in Perspective of Discontinuous Control

For analysis of applicability of sliding mode controls, the valves installed on the test axes are considered in more detail, i.e. the pilot operated 4WRTE valve and a direct operated 4WREE valve, both with an integrated electrical amplification stage and the valve spool in closed loop control. The dynamic responses of the valves when subjected to step-like inputs are readily evaluated from the data used in the model verification section, and are depicted in figures 4.4, 4.5, for the 4WRTE- and 4WREE valves, respectively. Besides the dynamic response of the 4WRTE valve in figure 4.4, also the supply pressure is shown as the pilot stage is internally supplied, i.e. the pilot supply pressure is the valve supply pressure.

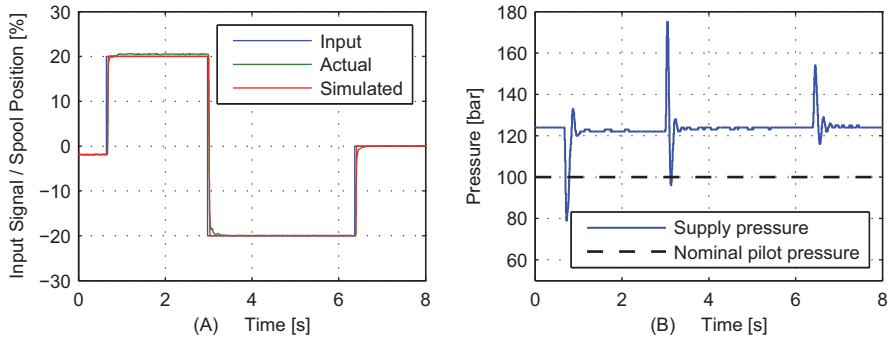

Figure 4.4: *Dynamic response of Bosch Rexroth 4WRTE 10 V1 100L two stage (pilot operated) proportional valve. (A) Input signal u_v (Input), measured spool position x_v (Actual) and simulated spool position x_v (Simulated). (B) Measured supply pressure P_S and nominal pilot pressure used in data sheet information for the valve.*

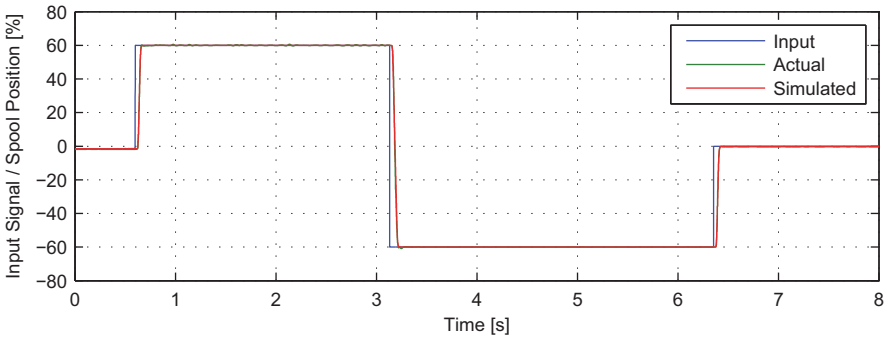

Figure 4.5: *Dynamic response of Bosch Rexroth 4WREE 10 V 50 direct operated proportional valve. Input signal u_v (Input), measured spool position x_v (Actual) and simulated spool position x_v (Simulated).*

From figures 4.4, 4.5 it is found that valve model responses closely resemble the measured responses, only minor inaccuracies in the 4WRTE valve model response is present, which is assumed to result from the contemporary variations in the valve supply-, hence the pilot supply pressure, not taken into account in the valve model. The verified valve models provide approximate dynamic characteristics of the valves under consideration, and in both cases the dynamic responses exhibit significant impact from slew rate limitations and time delays, resulting from saturation phenomena in the electro-mechanical amplification stages. The slew rate $|\dot{x}_\mathrm{v}|_\mathrm{max}$ and time delay τ_vd of the valve models are outlined in (4.27), (4.28).

$$\text{4WRTE:} \quad |\dot{x}_\mathrm{v}|_\mathrm{max} = 1500\ [\%/s] \quad , \quad \tau_\mathrm{vd} = 0.021\ [s] \tag{4.27}$$

$$\text{4WREE:} \quad |\dot{x}_\mathrm{v}|_\mathrm{max} = 2400\ [\%/s] \quad , \quad \tau_\mathrm{vd} = 0.021\ [s] \tag{4.28}$$

Direct application of discontinuous control signals will ideally cause the valve amplification stages to be constantly saturated, switching between their $\pm$saturation limits. This, as well as time delay and nominal $x_\mathrm{v}/u_\mathrm{v}-$dynamics, will prevent the realization of the discontinuous control, and therefore result in chattering of the control input, and following the spool position through the natural filter effects of the valve. Such chattering effects may be extremely harmful to the valve, and cause increased wear and reduce life time. Furthermore, the chattering- or oscillating valve spool causes and oscillatory power inlet to the system, possibly exciting high order dynamics and resonant modes of pipe assemblies and load structures, even though the cylinder assembly and the attached load mechanically filters the high frequency oscillations further, dependent on the hydraulic capacitance, mechanical damping and inertia.

Impact of Slew Rate Limitations

The impact of slew rate and time delay in sliding mode control systems is illustrated with a simple example, considering the scalar control system (4.13), (4.15) with $h(x) = 0$, $g(x) = g = 1$, zero set point and initial condition $e(0) = 0.1\ [-]$. After some convergence period, the relay controller enforces a sliding mode on $e = 0$.
The slew rate prevents ideal switching of the control, and the switching period τ_sl and oscillation (limit cycle-like oscillations on $e = 0$) amplitude a_sr resulting from this is obtained as (4.29) (for

this simple example).

$$\tau_{\mathrm{sl}} = \frac{\alpha g}{|\dot{x}_{\mathrm{v}}|_{\max}} \quad , \quad a_{\mathrm{sr}} = \frac{1}{2}\int_0^{\tau_{\mathrm{sl}}} \alpha g \mathrm{d}t = \alpha g \tau_{\mathrm{sl}} = \frac{1}{2}\frac{g^2\alpha^2}{|\dot{x}_{\mathrm{v}}|_{\max}} \tag{4.29}$$

The effects of the slew rate when the relay controller is directly applied are depicted in figure 4.6 for control gains $\alpha = 1$, $\alpha = 2$, respectively, and a slew rate of $|\dot{x}_{\mathrm{v}}|_{\max} = 100\ [-/s]$. The switching period and oscillation amplitudes for this example are found as $\tau_{\mathrm{sl}}|_{\alpha=1} = 1e-2\ [s]$, $a_{\mathrm{sr}}|_{\alpha=1} = 5e-3\ [-]$ and $\tau_{\mathrm{sl}}|_{\alpha=2} = 5e-1\ [s]$, $a_{\mathrm{sr}}|_{\alpha=2} = 2e-2\ [-]$.

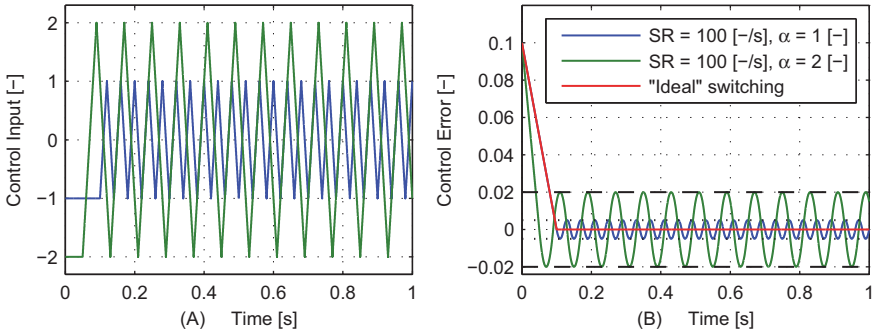

Figure 4.6: *(A) Input of control under slew rate impact, with $\alpha = 1$, $\alpha = 2$, respectively. Here, the ideal control is not depicted, as this is constituted by switching between ± 1 with a frequency of $100\ [kHz]$. (B) Control errors of the ideal (no slew rate) system, and system under slew rate impact, with $\alpha = 1$, $\alpha = 2$, respectively. The dashed- and dotted lines indicates the expected oscillation amplitude a_{sr} under slew rate impact for $\alpha = 1$, $\alpha = 2$, respectively.*

Note also that the switching time denotes the time it takes to realize one change of the discontinuous control, hence one oscillation period of the control input and / or of the control error will last at least three times longer than the switching period when a *sliding mode* is present.

Impact of Time Delays

An even more urgent obstacle is the presence of time delays involved in the amplification procedure. Such a time delay can be interpreted in a way similar to the sample frequency of discrete time systems, hence reducing the switching frequency. The performance of the *ideal* control system (as the one used above), is depicted in figure 4.7 when compared to the same control system with a time delay on the control input of $\tau_{\mathrm{d}} = 0.01\ [s]$ (the simulation time step is $1e-5\ [s]$). As depicted in figure 4.7, the convergence with $e = 0$ occur at time $t = 0.01\ [s]$, for the ideal relay control, as expected from (4.19) for $g = \alpha = 1$. The delayed relay control intersects $e = 0$ with the delay $\tau_{\mathrm{d}} = 0.01\ [s]$. Hereafter, the ideal relay controller provides for an ideal sliding mode on $e = 0$. However, τ_{d} of the delayed relay controller increases the switching amplitude and switching period compared to the ideal controller.

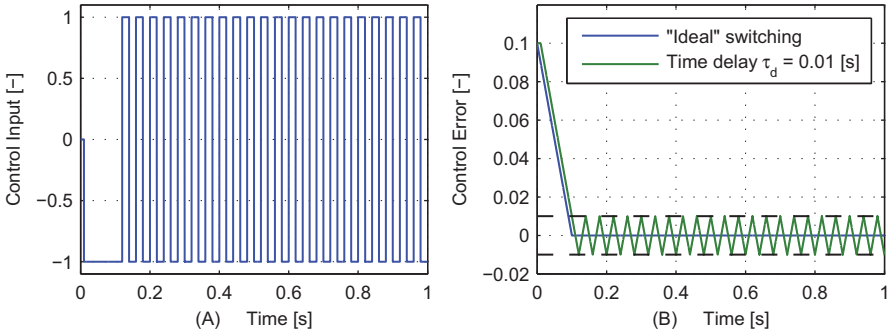

Figure 4.7: *(A) Input of delayed relay control. Here, the ideal control is not depicted, as this is constituted by switching between* ± 1 *with a frequency of* $100\ [kHz]$*. (B) Control error of the system with and without delayed relay control. The dotted lines indicates the expected oscillation amplitude* a_{ds}*, resulting from the time delay* τ_d*.*

For this simple control system, the reduced switching frequency is given by $\omega_{\mathrm{ds}} = \tau_{\mathrm{d}}^{-1}$, and the amplitude a_{sw} is obtained from integration as (4.30).

$$a_{\mathrm{ds}} = \int_0^{\tau_{\mathrm{d}}} \alpha g \mathrm{d}t = \alpha g \tau_{\mathrm{d}} \tag{4.30}$$

Perspectives of Hydraulic Drives

In general a hydraulic drive may not be represented by an ideal integrator as in the above analysis. In reality the system gain is state dependent, and possibly exhibits significant variations dependent on the load pressure, valve flow gain characteristics, supply pressure variations etc. Hence, from the above, the amplitude of the limit cycle-like oscillations on $e = 0$ as well as the switching frequency will change dependent on the system states, making estimation procedures for these quantities somewhat elaborate. However, the above considerations may be used to estimate minimum quantities of control switching period and frequency- and amplitude of oscillations on $e = 0$ if the valve time delay τ_{d} and the bound K_{m} can be estimated fairly accurately, and nonlinear friction phenomena are negligible compared to the remaining load components.
In the above an oscillation period on $e = 0$ may be restricted to last at least three times the switching time, however, in a hydraulic drive the pressure dynamics is not infinitely fast (analogue to the system above), and the response from the system to the switching action may last several switching periods dependent on the control gain, system gain etc. Furthermore, if friction phenomena are dominant the switching period and amplitude may be further increased.
The undesired dynamic features of hydraulic valves considered above, call for methods to reduce- or attenuate control chattering in order to achieve a successful application of sliding mode control. In the following subsections different approaches to achieve this is considered.

4.4.2 Chattering Attenuation by Continuous Approximations of Discontinuities

A popular and widely applied approach (see the following section for references) to reduce control chattering is by use of the so-called saturation function [Slotine and Li, 1991], given by (4.31).

This may be substituted with the sgn-function in e.g. the controller (4.15) (for $e \in \mathbb{R}$).

$$B = \text{sat}(e) = \begin{cases} \text{sgn}\left(\dfrac{e}{\varphi_b}\right) & \text{for } |e| > \varphi_b \\ \dfrac{e}{\varphi_b} & \text{for } |e| \leq \varphi_b \end{cases} \tag{4.31}$$

Outside the boundary layer φ_b the control (4.15) with (4.31) is invariant with respect to uncertain parameters and bounded disturbances for α sufficiently large, and the surface S is attractive for $|e| > \varphi_b$. Inside the boundary layer φ_b, the control is essentially a high gain control proportional to e with the gain φ_b^{-1}, and robustness in terms of invariance is lost.

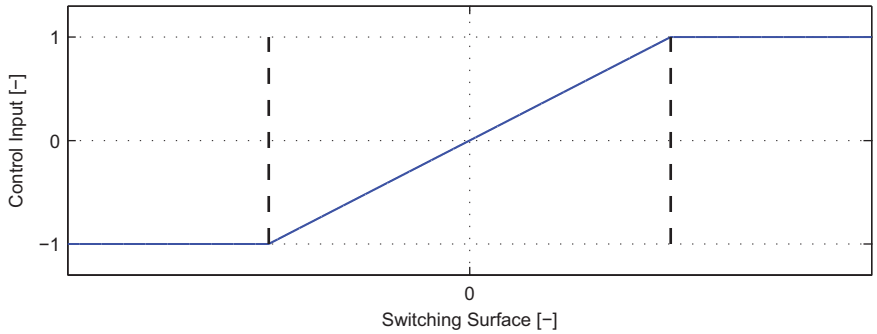

Figure 4.8: *Saturation function* (4.31). *The blue graph shows the output of the* sat*-function, and the black dotted lines indicates the boundary layer φ_b (width).*

Figure 4.8 illustrates the resulting control from the saturation function (4.31). The implementation of the saturation function implies that precision of the states in $e(x)$ is confined to the boundary layer *thickness* (or *width*) φ_b. Furthermore, if φ_b is chosen small, the gain φ_b^{-1} is large and may compromise stability within the boundary layer. Hence, performance within the boundary may be unstable, and stable outside the boundary layer, and therefore lead to limit cycles. Other popular approaches used for continuous approximations of the discontinuity are given by (4.32).

$$B_{ht} = \tanh\left(\frac{e}{\varepsilon_{ht}}\right) \quad , \quad B_{cs} = \frac{e}{|e| + \varepsilon_{cs}} \tag{4.32}$$

The functions (4.32) are bounded by $-1 < B_{th} < 1$, $-1 < B_{cs} < 1$. However, choosing ε_{ht}, ε_{cs} according to (4.33), then φ_{ht}, φ_{cs} approximates boundary layers resembling that of the saturation function (4.31).

$$\varepsilon_{ht} = \frac{\varphi_{ht}}{\pi} \quad , \quad \varepsilon_{cs} = \frac{\varphi_{cs}}{100} \tag{4.33}$$

Figure 4.9 illustrates the resulting controls from the discontinuity approximations (4.32).

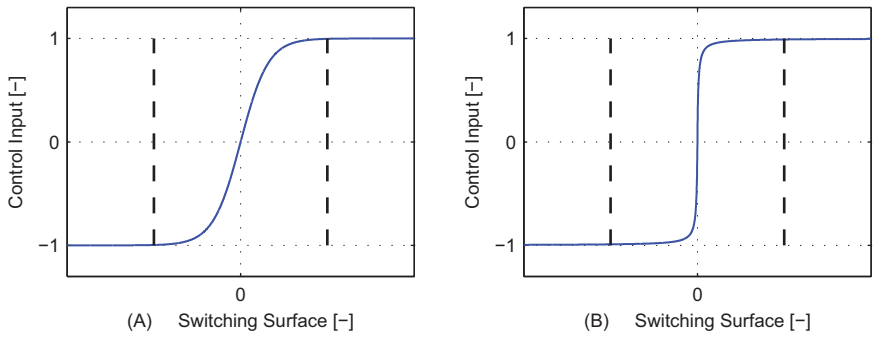

Figure 4.9: *(A) Continuous approximation of the* sgn *−function B_{ht} of* (4.32)*. (B) Continuous approximation of the* sgn *−function B_{cs} of* (4.32)*. The blue graphs shows the control inputs B_{ht}, B_{cs}, and the black dotted lines indicates the boundary layers φ_{ht}, φ_{cs}.*

In the context of the analysis of Section 4.4.1, it is crucial that e.g. the boundary layer φ_b is chosen sufficiently large and the control gain sufficiently small, such that the discontinuous control does not compromise the valve slew rate. Hence, in order to avoid deteriorating the control performance by saturation, a proper choice of φ_b is dependent of the control gain. Furthermore, one should take into account also possible continuous controller terms, that may require increasing the boundary layer further.

4.4.3 Chattering Attenuation Using High Order Sliding Algorithms

Another and more intriguing approach to avoid control chattering may be the application of high order sliding mode controls. Indeed, choosing a sliding mode controller of order $r = n+1$ (with n being the system order) allows the control input to be continuous, without the introduction of the boundary layer discussed in the previous subsection, i.e. the main features of sliding mode control are preserved with a continuous control input. Consider the second time derivative of the output function e given by (4.34), and the time derivative of the first order scalar system (4.7), given by (4.35).

$$\ddot{e}(x) = \frac{\mathrm{d}^2 e(x)}{\mathrm{d}t^2} = \frac{\partial^2 e(x)}{\partial x^2}\left(\frac{\mathrm{d}x}{\mathrm{d}t}\right)^2 + \frac{\partial e(x)}{\partial x}\frac{\mathrm{d}^2 x}{\mathrm{d}t^2} = \frac{\partial^2 e(x)}{\partial x^2}\dot{x}^2 + \frac{\partial e(x)}{\partial x}\ddot{x} \tag{4.34}$$

$$\ddot{x} = \frac{\partial a(x)}{\partial x}\frac{\mathrm{d}x}{\mathrm{d}t} + \frac{\partial b(x)}{\partial x}\frac{\mathrm{d}x}{\mathrm{d}t}u + b(x)\frac{\mathrm{d}u}{\mathrm{d}t} = \frac{\partial a(x)}{\partial x}\dot{x} + \frac{\partial b(x)}{\partial x}\dot{x}u + b(x)\dot{u} \tag{4.35}$$

From (4.7), (4.35), the system (4.36) is obtained with (4.37).

$$\ddot{e}(x) = \bar{h}(x) + \bar{g}(x)\dot{u} \tag{4.36}$$

$$\bar{h}(x) = \frac{\partial^2 e(x)}{\partial x^2}\dot{x}^2 + \frac{\partial e(x)}{\partial x}\frac{\partial a(x)}{\partial x}\dot{x} + \frac{\partial e(x)}{\partial x}\frac{\partial b(x)}{\partial x}\dot{x}u \quad , \quad \bar{g}(x) = \frac{\partial e(x)}{\partial x}b(x) \tag{4.37}$$

Provided that the bounds (4.38) exist, then some second order sliding mode controller $\dot{u} = \dot{u}(e, \dot{e})$, may be applied, with this controller providing for a second order sliding mode on $|e| = |\dot{e}| = 0$ in finite time, for some bounded initial conditions.

$$0 < \bar{K}_m < \bar{g}(x) < \bar{K}_M \quad , \quad |\bar{h}(x)| \leq \bar{C} \tag{4.38}$$

This means that the actual control will be continuous in time. To outline the features, consider the simple closed loop system (4.39), with $\alpha = 1$. This system is finite-time globally convergent to a second order sliding mode on $|e| = |\dot{e}| = 0$.

$$\dot{e} = u \quad , \quad \dot{u} = -\alpha \,\mathrm{sgn}(\dot{e} + |e|^{\frac{1}{2}} \,\mathrm{sgn}(e)) \tag{4.39}$$

Under ideal conditions, and if both states $e, \dot{e}$ are available from measurements, chattering in the control input u will be completely absent, however if the switching frequency is finite, some level of control chattering will be present.

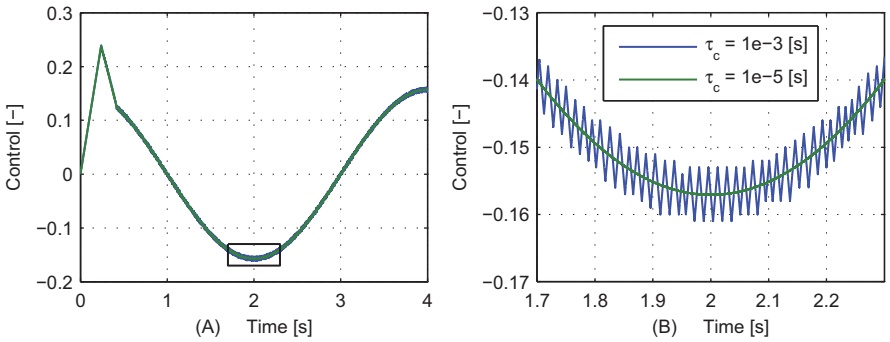

Figure 4.10: *(A) Control input for the discrete time version of* (4.39) *with different control time constants. (B) Zoom of the boxed area in (A).* τ_c *is the controller sampling time.*

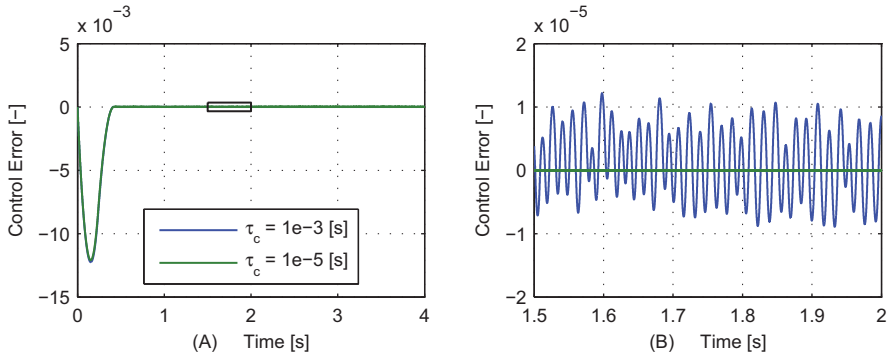

Figure 4.11: *(A) Control error for the discrete time version of* (4.39) *with different control time constants. (B) Zoom of the boxed area in (A).* τ_c *is the controller sampling time.*

Figures 4.10, 4.11 depict the control input and control error of the system (4.39) with the output function given by $x - x_\mathrm{d}$, with x_d being the desired trajectory of x. The desired trajectory is given by $x_\mathrm{d} = 0.1 \sin(\pi/2)$ [−], the *ideal* (infinite switching frequency) controller sample time is approximated by $\tau_c = 1e-5$ [s], and the *non-ideal* (bounded switching frequency) controller sample time is chosen $\tau_c = 1e-3$ [s]. Past convergence to $e = 0$ at $t \approx 0.4$ [s], the increased sample time influences the performance in terms of control chattering and increased magnitude of oscillations on

$e = 0$. However, for τ_c *sufficiently* small, then the chatter frequency and amplitude may resemble impact from sensor noise and / or the dither function used to minimize nonlinear friction effects related to the spool / housing contact surface(s). In such cases control chattering does not necessarily pose a significant problem. It is notable that using high order sliding mode controllers for this purpose on hydraulic drives with a proper valve choice, allow for sliding mode control *without* loss of robustness as opposed to boundary layer solutions.
Considering the analysis of Section 4.4.1, noting that $|\dot{u}|_{e_1,e_2\neq 0} = \alpha$, then the gain α of (4.39) should at least be restricted by $\alpha < |\dot{x}_v|_{\max}$. Furthermore, impact from time delays influences performance in a way similar to the bounded switching time.

4.4.4 Combining Saturation Functions & High Order Sliding Algorithms

The possible feature of achieving continuous control input without loss of robustness, makes high order sliding modes an attractive solution in control of hydraulic drives. However, in the event that time delays are significant, also this strategy will provide for oscillations of the output on $e = 0$, even with a high switching frequency. Also a possibility is that, in order to guarantee robustness, the control gain need to be of a size that causes slew rate saturation, which will also cause oscillations of the output near $e = 0$. Hence it may be feasible to combine e.g. the boundary layer approach with the usage of high order sliding modes, with the possibility of using a boundary layer significantly smaller than the conventional boundary layer approach. Such a controller may be realized as (4.40), (4.31).

$$\dot{e} = u \quad , \quad \dot{u} = -\alpha\,\mathrm{sat}(\dot{e} + |e|^{\frac{1}{2}}\,\mathrm{sgn}(e)) \tag{4.40}$$

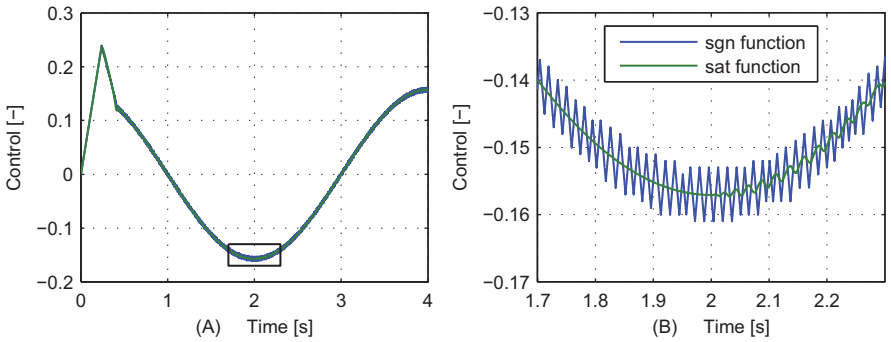

Figure 4.12: *(A) Control input for the system* (4.39) *implemented with* sgn *−function and* sat *−function, both with switching / control time constant* $\tau_c = 1e-3$ *[s]. (B) Zoom of the boxed area in (A).*

The resulting performance of the control system (4.40), (4.31) with $\varphi_b = 0.01$ $[-]$ in terms of control input and control error are depicted in figures 4.12, 4.13 and the surface $S = \dot{e} + |e|^{\frac{1}{2}}\,\mathrm{sgn}(e)$ in figure 4.14.

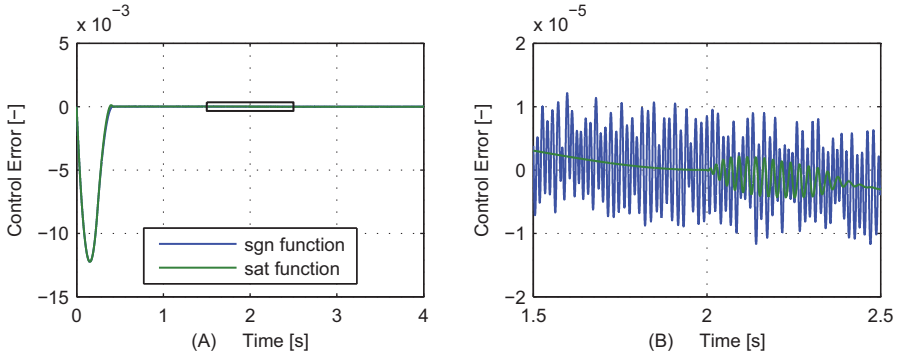

Figure 4.13: *(A) Output error e for the system* (4.39) *implemented with* sgn $-$*function and* sat $-$*function, both with switching / control time constant* $\tau_c = 1e-3$ *[s]. (B) Zoom of the boxed area in (A).*

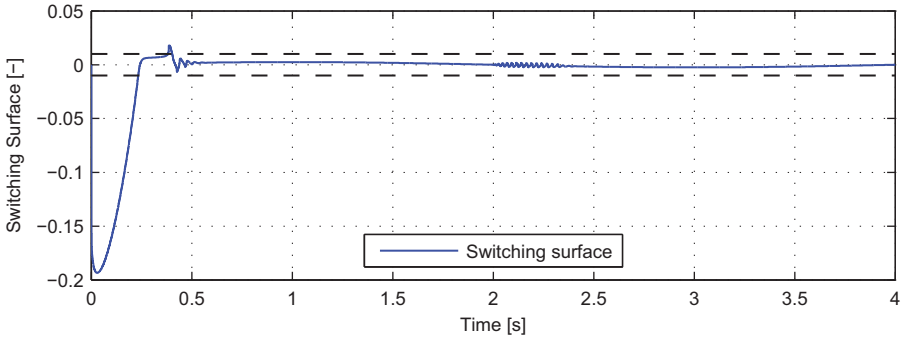

Figure 4.14: *Switching surface / function* $S = \dot{e} + |e|^{\frac{1}{2}} \operatorname{sgn}(e)$ *for the system* (4.39) *with the* sgn $-$*function replaced by a* sat $-$*function, with* $\varphi_b = 1e-2$ *[-], and with switching / control time constant* $\tau_c = 1e-3$ *[s]. The dashed lines indicate the boundary layer limit / width* φ_b.

It is found from figures 4.12, 4.13 that both control chattering as well as oscillations of the output near $e = 0$ are significantly reduced with the sat-function compared to the sgn-function. Also from figure 4.14 it is found that, in this example, the output function surface S is confined within this boundary layer.

4.5 State-of-the-Art for Application to Hydraulic Drives

This section outlines state-of-the-art for application of sliding mode control to hydraulic systems. Due to the *general purpose* objective of this project, focus is placed on the actual sliding control algorithms, and only limited attention is given to specific applications. Furthermore, limited attention is given to algorithms combining sliding mode controls with controllers such as adaptive controls etc. Investigating the literature, it turns out that most literature focus on conventional first order sliding control using different linear surface designs and different continuous approximations

of discontinuous control terms as those considered in Section 4.4.2. Furthermore, some attention has been given to the improvement of the (possibly poor) convergence speed resulting from discontinuous controller terms. Applications in which sliding mode controls have been applied are many and diverse, and ranges from active suspension systems, pitch systems for wind turbines to more conventional valve driven cylinders and motors actuating a variety of different types of loads. Hence state-of-the-art is highly related to different applications, which also emphasizes the applicability of sliding mode control in hydraulic systems.

4.5.1 Compensation of Discontinuities

As already discussed in previous sections of this chapter, the most profound obstacle for the application of sliding modes in hydraulic systems / drives is the possibility for control chattering. Hence, as expected, a study of the research literature also reveals that methods for smoothing of discontinuities are normally applied.
The, by far, most common method for this task, is the application of the saturation function (4.31) proposed in [Slotine and Li, 1991]. Position controls based on sliding modes (first order) with saturation function and linear surfaces representing some desired error dynamics similar to the method discussed in Section 4.2.2 was considered in [Hisseine, 2005], [Pi and Wang, 2011], [Yoon and Manurung, 2010], [Guo et al., 2008], [Wang and Su, 2007], [Komsta et al., 2010b], [Chiang, 2011], [Batur and Zhang, 2003], [Liu and Handroos, 1999], [Hwang and Lan, 1994], [Chen et al., 2005], [Habibi, 1995] and [Fung et al., 1997], in all cases based on continuous time designs. Also a discrete time sliding control design based on linear surface design, utilizing the sat-function (4.31), was proposed in [Wang et al., 2011].

As discussed in Section 4.4.2, continuous approximations of the sgn-term may also be successfully realized utilizing a hyperbolic tangent function B_{ht} of (4.32) or the function B_{cs} of (4.32).
The approach using the function B_{ht} was applied for position control based on linear surfaces in [Ghazali et al., 2010], [Hansen et al., 2005], [Bonchis et al., 2001] and for force control in [Nguyen et al., 2000] with the sliding constraint being the force error itself, and not a surface, similar to the approach considered in the relative degree one case of Section 4.2.1. It should be noted that in [Bonchis et al., 2001], the controller considered was proposed in combination with a friction observer based on a sliding algorithm somewhat resembling the super twisting algorithm, which will be discussed in Chapter 6. The approach using the function B_{cs} of (4.32) was applied in [Chern and c. wu, 1991] for velocity control and in [Ghazy, 2001] and in [Sam et al., 2004] for position control.

4.5.2 Improvement of Convergence Speed

In general, most of the approaches considered above utilize a constant gain on the *switching* term of the controllers. However, dependent on the size of this gain (and possible continuous controller terms), the speed of convergence may be rather slow, even though convergent to a sliding mode in finite time. Several methods for improving the convergence speed have been proposed in literature concerning hydraulic applications, and are considered in the following.

Constant Plus Proportional Reaching Law

One method that may be applied in order to improve the speed of convergence, is the so-called *constant plus proportional reaching law*, that was proposed in [Fung and Yang, 1998], [Jerouane et al., 2004b], [Jerouane et al., 2004a], [Zulfatman et al., 2011]. Such a reaching law

may be implemented, such that the switching controller term is given by (4.41).

$$u_{\text{smc}} = -(\delta|e| + \alpha)\,\text{sgn}(e), \quad \alpha, \delta > 0 \tag{4.41}$$

Evidently, this reaching law includes a proportional term, which improves the speed of convergence, as a function of the constraint e while maintaining sliding mode features.

Power Rate Reaching Law

A rather similar way of improving the speed of convergence is by use of the power rate reaching law. This was considered in [Jerouane et al., 2004a], [Chin-Wen Chuang, 2005], and with this implemented the switching term may be expressed as (4.42).

$$u_{\text{smc}} = -(\delta|e|^{\gamma} + \alpha)\,\text{sgn}(e), \quad 1 > \gamma > 0, \;\; \alpha, \delta > 0 \tag{4.42}$$

This reaching law introduces an exponent to the proportional term. It may be found that the condition $1 > \gamma > 0$ causes the continuous term to reach $e = 0$ in finite time under certain conditions, but does not provide robustness as the sgn-term. The discussion of the finite time convergence conditions of a similar term is presented in detail in Chapter 7.

4.5.3 *Hybrid* Controllers Utilizing Sliding Modes

Having considered the characteristics of sliding controls discussed in literature, it is worth noting that there exist a number of contributions combining sliding control with other control strategies. Such approaches were proposed in [Loukianov et al., 2009] when combined with H_∞ controls and in [Angue-Mintsa et al., 2011], [Guan and Pan, 2008] when combined with adaptive control strategies. In [Komsta et al., 2010a] an integral sliding mode disturbance compensator was combined with input-output linearization methods. However, in many of such approaches, the combination of several control methods results in significant numbers of parameters. Hence such methods do in general not comply with the objectives of this project, and are not considered further.

Literature concerning high order sliding modes in hydraulic control systems appear limited, and only a few methods have been proposed. However, application of the so-called *twisting algorithm* was proposed in [Lizalde et al., 2005], [Loukianov et al., 2008], when combined with neural identification methods for force tracking control. The twisting algorithm is considered in detail in Chapter 6.

4.6 Summary

The fundamentals of sliding mode controls were considered and their features discussed. Conventional first order sliding mode controls were considered in regard systems of relative degree one and systems of higher relative degrees, and the concept and existence of high order sliding modes was outlined. Furthermore chattering issues in regard to implementation in physical- and particular hydraulic systems were considered. Analyzes emphasized that slew rate limitations as well as time delays in actuator amplification stages pose significant obstacles in the application of such controls. A discussion of chattering attenuation methods using continuous approximations of sgn-terms and high order sliding modes reveals that chattering may be effectively reduced, and their differences and possible combinations were presented.

Finally, state-of-the-art for application of sliding controls in hydraulic systems was outlined. It was found that sliding mode control applied in relation to control of hydraulic systems has become increasingly popular over the years. However, sliding controller terms applied are mainly restricted to conventional first order approaches, thoroughly elaborated in literature, and limited attention have been given to intriguing methods evolving in the field of high order sliding mode control.

5 First Order Sliding Mode Control

Having elaborated the fundamental theoretical framework of sliding mode control and considered the main features, drawbacks and possible compensation methods in regard to control of hydraulic drives, such controls can be designed. In this chapter different conventional sliding mode controllers (of the first order) are designed and evaluated.

5.1 Conventional First Order Sliding Mode Controls

Conventional first order sliding mode controllers are considered controllers taking their offset in the design framework presented in [Slotine and Li, 1991], and two such designs are considered in the following.

5.1.1 First Order Sliding Output Feedback Controller

This controller may be considered the most simple sliding controller possible, i.e. a relay controller providing for a sliding mode on the position control error $e = x_P - x_R = 0$. Consider the first order scalar model representation of a gain compensated hydraulic drive (3.41) with the output function $e = x_P - x_R$, assuming the open loop system stable with parameters bounded as (5.1).

$$0 < K_{\mathrm{m}} \leq \rho(\mathbf{x}) \leq K_{\mathrm{M}} \quad , \quad |F(\mathbf{x})| \leq C \tag{5.1}$$

If this system is closed by the relay controller with velocity feed forward $\bar{u}_{\mathrm{v}} = \dot{x}_R - \alpha\,\mathrm{sgn}(e)$, then a first order sliding mode on $e = 0$ is achieved in finite time. This conclusion may be verified by the radially unbounded Lyapunov candidate function $V(e) = e^2/2 > 0\ \forall e \neq 0$, with the time derivative (5.2).

$$\begin{aligned} \dot{V}(e) = e\dot{e} &= e(F(\mathbf{x}) - \dot{x}_R + \rho(\mathbf{x})\bar{u}_{\mathrm{v}}) \\ &= e(F(\mathbf{x}) - \dot{x}_R + \rho(\mathbf{x})(\dot{x}_R - \alpha\,\mathrm{sgn}(e))) \\ &= eF(\mathbf{x}) + e(\rho(\mathbf{x}) - 1)\dot{x}_R - \alpha\rho(\mathbf{x})|e| \end{aligned} \tag{5.2}$$

If the compensator (3.30), (3.39) is properly designed, then $\rho(\mathbf{x}) \simeq 1$, leading to (5.3).

$$\dot{V}(e) = eF(\mathbf{x}) - \alpha|e| \tag{5.3}$$

From (5.3) it is found that $\dot{V}(e) < 0\ \forall e \neq 0$ provided that $\alpha \geq C$ is satisfied. If furthermore $\alpha > C$, then $\dot{V}(e) < 0\ \forall e$, and the closed loop system is globally convergent to a first order sliding mode $e = 0$ in finite time. To avoid control chattering, the sgn-function is substituted by the saturation function (4.31), confining $|e|$ to the boundary layer φ_b in finite time. If the discontinuity gain is chosen such that robustness is guaranteed outside the boundary layer φ_b, and such that slew

rate saturation does not occur, then the convergence time may be somewhat significant (but finite). This may be effectively compensated by altering the discontinuity gain according to the *power rate reaching law* discussed in Section 4.5, altering the simple relay controller to (5.4).

$$\bar{u}_{\mathrm{v}} = \dot{x}_R - (\delta|e|^{\gamma} + \alpha)\,\mathrm{sgn}(e) = \dot{x}_R - \delta|e|^{\gamma}\mathrm{sgn}(e) - \alpha\,\mathrm{sgn}(e), \quad 1 > \gamma > 0, \;\; \delta > 0 \tag{5.4}$$

The finite time convergence properties may, as before, be evaluated by the Lyapunov candidate function $V(e) = e^2/2$, leading to the derivative (5.5).

$$\dot{V}(e) = eF(\mathbf{x}) - \delta|e|^{\gamma} - \alpha|e| \tag{5.5}$$

From (5.5), parameters δ, γ can be adjusted to achieve the desired convergence speed, without compromising the invariance property.

Note; When $|e| \leq \varphi_b$, the discontinuous controller term is analogue to a proportional controller, hence a steady state error must be expected.

5.1.2 First Order Sliding Surface Controller

In order to reduce the steady state error possibly occurring using the control (5.4) with the saturation function (4.31) introducing a boundary layer on $e = 0$, an integral term may be included in the sliding constraint. Consider again the system (3.41), with the output function $\int_t (x_P - x_R)\mathrm{d}t = \int_t e\mathrm{d}t$. In this case, the system (3.41) has degree $r = 2$, relative to the output function, and the simple relay controller does not guarantee asymptotic stability of the closed loop system states. Hence, consider instead the surface constituted by a linear combination of the error states (following the approach in [Slotine and Li, 1991]), given by (5.6).

$$S(\mathbf{e}) = S = e + \lambda \int_t e\mathrm{d}t, \quad \lambda > 0 \tag{5.6}$$

Relating to the geometric considerations of the Filippov solution in Section 4.1.2, the vector $\dot{x} = f_0$ represents the average of the limit of motions on $S = 0$. Hence, the dynamics of the surface S when a sliding mode takes place (on $S = 0$) is ideally $\dot{S} = 0$. These considerations may be utilized to establish the dynamics of the closed loop system, that is equivalent to the motion on $S(\mathbf{e}) = 0$. Hence, solving $\dot{S} = 0$, obtain an equivalent control similar to the approach [Slotine and Li, 1991] as (5.7).

$$\hat{\bar{u}}_{\mathrm{v}} = \hat{\rho}(\mathbf{x})^{-1}(\dot{x}_R - F(\mathbf{x}) - \lambda e) \tag{5.7}$$

Utilizing the equivalent control (5.7), a controller may be synthesized, being robust toward parameter uncertainties of the model (3.41) for $K_{\mathrm{m}}\alpha > C$, as (5.8) (with $\hat{\rho}(\mathbf{x})$ being the estimate of $\rho(\mathbf{x})$).

$$\bar{u}_{\mathrm{v}} = \hat{\bar{u}}_{\mathrm{v}} - \hat{\rho}(\mathbf{x})^{-1}\alpha\,\mathrm{sgn}(S) = \hat{\rho}(\mathbf{x})^{-1}(\dot{x}_R - \lambda e - \alpha\,\mathrm{sgn}(S)) \tag{5.8}$$

The robustness of (5.8) is verified by the Lyapunov candidate function $V(S) = S^2/2$. The derivative of $V(S)$ is given by (5.9), with the notion $\bar{e} = \int_t e\mathrm{d}t$.

$$\begin{aligned}
\dot{V}(S) = \dot{V}(\bar{e}, e) = S\dot{S} &= S(\dot{e} + \lambda e) \\
&= S(\dot{x}_P - \dot{x}_R + \lambda e) \\
&= S(F(\mathbf{x}) + \rho(\mathbf{x})\bar{u}_{\mathrm{v}} - \dot{x}_R + \lambda e) \\
&= S(F(\mathbf{x}) + \rho(\mathbf{x})(\hat{\rho}(\mathbf{x})^{-1}(\dot{x}_R - \lambda e - \alpha\,\mathrm{sgn}(S))) - \dot{x}_R + \lambda e) \\
&= SF(\mathbf{x}) - \hat{\rho}(\mathbf{x})^{-1}\alpha|S| + S(\rho(\mathbf{x})\hat{\rho}(\mathbf{x})^{-1} - 1)(\dot{x}_R - \lambda e)
\end{aligned} \tag{5.9}$$

As in the above, assuming a proper compensator design, then (5.9) is reduced to (5.10), with $\hat{\rho}(\mathbf{x}) = 1$.

$$\dot{V}(S) = \dot{V}(\bar{e}, e) = SF(\mathbf{x}) - \alpha|S| \tag{5.10}$$

It is found that $\dot{V}(S) < 0\ \forall S$ provided that $\alpha > C$, i.e. a first order sliding mode on $S = 0$ is achieved in finite time. Hence the states $\int_t e\mathrm{d}t, e \to 0$ for $t \to \infty$, and the error dynamics are ideally confined to $e = -\lambda \int_t e\mathrm{d}t$ in finite time by virtue of the sliding constraint $S = 0$.

As for the relay controller, control chattering is avoided by implementation of a saturation function similar to (4.31), meaning that sliding precision of S is guaranteed outside a boundary layer width φ_b. For $|S| < \varphi_b$, the control input is linearly proportional to S.

5.2 Chattering Attenuation Without Boundary Layer Using First Order Sliding Modes

In both the above controllers, the saturation function is considered in order to avoid chattering. However, bearing in mind the possible problems with slew rate limitation, then the size of the required boundary layer may compromise the minimum precision requirement. A possible solution to such a problem may be inspired by the chattering attenuation approach using high order sliding modes. This involves constructing a surface of the same order as the system under control, but with the highest state being one order lower than that of the system. Assume that the piston velocity measurement $\dot{x}_\mathrm{P}$ is available from measurements or some state reconstruction method, and furthermore that $F(\mathbf{x}) + \rho(\mathbf{x})\bar{u}_\mathrm{v} \in C^2$, $\rho(\mathbf{x}) \simeq 1$, $\dot{\rho}(\mathbf{x}) \simeq 0$, such that the system derivative is given by (5.11), with the bound $|\dot{F}(\mathbf{x})| \leq \bar{C}$.

$$\ddot{x}_\mathrm{P} = \dot{F}(\mathbf{x}) + \dot{\bar{u}}_\mathrm{v} \tag{5.11}$$

Now construct the surface S from the closed loop state variables as (5.12).

$$S = \dot{e} + 2\lambda e + \lambda^2 \int_t e\mathrm{d}t, \quad \lambda > 0 \tag{5.12}$$

Following the procedure of the previous subsection, however targeting the control derivative of (5.11), obtain a control design given by (5.13).

$$\dot{\bar{u}}_\mathrm{v} = \dot{\hat{\bar{u}}}_\mathrm{v} - \alpha\,\mathrm{sgn}(S), \quad \dot{\hat{\bar{u}}}_\mathrm{v} = \ddot{x}_\mathrm{R} - 2\lambda\dot{e} - \lambda^2 e \tag{5.13}$$

Consider again the Lyapunov candidate function $V(S) = S^2/2$, and its derivative (5.14) (recall the notation $\bar{e} = \int_t e\mathrm{d}t$).

$$\begin{aligned}\dot{V}(S) = \dot{V}(\bar{e}, e, \dot{e}) = S\dot{S} &= S(\ddot{x}_\mathrm{P} - \ddot{x}_\mathrm{R} + 2\lambda\dot{e} + \lambda^2 + e) \\ &= S(\dot{F}(\mathbf{x}) + \dot{\bar{u}}_\mathrm{v} - \ddot{x}_\mathrm{R} + 2\lambda\dot{e} + \lambda^2 e) \\ &= S\dot{F}(\mathbf{x}) - \alpha|S|\end{aligned} \tag{5.14}$$

Again $\dot{V}(S) < 0\ \forall S$ if $\alpha > \bar{C}$, and a sliding mode on $S = 0$ is guaranteed in finite time, and hence $\int_t e\mathrm{d}t, e, \dot{e} \to 0$ for $t \to \infty$. Dependent on controller sample time, valve slew rate and time delays the control (5.13) may be applied in combination with e.g. the saturation function (4.31) as discussed in Section 4.3.

5.3 Experimental Results

In the following, performance results for implementation of the relay- and sliding surface controllers as well as the sliding surface controller with boundary layer elimination are presented. A complete list of the control parameters used can be found in the Appendix.

5.3.1 Relay Controller (1SMC-e)

The relay controller with velocity feedforward $\bar{u}_v = \dot{x}_R - \alpha\,\mathrm{sgn}(e)$, $e = x_P - x_R$ (and the compensator (3.39), (3.30)) is applied with boundary layers $\varphi_b = 9\ [mm]$, $\varphi_b = 4\ [mm]$ and $\varphi_b = 10\ [mm]$ to the three test cases TC1, TC2, TC3, respectively, and results are depicted in figure 5.1. From

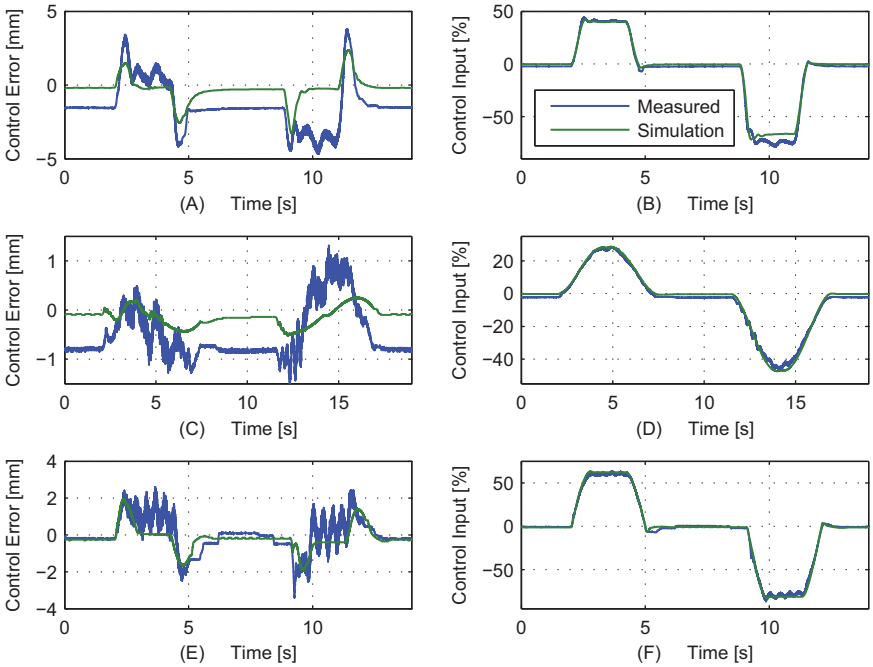

Figure 5.1: *Performance of first order sliding controllers. (A) Control error for TC1. (B) Control input for TC1. (C) Control error for TC2. (D) Control input for TC2. (E) Control error for TC3. (F) Control input for TC3.*

the results it is found that for all test cases, the control error is maintained within the boundary layers, and are essentially all operating in a proportional control mode. From this fact, the natural idea is to reduce the boundary layer further - however, experience during implementation revealed that further reduction of the boundary layer in all cases led to instability within the boundary layer, causing violent oscillations with the error passing through the boundary layer region, and essentially shifting between the convergence regions surrounding this. In all cases it is found that the control excites the resonant modes of the vehicle structure. Also it is found that steady state errors are present which is to be expected. The difference between measured- and simulation results

(steady state) is primarily due to inaccurate modeling of the leakage flow as discussed in Chapter 2. Note furthermore that for TC3, the settling properties are influenced by the profound friction phenomena of this axis.

5.3.2 Sliding Surface Controller (1SMC-S)

The implementation of the sliding surface controller (5.8) is for test cases TC1, TC2, TC3 carried out with boundary layers similar to those of the relay controller implementation, i.e. with $\varphi_b = 9\ [mm]$, $\varphi_b = 4\ [mm]$ and $\varphi_b = 10\ [mm]$, respectively, and also with the power rate reaching law as for the relay controller.

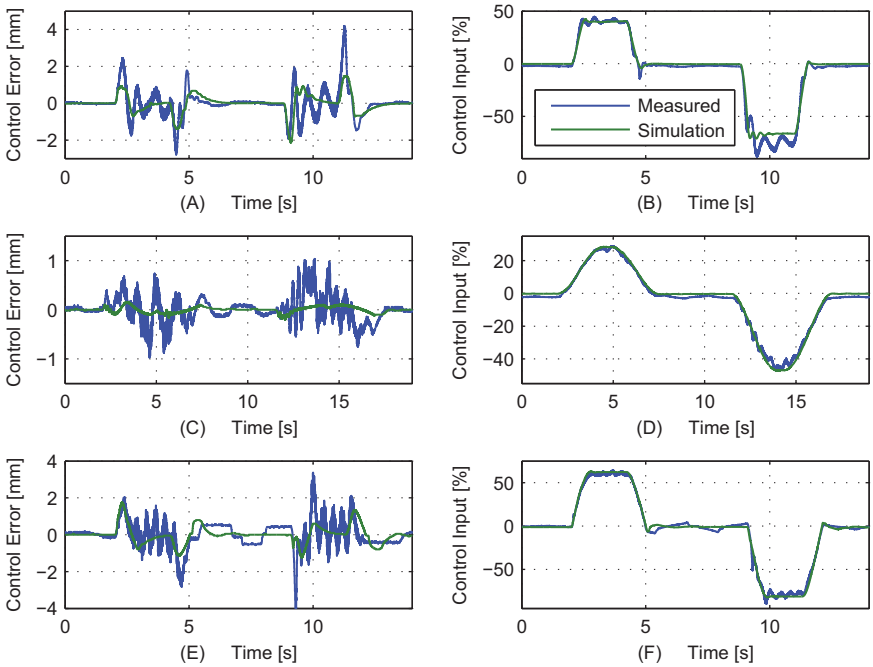

Figure 5.2: *Performance of first order sliding surface controllers. (A) Control error for TC1. (B) Control input for TC1. (C) Control error for TC2. (D) Control input for TC2. (E) Control error for TC3. (F) Control input for TC3.*

The performance results are depicted in figure 5.2. As for the relay controller, in all test cases it is found that the control operates within the boundary layer, hence operating in a PI control mode. However, opposite to the relay controller, the sliding surface controller reduces the error to zero which is to be expected from the integral term. Also in this case it is found that the vehicle resonant mode is excited. Experiences with boundary layer tuning are similar to those of the relay controller. However the additional parameter λ complicates the tuning process, as this parameter influences the allowable boundary layer limits for a satisfactory performance. Furthermore it is notable, that in TC3, the control error is prone to limit cycles, which is due to the presence of dominant friction

phenomena combined with the integral term of the switching surface.

5.3.3 First Order Sliding Controller Without Boundary Layer (1SMC-D)

The sliding control design targeting elimination of the boundary layer (5.13), is evaluated by simulation due to the lack of a velocity measurement, and considered in regard to Test Case 1. The control tracking error as well as the control input is depicted in figure 5.3, compared with the same controller with a boundary layer implemented.

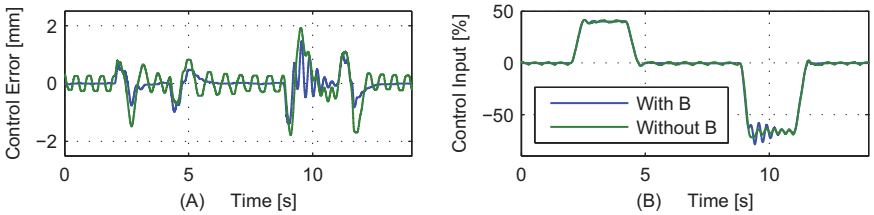

Figure 5.3: *Performance of first order sliding controller* (5.13)*. (A) Control error for TC1. (B) Control input for TC1.*

From figure 5.3 it is found that limit cycle-like behavior is present when using the controller without boundary layer. This is mainly caused by the nonlinear dynamic features of the valve discussed in Chapter 4. However, in the event that these features can be reduced by usage of more high performance valves, then this approach may be applied with satisfactory performance as a result.

5.4 Summary

Different approaches for output feedback control using first order sliding modes have been proposed, applying such methods as simple relay controls, or by subjecting a surface composed as some desired error dynamics, to a first order sliding constraint. In both cases, with direct application of the controls, chattering is inherent, and boundary layers were implemented, introducing an additional tuning parameter. An initiative to avoid the boundary layer was proposed, increasing the relative order of the error dynamics contained in the switching surface. Results showed that chattering was successfully reduced, however limit cycle-like behavior of the error dynamics was propound, and caused by the nonlinear dynamic valve characteristics.

During the implementation it was found that the closed loop systems were highly sensitive to the boundary layer thickness. This is due to the fact that the equivalent *linear* control performance within the boundary layer may become unstable, as the inverse of the boundary layer thickness gains the control error / surface. In such cases results were violent oscillations of the control error.

The experimental results are summarized in figure 5.4, and it is found that the sliding surface controller exhibits superior performance compared to the relay type controller in all test cases except regarding the maximum control error for Test Case 3. For Test Case 3, the sliding surface controller is prone to limit cycles due to the integral term included in the surface combined with the strong friction phenomena. Compared to the PI-AGC, in TC1 and TC2, performance is improved with the proposed controllers, and especially the sliding surface controller proved to be superior.

In TC3, performance of the proposed controllers are on a level with the PI-AGC in regard to RMS- and maximum errors. However, these improvements are achieved on the cost of increasing the number of tuning parameters compared to the PI-AGC.

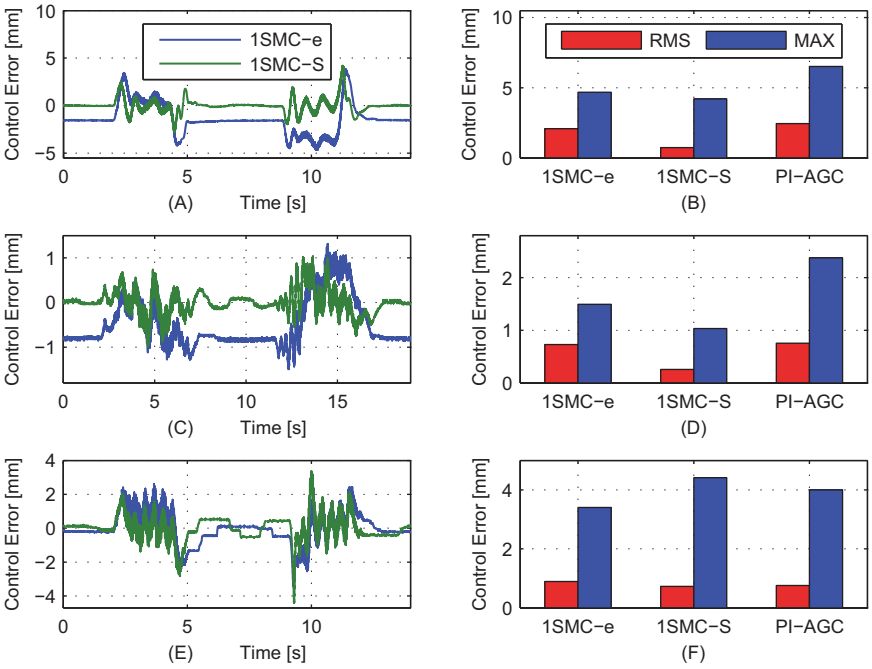

Figure 5.4: *Performance with application of the relay controller (1SMC-e) and the sliding surface controller (1SMC-S). (A) Control tracking errors for TC1. (B) RMS- and MAX control tracking errors for TC1. (C) Control tracking errors for TC2. (D) RMS- and MAX control tracking errors for TC2. (E) Control tracking errors for TC3. (F) RMS- and MAX control tracking errors for TC3.*

6 Second Order Sliding Mode Control

In the following, different controllers utilizing second order sliding algorithms are proposed, focusing on some of the most well known types, i.e. the prescribed convergence algorithm, the twisting algorithm and the super twisting algorithm. With the target of the presented work being simple and robust controls with limited parameter design, the second order sliding mode (SOSM) controls considered in the following are mainly focused on output feedback control for hydraulic drives.

6.1 Controller with Prescribed Convergence

The SOSM controller with prescribed convergence (PCA) considered in Section 4.3, is briefly summarized here in the context of the design model with relative degree $r = 1$ (i.e. in application for chattering attenuation) and for relative degree $r = 2$.

6.1.1 Application for Chattering Attenuation

Consider again the first order design model representation (3.41) with the output function being the position control error $e = x_P - x_R$, with assumptions similar to those of Section 5.2, i.e. that $\dot{x}_\mathrm{P} \in C^2$, $\rho(\mathbf{x}) \simeq 1$, $\dot{\rho}(\mathbf{x}) \simeq 0$ and $|\dot{F}(\mathbf{x})| \leq \bar{C}$. The prescribed convergence controller of Section 5.2 contain only the discontinuous control, possibly causing poor convergence speed. Hence, to improve this, a control design similar to that of Section 5.2 may be applied. However, instead of the surface constituted by linear error dynamics, the surface (6.1) is utilized.

$$S = \dot{e} + \lambda |e|^\gamma \mathrm{sgn}(e), \;\; 0.5 \leq \gamma < 1, \quad \lambda > 0 \tag{6.1}$$

The equivalent control is constructed as (6.2) for $\dot{S} = 0$ with $\dot{F}(\mathbf{x}) = 0$, from the model derivative (5.11). The combined control algorithm is given by (6.2).

$$\dot{\bar{u}}_\mathrm{v} = \dot{\hat{\bar{u}}}_\mathrm{v} - \alpha\,\mathrm{sgn}(S), \quad \dot{\hat{\bar{u}}}_\mathrm{v} = \ddot{x}_\mathrm{R} - \gamma\lambda|e|^{\gamma-1}\dot{e} \tag{6.2}$$

The stability and robustness of the controller is verified via $V(S) = S^2/2$ and its derivative is given by (6.3). Hence, $e, \dot{e} \to 0$ for $t \to t_1 < \infty$ following the reasoning of Section 4.3, providing for a second order sliding mode in finite time.

$$\dot{V}(S) = \dot{V}(e,\dot{e}) = S\dot{S} = S\dot{F}(\mathbf{x}) - \alpha|S| \quad \Rightarrow \quad \dot{V}(S) < 0 \;\forall S \;\text{ if }\; \alpha > \bar{C} \tag{6.3}$$

The actual control input is given by (6.4).

$$\bar{u}_\mathrm{v} = \dot{x}_\mathrm{R} - \lambda|e|^\gamma \mathrm{sgn}(e) - \alpha \int_t \mathrm{sgn}(S)\mathrm{d}t \tag{6.4}$$

6.1.2 Application in Relative Degree Two Design Model

The prescribed convergence controller may also be applied in a more conventional way. Consider the system (3.41) with the output function $\bar{e} = \int_t e dt$ with degree $r = 2$ relative to the system, and choose the sliding surface as (6.5).

$$S = e + \lambda |\bar{e}|^{\gamma} \operatorname{sgn}(\bar{e}), \;\; 0.5 \leq \gamma < 1, \quad \lambda > 0 \tag{6.5}$$

In this situation, the equivalent control approach is not found to feasible, as the control will be unbounded in this case, which is clear from (6.6) for $1 > \gamma$.

$$\dot{S} = \dot{e} + \gamma \lambda |\bar{e}|^{\gamma - 1} e \tag{6.6}$$

As discussed in Section 5.1.1, a strictly discontinuous control may cause low convergence speed, but may be improved similarly by usage of the power rate reaching law, leading to the controller (6.7) (including a velocity feed forward term).

$$\bar{u}_{\mathrm{v}} = \dot{x}_{\mathrm{R}} - (\delta |S|^{\gamma} + \alpha) \operatorname{sgn}(S), \quad 1 > \gamma, \;\; \alpha, \delta > 0 \tag{6.7}$$

The stability of the resulting closed loop system may be analyzed similarly to the analysis of the controller example in Section 4.3.

6.2 Twisting Controller

The controls considered until this point are somewhat similar in the sense that the control error- or a surface function representing some desired error dynamics have been subjected to first order sliding constraints. Another and very different approach to second order sliding control is the usage of the so-called twisting algorithm (TA), which was the first SOSM controller ever introduced [Fridman et al., 2012].

6.2.1 Application for Chattering Attenuation

Again, let system (3.41) have output function $e = x_P - x_R$ and assume that $\dot{x}_{\mathrm{P}} \in C^2$, $\rho(\mathbf{x}) \simeq 1$, $\dot{\rho}(\mathbf{x}) \simeq 0$, $|\dot{F}(\mathbf{x})| \leq \bar{C}$ are satisfied. Assume that the piston velocity is available, and consider the controller based on the TA with feedforward given by (6.8).

$$\dot{\bar{u}}_{\mathrm{v}} = \ddot{x}_{\mathrm{R}} - \alpha_1 \operatorname{sgn}(e) - \alpha_2 \operatorname{sgn}(\dot{e}) \tag{6.8}$$

The closed loop system is then given by (6.9), satisfying the inclusion (6.10).

$$\begin{aligned} \ddot{e} &= \dot{F}(\mathbf{x}) + \dot{\bar{u}}_{\mathrm{v}} - \ddot{x}_{\mathrm{R}} && (6.9) \\ &= \dot{F}(\mathbf{x}) - \alpha_1 \operatorname{sgn}(e) - \alpha_2 \operatorname{sgn}(\dot{e}) \quad \Rightarrow \\ \ddot{e} &\in [-\bar{C}, \bar{C}] - \alpha_1 \operatorname{sgn}(e) - \alpha_2 \operatorname{sgn}(\dot{e}) && (6.10) \end{aligned}$$

From inclusion (6.10) the closed loop system is found to be invariant with respect to $\dot{F}(\mathbf{x})$ if $|\alpha_1 - \alpha_2| > \bar{C}$ and $\alpha_1, \alpha_2 > \bar{C}$. This condition allows to carry out the stability analysis assuming that $\dot{F}(\mathbf{x}) = 0$, i.e. assuming that the system is represented by the simple system (6.11).

$$\ddot{e} = -\alpha_1 \operatorname{sgn}(e) - \alpha_2 \operatorname{sgn}(\dot{e}) \tag{6.11}$$

From (6.11) it is found that $\pm|\alpha_1 - \alpha_2|$ for $e\dot{e} < 0$, and $\pm|\alpha_1 + \alpha_2|$ for $e\dot{e} > 0$. The convergence conditions are established via analysis of the phase portrait. The gradient of the phase portrait is obtained using the identity $\ddot{e} = (\mathrm{d}\dot{e}\mathrm{d}e)/(\mathrm{d}e\mathrm{d}t) = (\mathrm{d}\dot{e})/(\mathrm{d}e)\dot{e}$, and is given by (6.12).

$$\frac{\mathrm{d}\dot{e}}{\mathrm{d}e} = \frac{-\alpha_1 \operatorname{sgn}(e) - \alpha_2 \operatorname{sgn}(\dot{e})}{\dot{e}} \tag{6.12}$$

Assuming initial conditions $(e(0), \dot{e}(0)) = (0, \dot{e}_{\mathrm{p}0})$ (see figure 6.1) the state trajectory sets off into the first quadrant defined by $e, \dot{e} > 0$ with $\dot{e} \to 0$. Using (6.12), then by separation of variables, obtain the intersection point $(e_{\mathrm{p}1}, 0)$ (figure 6.1), given by (6.13).

$$\int_0^{e_{\mathrm{p}1}} \mathrm{d}e = -\int_{\dot{e}_{\mathrm{p}0}}^{0} \frac{\dot{e}}{\alpha_2 + \alpha_1}\mathrm{d}\dot{e} \quad \Rightarrow \quad e_{\mathrm{p}1} = \frac{1}{2}\frac{\dot{e}_{\mathrm{p}0}^2}{\alpha_2 + \alpha_1} \tag{6.13}$$

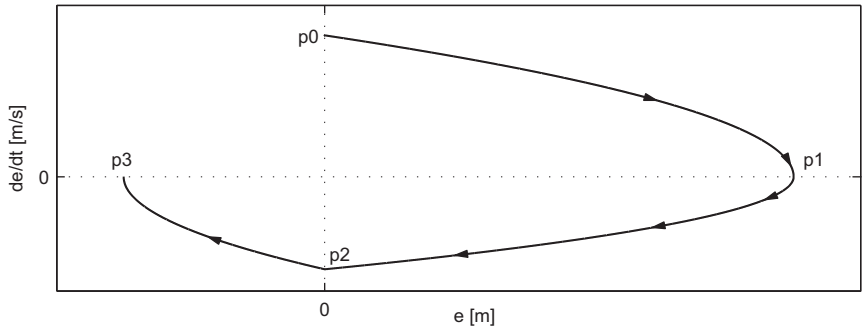

Figure 6.1: *Phase portrait for the system* (6.11).

Past the intersection $(e_{\mathrm{p}1}, 0)$, the state trajectory proceeds into the fourth quadrant defined by $e > 0, \dot{e} < 0$, $e \to 0$, if and only if $\alpha_1 > \alpha_2$. Otherwise, the trajectory will return into the first quadrant. Assuming $\alpha_1 > \alpha_2$, obtain the intersection $\dot{e} = \dot{e}_{\mathrm{p}2}$ similar to (6.13), as (6.14).

$$\int_{e_{\mathrm{p}1}}^{0} \mathrm{d}e = \int_0^{\dot{e}_{\mathrm{p}2}} \frac{\dot{e}}{\alpha_2 - \alpha_1}\mathrm{d}\dot{e} \quad \Rightarrow \quad -e_{\mathrm{p}1} = \frac{1}{2}\frac{\dot{e}_{\mathrm{p}2}^2}{\alpha_2 - \alpha_1} \tag{6.14}$$

From figure 6.1, if $|\dot{e}_{\mathrm{p}0}| > |\dot{e}_{\mathrm{p}2}|$, then $\dot{e}$ tends to zero. This criterion is realized combining (6.13), (6.14), yielding (6.15).

$$0 > \left|\frac{\dot{e}_{\mathrm{p}2}}{\dot{e}_{\mathrm{p}0}}\right| = \sqrt{\left|\frac{\alpha_1 - \alpha_2}{\alpha_2 + \alpha_1}\right|} \tag{6.15}$$

From (6.13), (6.14), (6.15) and the reasoning above it is found that $e, \dot{e} \to 0$ for $\alpha_1 > \alpha_2$. Furthermore, if $\pm|\alpha_1 - \alpha_2|\ \forall e\dot{e} < 0$, and $\pm|\alpha_1 + \alpha_2|\ \forall e\dot{e} > 0$, finite time convergence may be found from integral analysis using (6.10) for arbitrary initial conditions.

Output Feedback Version

Under certain conditions the TA controller may be applied as an output feedback controller in a discrete time implementation. In such an implementation, measurements may be obtained (sampled) at times $t_1, t_2, t_3, ..., t_n$, and the time interval between measurements as $\tau_c = t_k - t_{k-1}$. Assuming furthermore that $t \in [t_k, t_{k+1}]$ and defining $\Delta e_k = \Delta e(t_k) = e(t_k) - e(t_{k-1}) = e_k - e_{k-1}$, then a discrete time output feedback controller is obtained as (6.16).

$$\dot{\bar{u}}_{\mathrm{v},k} = \ddot{x}_{\mathrm{v},k} - \alpha_1 \operatorname{sgn}(e_k) - \alpha_2 \operatorname{sgn}(\Delta e_k) \tag{6.16}$$

For $\tau_c \to 0$, the controller (6.16) constitutes a second order real sliding algorithm [Levant, 1993]. Yet interesting, the controller (6.16) asserts significant requirements to the choice of position sensor in order to work properly. For a pure analogue sensor measurement, a change in Δe_k can be detected regardless of the sample interval τ_c. However, in the situation when the measurement is *discrete in state*, i.e. the sensor resolution in finite with a minimum detectable change $|x_{\mathrm{P}}|_{\min}$, then $\Delta x_{\mathrm{P},k}$ takes on values only if the change of $x_{\mathrm{P},k}$ exceeds $|x_{\mathrm{P}}|_{\min}$ within a sample step.

$$\Delta x_{\mathrm{P},k} = \begin{cases} \neq 0 & \text{for } |\dot{x}_{\mathrm{P}}| \geq \dfrac{|x_{\mathrm{P}}|_{\min}}{\tau_c} \\ 0 & \text{for } |\dot{x}_{\mathrm{P}}| < \dfrac{|x_{\mathrm{P}}|_{\min}}{\tau_c} \end{cases} \tag{6.17}$$

From (6.17) it is found that, in order for (6.16) to work properly, the sensor resolution must be chosen sufficiently high, such that a *small* τ_c will not deteriorate performance. In turn, with τ_c too small, the sliding performance will result in limit cycle behavior on the target $e, \dot{e} = 0$.

6.2.2 Direct Application

The direct application of the TA controller poses a problem similar to that of e.g. the relay controller. Consider now such a controller given by (6.18).

$$\bar{u}_{\mathrm{v}} = \dot{x}_{\mathrm{R}} - \alpha_1 \operatorname{sgn}\left(\int_t e \mathrm{d}t\right) - \alpha_2 \operatorname{sgn}(e) \tag{6.18}$$

In the event that the system (3.41) is closed by (6.18), chattering of the control is inherent, and boundary layers are necessary in order to achieve satisfactory performance. Application of e.g. the boundary layer approach (4.31), will expand the zero set to some vicinity of the second order sliding constraint $\int_t e \mathrm{d}t, e = 0$, defined by $|\alpha_1 \operatorname{sat}(\int_t e \mathrm{d}t) - \alpha_2 \operatorname{sat}(e)|$. Within this vicinity, the control (6.18) is essentially a PI controller, and the parameters that guarantee convergence of $\int_t e \mathrm{d}t, e$ to this vicinity do not necessarily guarantee convergence to $\int_t e \mathrm{d}t, e = 0$ within this vicinity. Hence, an instability mode may occur near the origin. However, for a boundary layer sufficiently large, a globally stable closed loop system may be achieved. The convergence properties may be improved similar to the relay controller (5.4) with the power rate reaching law, resulting in the control (6.19).

$$\bar{u}_{\mathrm{v}} = \dot{x}_R - (\delta |e|^{\gamma} + \alpha_2) \left(\alpha_1 \alpha_2^{-1} \operatorname{sat}\left(\int_t e \mathrm{d}t\right) + \operatorname{sat}(e) \right), \quad 1 > \gamma > 0, \;\; \delta > 0 \tag{6.19}$$

6.3 Super Twisting Controller

Another approach to second order sliding mode control may be realized by utilization of the super twisting algorithm (STA) [Emelyanov et al., 1990], [Levant, 1993]. This controller is rather different from the controllers based on the prescribed convergence- and twisting algorithms in the sense,

that it provides for a second order sliding mode on some control constraint *and* its derivative, using only the constraint itself as feedback. Hence, the application of the STA for output feedback control is of significant interest in regard to the objective of this project.

6.3.1 Application for Output Feedback Control

Consider again the system (3.41) with output function $e = x_P - x_R$, assume the same conditions satisfied as in Section 6.2, and consider furthermore a controller based on the STA given by (6.20).

$$\bar{u}_{\mathrm{v}} = \dot{x}_{\mathrm{R}} - \lambda\sqrt{|e|}\,\mathrm{sgn}(e) - \alpha\int_t \mathrm{sgn}(e)\mathrm{d}t \tag{6.20}$$

The closed loop system is analyzed combining the derivative of the closed loop system (3.41), $e = x_P - x_R$, (6.20) at some intersection $e \neq 0$, given by (6.21).

$$\ddot{e} = \dot{F}(\mathbf{x}) + \dot{\bar{u}}_{\mathrm{v}} - \ddot{x}_{\mathrm{R}} = \dot{F}(\mathbf{x}) - \frac{\lambda}{2}\frac{\dot{e}}{\sqrt{|e|}} - \alpha\,\mathrm{sgn}(e) \quad \Rightarrow \tag{6.21}$$

$$\ddot{e} \in [-\bar{C},\bar{C}] - \frac{\lambda}{2}\frac{\dot{e}}{\sqrt{|e|}} - \alpha\,\mathrm{sgn}(e) \tag{6.22}$$

In order to verify convergence of the states $e, \dot{e}$, consider now a conservative analysis of the closed loop system, based on figure (6.2) (similar to the *majorant curve* approach [Davila et al., 2005]).

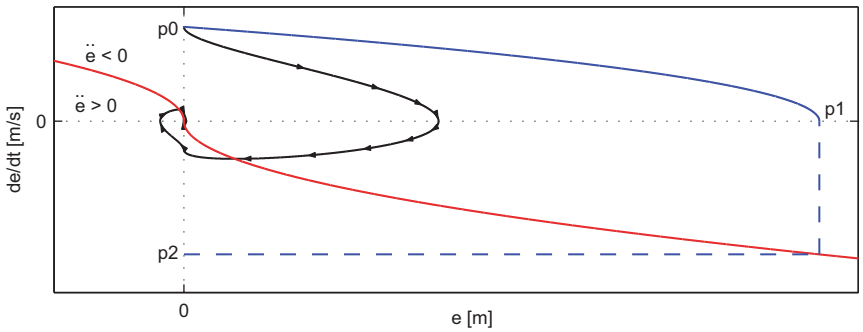

Figure 6.2: *Phase portrait for closed loop system* (6.21)*. The red graph indicates the deflection tangent* $\ddot{e} = 0$*, the black line a stable trajectory and the blue solid line the trajectory resulting from only the term* $\alpha\,\mathrm{sgn}(e)$ *for initial conditions at point* $p1$*.*

Consider the situation with initial conditions $(e(0),\dot{e}(0)) = (0,\dot{e}_{\mathrm{p0}})$, similar to the analysis of the TA type controller above. Note from (6.21), that the deflection tangent $\ddot{e} = 0$ separates the state space into two parts as depicted in figure 6.2. Hence, if $\alpha > \bar{C}$, then from the initial condition, the state trajectory will set off into the first quadrant, in the direction of the fourth quadrant, regardless of the magnitude of $(\lambda\dot{e})/(2\sqrt{|e|})$. However, as both terms of the right hand side of (6.21) are negative, then the state trajectory is indeed confined within the trajectory resulting from $\alpha\,\mathrm{sgn}(e)$ as depicted in figure 6.2. Noting this, denoting $\Gamma = \alpha - \bar{C}$ and assuming that $\alpha\dot{F}(\mathbf{x}) < 0$, $|\dot{F}(\mathbf{x})| = \bar{C}$ is always satisfied, obtain a *conservative* estimate of the first intersection with the e-axis, from the trajectory resulting from $\ddot{e} = \dot{F}(\mathbf{x}) - \alpha\,\mathrm{sgn}(e)$, by separation of variables, again using the identity

$\ddot{e} = (\mathrm{d}\dot{e}\mathrm{d}e)/(\mathrm{d}e\mathrm{d}t) = (\mathrm{d}\dot{e})/(\mathrm{d}e)\dot{e}$ as (6.23).

$$\int_0^{e_{\mathrm{p1}}} \Gamma \mathrm{d}e = -\int_{\dot{e}_{\mathrm{p0}}}^{0} \dot{e}\mathrm{d}\dot{e} \quad \Rightarrow \quad e_{\mathrm{p1}} = \frac{1}{2}\frac{\dot{e}_{\mathrm{p0}}^2}{\Gamma} \tag{6.23}$$

Using this and the deflection tangent, obtain the worst case intersection $\dot{e}_{\mathrm{p2}}$ as (6.24) (notion the assumption $\alpha\dot{F}(\mathbf{x}) < 0$).

$$\dot{e}_{\mathrm{p2}} = -\frac{2}{\lambda}\sqrt{|e_{\mathrm{p1}}|\Gamma} = -\frac{2}{\lambda}\sqrt{\left|\frac{1}{2}\frac{\dot{e}_{\mathrm{p0}}^2}{\Gamma}\right|\Gamma} = -\frac{\sqrt{2\Gamma}}{\lambda}\dot{e}_{\mathrm{p0}} \tag{6.24}$$

Using again the criterion for convergence of $\dot{e}$ by intersection of axes, given by $|\dot{e}_{\mathrm{p0}}| > |\dot{e}_{\mathrm{p2}}|$, obtain the convergence criterion (6.25).

$$\frac{|\dot{e}_{\mathrm{p2}}|}{|\dot{e}_{\mathrm{p0}}|} = \frac{\sqrt{2\Gamma}}{\lambda} < 1 \quad \Rightarrow \quad \lambda > \sqrt{2\Gamma} \tag{6.25}$$

In [Fridman et al., 2012] an appropriate choice of parameters was proposed as (6.26), which satisfies (6.25).

$$\lambda = 1.5\sqrt{\bar{C}}, \;\; \alpha = 1.1\bar{C} \tag{6.26}$$

Hence, the controller (6.20) with parameters (6.26) provides for a second order sliding mode output feedback controller for the system (3.41), $e = x_P - x_R$ with only a single tuning parameter.

6.3.2 Extension with Boundary Layer

Even though the controller (6.20), (6.26) appears highly attractive in the context of the objective of this work, the dynamic characteristics of the valve may deteriorate controller performance as discussed in Section 4.4.1. Hence, the obvious modification is the extension with the boundary layer approach (4.31), replacing the sgn-function with a sat-function. As discussed previously, this causes a partial loss of robustness and restricts guaranteed convergence to a vicinity of the origin $(e, \dot{e}) = (0, 0)$, but may improve the overall performance. This introduces an additional parameter in terms of the boundary layer thickness, but this may be easily tuned based on the *desired* control precision.

6.4 Experimental Results

In the following, results of implementation of the controllers are presented. A complete list of controller parameters applied can be found in the Appendix.

6.4.1 Prescribed Convergence Controller (Direct Application) (PCA)

The prescribed convergence type controller (6.7) has been implemented experimentally using the same controller parameters as the linear surface type controller (5.8) (also the boundary layer), with the parameter $\gamma = 0.875$. The results are shown in figure 6.3, and from figures 6.3 (A)-(F) it is found that this controller closely tracks the trajectory, similar to e.g. the controller (5.8), and that chattering is absent.

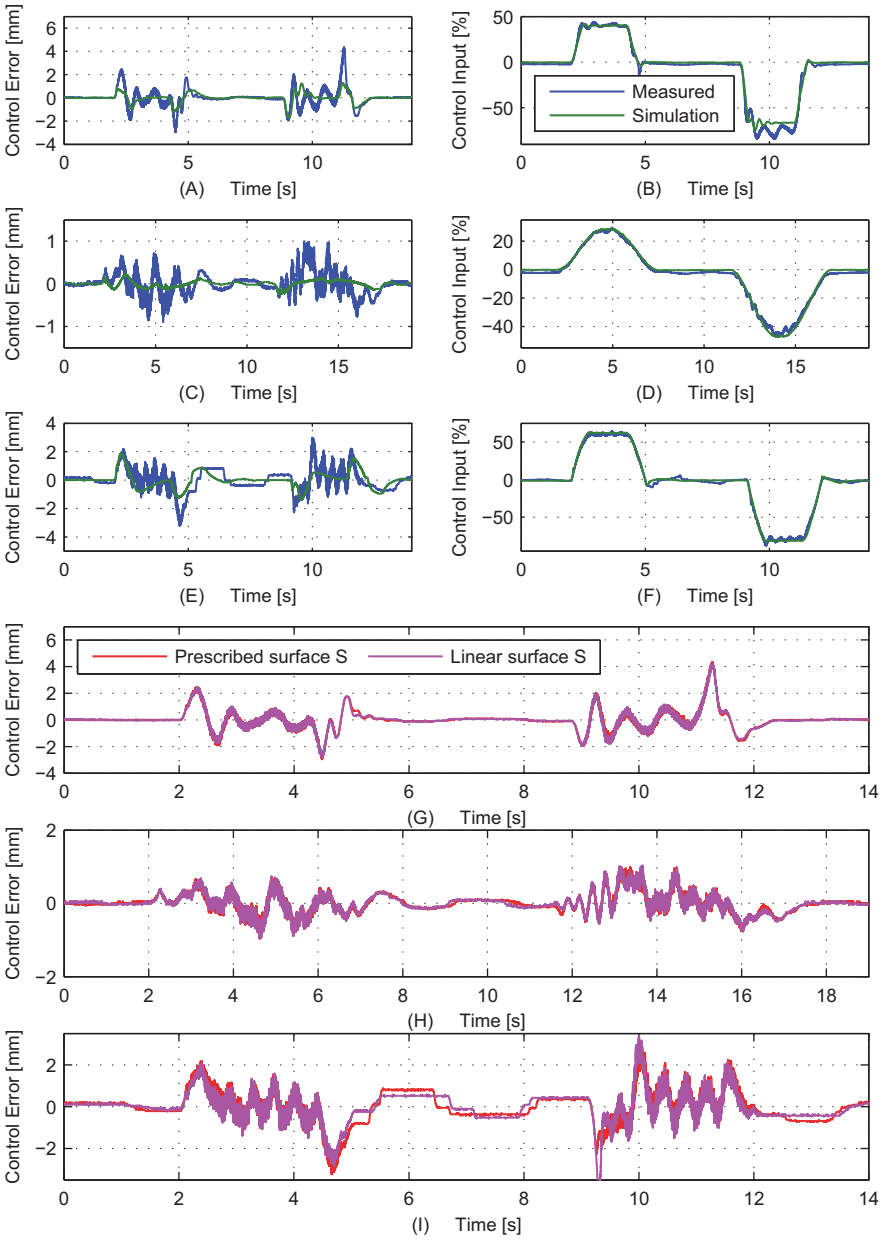

Figure 6.3: *Performance with application of the control* (6.7)*, and comparison with* (5.8)*. (A) Control tracking error for TC1. (B) Control input for application to TC1. (C) Control tracking error for TC2. (D) Control input for application to TC2. (E) Control tracking error for TC3. (F) Control input for application to TC3. (G) Control tracking error for TC1. (H) Control tracking error for TC2. (I) Control tracking error for TC3.*

However, from figures 6.3 (G)-(I), performance is somewhat similar to the linear surface type controller (5.8), and it is found that introduction of the surface (6.5) not significantly alters performance.

An initiative to improve performance by reducing γ, caused the closed loop system to be prone to oscillations. Hence, it is found that introduction of the surface (6.5) does not provide any relevant improvement of performance compared to the linear surface counterpart, but merely complicates the parameter design.

6.4.2 Twisting Controller (Direct Application) (TA)

The controller based on the twisting controller (6.19) has been implemented with identical boundary layers, in order to maintain tuning parameters at a minimum. The boundary layers applied are $\varphi_b = 4$ $[mm]$ for test cases TC1, TC3 and $\varphi_b = 3$ $[mm]$ for TC2. The results are shown in figure 6.4.

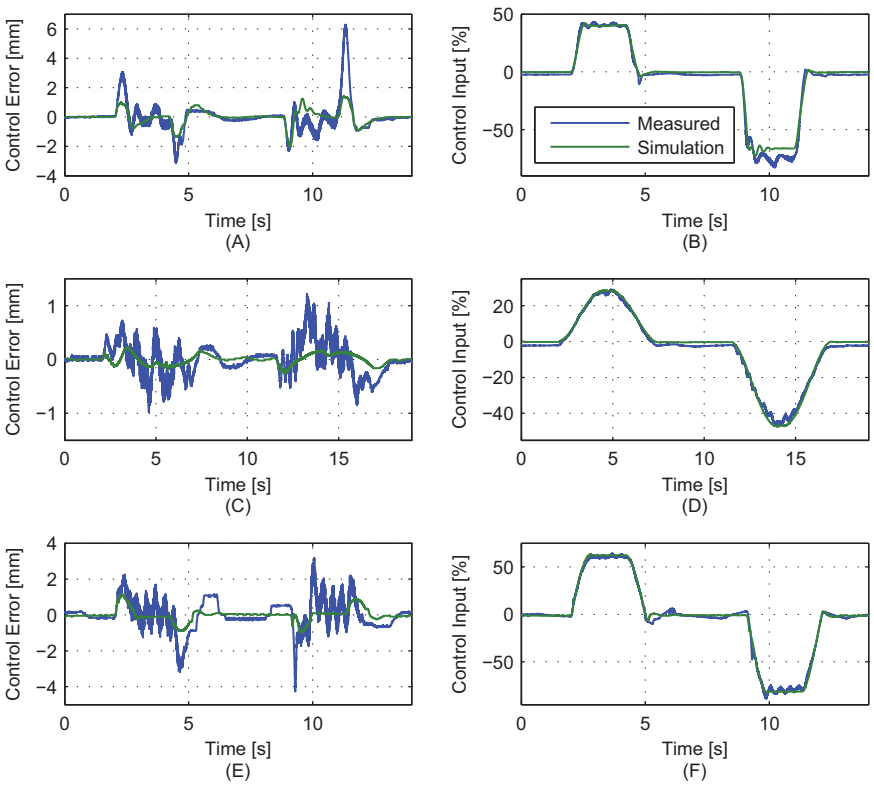

Figure 6.4: *Performance with application of the control* (6.19)*. (A) Control tracking error for TC1. (B) Control input for application to TC1. (C) Control tracking error for TC2. (D) Control input for application to TC2. (E) Control tracking error for TC3. (F) Control input for application to TC3.*

From figure 6.4 it is found that a stable system is achieved for all test cases, and that convergence to the origin is achieved similar to a PI controller as expected. Furthermore, as for the controllers considered until this point, resonant modes of the vehicle / Axis 1 are excited. In all cases parameters $\alpha_1 = 2.1$, $\alpha_2 = 1$, $\gamma = 0.875$ were chosen, and only tuning of δ, α was carried out individually. The results do not differ significantly from those of the prescribed convergence controller, but this controller has a more simple mathematical structure, and may be more appropriate bearing in mind the objective of the project.

6.4.3 Super Twisting Controller (Direct Application) (STA)

The performance results of the direct implementation of the super twisting controller, with parameters tuned according to the rules (6.26), are depicted in figure 6.5. It is found that a *sliding mode* takes place on e, but appear as limit cycle-like behavior as discussed in Chapter 4, which is naturally undesirable.

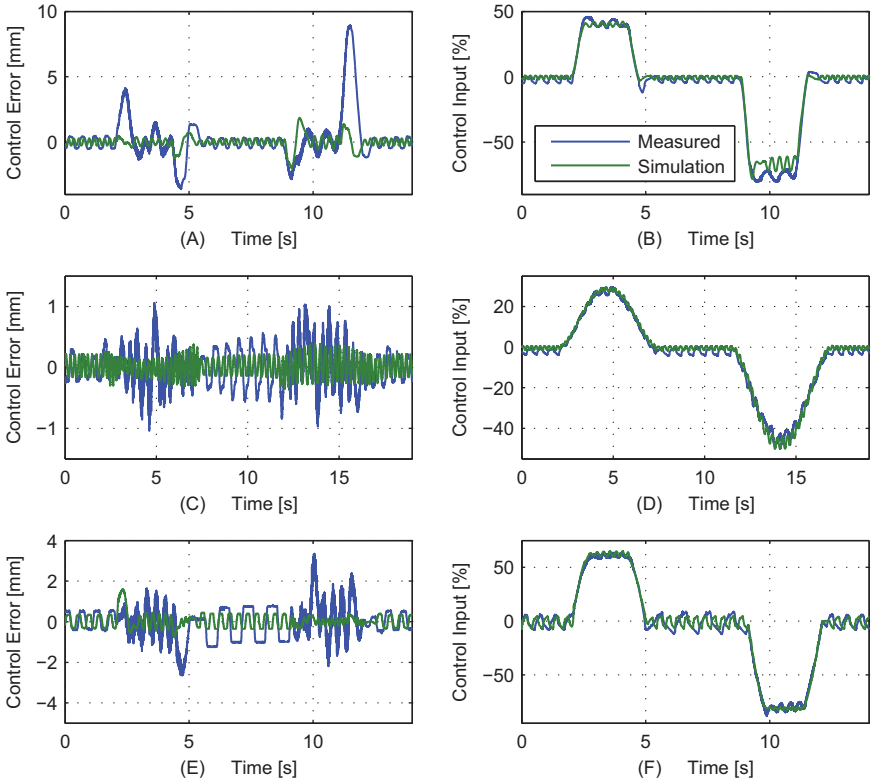

Figure 6.5: *Performance with application of the control* (6.20)*. (A) Control tracking error for TC1. (B) Control input for application to TC1. (C) Control tracking error for TC2. (D) Control input for application to TC2. (E) Control tracking error for TC3. (F) Control input for application to TC3.*

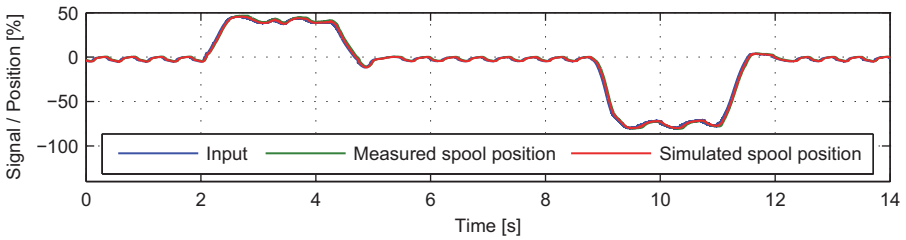

Figure 6.6: *Measured input, measured spool position, valve model output with measured input for TC1.*

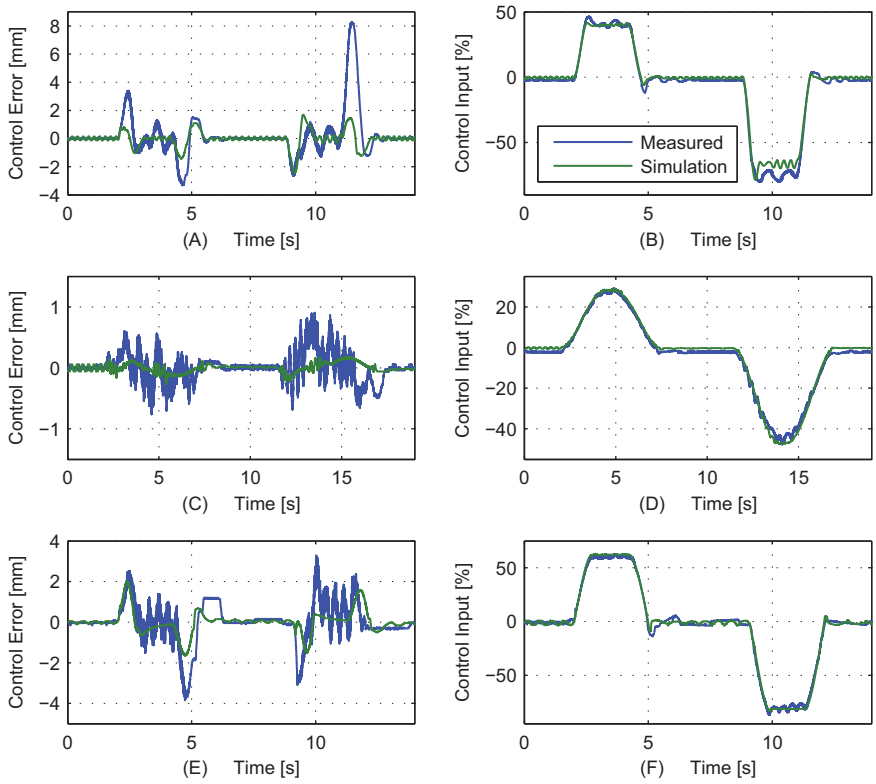

Figure 6.7: *Performance with application of the control* (6.20) *with a boundary layer of* $\varphi_b = 0.5$ *[mm]. (A) Control tracking error for TC1. (B) Control input for application to TC1. (C) Control tracking error for TC2. (D) Control input for application to TC2. (E) Control tracking error for TC3. (F) Control input for application to TC3.*

Also it is found that the oscillation frequency when implemented in the test bench is smaller than

that of the model, leading to the idea that the valve model may not represent the actual dynamics sufficiently in regard to this type of controls. However, comparing the valve model output with the measured input signal fed to the model, does not reveal significant differences between the modeled spool position and the measured spool position, which should lead to the observed difference in oscillation frequencies (see in figure 6.6). The main reason for the difference in oscillation frequencies is assumed to be inaccuracies in the modeled time delays and dynamics of sensors, inaccurate friction models- and static gains of the valves, hence the gain compensator.

6.4.4 Super Twisting Controller with Boundary Layer (STA-B)

Replacing the sgn-term of the STA controller would expectedly reduce oscillations of the output as discussed previously, with some loss of robustness. Application of a boundary layer of 0.5 [mm] to the algorithm leads to the results of figure 6.7 (with the same parameters as in the results of figure 6.5). It is worth noting that the boundary layer width is significantly smaller that those applied in controllers considered previously, and robustness is preserved *to a higher extend* than for these controllers. It is found that the implementation of this boundary layer significantly alters performance compared to the *conventional* STA controller, with maximum errors being on the level with the STA controller. Hence, with a boundary layer, the super twisting algorithm (STA-B) can be successfully applied for output feedback control.

6.5 Summary

Three of the most popular second order sliding algorithms were considered for application in control structures together with the gain compensator and velocity feed forward control. The controllers considered were the prescribed convergence algorithm (PCA), the twisting algorithm (TA) and the super twisting algorithm (STA).

These second order sliding mode controllers were considered in relation to application for chattering reduction, as well as their direct application in hydraulic control structures. In regard to the controllers based on the direct application of the prescribed convergence algorithm and the twisting algorithm, boundary layers were utilized in order to avoid control chattering. Furthermore, in order to improve convergence speed the power rate reaching law discussed previously was applied, similar to e.g. the relay controller in Chapter 5. With boundary layers implemented, the PCA and TA type controllers demonstrate satisfactory performance, however, with the usage of several parameters.

The controller based on the STA appears in general more intriguing due to the single tuning parameter (when using the proposed tuning guide line), however the presence of undesirable nonlinear characteristics of the valve dynamics, causes a limit cycle-like behavior of the control. These effects were effectively reduced by implementation of a (rather small) boundary layer, having the effect that a satisfactory performance can be achieved.

The performance of the considered controllers in terms of RMS- and maximum errors have been compared with the PI-AGC controller in figure 6.8. The main conclusion is that the second order controllers considered in this section, in general provide for improved tracking accuracy, in particular when low speed motion is required as in TC2. However, in high velocity applications and applications with strong friction phenomena no significant improvement of performance is evident. At least not when applied for output feedback control as considered here, and the additional tuning

effort required by the PCA- and TA type controllers (compared to the PI-AGC) does not yield a feasible usage of these controllers. However, the simple structures seem intriguing, and some of the elements may be applied in the development of controllers more applicable for the objective of this project.

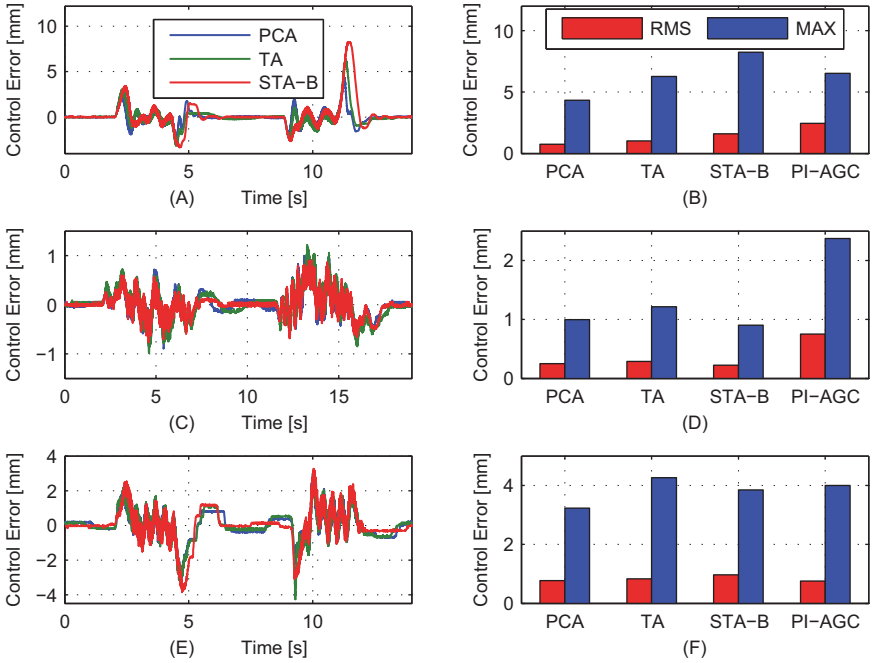

Figure 6.8: *Performance with application of controllers PCA, TA, STA-B, compared with the PI-AGC controller. (A) Control tracking errors for TC1. (B) RMS- and MAX control tracking errors for TC1. (C) Control tracking errors for TC2. (D) RMS- and MAX control tracking errors for TC2. (E) Control tracking errors for TC3. (F) RMS- and MAX control tracking errors for TC3.*

7 Finite-Time Continuous Approximations of Sliding Controls

Having studied selected second order sliding controllers, their main features and drawbacks in regard to application in hydraulic drives, some modifications are proposed in this chapter. In the following, homogeneous extensions of these second order sliding controllers are proposed allowing for absolutely continuous control inputs, which may prove more appropriate than the controls considered until this point.

7.1 Weighted Homogeneity & Finite-Time Convergence Properties

A system $f(\mathbf{e})$ is a homogenous function of degree ξ, if it satisfies (7.1).

$$f(\kappa\mathbf{e}) = \kappa^{\xi} f(\mathbf{e}) \ , \ \forall \mathbf{e} = (e_1, e_2, ..., e_n) \in \mathbb{R}^n, \ 0 < \forall \kappa \in \mathbb{R} \tag{7.1}$$

A system $f(\mathbf{e})$ satisfying (7.1) is considered scale invariant, i.e. it holds the property that it does not change if variables within the system are multiplied by the same e.g. constant, and is as such a structure preserving property. From a geometrical point of view this means that the *shape* of the system in the state space is preserved if the system states are *uniformly* scaled. The more formal notion of this is, that a system satisfying (7.1) is said to be homogenous of degree ξ with respect to the dilation (7.2).

$$d_\kappa : \mathbf{e} \mapsto \kappa^{\xi}\mathbf{e} \tag{7.2}$$

The concept of weighted homogeneity is an extension of the homogeneity property above, and turns out to have an intriguing relevance in relation to control systems, as will be clear in the following. For this situation, the common factor κ is assigned different weights for the different states, and the dilation (transformation) is extended to (7.3).

$$d^r_\kappa : (e_1, e_2, ..., e_n) \mapsto (\kappa^{r_1} e_1, \kappa^{r_2} e_2, ..., \kappa^{r_n} e_n), \ \forall \kappa, r_i > 0, \ i = 1, 2, ..., n \tag{7.3}$$

Then a system $f(\mathbf{e}) : \mathbb{R}^n \to \mathbb{R}^n$ is said to be d^r-homogeneous of degree ξ with respect to the dilation (7.3), if each component f_i is d^r-homogeneous of degree $\xi + r_i$, meaning that it satisfies (7.4) [Bacciotti and Rosier, 2005].

$$f_i(\kappa^{r_1} e_1, \kappa^{r_2} e_2, ..., \kappa^{r_n} e_n) = \kappa^{\xi + r_i} f_i(e_1, e_2, ..., e_n), \ 0 < \forall \kappa \in \mathbb{R}, \ i = 1, 2, ..., n \tag{7.4}$$

This leads to the main property of interest, that if the system $f(\mathbf{e}) : \mathbb{R}^n \to \mathbb{R}^n$ satisfies (7.4), then a stable origin $(e_1, e_2, ..., e_n) = (0, 0, ..., 0)$ is stable in finite time, based on Theorem 1.

Theorem 1 *[Bhat and Bernstein, 1997]*
The origin $(e_1,e_2,...,e_n)=(0,0,...,0)$ *is a finite-time stable equilibrium of* $f(\boldsymbol{e})$, $\boldsymbol{e}=(e_1,e_2,...,e_n)$ *if and only if the origin is an asymptotically stable equilibrium of* $f(\boldsymbol{e})$ *and* $\xi<0$.

The finite-time stability property implies faster convergence, and some kind of robustness property, even though it may not be invariant with respect to parameter uncertainties and bounded disturbances as sliding controls. However, in light of the dynamical features of hydraulic valves discussed in Section 4.4.1 and the possible limit cycle oscillations resulting from this, finite-time convergent continuous controls may offer a more reasonable compromise between robustness and performance compared to sliding mode controls.

In the sequel finite-time convergent continuous controls are developed, taking their offset in some of the sliding algorithms considered in previous chapters. The controllers developed in this chapter are based on the simple representation (2.98) (with gain compensation), representable for a hydraulic drive in some limited frequency range below its natural frequency.

7.2 Modified Relay Control

Consider the scalar system with the parameter bound assumption (7.5), and the output function $e=x_P-x_R$.

$$\dot{x}_{\mathrm{P}}=\rho(\mathbf{x})\bar{u}_{\mathrm{v}},\ \ 0<K_{\mathrm{m}}\leq\rho(\mathbf{x})\leq K_{\mathrm{M}} \tag{7.5}$$

Extend the simply relay controller with velocity feedforward (5.4) to (7.6).

$$\bar{u}_{\mathrm{v}}=\dot{x}_{\mathrm{R}}-\alpha|e|^{\gamma}\mathrm{sgn}(e)\ ,\ \ 1>\gamma>0,\ \alpha>0 \tag{7.6}$$

The resulting closed loop system is then given by (7.7).

$$\dot{e}=-\alpha|e|^{\gamma}\mathrm{sgn}(e) \tag{7.7}$$

From (7.7), $e=0$ is asymptotically stable as $e\dot{e}<0,\ \ \forall e\neq 0$. The convergence time t_{s} is found by separation of variables similar to the process in Section 4.3 as (7.9), with initial conditions $e(0)$ and $t_0=0$.

$$\dot{e}=\frac{\mathrm{d}e}{\mathrm{d}t}=-\alpha|e|^{\gamma}\mathrm{sgn}(e)\ \ \Rightarrow\ \ \mathrm{d}t=-\frac{1}{|e|^{\gamma}\mathrm{sgn}(e)}\mathrm{d}e\ \ \Rightarrow \tag{7.8}$$

$$\int_0^{t_{\mathrm{s}}}\mathrm{d}t=-\int_{e(0)}^{0}\frac{1}{\alpha|e|^{\gamma}\mathrm{sgn}(e)}\mathrm{d}e\ \ \Rightarrow\ \ t_{\mathrm{s}}=\frac{1}{\alpha(1-\gamma)}|e(0)|^{1-\gamma} \tag{7.9}$$

Evidently, from (7.9), the convergence time $t_{\mathrm{s}}<0$ by virtue of $\gamma<1$, and may be considered a finite-time *proportional* controller. Considering the entire frequency range, i.e. taking into account that $F(\mathbf{x})\neq 0$ and bounded by $|F(\mathbf{x})|\leq\bar{C}$, then from the above analysis, precision can only be guaranteed to a vicinity of the origin bounded by $|e|=(\bar{C}/\alpha)^{\gamma^{-1}}$.

7.3 Modified Twisting Controller

Consider again the controller (6.8) based on the twisting algorithm with velocity feedforward, and the system (7.5) with output function $\int_t e\mathrm{d}t$. Modifying the control (6.8) similarly to the relay

control in the previous section, obtain the continuous controller (7.10), denoting the closed loop state vector $\mathbf{e} = (\int_t e dt, e) = (e_1, e_2)$.

$$\bar{u}_v = \dot{x}_R - \alpha_1 |e_1|^{\gamma_1} \operatorname{sgn}(e_1) - \alpha_2 |e_2|^{\gamma_2} \operatorname{sgn}(e_2) \ , \ \ 1 > \gamma_1, \gamma_2 > 0, \ \alpha_1, \alpha_2 > 0 \tag{7.10}$$

By examination of the limits for the exponents γ_1, γ_2, obtain (7.11), being coincident either with the second order sliding mode controller (6.8), or a conventional linear PI controller with velocity feed forward.

$$\lim_{\gamma_1, \gamma_2 \to 0} \bar{u}_v = \dot{x}_R - \alpha_1 \operatorname{sgn}(e_1) - \alpha_2 \operatorname{sgn}(e_2) \quad , \quad \lim_{\gamma_1, \gamma_2 \to 1} \bar{u}_v = \dot{x}_R - \alpha_1 e_1 - \alpha_2 e_2 \tag{7.11}$$

The closed loop system under consideration may be represented by the state space representation (7.12), assuming that $\rho(\mathbf{x}) \approx 1$.

$$\begin{bmatrix} f_1(\mathbf{e}) \\ f_2(\mathbf{e}) \end{bmatrix} = \begin{bmatrix} \dot{e}_1 \\ \dot{e}_2 \end{bmatrix} = \begin{bmatrix} e_2 \\ -\alpha_1 |e_1|^{\gamma_1} \operatorname{sgn}(e_1) - \alpha_2 |e_2|^{\gamma_2} \operatorname{sgn}(e_2) \end{bmatrix} \tag{7.12}$$

Consider a radially unbounded positive definite Lyapunov-like function and its derivative, given by (7.13).

$$V(e_1, e_2) = \frac{1}{2} e_2^2 + \frac{\alpha_1}{1+\gamma_1} |e_1|^{\gamma_1 + 1} \quad , \quad \dot{V}(e_1, e_2) = e_2 \dot{e}_2 + \alpha_1 |e_1|^{\gamma_1} e_2 \operatorname{sgn}(e_1) \tag{7.13}$$

Substituting $\dot{e}_2$ of (7.12) into $\dot{V}$, obtain (7.14).

$$\dot{V}(e_1, e_2) = -\alpha_2 |e_2|^{\gamma_2 + 1} \tag{7.14}$$

From (7.14) $\dot{V}$ is only negative semi-definite, however the system is stable in the sense of Lyapunov, and the states are bounded. Consider the time derivative of $\dot{V}_2(e_1, e_2)$ given by (7.17).

$$\ddot{V}(e_1, e_2) = -\alpha_2(\gamma_2 + 1)|e_2|^{\gamma_2} \operatorname{sgn}(e_2) \dot{e}_2 \tag{7.15}$$

$$= \alpha_2(\gamma_2 + 1)|e_2|^{\gamma_2} \operatorname{sgn}(e_2)(\alpha_1 |e_1|^{\gamma_1} \operatorname{sgn}(e_1) + \alpha_2 |e_2|^{\gamma_2} \operatorname{sgn}(e_2)) \tag{7.16}$$

$$\sim \pm \alpha_1 \alpha_2 (\gamma_2 + 1)|e_2|^{\gamma_2} |e_1|^{\gamma_1} + \alpha_2^2 (\gamma_2 + 1)|e_2|^{2\gamma_2} \tag{7.17}$$

From (7.17) it is found that $\ddot{V}$ is bounded, hence uniformly continuous, and Barbalat' Lemma [Slotine and Li, 1991] implies that $e_2 \to 0$, i.e. that $e \to 0$, for $t \to \infty$. However, it cannot be concluded that the origin $(e_1, e_2) = (0, 0)$ is asymptotically stable. However, assume for now that this is the case.

7.3.1 Finite-Time Convergence Conditions

In order to establish finite-time convergence conditions for the closed loop system (7.12), the homogeneity considerations discussed in Section 7.1 are utilized. It turns out that the closed loop system (7.12) is homogeneous of degree $\xi = -1 \ \forall \ \delta > 1, \kappa > 0$ provided that weights are chosen as $r_1 = \delta + 1, r_2 = \delta$, and controller exponents as (7.18).

$$\gamma_1 = \frac{\delta - 1}{\delta + 1} \quad , \quad \gamma_2 = \frac{\delta - 1}{\delta} \tag{7.18}$$

This statement becomes evident from the following considerations. Consider $\dot{e}_1$ of (7.12), and obtain the degree (7.20).

$$f_1(d_\kappa^r \mathbf{e}) = f_1(\kappa^{\delta+1} e_1, \kappa^\delta e_2) = \kappa^\delta e_2 = \kappa^\delta f_1(\mathbf{e}) \ \Rightarrow \tag{7.19}$$

$$\xi + r_1 = \xi + \delta + 1 = \delta \ \Rightarrow \ \xi = -1 \tag{7.20}$$

Regarding the second component $\dot{e}_2$ of (7.12), obtain (7.21).

$$\begin{aligned} f_2(d^r_\kappa \mathbf{e}) =& -\alpha_1 |\kappa^{\delta+1} e_1|^{\gamma_1} \operatorname{sgn}(\kappa^{\delta+1} e_1) \alpha_2 |\kappa^{\delta} e_2|^{\gamma_2} \operatorname{sgn}(\kappa^{\delta} e_2) \\ =& -\alpha_1 \kappa^{(\delta+1)\gamma_1} |e_1|^{\gamma_1} \operatorname{sgn}(e_1) - \alpha_2 \kappa^{\delta\gamma_2} |e_2|^{\gamma_2} \operatorname{sgn}(e_2) \end{aligned} \tag{7.21}$$

Substituting (7.18) into (7.21), obtain (7.22).

$$\begin{aligned} f_2(d^r_\kappa \mathbf{e}) =& -\alpha_1 \kappa^{\frac{(\delta+1)(\delta-1)}{\delta+1}} |e_1|^{\gamma_1} \operatorname{sgn}(e_1) - \alpha_2 \kappa^{\frac{\delta(\delta-1)}{\delta}} |e_2|^{\gamma_2} \operatorname{sgn}(e_2) \\ =& -\alpha_1 \kappa^{\delta-1} |e_1|^{\gamma_1} \operatorname{sgn}(e_1) - \alpha_2 \kappa^{\delta-1} |e_2|^{\gamma_2} \operatorname{sgn}(e_2) \\ =& -\kappa^{\delta-1} (\alpha_1 |e_1|^{\gamma_1} \operatorname{sgn}(e_1) + \alpha_2 |e_2|^{\gamma_2} \operatorname{sgn}(e_2)) \\ =& \kappa^{\delta-1} f_2(\mathbf{e}) \end{aligned} \tag{7.22}$$

Using (7.22), obtain the homogeneity degree (7.23).

$$\xi + r_2 = \xi + \delta = \delta - 1 \;\; \Rightarrow \xi = -1 \tag{7.23}$$

From (7.20), (7.23) it is found that the closed loop system (7.12) is d^r-homogeneous of degree $\xi = -1$ for $r_1 = \delta + 1, r_2 = \delta, \delta > 0$, and (7.18) satisfied. Hence, according to Theorem 1, the origin $(e_1, e_2) = (0,0)$ of the system (7.12) is finite-time asymptotically stable, if the origin is an asymptotically stable equilibrium. With (7.18) satisfied, the tuning parameters have been reduced by one, which is useful in further considerations on the stability of the origin, and this problem is reduced to an investigation of how parameters $\gamma_1,\ \gamma_2$ influences stability. This leads to the possible scenarios (7.24).

$$2\alpha_2 > \alpha_1 > \alpha_2 \quad , \quad 2\alpha_1 > \alpha_2 > \alpha_1 \quad , \quad \alpha_1 > 2\alpha_2 \quad , \quad \alpha_2 > 2\alpha_1 \quad , \quad \alpha_1 = \alpha_2 \tag{7.24}$$

Utilizing the state space representation (7.12), the phase portrait for each possible scenario (7.24) may be established as depicted in figure 7.1, indicating that the origin $(e_1, e_2) = (0,0)$ is globally asymptotically stable for all five parameter scenarios. Besides providing information on stability, the phase portraits of figure 7.1 also provide some relevant information on the convergence properties. Figure 7.1 (D) and (E) suggest that for $\alpha_1 > \alpha_2$, the state trajectory continuously encircles the origin, implying an oscillatory (yet stable) trajectory. On the other hand figure 7.1 (A), (B) and (C) implies that for $\alpha_1 = \alpha_2$ and $\alpha_1 < \alpha_2$ oscillation during transient stages may be limited. These observations are further supported by the responses of figure 7.2, when implemented in a pure integral system (ideal system). However, from figure 7.2 it is also observed that convergence time is increased for parameters $\alpha_1 = \alpha_2$ and $\alpha_1 < \alpha_2$ compared to parameters $\alpha_1 > \alpha_2$.

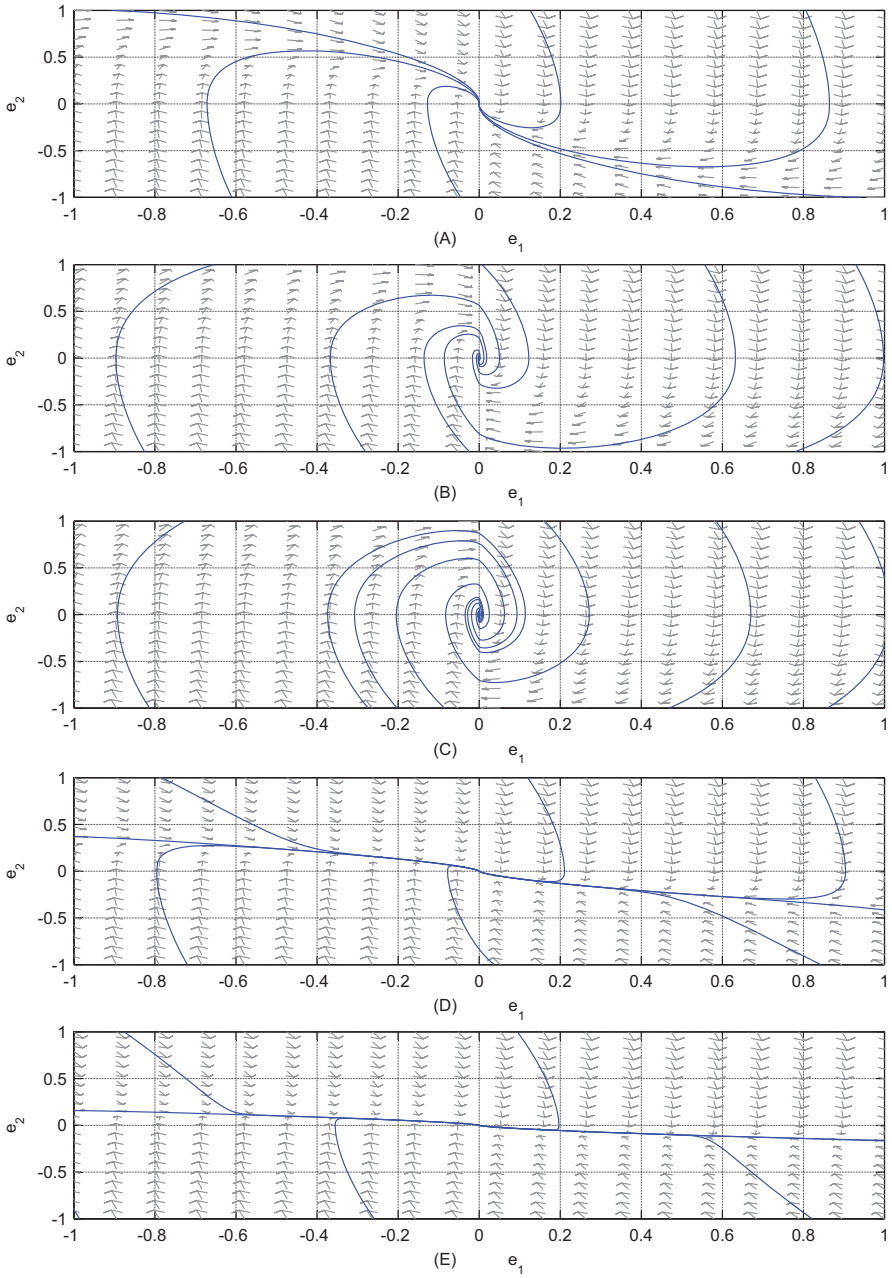

Figure 7.1: *Phase portraits of the closed loop system* (6.8), (7.10), $\rho(\boldsymbol{x}) = 1$. *In all cases* $\delta = 3$. *(A) Parameters:* $\alpha_1 = 5$, $\alpha_2 = 5$. *(B) Parameters:* $\alpha_1 = 3$, $\alpha_2 = 5$. *(C) Parameters:* $\alpha_1 = 2$, $\alpha_2 = 5$. *(D) Parameters:* $\alpha_1 = 5$, $\alpha_2 = 3$. *(E) Parameters:* $\alpha_1 = 5$, $\alpha_2 = 2$.

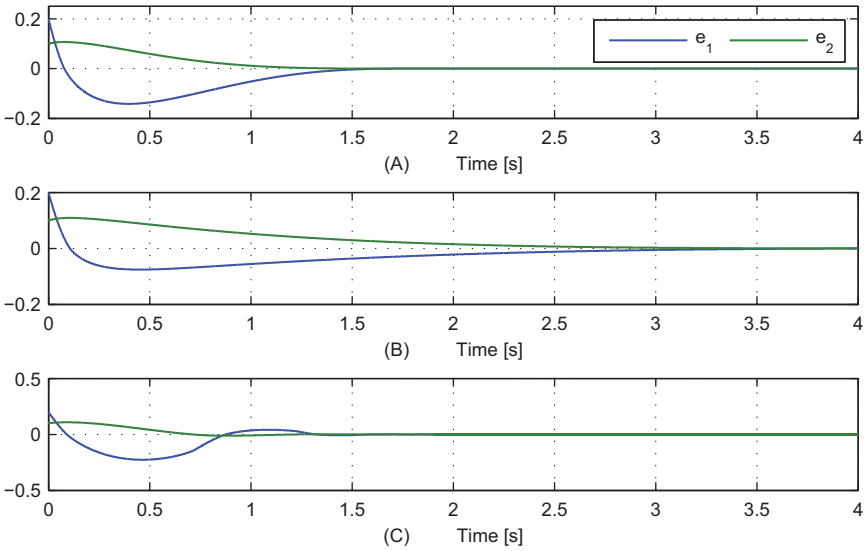

Figure 7.2: *State trajectories for the closed loop system* (6.8), (7.10), $\rho(\boldsymbol{x}) = 1$ *and simulation time step* $T_{sim} = 1e-4$ *[s]. In all cases* $\delta = 3$. *(A) Trajectory for* $\alpha_1 = \alpha_2 = 5$. *(B) Trajectory for* $\alpha_1 = 3$, $\alpha_2 = 5$. *(C) Trajectory for* $\alpha_1 = 5$, $\alpha_2 = 3$.

The finite time convergence properties imply that, after convergence to $(e_1, e_2) = (0,0)$, motion of the states e_1, e_2 should consist of Filippov sense trajectories. This reasoning is confirmed by considering e.g. the states of figure 7.2 (C), after convergence which are depicted in figure 7.3. Here the amplitude of the *oscillations* on $e_1 = 0$, $e_2 = 0$ would vanish for $T_{\text{sim}} \to 0$.

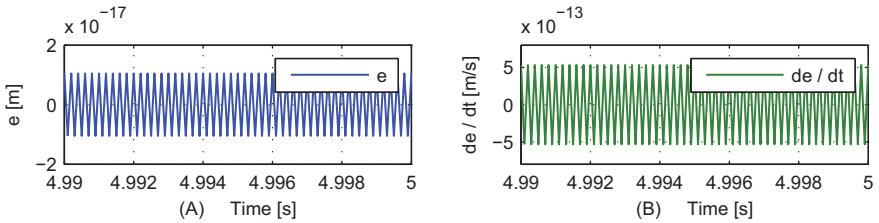

Figure 7.3: *Zoom of figure 7.2. (A) The state* e_1. *(B) The state* e_2.

Note furthermore from the limits (7.25), that the homogeneous controller (7.10), (7.18) is coincident with the second order sliding controller (6.8) or a linear controller. Hence the controller (7.10), (7.18) proves to be a rather versatile control structure, and the parameter δ may be regarded as a *robustness* parameter.

$$\lim_{\delta \to 1} \bar{u}_{\text{v}} = \dot{x}_{\text{R}} - \alpha_1 \operatorname{sgn}(e_1) - \alpha_2 \operatorname{sgn}(e_2) \quad , \quad \lim_{\delta \to \infty} \bar{u}_{\text{v}} = \dot{x}_{\text{R}} - \alpha_1 e_1 - \alpha_2 e_2 \tag{7.25}$$

7.4 Modified Super Twisting Controller

Based on ideas somewhat similar to those of the previous section, a finite-time convergent controller based on the super twisting algorithm (STA) is now developed. The development is again based on the model (7.5), but with output function $e = x_{\mathrm{P}} - x_{\mathrm{R}}$. Taking its offset in the controller (6.20), consider now a modified version of this, given by (7.26).

$$\bar{u}_{\mathrm{v}} = \dot{x}_{\mathrm{R}} - \lambda |e|^{\gamma_1} \operatorname{sgn}(e) - \alpha \int_t |e|^{\gamma_2} \operatorname{sgn}(e) \mathrm{d}t, \;\; 1 > \gamma_1, \gamma_2 > 0, \; \lambda, \alpha > 0 \tag{7.26}$$

To analyze the properties of this controller, consider the time derivative of the closed system (7.5), (7.26) assuming $\rho(\mathbf{x}) \approx 1$, given by (7.27).

$$\ddot{e} = \ddot{x}_{\mathrm{P}} - \ddot{x}_{\mathrm{R}} = \bar{u}_{\mathrm{v}} - \ddot{x}_{\mathrm{R}} = -\lambda \gamma_1 \dot{e} |e|^{\gamma_1 - 1} - \alpha |e|^{\gamma_2} \operatorname{sgn}(e) \tag{7.27}$$

The analysis of the closed loop system (7.27) is initiated by homogeneity reasoning, as this proves useful in the stability analysis.

7.4.1 Homogeneity Considerations

This subsection is devoted solely to homogeneity considerations in regard to the closed loop system (7.27). Denote the closed loop state vector $\mathbf{e} = (e, \dot{e}) = (e_1, e_2)$, and consider the state space representation of the closed loop system (7.28).

$$\begin{bmatrix} f_1(\mathbf{e}) \\ f_2(\mathbf{e}) \end{bmatrix} = \begin{bmatrix} \dot{e}_1 \\ \dot{e}_2 \end{bmatrix} = \begin{bmatrix} e_2 \\ -\lambda \gamma_1 \dot{e} |e|^{\gamma_1 - 1} - \alpha |e|^{\gamma_2} \operatorname{sgn}(e) \end{bmatrix} \tag{7.28}$$

As it will be shown in the following, the closed loop system (7.28) is homogeneous of degree $\xi = -1 \; \forall \; \delta > 1$ provided that weights are chosen as $r_1 = \delta + 1, r_2 = \delta$, and controller exponents as (7.29).

$$\gamma_1 = \frac{\delta}{\delta + 1} \; , \; \gamma_2 = \frac{\delta - 1}{\delta + 1} \tag{7.29}$$

Consider first f_1 of (7.28), and obtain the homogeneity degree (7.31).

$$f_1(d_\kappa^r \mathbf{e}) = \kappa^\delta e_2 = \kappa^\delta f_1(\mathbf{e}) \;\; \Rightarrow \tag{7.30}$$

$$\xi + r_1 = \xi + \delta + 1 = \delta \;\; \Rightarrow \xi = -1 \tag{7.31}$$

Turning the attention to the second component f_2 of (7.28), then using (7.29), obtain (7.32).

$$\begin{aligned} f_2(d_\kappa \mathbf{e}) &= -\gamma_1 \lambda \kappa^\delta e_2 |\kappa^{\delta+1} e_1|^{\gamma_1 - 1} - \alpha |\kappa^{\delta+1} e_1|^{\gamma_2} \operatorname{sgn}(\kappa^{\delta+1} e_1) \\ &= -\gamma_1 \lambda \kappa^\delta \kappa^{(\delta+1)(\gamma_1 - 1)} e_2 |e_1|^{\gamma_1 - 1} - \alpha \kappa^{(\delta+1)\gamma_2} |e_1|^{\gamma_2} \operatorname{sgn}(\kappa^{\delta+1} e_1) \\ &= -\gamma_1 \lambda \kappa^{\delta + (\delta+1)(\gamma_1 - 1)} e_2 |e_1|^{\gamma_1 - 1} - \alpha \kappa^{(\delta+1)\gamma_2} |e_1|^{\gamma_2} \operatorname{sgn}(\kappa^{\delta+1} e_1) \\ &= -\gamma_1 \lambda \kappa^{(\delta+1)\gamma_1 - 1} e_2 |e_1|^{\gamma_1 - 1} - \alpha \kappa^{(\delta+1)\gamma_2} |e_1|^{\gamma_2} \operatorname{sgn}(\kappa^{\delta+1} e_1) \\ &= -\gamma_1 \lambda \kappa^{\delta - 1} e_2 |e_1|^{\gamma_1 - 1} - \alpha \kappa^{\delta - 1} |e_1|^{\gamma_2} \operatorname{sgn}(\kappa^{\delta+1} e_1) \\ &= \kappa^{\delta - 1} (-\gamma_1 \lambda e_2 |e_1|^{\gamma_1 - 1} - \alpha |e_1|^{\gamma_2} \operatorname{sgn}(e_1)) \\ &= \kappa^{\delta - 1} f_2(\mathbf{e}) \end{aligned} \tag{7.32}$$

From (7.32), obtain the homogeneity degree (7.33).

$$\xi + r_2 = \xi + \delta = \delta - 1 \;\; \Rightarrow \xi = -1 \tag{7.33}$$

From these considerations it is concluded that the system (7.28) is d^r-homogeneous of degree $\xi = -1$ for (7.29) satisfied, and $r_1 = \delta + 1, r_2 = \delta, \delta > 0$.

Asymptotic Stability

The stability of $(e,\dot{e}) = (0,0)$ is shown via phase plane considerations, similarly to the STA controller in Section 6.3. The gradient of the phase trajectory is obtained using the identity $\ddot{e} = (\mathrm{d}\dot{e}\mathrm{d}e)/(\mathrm{d}e\mathrm{d}t) = (\mathrm{d}\dot{e})/(\mathrm{d}e)\dot{e}$, and the closed loop system (7.28), (7.29) as (7.34).

$$\frac{\mathrm{d}\dot{e}}{\mathrm{d}e} = -\lambda\frac{\delta}{\delta+1}|e|^{\frac{\delta}{\delta+1}-1} - \alpha\frac{|e|^{\frac{\delta-1}{\delta+1}}}{\dot{e}}\,\mathrm{sgn}(e) \tag{7.34}$$

Now, consider the phase trajectory for (7.28), (7.29) for properly chosen parameters λ, α in figure 7.4.

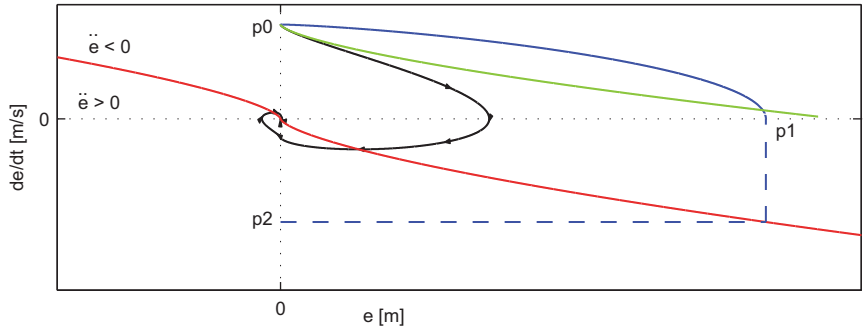

Figure 7.4: *Phase portrait for closed loop system* (7.28)*. The red graph indicates the deflection tangent* $\ddot{e} = 0$*, the black line a stable trajectory, the green solid line the trajectory resulting from the first term of the r.h.s. of* f_2 *in* (7.28) *and the blue solid line the trajectory resulting from the second term of the r.h.s. of* f_2 *in* (7.28)*.*

For simplicity consider the first quadrant of the phase plane, with initial conditions $(e(0),\dot{e}(0)) = (0,\dot{e}_{\mathrm{p0}})$. For this situation, the trajectory sets off into the first quadrant, in the direction of the fourth quadrant, and furthermore trajectories are *confined within the regions* produced by its individual components as depicted in figure 7.4. Inspired by the majorant curve approach [Davila et al., 2005] (as in Section 6.3), a conservative estimate of the first intersection with the e-axis $(e_{\mathrm{p1}},0)$ (at point $p1$ in figure 7.4) is established from the second term of the r.h.s. of (7.34), neglecting the first term. Hence, (7.34) is reduced to (7.35) (for the first quadrant).

$$\frac{\mathrm{d}\dot{e}}{\mathrm{d}e} = -\alpha\frac{e^{\frac{\delta-1}{\delta+1}}}{\dot{e}} \tag{7.35}$$

By separation of variables of obtain (7.36).

$$\int_{\dot{e}_{\mathrm{p0}}}^{0}\dot{e}\mathrm{d}\dot{e} = -\int_{0}^{e_{\mathrm{p1}}}\alpha e^{\frac{\delta-1}{\delta+1}}\mathrm{d}e \quad\Rightarrow\quad -\frac{1}{2}\dot{e}_{\mathrm{p0}}^2 = -\frac{1}{2}\frac{\alpha(\delta+1)}{\delta}e_{\mathrm{p1}}^{\frac{2\delta}{\delta+1}} \tag{7.36}$$

From (7.36), the intersection with the $e-$axis at point $(e_{\mathrm{p1}},0)$ is obtained as (7.37).

$$e_{\mathrm{p1}} = \left(\frac{\delta}{\alpha(\delta+1)}\dot{e}_{\mathrm{p0}}^2\right)^{\frac{\delta+1}{2\delta}} \tag{7.37}$$

Indeed, $\dot{e}$ will attain its maximum value on the deflection tangent, i.e. on (7.27), (7.29) for $\ddot{e}=0$, given by (7.38).

$$\dot{e} = -\frac{\alpha(\delta+1)}{\lambda\delta}|e|^{\frac{\delta}{\delta+1}}\,\mathrm{sgn}(e) \tag{7.38}$$

Substituting (7.37) into (7.38) a *worst case* intersection with the $\dot{e}-$axis at $(0,\dot{e}_{\mathrm{p2}})$ is obtained as (7.40) (see figure 7.4).

$$\dot{e}_{p2} = -\frac{\alpha(\delta+1)}{\lambda\delta}e_{p1}^{\frac{\delta}{\delta+1}} = -\frac{\alpha(\delta+1)}{\lambda\delta}\left(\left(\frac{\delta}{\alpha(\delta+1)}\dot{e}_{p0}^2\right)^{\frac{\delta+1}{2\delta}}\right)^{\frac{\delta}{\delta+1}} \tag{7.39}$$

$$= -\frac{\sqrt{\alpha(\delta+1)}}{\lambda\sqrt{\delta}}\dot{e}_{p0} \tag{7.40}$$

Convergence of $e,\dot{e}\to 0$ may, as for the analysis of the STA controller, be established by the condition $|\dot{e}_{p2}|<|\dot{e}_{p0}|$, as intersection with axes is dependent only on past axis-intersection points and tuning parameters. Then from (7.40), with (7.41) satisfied, the origin is asymptotically stable, and furthermore finite-time asymptotically stable noting the homogeneity reasoning above.

$$\lambda\sqrt{\delta} > \sqrt{\alpha(\delta+1)} \tag{7.41}$$

It is notable, that for the limits of δ, the controller (7.26) is identical with the STA controller (6.20), with the exact same convergence criterion, or a conventional linear PI type controller. Hence, the versatility of the controller structure is similar to that of the previous section.

$$\lim_{\delta\to 1}\bar{u}_{\mathrm{v}} = \dot{x}_{\mathrm{R}} - \lambda|e|^{\frac{1}{2}}\,\mathrm{sgn}(e) - \alpha\int_t \mathrm{sgn}(e)\mathrm{d}t \quad , \quad \lim_{\delta\to\infty}\bar{u}_{\mathrm{v}} = \dot{x}_{\mathrm{R}} - \lambda e - \alpha\int_t e\mathrm{d}t \tag{7.42}$$

As for the controller proposed in the previous section, the finite-time convergence properties imply that motion on $|e|=|\dot{e}|=0$, should consist of Filippov sense trajectories. This is confirmed by figure 7.5, also indicating the time response, using tuning rules inspired by (6.25) with $\delta=3,\lambda=1.5\sqrt{\bar{\gamma}},\alpha=1.1\bar{\gamma},\bar{\gamma}=1$ (and applied to an ideal double integrator).

7.5 Modified Prescribed Convergence Controller

The controller with prescribed convergence discussed in Section 6.1 may be modified in a way similar to the remaining controllers considered in this chapter. Based on the controller (6.4), a continuous homogeneous version of this controller may be composed as (7.43).

$$\bar{u}_{\mathrm{v}} = \dot{x}_{\mathrm{R}} - \lambda|e|^{\gamma_1}\,\mathrm{sgn}(e) - \alpha\int_t |e|^{\gamma_2}\,\mathrm{sgn}(\dot{e}+\lambda|e|^{\gamma_1}\,\mathrm{sgn}(e))\mathrm{d}t,\;\; 0.5\le\gamma<1,\quad \lambda>0 \tag{7.43}$$

Choosing parameters γ_1,γ_2 according to (7.44), and weights as $r_1=\delta+1,r_2=\delta$, then from similar considerations as in the above, it may be shown that the closed loop system (7.5), (7.43) is d^r-homogeneous with homogeneity degree $\xi=-1$.

$$\gamma_1 = \frac{\delta}{\delta+1}\;,\;\gamma_2 = \frac{\delta-1}{\delta+1} \tag{7.44}$$

Furthermore the origin may be found to be asymptotically stable via Lyapunov arguments. Then from Theorem 1, the origin is finite-time asymptotically stable. The homogeneity- and stability properties are considered in detail in [Schmidt et al., 2013]. The obvious drawback of this controller compared to the remaining controls proposed in this chapter, is the fact that a velocity measurement is necessary.

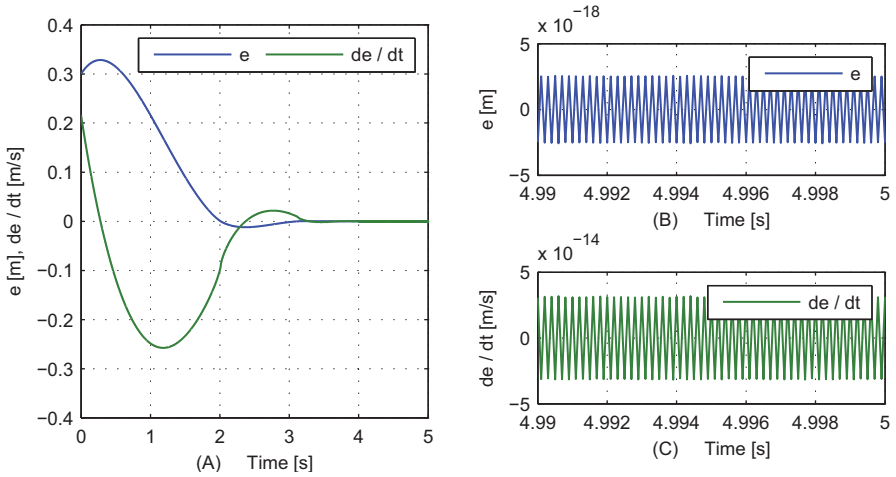

Figure 7.5: *State trajectories. In all cases* $\delta = 3, \lambda = 1.5\sqrt{\bar{\gamma}}, \alpha = 1.1\bar{\gamma}, \bar{\gamma} = 1$. *(A) Convergence of e, ė. (B) e after convergence to* $e = 0$. *(C)* $\dot{e}$ *after convergence to* $\dot{e} = 0$.

7.6 Experimental Results

In the following the modified relay controller, modified twisting- and super twisting controllers are evaluated experimentally, and are furthermore denoted M-P controller, M-TA controller and M-STA controller, respectively. A complete list of control parameters applied can be found in the Appendix.

7.6.1 Modified Relay Controller (M-P)

The performance results in terms of tracking control error and control input are depicted in figure 7.6 for the three test cases. The gain α is designed based on a standard linear proportional control design approach, targeting a gain margin $GM \approx 8$ [dB]. The remaining tuning effort for the controller is rather straight forward, and the exponent γ is simply reduced (from an initial value $\gamma = 1$) until a satisfactory performance is achieved. From figure 7.6 (A)-(F) it is found that the control error is stable and exhibits a steady state error, as would be expected. The steady state error settles at the corresponding leakage flow level. Also it is found that the controller excites the (un-modeled) vehicle / Axis 1 resonant modes. Figure 7.6 (H)-(I) depicts the control errors when compared to those of the PI-AGC controller of Section 3.2. Here it is found that the modified relay control exhibits significantly improved tracking performance compared to the PI-AGC controller, in terms if the maximum error. This fact may be interpreted in the intuitive way for this simple controller - the exponent $1 > \gamma > 0$ causes a larger controller response to a certain error value, than e.g. the proportional term of the PI type controller, causing the proposed controller to be more *pro-active* in compensating the error.

7.6.2 Modified Twisting Controller (M-TA)

The parameters α_1, α_2 for the M-TA controller are chosen identically to those of the PI-AGC controllers of Section 3.2, in order to explicitly evaluate the consequences of the homogeneous modification. Also similarly to the relay controller, satisfactory performance is achieved simply

by reducing the parameter δ from some *large* value (e.g. from $\delta = 100$). Results are depicted in figure 7.7 (A)-(F). Here it is found that fast convergence to $e = 0$ is achieved after transients, and from figure 7.7 (H)-(I), the M-TA exhibits significantly smaller maximum errors and faster convergence to $e = 0$ after transients, compared to the PI-AGC. However, results for TC3 suggest that the M-STA controller is more prone to limit cycles in the presence of significant friction phenomena than the PI-AGC, hence in such cases the parameter δ should be chosen *large enough*. In general it is found that the homogeneity properties improve control performance in terms of tracking performance, while maintaining satisfactory control inputs.

7.6.3 Modified Super Twisting Controller (M-STA)

The basic parameter design for the M-STA was chosen according to (6.26) which satisfies the convergence criterion (7.41). From the tuning process it was found that for this choice of parameter relations the controller was prone to oscillations. Instead the parameter relation (7.45) (also satisfying the convergence criterion (7.41)) was found to be appropriate for all test cases. It should be noted that with (7.45), only two parameters need to be tuned for this controller.

$$\lambda = 3.5\sqrt{\bar{\gamma}}, \;\; \alpha = 1.1\bar{\gamma} \tag{7.45}$$

The results are depicted in figure 7.8 (A)-(F), and demonstrate performance similar to the M-TA controller, with satisfactory tracking error, fast convergence to $e = 0$ after transients and a satisfactory control input. Figure 7.8 (G)-(I) illustrates, as for the M-TA, that the M-STA produces significantly improved tracking performance compared to the PI-AGC controller in terms of maximum control error and faster convergence to $e = 0$ after transients.

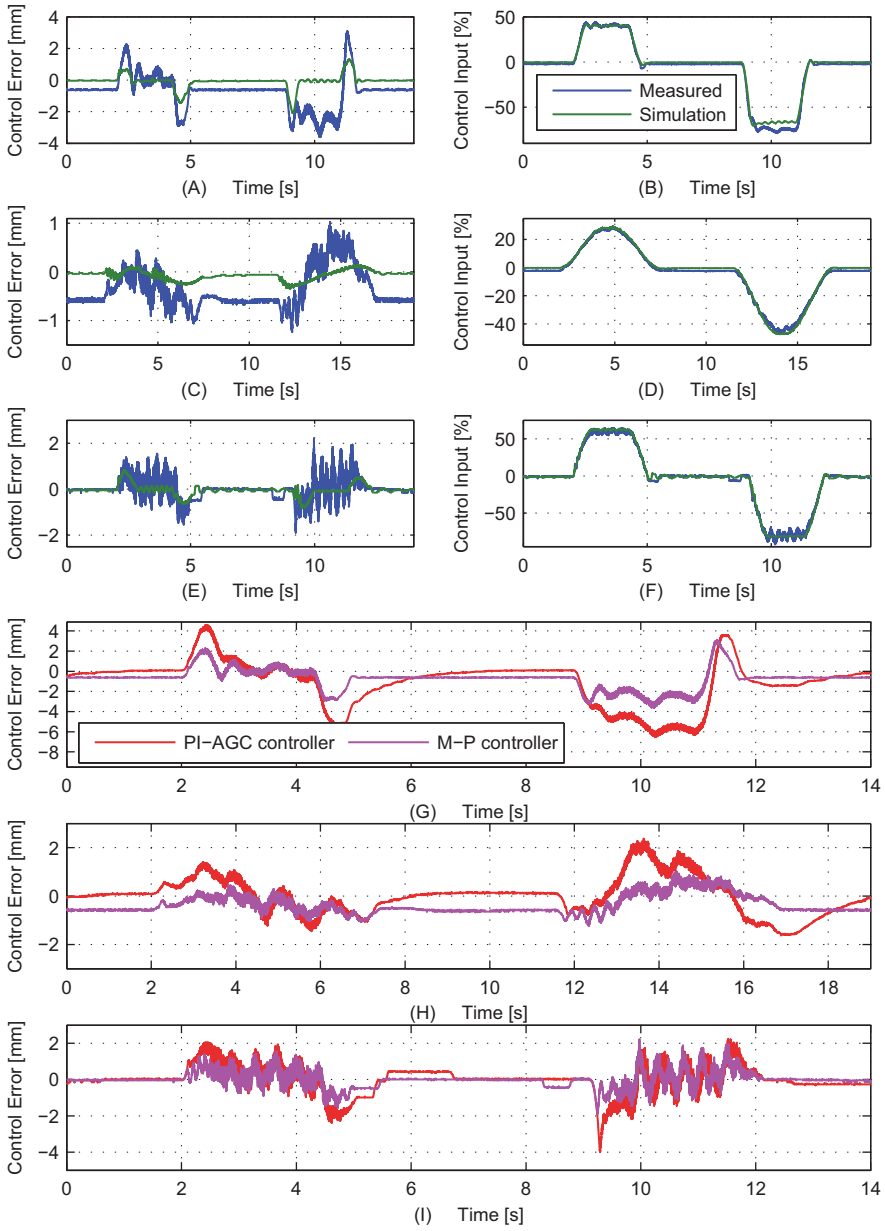

Figure 7.6: *Performance with application of the control* (7.6)*. (A) Control tracking error for TC1. (B) Control input for application to TC1. (C) Control tracking error for TC2. (D) Control input for application to TC2. (E) Control tracking error for TC3. (F) Control input for application to TC3. (G) Comparison of* (7.6) *to* (3.42) *for TC1. (H) Comparison of* (7.6) *to* (3.42) *for TC2. (I) Comparison of* (7.6) *to* (3.42) *for TC3.*

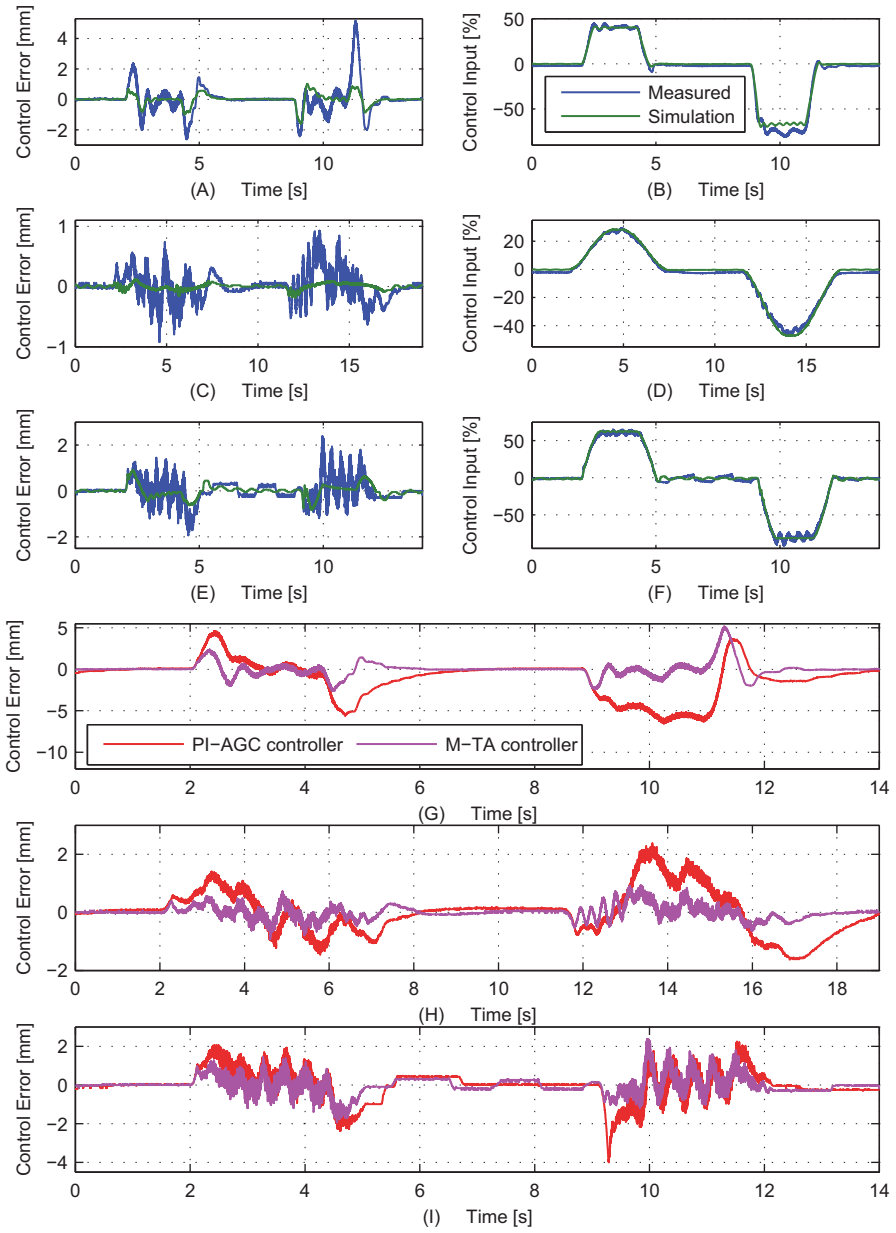

Figure 7.7: *Performance with application of the control* (7.6)*. (A) Control tracking error for TC1. (B) Control input for application to TC1. (C) Control tracking error for TC2. (D) Control input for application to TC2. (E) Control tracking error for TC3. (F) Control input for application to TC3. (G) Comparison of* (7.6) *to* (3.42) *for TC1. (H) Comparison of* (7.6) *to* (3.42) *for TC2. (I) Comparison of* (7.6) *to* (3.42) *for TC3.*

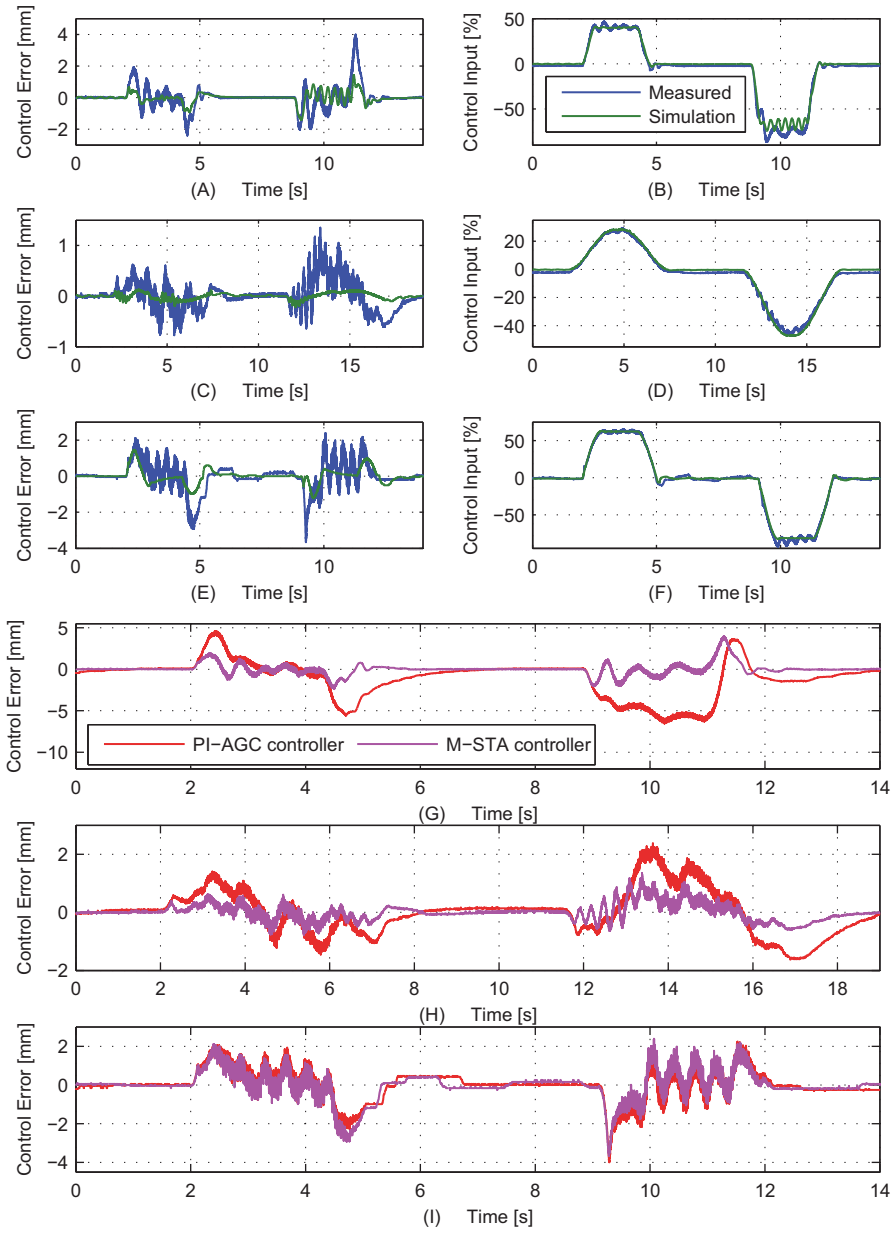

Figure 7.8: *Performance with application of the control* (7.6)*. (A) Control tracking error for TC1. (B) Control input for application to TC1. (C) Control tracking error for TC2. (D) Control input for application to TC2. (E) Control tracking error for TC3. (F) Control input for application to TC3. (G) Comparison of* (7.6) *to* (3.42) *for TC1. (H) Comparison of* (7.6) *to* (3.42) *for TC2. (I) Comparison of* (7.6) *to* (3.42) *for TC3.*

7.7 Summary

In this chapter several homogeneous continuous controllers were proposed, with the designs being founded on some of the sliding mode control structures discussed in previous chapters. The homogeneous controls include an additional tuning parameter compared to their linear counterparts, which is found to be easily tuned. The structures of these controls turn out to be highly versatile, and in the limit cases they may resemble either their sliding counterparts, or conventional linear P / PI controls. Results demonstrate improved tracking robustness compared to the (linear) PI-AGC controller. Also, the controller gain tuning used suggests that the controllers may be tuned using parameters appropriate for conventional linear methods (at least for the test cases considered here). In the specific case of the homogeneous extension of the super twisting algorithm, a modified version of a known tuning approach was proposed. Hence, this controller may be tuned using only two parameters in total.

It should furthermore be noted that in the general case, the feedback should be normalized to one in order for the homogeneous controllers to work as expected and as demonstrated here.

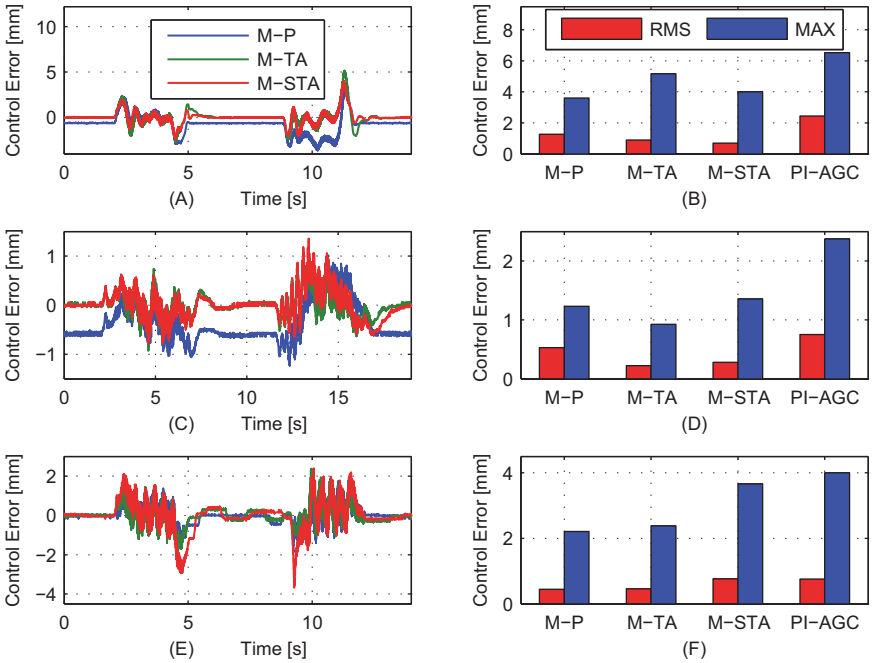

Figure 7.9: *Performance with application of controllers M-P, M-TA and M-STA controllers, compared with then PI-AGC controller. (A) Control tracking errors for TC1. (B) RMS- and MAX errors for TC1. (C) Control tracking errors for TC2. (D) RMS- and MAX errors for TC2. (E) Control tracking errors for TC3. (F) RMS- and MAX errors for TC3.*

The performance results for the proposed homogeneous controls are outlined in figure 7.9, and it is

found that performance of the different controllers resemble each other, with the M-TA and M-STA controllers producing the more precise overall tracking performance for TC1 and TC2. The M-P appears to be a more appropriate choice in the case of TC3, due to the lack of an integral term, hence avoiding possible limit cycles.

8 Third- & Higher Order Sliding Control

From the control designs discussed in the previous chapters, second order sliding controllers are attractive in the sense that chattering may be attenuated if the nominal open loop system is uniformly continuous, disturbances are bounded, the slew rate limitation of the valve is sufficiently large and time delays are minimal. Another interesting feature is that e.g. the twisting algorithm may be designed to steer the output function and its derivative to zero using boundary layers without detailed knowledge of the system dynamics as opposed to conventional surface-based sliding controls. As discussed in Section 4.3 there exist several high order sliding mode control structures, even applicable to *arbitrary order* systems. However, also many of these approaches involve several sensors, and tuning of a number of parameters which should be avoided to the extend possible in this project. Instead, in the following an extension of the twisting algorithm to the third order is proposed, with the result not strictly a relay controller as the TA controller, but similar to. Furthermore, a partial framework for a controller based on a homogeneous surface design is established, which may be considered a homogeneous extension of the PCA controller discussed previously.

8.1 Third Order Extension of the Twisting Controller

The simple structure of the TA controller, and the simple parameter tuning, is interesting from several reasons as discussed in Section 6.2, and the expansion of the TA structure would be desirable, allowing for both chattering attenuation while including several derivatives of the output function, using multiple state measurements and (possibly) as an output feedback controller. In the sequel of this section, an extension of the TA controller to the third order is considered. Let the system (3.41) satisfy conditions as in Section 6.2.1, and have the output function $\int_t e\mathrm{d}t$. Defining the closed loop state vector as $e = (\int_t e\mathrm{d}t, e, \dot{e}) = (e_1, e_2, e_3)$, then the closed loop system may be represented as (8.1) (assuming $\dot{\rho}(\mathbf{x}) \approx 0$).

$$\begin{bmatrix} \dot{e}_1 \\ \dot{e}_2 \\ \dot{e}_3 \end{bmatrix} = \begin{bmatrix} e_2 \\ e_3 \\ \dot{F}(\mathbf{x}) - \ddot{x}_\mathrm{R} + \rho(\mathbf{x})\dot{\bar{u}}_\mathrm{v} \end{bmatrix} \quad , \quad 0 < \bar{K}_\mathrm{m} < \rho(\mathbf{x}) < \bar{K}_\mathrm{M} \quad , \quad |\dot{F}(\mathbf{x})| \leq \bar{C} \tag{8.1}$$

Let the state space be defined as $\Sigma = \{(e_1, e_2, e_3) \in \mathbb{R}^3\}$. Taking into account signs of the states, the complete state space is constituted by eight octants, given by (8.5) through (8.9).

$$\Sigma^{+++} = \{(e_1, e_2, e_3) \ \in \mathbb{R}^3 | e_1 > 0, e_2 > 0, e_3 > 0\} \tag{8.2}$$

$$\Sigma^{++-} = \{(e_1, e_2, e_3) \ \in \mathbb{R}^3 | e_1 > 0, e_2 > 0, e_3 < 0\} \tag{8.3}$$

$$\Sigma^{+--} = \{(e_1, e_2, e_3) \ \in \mathbb{R}^3 | e_1 > 0, e_2 < 0, e_3 < 0\} \tag{8.4}$$

$$\Sigma^{---} = \{(e_1,e_2,e_3) \in \mathbb{R}^3 | e_1 < 0, e_2 < 0, e_3 < 0\} \tag{8.5}$$

$$\Sigma^{-++} = \{(e_1,e_2,e_3) \in \mathbb{R}^3 | e_1 < 0, e_2 > 0, e_3 > 0\} \tag{8.6}$$

$$\Sigma^{--+} = \{(e_1,e_2,e_3) \in \mathbb{R}^3 | e_1 < 0, e_2 < 0, e_3 > 0\} \tag{8.7}$$

$$\Sigma^{+-+} = \{(e_1,e_2,e_3) \in \mathbb{R}^3 | e_1 > 0, e_2 < 0, e_3 > 0\} \tag{8.8}$$

$$\Sigma^{-+-} = \{(e_1,e_2,e_3) \in \mathbb{R}^3 | e_1 > 0, e_2 > 0, e_3 > 0\} \tag{8.9}$$

Noting the definition (4.4), in the sequel, limit points are denoted $e_{i\pm},\ i = 1,2,3$. Inspired by the TA controller (6.8), consider the extended version (8.10) with $\alpha_1, \alpha_2, \alpha_3 > 0$.

$$\dot{\tilde{u}}_{\mathrm{v}} = \ddot{x}_{\mathrm{R}} - \alpha_1 \operatorname{sgn}(e_1) - \alpha_2 \operatorname{sgn}(e_2) - \alpha_3 \operatorname{sgn}(e_3), \quad \operatorname{sgn}(e_i) \triangleq \begin{cases} 1, & e_i \geq 0 \\ - & 1, \ e_i < 0 \end{cases} \tag{8.10}$$

In order to reduce complexity of the analysis, defining coefficients $\alpha = \alpha_2$, $\lambda = \alpha_1/\alpha_2$, $\gamma = \alpha_3/\alpha_2$, the identity (8.11) holds true.

$$-\alpha_1 \operatorname{sgn}(e_1) - \alpha_2 \operatorname{sgn}(e_2) - \alpha_3 \operatorname{sgn}(e_3) \equiv -\alpha(\lambda \operatorname{sgn}(e_1) + \operatorname{sgn}(e_2) + \gamma \operatorname{sgn}(e_3)) \tag{8.11}$$

Closing the system (8.1) by the control (8.10) utilizing the identity (8.11), satisfies the system (8.12).

$$\begin{bmatrix} \dot{e}_1 \\ \dot{e}_2 \\ \dot{e}_3 \end{bmatrix} = \begin{bmatrix} e_2 \\ e_3 \\ \dot{F}(\mathbf{x}) - \alpha\rho(\mathbf{x})(\lambda \operatorname{sgn}(e_1) + \operatorname{sgn}(e_2) + \gamma \operatorname{sgn}(e_3)) \end{bmatrix} \tag{8.12}$$

Choosing the control gain α according to (8.13) noting the bounds (8.1), then $\operatorname{sgn}(\dot{e}_3)$ is uniquely determined by the control (8.10) (rewritten with the identity (8.11)).

$$\alpha > \frac{\bar{C}}{\bar{K}_m} \frac{1}{\inf(|\lambda \operatorname{sgn}(e_1) + \operatorname{sgn}(e_2) + \gamma \operatorname{sgn}(e_3)|)} \tag{8.13}$$

The closed system (8.12), (8.13) is invariant with respect to uncertain bounded parameters and disturbances from [Utkin et al., 2009]. This invariance property allows to conduct the convergence analysis considering the controlled system as a triple integrator closed by (8.10) with $\alpha = \alpha_2$, $\lambda = \alpha_1/\alpha_2$, $\gamma = \alpha_3/\alpha_2$, by virtue of (8.13). From these considerations, the analysis will be based on the inclusion (8.14).

$$\dot{\mathbf{e}} = \begin{bmatrix} \dot{e}_1 \\ \dot{e}_2 \\ \dot{e}_3 \end{bmatrix} \in \begin{bmatrix} e_2 \\ e_3 \\ -\alpha(\lambda \operatorname{sgn}(e_1) + \operatorname{sgn}(e_2) + \gamma \operatorname{sgn}(e_3)) \end{bmatrix} \tag{8.14}$$

From (8.14), in each of the octants defined above, $\dot{e}_3$ is constant. Consider the inequalities (8.15), (8.16), (8.17). If one of these inequalities is satisfied, then the corresponding state determines $\operatorname{sgn}(\dot{e}_3)$, not implying a stable origin.

$$\lambda > 1 + \gamma \ \Rightarrow \ \operatorname{sgn}(e_1) = \operatorname{sgn}(\dot{e}_3) \tag{8.15}$$

$$1 > \gamma + \lambda \ \Rightarrow \ \operatorname{sgn}(e_2) = \operatorname{sgn}(\dot{e}_3) \tag{8.16}$$

$$\gamma > 1 + \lambda \ \Rightarrow \ \operatorname{sgn}(e_3) = \operatorname{sgn}(\dot{e}_3) \tag{8.17}$$

Hence in order to achieve influence from all states, the restrictions (8.18) are imposed.

$$\lambda < 1+\gamma,\ \ 1 < \gamma+\lambda,\ \ \gamma < 1+\lambda \tag{8.18}$$

An unfortunate property of the closed loop system (8.14) may be observed from these considerations. In the event that $e_2 = 0, e_3 = 0$, then e_1 is ideally constant due to $\lambda < 1+\gamma$, and the existing sliding mode on $|e_2| = |e_3| = 0$. Hence, for initial conditions $\mathbf{e}(0) = (e_1(0),0,0)$, the solution is $\mathbf{e}(t) = (e_1(0),0,0),\ \forall t > 0$, i.e. $\mathbf{e} = (e_1(0),0,0)$ is an equilibrium point. This fact was proved in [Anosov, 1959] as far back as 1959 [Bartolini et al., 2007], [Kryachkov et al., 2010]. A particular interesting alternative to the controller (8.10) was presented in [Bartolini et al., 2007] where a simple relay controller denoted *Anosov Unstable* was combined with the twisting algorithm, i.e. combining the two relay controls (8.19). The activation of signals u_1, u_2 is controlled by a logic scheme to achieve a stable origin.

$$u_1 = -\alpha_1 \operatorname{sgn}(e_1) \quad ,\ \ u_2 = -\alpha_2 \operatorname{sgn}(e_2) - \alpha_3 \operatorname{sgn}(e_3) \tag{8.19}$$

However, the invariance property of the controller (8.10), (8.13) does in fact allow convergence to the origin $\forall\ \mathbf{e}(0) \neq (e_1(0),0,0)$, making the analysis of this controller still relevant for such initial conditions. Furthermore, in the following a solution that effectively compensates for the above mentioned problem, is proposed.

8.1.1 Convergence Analysis

Consider $\dot{e}_3$ of (8.14) given by (8.20).

$$\dot{e}_3 \in -\alpha(\lambda \operatorname{sgn}(e_1) + \operatorname{sgn}(e_2) + \gamma \operatorname{sgn}(e_3)) \tag{8.20}$$

By inspection of (8.20) it is found that $\mathbf{e}$ is *diagonally* equivalent with respect to the octants, i.e. $\mathbf{e} \in \Sigma^{+++} \sim \mathbf{e} \in \Sigma^{---}$, $\mathbf{e} \in \Sigma^{++-} \sim \mathbf{e} \in \Sigma^{--+}$ and so fourth. This allows to consider only half of the state space in the analysis. As $\dot{e}_3$ is constant in each octant, simple integral analysis allows for determining the direction of $\mathbf{e}$, i.e. to which octant this is directed. Noting the restrictions (8.18), this leads to the statements (8.21), (8.22), (8.23), (8.24) .

$$\dot{e}_3 = -\lambda - 1 - \gamma < 0,\ \ e_3 > 0,\ \ e_2 > 0,\ \ e_1 > 0 \ \text{ for } \ \mathbf{e}, \in \Sigma^{+++} \tag{8.21}$$

$$\dot{e}_3 = -\lambda - 1 + \gamma < 0,\ \ e_3 < 0,\ \ e_2 > 0,\ \ e_1 > 0 \ \text{ for } \ \mathbf{e}, \in \Sigma^{++-} \tag{8.22}$$

$$\dot{e}_3 = -\lambda + 1 + \gamma > 0,\ \ e_3 < 0,\ \ e_2 < 0,\ \ e_1 > 0 \ \text{ for } \ \mathbf{e}, \in \Sigma^{+--} \tag{8.23}$$

$$\dot{e}_3 = -\lambda + 1 - \lambda < 0,\ \ e_3 > 0,\ \ e_2 < 0,\ \ e_1 > 0 \ \text{ for } \ \mathbf{e}, \in \Sigma^{+-+} \tag{8.24}$$

From (8.21) it is found that $\mathbf{e} \in \Sigma^{+++} \to \Sigma^{++-}$ (respectively $\mathbf{e} \in \Sigma^{---} \to \Sigma^{--+}$), from (8.22) that $\mathbf{e} \in \Sigma^{++-} \to \Sigma^{+--}$ (respectively $\mathbf{e} \in \Sigma^{--+} \to \Sigma^{-++}$), from (8.23) that $\mathbf{e} \in \Sigma^{+--} \to \Sigma^{+-+}, \Sigma^{---}$ (respectively $\mathbf{e} \in \Sigma^{-++} \to \Sigma^{--+}, \Sigma^{+++}$) and from (8.24) that $\mathbf{e} \in \Sigma^{+-+} \to \Sigma^{+++}, \Sigma^{+--}, \Sigma^{---}$ (respectively $\mathbf{e} \in \Sigma^{--+} \to \Sigma^{---}, \Sigma^{-++}, \Sigma^{++-}$). Hence for $\mathbf{e} \in \Sigma^{+--}$ and $\mathbf{e} \in \Sigma^{+-+}$, the direction of $\mathbf{e}$ is not unique which is visualized in the phase planes of the state space in figure 8.1.

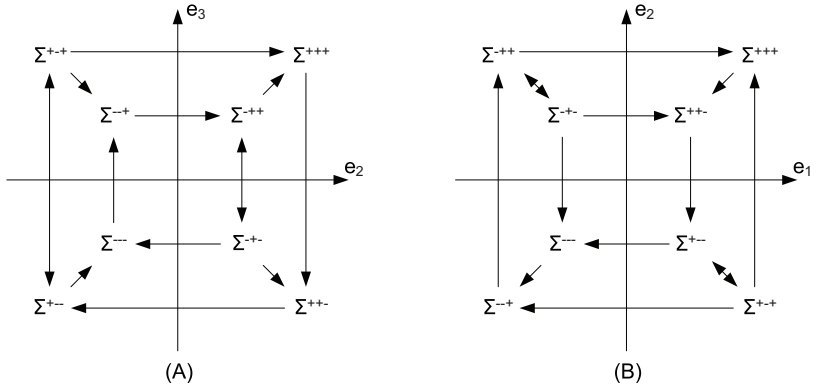

Figure 8.1: *(A) Illustration of possible directions of* $\mathbf{e}$ *in the* $(e_3,e_2)-$*plane. (B) Illustration of possible directions of* $\mathbf{e}$ *in the* $(e_2,e_1)-$*plane. The arrows symbolize the direction of* $\mathbf{e}$*.*

Uniqueness of State Trajectory

The convergence analysis in the following is based on geometrical considerations in regard to the state trajectory. Furthermore, the analysis is carried out sequentially with respect to transitions of the state trajectory between octants. Consider the situation $\mathbf{e} \subseteq \Sigma^{++-} \cap \Sigma^{+--}$ and recall (8.23). Whether $\mathbf{e}$ tends to Σ^{---} or Σ^{+-+} depends on $|e_1|$, $|e_3|$ at the instant $\mathbf{e} \in \Sigma^{++-} \cap \Sigma^{+--}$ and λ, γ, i.e. whether $\mathbf{e}$ exits Σ^{+--} via $e_3 = 0$ or via $e_1 = 0$. Provided that $\mathbf{e}$ sets off into Σ^{++-} with initial conditions $\mathbf{e}_0 = [e_{1+}\ e_{02}\ e_{3-}]$, $|e_{02}| > 0$ (i.e. when $|\mathbf{e}_0| = |e_{02}|$), then $\mathbf{e}$ enters Σ^{+--} with least possible $|e_1|$, $|e_3|$.
Consider the time instants relative to the states at $\mathbf{e} \in \Sigma^{++-} \cap \Sigma^{+--}$ and $\mathbf{e} \in \Sigma^{+--} \cap \Sigma^{---} \cap \Sigma^{+-+}$ defined by (8.25). The situation at time t_2 when $\mathbf{e}$ exits Σ^{+--} via the boundary $\Sigma^{---} \cap \Sigma^{+-+}$, i.e. when $|e_1(t_2)| = |e_3(t_2)| = 0$, is considered a critical situation.

$$t_0 = 0 \ , \ t_1 = t|_{e_2=0} \ , \ t_2 = t|_{|e_1|,|e_3|=0} \tag{8.25}$$

Indeed, when $\mathbf{e} \in \Sigma^{++-}$ the state trajectory tends to Σ^{+--} via $|e_2| = 0$, yielding (8.26) with $\mathbf{e}_0 = (e_{1+}, e_{02}, e_{3-})$, $e_{02} > 0$.

$$e_2(t_1) = \int_{t_0}^{t_1} \left(\int_{t_0}^{t} (\gamma - \lambda - 1)\mathrm{d}t + e_3(t_0) \right) \mathrm{d}t + e_2(t_0) \tag{8.26}$$

$$= \int_{0}^{t_1} \left(\int_{0}^{t} (\gamma - \lambda - 1)\mathrm{d}t \right) \mathrm{d}t + e_2(t_0) = 0 \ \Rightarrow \ t_1 = \sqrt{\frac{2e_2(t_0)}{\lambda + 1 - \gamma}} \ \Rightarrow \tag{8.27}$$

$$e_3(t_1) = -\sqrt{2(\lambda + 1 - \gamma)e_2(t_0)} \ , \quad e_1(t_1) = \frac{2}{3}\sqrt{\frac{2}{\lambda + 1 - \gamma}} e_2(t_0)^{3/2} \tag{8.28}$$

The time instant t_2 and corresponding states are found by straightforward integration as (8.29),

(8.30), respectively.

$$e_3(t_2) = \int_0^{t_2} (1+\gamma-\lambda)\mathrm{d}t + e_3(t_1) = (1+\gamma-\lambda)t_2 - \sqrt{2(\lambda+1-\gamma)e_2(t_0)} = 0 \;\Rightarrow \quad (8.29)$$

$$t_2 = \frac{\sqrt{2(\lambda+1-\gamma)e_2(t_0)}}{1+\gamma-\lambda} \;\Rightarrow$$

$$\begin{aligned} e_1(t_2) &= \int_0^{t_1} \left(\int_0^t \left(\int_0^t (1+\gamma-\lambda)\mathrm{d}t + e_3(t_1) \right) \mathrm{d}t + e_2(t_1)) \right) \mathrm{d}t + e_1(t_1) \\ &= \int_0^{t_1} \left(\int_0^t \left(\int_0^t (1+\gamma-\lambda)\mathrm{d}t + e_3(t_1) \right) \mathrm{d}t) \right) \mathrm{d}t + e_1(t_1) \\ &= \frac{1}{6}(1+\gamma-\lambda)t_2^3 - \frac{1}{2}\sqrt{2(\lambda+1-\gamma)e_2(t_0)}t_2^2 + \frac{2}{3}\sqrt{\frac{2}{\lambda+1-\gamma}}e_2(t_0)^{3/2} \qquad (8.30) \\ &= 0 \;\Rightarrow \end{aligned}$$

$$\lambda = \gamma \qquad (8.31)$$

Reducing (8.30) leads to the criterion (8.31), hence critical for the direction of $\mathbf{e}$ when $\mathbf{e} \subseteq \Sigma^{+--}$. By inspection of (8.29), (8.30) it is found that $\mathbf{e} \subseteq \Sigma^{+--}$ tends to Σ^{---} for $\lambda > \gamma$ and $\mathbf{e} \subseteq \Sigma^{+--}$ tends to Σ^{+-+} for $\lambda < \gamma$, which is also illustrated in figure 8.2.

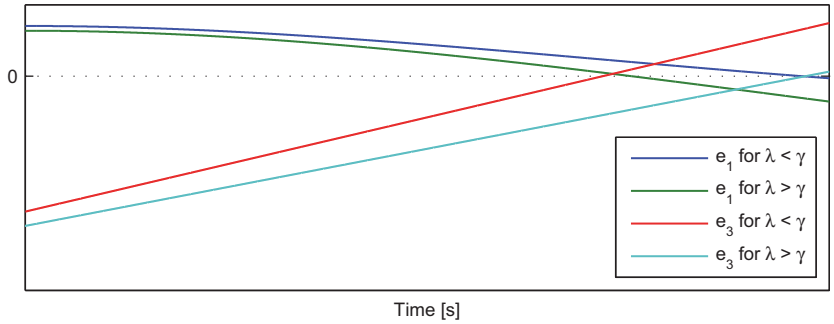

Figure 8.2: *Illustration of the impact of* $\lambda \lessgtr \gamma$.

Consider now the fact (8.32) following from (8.20), (8.18) with $\lambda < \gamma$.

$$\dot{e}_3 = 1+\gamma-\lambda > 0 \;\; \forall\, \mathbf{e} \subseteq \Sigma^{+--} \quad , \quad \dot{e}_3 = 1-\gamma-\lambda < 0 \;\; \forall\, \mathbf{e} \subseteq \Sigma^{+-+} \qquad (8.32)$$

From (8.32), when $\mathbf{e} \subseteq \Sigma^{+--}$ then $\mathbf{e}$ tends to Σ^{+-+} (at the intersection $e_3 = e_{3+}$), $\dot{e}_3$ changes sign and $\mathbf{e}$ is instantaneously driven back towards Σ^{+--} (the intersection $e_3 = e_{3-}$), enforcing a sliding mode *locally* on $e_3 = 0$. Hence, ideally $|e_3| = 0$ leading to $e_2 =$constant< 0, and due to $e_1 e_2 < 0$, $e_1 \to 0$.
At the instant e_1 intersects the limit $e_{1\text{-}}$, then $\mathbf{e} \subseteq \Sigma^{+-+}$ and tends to Σ^{--+} or Σ^{---} dependent on whether $e_3 = e_{3+}$ or $e_3 = e_{3-}$. However, as $|e_3| = 0$, then instantaneously $\mathbf{e} \subseteq \Sigma^{---}$ tends to Σ^{--+} by virtue of infinite switching frequency. As $\mathbf{e} \subseteq \Sigma^{--+} \sim \mathbf{e} \subseteq \Sigma^{++-}$, then $\mathbf{e}$ will resemble the description above.

The considerations above imply that for initial conditions $\mathbf{e}_0 \in \Sigma^{++-} = (e_{1+}, e_{02}, e_{3-}),\ |e_{02}| > 0$, $\lambda < \gamma$ and (8.18) satisfied, then the direction of the trajectory $\mathbf{e}$ is unique / predictable. However for arbitrary initial conditions $\mathbf{e}_0 \in \Sigma^{+--}$ or $\mathbf{e}_0 \in \Sigma^{+-+}$ additional considerations must be made. For arbitrary $\mathbf{e}_0 \in \Sigma^{+--}$ or $\mathbf{e}_0 \in \Sigma^{+++}$ either of (8.33)−(8.38) may occur, from which it is found that in any case, $\mathbf{e}$ will eventually enter a region where the state trajectory resembles the one described above.

$$\text{For } \mathbf{e}_0 \in \Sigma^{+--},\ \mathbf{e} \text{ tends to } \Sigma^{---} \tag{8.33}$$

$$\text{For } \mathbf{e}_0 \in \Sigma^{+--},\ \mathbf{e} \text{ tends to } \Sigma^{+-+} \tag{8.34}$$

$$\text{For } \mathbf{e}_0 \in \Sigma^{+-+},\ \mathbf{e} \text{ tends to } \Sigma^{+--},\ \text{then to } \Sigma^{+-+} \qquad (\text{SM on } e_3 = 0) \tag{8.35}$$

$$\text{For } \mathbf{e}_0 \in \Sigma^{+-+},\ \mathbf{e} \text{ tends to } \Sigma^{--+},\ \text{then to } \Sigma^{-++},\ \text{then to } \Sigma^{-+-} \qquad (\text{SM on } e_3 = 0) \tag{8.36}$$

$$\text{For } \mathbf{e}_0 \in \Sigma^{+-+},\ \mathbf{e} \text{ tends to } \Sigma^{+--},\ \text{then to } \Sigma^{---} \tag{8.37}$$

$$\text{For } \mathbf{e}_0 \in \Sigma^{+-+},\ \mathbf{e} \text{ tends to } \Sigma^{--+},\ \text{then to } \Sigma^{-++},\ \text{then to } \Sigma^{+++} \tag{8.38}$$

Hence, for $\lambda < \gamma$ and (8.18) satisfied, the direction of $\mathbf{e}$ is predictable in the entire state space, and furthermore encircles the origin. The phase planes of the state space with $\lambda < \gamma$ and (8.18) satisfied, are shown in figure 8.3.

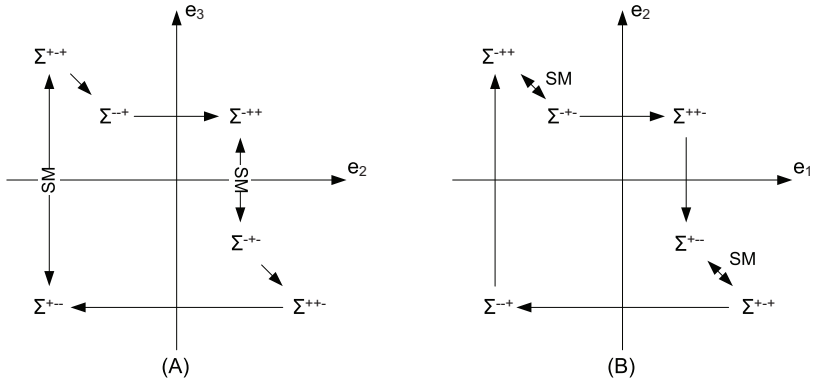

Figure 8.3: *(A) Illustration of resulting directions of* $\mathbf{e}$ *in the* $(e_2, e_3)-$*plane, with* $\lambda < \gamma$ *and* (8.18) *satisfied. (b) Illustration of resulting directions of* $\mathbf{e}$ *in the* $(e_1, e_2)-$*plane, with* $\lambda < \gamma$ *and* (8.18) *satisfied. The arrows symbolize the direction of* $\mathbf{e}$*, and* SM *indicates a sliding mode locally on* e_3*.*

Having determined the criterion for trajectory uniqueness for $\mathbf{e}$, and that this encircles the origin for $\lambda < \gamma$ and (8.18) satisfied, it is necessary to show that $|\mathbf{e}| \to 0$ in finite time.

8.1.2 Finite-Time Stability of the Origin

Using t_2 of (8.29) to derive $e_2(t_2)$, (8.40) is obtained. e_2 converges towards zero if $|e_2(t_2)| < |e_2(t_0)|$, which is satisfied provided that $\lambda < \gamma$ and (8.18) hold true.

$$e_2(t_2) = \frac{1}{2}(1+\gamma-\lambda)t_2^2 - \sqrt{2(1+\lambda-\gamma)e_1(t_0)}t_2 \tag{8.39}$$

$$= \frac{1}{2}(1+\gamma-\lambda)\left(\frac{\sqrt{2(1+\lambda-\gamma)e_2(t_0)}}{1+\gamma-\lambda}\right)^2 - \sqrt{2(1+\lambda-\gamma)\dot{e}_0}\left(\frac{\sqrt{2(1+\lambda-\gamma)\dot{\sigma}_0}}{1+\gamma-\lambda}\right)$$

$$= -\frac{1+\lambda-\gamma}{1+\gamma-\lambda}e_2(t_0) \tag{8.40}$$

From Section 8.1.1 it is found that past time $t = t_2$, a sliding mode will occur on $e_3 = 0$ with $\lambda < \gamma$ and (8.18) satisfied, which is maintained until the intersection $e_1 = e_{1\text{-}}$. Past this intersection $\mathbf{e}$ sets off into Σ^{--+} with initial conditions $\mathbf{e}_0 = (e_{1\text{-}}, e_{02}, e_{3+})$, hence $\mathbf{e} \subseteq \Sigma^{--+}$ resembles the critical situation described in Section 8.1.1.
As $\mathbf{e} \subseteq \Sigma^{--+} \sim \mathbf{e} \subseteq \Sigma^{++-}$ it is found that for $\mathbf{e} \subseteq \Sigma^{--+}$, then $\mathbf{e}$ will tend to Σ^{-++}. Denote the relative time instant and initial condition for e_2 when $\mathbf{e} \in \Sigma^{--+} \cap \Sigma^{-++}$ as (8.41).

$$t = t_3, \;\; e_2(t_3) = 0 \tag{8.41}$$

$|\dot{e}_2|$ is identical for $\mathbf{e} \in \Sigma^{++-}$ and $\mathbf{e} \in \Sigma^{--+}$, hence $e_1(t_3), e_3(t_3)$ resembles $e_1(t_1), e_3(t_1)$, and are given by (8.42), (8.43), respectively.

$$e_3(t_3) = \sqrt{2(\lambda+1-\gamma)e_2(t_2)} \tag{8.42}$$

$$e_1(t_3) = -\frac{2}{3}\sqrt{\frac{2}{\lambda+1-\gamma}}e_2(t_2)^{3/2} \tag{8.43}$$

Hence convergence criteria may be established as (8.44).

$$|e_3(t_3)| < |e_3(t_1)|, |e_1(t_3)| < |e_1(t_1)| \;\text{ for }\; |e_2(t_2)| < |e_2(t_0)| \tag{8.44}$$

The convergence criteria (8.44) are satisfied by virtue of (8.40), provided that $\lambda < \gamma$ and (8.18) hold true. The finite-time convergence properties, i.e. that $|\mathbf{e}| \to 0$ for $t \to T < \infty$, are established from the following reasoning. As $|\dot{e}_3|$ is identical for $\mathbf{e} \subseteq \Sigma^{++-}$ and $\mathbf{e} \subseteq \Sigma^{--+}$, the time instant t_3 is obtained similar to the time instant t_1 of (8.26). From (8.40) then $t_1, t_3 < \infty$ with $\lambda < \gamma$, (8.18) satisfied and bounded initial conditions - this implies that e_1, e_2, e_3 converge to the origin in finite time. The dependence of t_1, t_3 on initial conditions, further implies that $t_3 < t_1 < \infty$, i.e. that convergence speed increases as $|\mathbf{e}| \to 0$, at least for the control gain α large enough. The characteristic trajectory of $\mathbf{e}$ viewed in the individual phase planes of the state space are depicted in figure 8.4, and in the state space itself in figure 8.5.

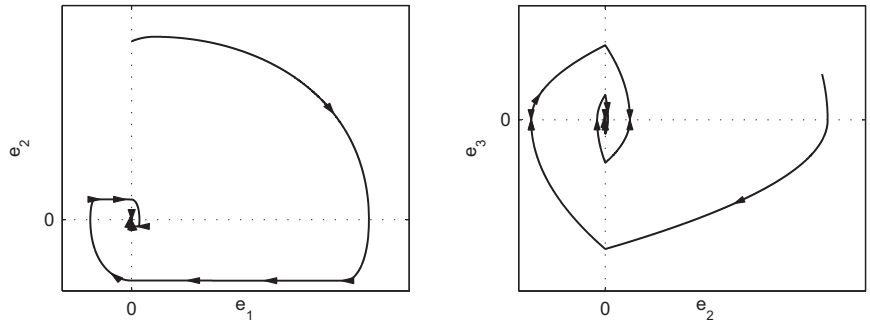

Figure 8.4: *Characteristic (e_1,e_2)- and $(e_2,e_3)-$trajectories of the algorithm* (8.13)*,* (8.10) *with $\lambda < \gamma$.*

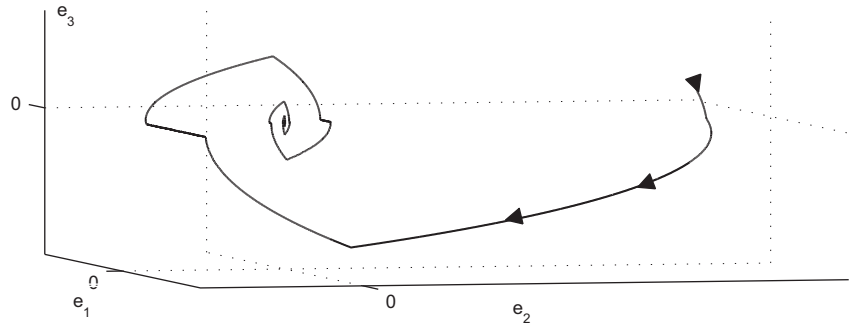

Figure 8.5: *Characteristic state trajectory* $\mathbf{e}$ *of the control algorithm* (8.13)*,* (8.10) *with $\lambda < \gamma$.*

8.1.3 Parameter Reduction & Adjustment of Transient Performance

Bearing in the mind the objective of this work, tuning parameters should be reduced to the extend it is possible, in order to limit commissioning efforts. By inspection of (8.18) and the criterion $\lambda < \gamma$ from the analysis above, then choosing $\gamma = 1$, $0 < \lambda < 1$ yield the final control and convergence criteria (8.45).

$$\bar{u}_{\mathrm{v}} = -\alpha(\lambda\,\mathrm{sgn}(e_1) + \mathrm{sgn}(e_2) + \mathrm{sgn}(e_3)), \quad \alpha > \frac{C}{K_m\lambda}, \quad 0 < \lambda < 1 \tag{8.45}$$

With this choice of γ, the controller utilizes only two parameters. This allows for limited ability to influence the transients, but also allow for obtaining distinct guidelines on how to tune the controller. From the analysis above and (8.45), then $e_1, e_2, e_3 \to 0$ for $t \to T < \infty$, for α sufficiently large, whereas λ *shapes* the transients. Figure 8.6 illustrates the transient performance for initial conditions $\mathbf{e}(0) = (0, e_{02}, e_{03})$, $e_{02}, e_{03} \neq 0$ for different values of λ and α sufficiently large. If λ is chosen near zero, the overshoot and the convergence time are increased compared to $\lambda = 0.5$, and the number of *periods* are reduced. Choosing λ near one causes the opposite behavior, increasing the number of periods and decreasing the overshoot and convergence time.

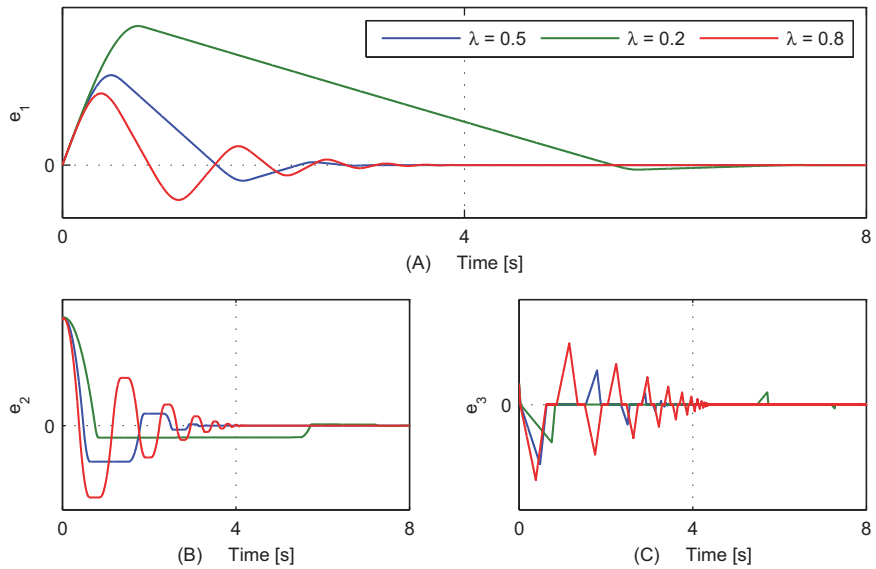

Figure 8.6: *Transient performance of e_1, e_2, e_3 for different values of λ.*

8.1.4 Compensation for Multiple Equilibria

As discussed previously, a serious drawback of this controller is the equilibrium points $(e_1, e_2, e_3) = (e_{01}, 0, 0)$ for some $e_{01} \neq 0$, which only causes a problem if $\mathbf{e}(0) = (e_{01}, 0, 0)$, provided that α is chosen properly. However, in the context of commissioning of industrial hydraulic drive applications, such initial conditions are most likely to be present, and some type of compensation need to be implemented. The problem is depicted in figure 8.7 (B), from which it is found that the closed loop system is stationary. To compensate for this problem, a simple filter and activation logic is proposed, resulting in the controller (8.46), with α, λ as in (8.45).

$$\dot{\tilde{u}}_v = -\alpha(\lambda \operatorname{sgn}(e_1) + \delta_f(\operatorname{sgn}(e_2) + \operatorname{sgn}(e_3))), \quad \dot{\delta}_f \tau_f + \delta_f = \delta, \; \delta = \begin{cases} 0, & e_2, e_3 = 0 \\ 1, & e_2, e_3 \neq 0 \end{cases} \tag{8.46}$$

When $e_2, e_3 = 0$, i.e. $\delta_f = 0$, the third order system is controlled by the single relay dependent on e_1, and the origin of the closed loop system is essentially unstable, and e_2, e_3 will tend away from the origin. However, when $e_2, e_3 \neq 0$, $\delta_f \to 1$ with a rate dependent on the filter time constant τ_f. Then e_2, e_3 tends away from the origin, and after a certain delay dependent on τ_f, the parameters of the relay scheme are such that it stabilizes the origin, leading to convergence of $e_1, e_2, e_3 \to 0$. The response from the controller (8.46) when implemented for stabilization of a triple integrator $\dot{e}_1 = e_2, \dot{e}_2 = e_3, \dot{e}_3 = \dot{\tilde{u}}_v$ is depicted in figure 8.7 (A), and the filter response in 8.7 (C). From these figures it is found the filter effectively compensates the undesired equilibria.

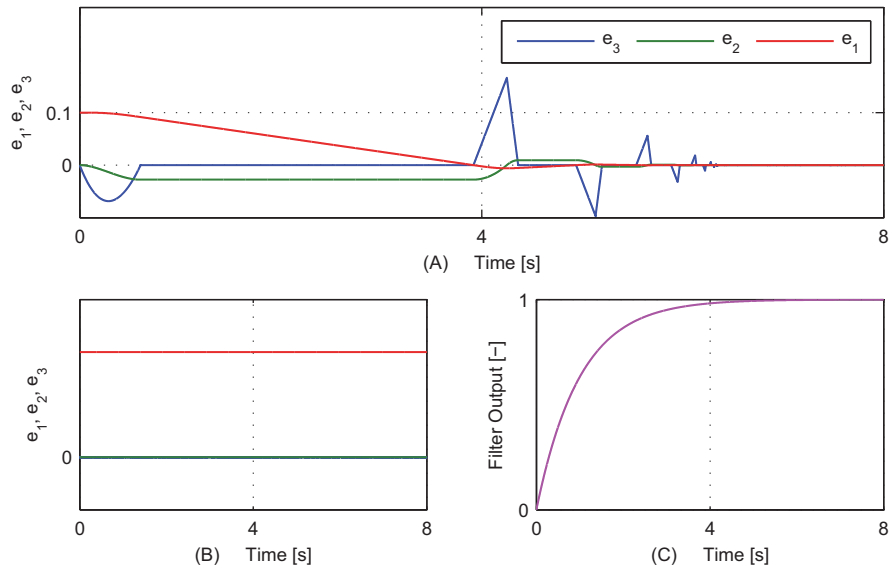

Figure 8.7: *(A) Response from the controller* (8.46) *with initial conditions* $\boldsymbol{e}(0) = (0.1, 0, 0)$*, proper* α, λ *and* $\tau_f = 1$ *[s]. (B) Response from the controller* (8.45) *with initial conditions* $\boldsymbol{e}(0) = (0.1, 0, 0)$*, i.e. without the filter compensation and proper* α, λ*. (C) Filter output* δ_f*, for the response of figure (A).*

8.2 Arbitrary Order Sliding Surface Design − A Partial Framework

With sensor technology evolving, allowing for measurement / calculation of multiple derivatives, another intriguing idea is to generalize the switching surface of the prescribed convergence controller (4.24) [Levant, 1993], such that the controller may be applied for chattering attenuation for arbitrary relative order systems. Furthermore, systematization of the surface design regardless of relative order and least possible tuning parameters are highly relevant properties. A partial framework for such a surface / controller design is proposed in the following, and has, to the knowledge of the author, not previously been presented in literature.
Consider an r^{th}-order closed loop system given by (8.47), with the sliding mode controller (8.48).

$$\mathbf{f}(\mathbf{e}) = \begin{bmatrix} f_1(\mathbf{e}) \\ f_2(\mathbf{e}) \\ \vdots \\ f_{\mathrm{r}}(\mathbf{e}) \end{bmatrix} = \begin{bmatrix} \dot{e}_1 \\ \dot{e}_2 \\ \vdots \\ \dot{e}_{\mathrm{r}} \end{bmatrix} = \begin{bmatrix} e_2 \\ e_3 \\ \vdots \\ e_{\mathrm{r+1}} \end{bmatrix} = \begin{bmatrix} e_2 \\ e_3 \\ \vdots \\ H(\mathbf{x}) + G(\mathbf{x})\dot{u} \end{bmatrix} \tag{8.47}$$

$$\dot{u} = -\alpha\,\mathrm{sgn}(S), \;\; S = \lambda_1 |e_1|^{\gamma_1}\,\mathrm{sgn}(e_1) + \ldots + \lambda_{\mathrm{r\text{-}1}} |e_{r-1}|^{\gamma_{\mathrm{r\text{-}1}}}\,\mathrm{sgn}(e_{r-1}) + e_r \tag{8.48}$$

Furthermore, assume that the open loop system is C^2 and the bounds (8.49) exist.

$$0 < G_{\mathrm{m}} < G(\mathbf{x}) < G_{\mathrm{M}} \quad , \quad |H(\mathbf{x})| \leq H_{\max} \tag{8.49}$$

Choosing the control gain α such that it satisfies $G_{\mathrm{m}}\alpha > H_{\max}$, then ideally $S\dot{S} < 0$ and a (first order) sliding mode on $S = 0$ is achieved in finite time for any initial condition $S(0)$, as discussed in Section 5.1.2. After a sliding mode has been enforced on $S = 0$, the ideal closed loop system is given by (8.50).

$$\begin{aligned}\mathbf{f}(\mathbf{e}) &= \begin{bmatrix} f_1(\mathbf{e}) \\ f_2(\mathbf{e}) \\ \vdots \\ f_{\text{r-1}}(\mathbf{e}) \end{bmatrix} = \begin{bmatrix} \dot{e}_1 \\ \dot{e}_1 \\ \vdots \\ \dot{e}_{\text{r-1}} \end{bmatrix} = \begin{bmatrix} e_2 \\ e_3 \\ \vdots \\ e_{\mathrm{r}} \end{bmatrix} \\ &= \begin{bmatrix} e_2 \\ e_3 \\ \vdots \\ -\lambda_1|e_1|^{\gamma_1}\operatorname{sgn}(e_1) - \lambda_2|e_2|^{\gamma_2}\operatorname{sgn}(e_2) - \ldots - \lambda_{\text{r-1}}|e_{r-1}|^{\gamma_{\text{r-1}}}\operatorname{sgn}(e_{r-1}) \end{bmatrix}\end{aligned} \tag{8.50}$$

Noting the discussion of Section 7.1, then weights may be assigned based on homogeneity considerations. Choosing weights and exponents of the surface S according to (8.51), then the ideal closed loop system (8.50) is homogeneous of degree $\xi = -1$.

$$r_{\mathrm{i}} = \delta + r - 1 - i \ , \ \ \gamma_{\mathrm{i}} = \frac{\delta - 1}{\delta + r - 1 - i}, \ \ i = 1, 2, ..., r-1 \tag{8.51}$$

Hence, with parameters (8.51) satisfied, the origin of the state space $(e_1, e_2, ..., e_r) = (0, 0, ..., 0)$ is finite-time asymptotically stable, if it is asymptotically stable. In the event that this is in fact the case, then the controller (8.48), (8.51) is an r^{th}-order sliding sliding controller according to Definition 1. The homogeneous controller version (8.48), (8.51) may be written in the more compact form (8.52).

$$\dot{u} = -\alpha\operatorname{sgn}(S), \ \ S = e_r + \sum_{i=1}^{r-1} \lambda_{\mathrm{i}}|e_i|^{\frac{\delta-1}{\delta+r-1-i}}\operatorname{sgn}(e_i) \tag{8.52}$$

The remaining problem is regarding stability of the closed loop system variables after a sliding mode is enforced on $S = 0$, i.e. for which parameters $\lambda_1, \lambda_2, ..., \lambda_{\text{r-1}}$, will state trajectories $\in S = 0$ converge to the origin! If it is possible to design a method that relates $\lambda_1, \lambda_2, ..., \lambda_{\text{r-1}}$ to each other through a single parameter e.g. as possible for surfaces representing linear closed loop dynamics [Slotine and Li, 1991], then the controller will be tunable via three parameters, however, this issue is still open.

In the event that the parameter design issue is solved, then the simple systematic design procedure for the control structure, and the possibility to commission the controller via only three parameters, would make this controller extremely attractive in many physical systems, and especially in hydraulic systems, in the event that slew rate limitations and time delays do not pose serious restrictions.

8.2.1 Examples of Control Structure Designs

In regard to a hydraulic drive, assuming a first order model description sufficiently accurate, then the order of the system derivative relative to the position $e = x_{\mathrm{P}} - x_{\mathrm{R}}$ is $r = 2$, and the resulting switching surface S appear as (8.53). Note, that in this case the switching surface is coincident with

that of the prescribed convergence controller for $\delta \geq 2$ discussed in Section 6.1, when applied for chattering attenuation.

$$S = e_2 + \sum_{i=1}^{1} \lambda_i |e_i|^{\frac{\delta-1}{\delta+r-1-i}} \operatorname{sgn}(e_i) = e_2 + \lambda_1 |e_1|^{\frac{\delta-1}{\delta}} \operatorname{sgn}(e_1) \tag{8.53}$$

In the event that the output function is $\int_t e\mathrm{d}t = \int_t (x_\mathrm{P} - x_\mathrm{R})\mathrm{d}t$ (i.e. e_1), then $r = 3$, leading to the switching surface (8.54).

$$S = e_3 + \sum_{i=1}^{2} \lambda_i |e_i|^{\frac{\delta-1}{\delta+r-1-i}} \operatorname{sgn}(e_i) = e_3 + \lambda_2 |e_2|^{\frac{\delta-1}{\delta}} \operatorname{sgn}(e_2) + \lambda_1 |e_1|^{\frac{\delta-1}{\delta+1}} \operatorname{sgn}(e_1) \tag{8.54}$$

Considering the third order drive model representation (2.85), still assuming the output function $\int_t e\mathrm{d}t = e_1$, then the relative order between the output function and the system derivative is $r = 5$, resulting in the switching surface (8.55).

$$\begin{aligned} S &= e_5 + \sum_{i=1}^{4} \lambda_i |e_i|^{\frac{\delta-1}{\delta+r-1-i}} \operatorname{sgn}(e_i) \\ &= e_5 + \lambda_4 |e_4|^{\frac{\delta-1}{\delta}} \operatorname{sgn}(e_4) + \lambda_3 |e_3|^{\frac{\delta-1}{\delta+1}} \operatorname{sgn}(e_3) + \lambda_2 |e_2|^{\frac{\delta-1}{\delta+2}} \operatorname{sgn}(e_2) + \lambda_1 |e_1|^{\frac{\delta-1}{\delta+3}} \operatorname{sgn}(e_1) \end{aligned} \tag{8.55}$$

8.3 Simulation Results

Consider a controller based on the algorithm (8.46) with the target of reducing control chattering, given by (8.56) (here with $\delta_\mathrm{f} = 1$), with identical boundary layers, velocity feed forward and power rate reaching law based on the actual control error e.

$$\bar{u}_\mathrm{v} = \dot{x}_R - \int_t \left((\delta |e|^\gamma + \alpha) \left(\lambda \operatorname{sat}\left(\int_t e\mathrm{d}t \right) + \operatorname{sat}(e) + \operatorname{sat}(\dot{e}) \right) \right) \mathrm{d}t, \quad 1 > \gamma > 0, \;\; \delta > 0 \tag{8.56}$$

The controller (8.56) (denoted 3TA) is verified by simulation for TC2 and compared with its TA counterpart (6.19), both with boundary layer widths of $\varphi_\mathrm{b} = 4$ [mm]. The results are depicted in figure 8.8. From figures 8.8 (A) and (B) it is found that performance of the 3TA controller somewhat resembles that of the TA controller in regard to tracking error and control input. However, from figures 8.8 (C) and (D) it is found that chattering of the *sliding* control signal for the 3TA is somewhat reduced compared to that of the TA controller. This is naturally due to the integral action on the sliding control part in the 3TA controller. It is notable that the number of tuning parameters remain the same for the TA and 3TA controllers, and as such similar tuning efforts are required. However, the usage of the piston velocity in the 3TA controller is naturally a drawback compared to the TA controller. However, as discussed in Chapter 6, if the position sensor satisfies certain requirements, a discrete implementation $\dot{e}_k$ may be substituted with $\Delta e_k = e_k - e_{k-1}$, causing this controller to be somewhat attractive compared to the TA controller.

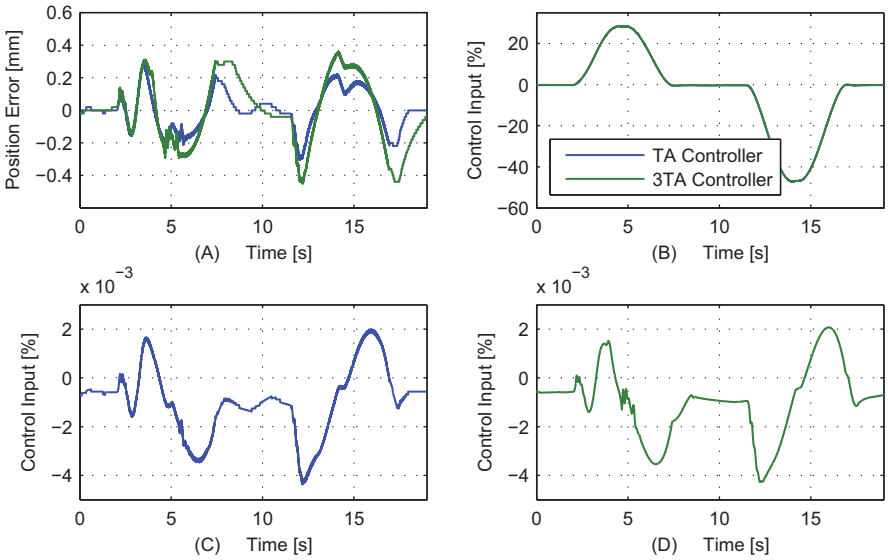

Figure 8.8: *Control performance for the 3TA and TA controllers (*(8.56)*,* (6.19)*, respectively) when implemented with Test Case 2. (A) Position tracking error. (B) Total input signals. (C) Output from sliding control part of the TA controller. (D) Output from sliding control part of the 3TA controller.*

8.4 Summary

An extension of the twisting algorithm to the third order was proposed, and theoretically elaborated. It was found that such an extension can be realized without increasing the number of tuning parameters compared to the twisting algorithm. Such an extension has the unfortunate property that the lowest order state axis is constituted by (ideally) an infinite number of equilibrium points. This undesirable feature was proposed solved by incorporation of a simple first order filter, and results demonstrate a satisfactory performance with this modification. When used in combination with boundary layers (identical for all states), velocity feed forward and the power rate reaching law, implemented with the purpose of chattering reduction, the controller proves to perform on the level with the controller based on the twisting algorithm. However, with significant reduction in control chattering. The proposed controller is found to be industrially applicable, if the position sensor satisfies certain requirements.

Targeting *high performance* systems, also a partial framework for a systematic arbitrary order sliding controller design was proposed, taking its offset in the prescribed convergence algorithm and homogeneity reasoning. The main idea is founded on the ability to reduce control chattering, while providing a systematic approach to guarantee finite-time convergence of the states included in a switching surface. The main problem with the completion of the framework arises with difficulties in establishing the necessary stability criteria for the switching surface, which is considered future work.

9 Evaluation & Final Control Structure

In the following the results for the controllers considered in previous chapters are compared quantitatively based on experimental results in terms of RMS- and maximum errors and the number of tuning parameters. Furthermore, a final control structure is proposed based on the quantitative performance results and experiences made in regard to controller tuning.

9.1 Quantitative Evaluation of Controllers

In order to evaluate *industrial* applicability of controllers, these are considered in terms of RMS- and maximum position tracking errors and the number of tuning parameters which in some sense emphasize the complexity of the tuning process. Hence, the evaluation complies (quantitatively) to the evaluation criteria discussed in Section 2.8. Furthermore, experiences with the tuning process in the implementation are taken into account. The results of the controllers that have been experimentally tested *and* found to provide for satisfactory control performance are outlined in figure 9.1 for the three test cases.

In general it is found that the gain compensator (AGC) proposed in Section 3.2 improves control performance significantly, which is also the reason for the rather accurate performance of all controllers under consideration. From an overall perspective, the proposed homogeneous controllers M-P, M-TA and M-STA demonstrate the most beneficial performance with few tuning parameters. Also these controllers were found to be easily tuned and rather insensitive to parameter variations compared to the sliding controllers. For these controllers, a too *small* boundary layer was found to cause violent oscillations and the limit case between a too small boundary layer- and a sufficiently large boundary layer was found to be somewhat narrow.

Considering specifically the homogeneous controllers, the M-TA and M-STA controllers are found to be the appropriate choices for TC1 and TC2, whereas the M-P controller is the more appropriate choice for TC3 where that lack of an integral term avoids possible limit cycles.

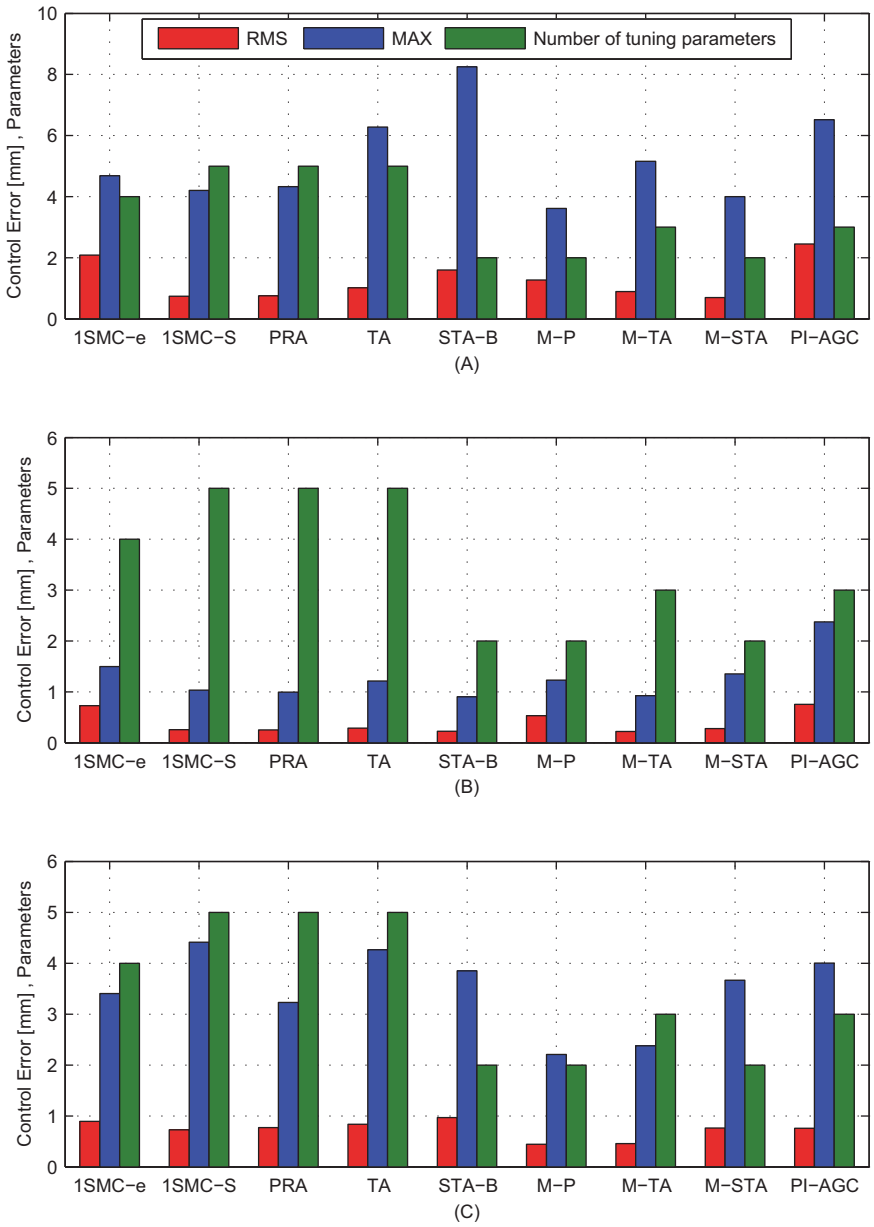

Figure 9.1: *Performance results for controllers considered in the project along with the number of tuning parameters. (A) Test Case 1. (B) Test Case 2. (C) Test Case 3.*

9.2 Outline of Final Control Structure

Based on these considerations, and in order to maintain the number of tuning parameters at a minimum, a *general* control structure that satisfies the requirements for industrial applicability, may be composed from the M-STA controller with a switching integral term, also enabling the possibility to eliminate the integral effect. Hence a novel industrial applicable control algorithm and a (possible) tuning guide line is outlined as:

Proposed control algorithm:

$$u_{\mathrm{v}} = \frac{1}{\hat{G}}\left(\dot{x}_{\mathrm{R}} - 3.5\sqrt{\bar{\gamma}}|e|^{\frac{\delta}{\delta+1}}\,\mathrm{sgn}(e) - 1.1\bar{\gamma}K_{\mathrm{isw}}\int_t |e|^{\frac{\delta-1}{\delta+1}}\,\mathrm{sgn}(e)\mathrm{d}t\right) \tag{9.1}$$

$$\hat{G} = \frac{\sigma\hat{K}_{\mathrm{vA}}}{A_{\mathrm{A}}\sqrt{\sigma^2+\mu^3}}\begin{cases}\sqrt{P_{\mathrm{S}} - \mathrm{sgn}(x_{\mathrm{v}})P_{\mathrm{L}}} & \text{for} \quad x_{\mathrm{v}} > 0\\ \sqrt{\mu P_{\mathrm{S}} - \mathrm{sgn}(x_{\mathrm{v}})P_{\mathrm{L}}} & \text{for} \quad x_{\mathrm{v}} < 0\end{cases} \tag{9.2}$$

$$K_{\mathrm{isw}} = \begin{cases}1 & \text{for } |e| \le \delta_{\mathrm{isw}}\\ 0 & \text{for } |e| > \delta_{\mathrm{isw}}\end{cases} \tag{9.3}$$

A tuning guide line:

1. Obtain $\hat{K}_{\mathrm{vA}}$, A_{A}, μ, σ from valve- and cylinder data sheet information.
2. Set $\delta = 100$, $\delta_{\mathrm{isw}} = 0$ and increase $\bar{\gamma}$ until desired performance is achieved
3. Set δ_{isw} such that the steady state error is reduced at stationary reference input
4. Reduce δ until a satisfactory performance is achieved

Evidently, bearing in mind that Bosch Rexroth, among many other things, is a manufacturer of valves and control electronics, the tuning of the algorithm (9.1), (9.2), (9.3) may be simplified even further. With the structure implemented in standard, commercially available closed loop control electronics, the parameters related to the valve $\hat{K}_{\mathrm{vA}}$, σ may be tabulated in the controller memory. This may enable the commissioning personnel of a given system just to choose the valve installed and feed in the cylinder dimensions, and not care further about the parameters $\hat{K}_{\mathrm{vA}}$, A_{A}, μ, σ. Hence, it is left to adjust $\bar{\gamma}$, δ, δ_{isw}.

10 Summary

The development of electro-hydraulic components has provided the market with opportunity for developing high performance hydraulic applications, posing strong requirements to hydraulic drives operating in closed loop control regarding performance in terms of tracking accuracy, tracking consistency and simple / easy commissioning etc. The intrinsic nonlinearities of hydraulic drives- and systems in general make it difficult to comply with these requirements using conventional linear methods, and commissioning processes are often difficult, time consuming and of an iterative nature. The work presented in this dissertation, has been concerned with the development of control structures for industrial hydraulic cylinder drives with the focus on accurate and consistent performance, limited requirements for system information, and a limited number of tuning parameters in order to facilitate a simple commissioning process.

Initially a classification of applications has been conducted in order to outline load- and hydraulic component characteristics that can be expected in regard to industrial hydraulic cylinder drives, and a test bench representing such characteristics has been established, modeled in detail, and verified. A generalized model framework has been established, representing any such hydraulic cylinder drive, taking into account possible unmatched valve- and cylinder asymmetries. Three different test cases / scenarios have been outlined, and benchmark controllers have been established based on *best industrial practice*, i.e. being linear controllers commonly applied in industry, with their parameter designs based on conventional linear methods.

Generally, the ability to monitor system parameters online during operation, may provide the possibility to enhance system performance through compensation of e.g. nonlinearities and / or online tuning of controller parameters. In this regard the applicability of the recursive least squares algorithm was investigated with main emphasis on controlling the algorithm update gain in a proper way. Doing this in a reliable way necessitates that signals applied in this process are rich enough such that the parameter set providing for zero model estimation error is unique. Such a condition contradicts with the motion performance, commonly required in industry. This fact asserts strong requirements to the update gain control, and an evaluation of state-of-the-art methods for this in the context of hydraulic drives were considered. It was found that as few as three parameters cannot be estimated reliably, to an extend where such a method is industrially applicable. However, the system gain may be estimated fairly accurately online, under certain model assumptions. Also a model based approach for online estimation of the system gain using common data sheet information and available sensors, has been proposed. When implemented for compensation of the system gain, this compensator provides significant improvement of control performance. Based on these results, all remaining developments of the project have been targeting such compensated cylinder

drives.

In order to achieve accurate- and consistent position control performance with little commissioning effort, sliding mode control strategies were considered, with special focus on output feedback control. The theoretical framework in regard to sliding mode control, and the applicability of such controllers to hydraulic cylinder drives has been discussed. The successful application of sliding mode controls was found to be strongly related to the slew rate, time delays and nominal dynamics of hydraulic control valves. These features outline the main drawback for the application of sliding modes controls, as the inability to realize discontinuous control inputs, possibly leads to control chattering and high frequent oscillations in the system. Several different methods to avoid chattering were considered, ranging from different continuous approximations of the discontinuous control input, to the usage of high order sliding modes. Continuous approximations of the discontinuous terms imposes boundary layers on control constraints, to which sliding precision can be guaranteed. However, within this boundary layer a proportional control is realized, and possible instability modes may occur here dependent on the boundary layer width. The application of high order sliding mode algorithms for chattering attenuation appear a simple and efficient solution, at least under ideal conditions. However, the presence of finite sampling frequency, slew rate limitations and time delay may significantly deteriorate performance, possibly leading to limit cycles.

Different controllers based on first order sliding modes with boundary layer were proposed, including the power rate reaching law to improve speed of convergence. From the implementation to the three test cases, it was found that such methods may enhance performance compared to the linear benchmark controllers, also implemented with the proposed compensator. Similarly, the second order sliding controllers based and the so-called prescribed convergence algorithm- and the twisting algorithm has been utilized in control designs for chattering attenuation, and for direct application in combination with boundary layers. From the experimental verification of these controllers, these were found to perform on the level with the first order sliding controllers. A main conclusion for the application of such controls is, that performance is highly sensitive to the boundary layer width / thickness. The (direct) usage of the super twisting controller was also considered. Results demonstrate that slew rate limitations and time delays significantly deteriorate the, ideally, perfect performance, leading to limit cycles in the experimental tests conducted in this project. However, the replacement of the switching term with a boundary layer function significantly alters performance, and limit cycles can be avoided. Furthermore, it should be noted that the boundary width applied here, is chosen somewhat smaller than those of the remaining controllers, due to the integral action on the boundary layer function output. Hence, a *higher level* of robustness can be achieved in comparison to conventional sliding controllers utilizing boundary layers.

The conclusion in regard to the general application of first- and second order sliding mode algorithms in hydraulic output feedback control systems is, that in the event that more high performance valves- and sensors are utilized, such control methods are applicable. However, for valves and sensors commonly applied in industry today, such methods has limited applicability from a general point of view.

Based on these findings, homogeneous extensions / modifications of the considered sliding algorithms were proposed. The main features are, that these algorithms are continuous hence avoiding boundary layers, and furthermore provide for finite-time convergence of controlled states to zero, under certain model assumptions. The algorithms have been developed using weighted homogene-

ity considerations, and finite-time convergence properties have been established from elaborated research literature. The proposed homogeneous controllers are highly versatile in the sense that, dependent of parameters, the resulting performance resembles that of their sliding mode counterparts- or conventional linear controllers. This feature emphasizes their properties of being generally applicable to a wide ranges of systems, and especially to hydraulic drives. Experimental results demonstrate the announced properties, and the controllers are furthermore easily tuned. Furthermore, these controllers exhibit significant improvement of control performance, compared to their linear counterparts, in all cases implemented with the proposed compensator. In the specific case with the homogeneous extension of the super twisting controller, only two parameters need to be tuned, rendering this highly applicable from an industry point of view. Hence, this control structure together with the proposed gain compensator are considered the main result in regard to the objective of this project.

Finally, an extension of the intriguingly simple structure of the twisting algorithm, was proposed, constituting an algorithm containing three relay functions. A system controlled by such a controller contain, ideally, infinitely many equilibrium point, which was proposed compensated using a simple logic and a first order filter. The three relay algorithm was analyzed via geometric considerations on the state trajectory, and was found to be asymptotically stable for certain initial conditions. Simulation results demonstrate performance on the level with the twisting algorithm, but with reduced control chattering. Furthermore, a partial framework for a controller with a systematic surface design, applicable to arbitrary order systems has been proposed. The main idea is founded in an arbitrary order homogenous surface design, and stability issues for motion on this surface remains an open topic, and an objective for future work. The application of these controllers necessitates at least an additional measurement in terms of the velocity, and is hence not directly applicable in many present day industrial applications. This summary answers the research questions of the Introduction.

A Appendix

A.1 Main Components of Hydraulic Test Bench

Component	Description
4WRKE 10 E1-100L-3X/6EG24EK31/F1D3M	Proportional flow control valve
4WRTE 10 V1-100L-4X/6EG24EK31/F1M	Proportional flow control valve
4WREE 10 V50-2X/G24K31/F1V	Proportional flow control valve
4WREE 6 V32-2X/G24K31/F1V	Proportional flow control valve
A10VSO100 DFR /31R-PPA12N00	Variable axial displacement pump
DBETE-6X/315G24K31A1V	Pressure control valve (pump LS)
HM 17-1X/250-C/V0/0	Pressure sensor

Table A.1: *Main hydraulic components in test bench.*

A.2 Parameters - Chapter 2

Parameter	Axis 1	Axis 2	Axis 3	Axis 4
B_h [Ns/m]	9075	10900	30129	3300
B_m [Nms/rad]	8775	6830	–	2372
F_fC [Nm]	2280	500	2045	500
F_fS [Nm]	3000	300	174	50
c_f1 [m/s]	0.011	0.0011	0.0010	0.02
c_f2 [-]	2000	2000	2000	2000
A_A [m^2]	0.0127	0.0127	0.0045	0.0062
A_B [m^2]	0.0101	0.0096	0.0030	0.0031
C_L [m^3/s/Pa]	$1e-13$	$2e-12$	$2.0e-12$	$2.1e-10$
β_F [Pa]	$5.3e8$	$5.3e8$	$5.3e8$	$5.3e8$
V_0A [m^3]	0.0030	0.0011	0.0011	0.0011
V_0B [m^3]	0.0103	0.0061	0.0035	0.0038
ε_Air [-]	0.04	0.04	0.03	0.04
C_ad [-]	1.4	1.4	1.4	1.4

Table A.2: *Friction-, cylinder and hydraulic parameters.*

Parameter	
L_{AO0}	425 [mm]
L_{BO0}	1588 [mm]
L_{BC}	487 [mm]
L_{CO0}	1170 [mm]
L_{CO1}	1220 [mm]
L_{DO1}	350 [mm]
L_{EG}	229 [mm]
L_{EH}	1630 [mm]
L_{FH}	474 [mm]
L_{FI}	380 [mm]
L_{GH}	1491 [mm]
L_{HO3}	185 [mm]
L_{IO3}	375 [mm]
L_{IO4}	1133 [mm]
L_{O3O4}	902 [mm]
L_{O0O1}	2398 [mm]
L_{ABmin}	1170 [mm]
L_{CDmin}	930 [mm]
$L_{O2O3min}$	2005 [mm]
L_{EFmin}	1185 [mm]
L_{CM1x}	-0.972 [mm]
L_{CM1y}	0 [mm]
L_{CM2x}	0 [mm]
L_{CM2z}	0.68 [mm]
L_{CM3x}	0.14 [mm]
L_{CM3y}	0.819 [mm]
m_1	508.8 [kg]
m_2	312.5 [kg]
m_3	149.3 [kg]
m_4	213 [kg]
I_{zz1}	129.96 [kgm^2]
I_{yy2}	74.44 [kgm^2]
I_{zz3}	67.8 [kgm^2]
I_{zz4}	70 [kgm^2]
φ_{H1}	0.1168 [rad]
φ_{33}	1.8382 [rad]
φ_{01}	1.3781 [rad]
φ_{03}	0.1836 [rad]
Stroke - Cylinder 1	827 [mm]
Stroke - Cylinder 3	1050 [mm]
Stroke - Cylinder 2	583 [mm]
Stroke - Cylinder 4	892 [mm]

Table A.3: *Manipulator parameters.*

Parameter		Parameter	
C_{Lp}	$10e-11$ [m^3/s/Pa]	V_{S}	0.0030 [m^3]
D_{P}	$3.18e-05$ [m^3/rad]	β_{PS}	$8e8$ [Pa]
ω_{m}	152 [rad/s]	η_{P}	0.95 [mm]
ζ_{ps}	10 [-]	ω_{s}	5.45π [rad/s]

Table A.4: *HPU parameters.*

Parameter	4WRKE	4WRTE	4WREE 10	4WREE 6
ω_{v1} [rad/s]	150π	150π	120π	90π
ω_{v2} [rad/s]	220π	220π	138π	200π
ζ_{v} [-]	1.0	0.6	0.6	0.6

Table A.5: *Valve parameters (dynamic).*

Parameter	K_{P}	K_{i}	$K_{\mathrm{f+}}$	$K_{\mathrm{f-}}$
TC1	4.00	4.00	0.0045	0.0029
TC2	4.00	4.00	0.0045	0.0029
TC3	11.62	8.30	0.0034	0.0027

Table A.6: *Benchmark controller parameters, with the input normalized to* 100 %.

A.3 Parameters - Chapter 5

Parameter	δ	γ	α	φ_{b} [mm]
TC1	4.00	0.875	0.025	9
TC2	4.00	0.875	0.025	4
TC3	11.62	0.875	0.055	10

Table A.7: *1SMC-e controller parameters, with the input normalized to* 100 %.

Parameter	δ	γ	α	λ	φ_{b} [mm]
TC1	4.00	0.875	0.025	π	9
TC2	4.00	0.875	0.025	π	4
TC3	11.62	0.875	0.025	π	10

Table A.8: *1SMC-S controller parameters, with the input normalized to* 100 %.

A.4 Parameters - Chapter 6

Parameter	δ	γ	α	λ	φ_b [mm]
TC1	4.00	0.875	0.025	1.0	9
TC2	4.00	0.875	0.025	1.0	4
TC3	11.62	0.875	0.030	0.7	10

Table A.9: *PCA controller parameters, with the input normalized to* 100 %.

Parameter	δ	γ	α_1	α_2	φ_b [mm]
TC1	4.00	0.875	0.042	0.020	4
TC2	4.00	0.875	0.042	0.020	3
TC3	4.00	0.875	0.053	0.025	4

Table A.10: *TA controller parameters, with the input normalized to* 100 %.

Parameter	$\bar{C}$
TC1	0.03
TC2	0.02
TC3	0.05

Table A.11: *STA controller parameters, with the input normalized to* 100 %.

Parameter	$\bar{C}$	φ_b [mm]
TC1	0.03	0.5
TC2	0.02	0.5
TC3	0.05	0.5

Table A.12: *STA-B controller parameters, with the input normalized to* 100 %.

A.5 Parameters - Chapter 7

Parameter	α	γ
TC1	0.03	0.5
TC2	0.02	0.5
TC3	0.05	0.5

Table A.13: *M-P controller parameters, with the input normalized to* 100 %.

Parameter	α_1	α_1	δ
TC1	4.00	4.00	7
TC2	4.00	4.00	8
TC3	11.62	8.30	13

Table A.14: *M-TA controller parameters, with the input normalized to* 100 %.

Parameter	$\bar{\gamma}$	δ
TC1	4	8
TC2	2	8
TC3	3	8

Table A.15: *M-STA controller parameters, with the input normalized to* 100 %.

A.6 Working Paper Referred in Chapter 3

Recursive Parameter Estimation of Electro-Hydraulic Actuator Systems - A Review

Lasse Schmidt
Bosch Rexroth A/S, Denmark
Email: lasse.schmidt@boschrexroth.dk

Torben O. Andersen
Department of Energy Technology
Aalborg University, Denmark
Email: toa@et.aau.dk

***Abstract*—This paper provides a review of contributions in the literature related to on-line parameter estimation of electro-hydraulic actuator systems by use of the recursive least squares method. Variations in contributions are primarily restricted to be within the approach to control the algorithm update gain, and these are classified as the *exponential forgetting factor* approach, the *variable forgetting factor* approach, the *variable forgetting factor approach with dead zone*, the *covariance matrix regularization* approach and the *controlled covariance trace* approach. The contributions are each evaluated with emphasis on system type on which the scheme is applied, type of regression model used, the ability of the algorithms to track parameter variations and the boundedness of the algorithms. This review is carried out bearing in mind the possibility of application to EHA systems continuously operating under industrial conditions.**

I. Abbreviations

The abbreviations used throughout this paper are:

CCT:	Controlled covariance trace.
DZ:	Dead zone.
EA:	Estimation algorithm.
EFF:	Exponential forgetting factor.
EHA:	Electro-hydraulic actuator.
LP:	Linear-in-parameters.
LS:	Least squares.
PE:	Persistent excitation.
RC:	Regularization of covariance matrix.
RLS:	Recursive least squares.
VFCR:	Variable forgetting factor and covariance resetting.
VFF:	Variable forgetting factor.

II. Introduction

With the development of reliable proportional flow control components with medium transient performance characteristics to acceptable prices, trends and demands are increasingly to develop and deliver high performance, energy efficient *turn-key* solutions. The great majority of hydraulic systems developed are produced in a limited number for specialized applications, where budgets are too limited to design professionally engineered model based motion control systems. In these cases *stand alone* economically feasible digital controllers employing traditional linear control schemes, dedicated to control electro-hydraulic components with *ease-of-use* interfaces, are widely used. However, the often limited knowledge on control theory, usually results in poor performance with no indications of stability margins, robustness to perturbations in system parameters due the inherently nonlinear dynamics, and parameters such as viscosity-temperature relations, friction factors, air content, variant inertia load and so forth. Due to this, commissioning of electro-hydraulic motion control systems is often an iterative and hence expensive process making it difficult to comply with tight budgets and delivery deadlines. This, and the fact that performance requirements are constantly increasing, naturally leads to the idea of employing more advanced control schemes in order to improve control performance. However, such approaches often require extensive system knowledge, which do not comply with the industry in general, as system dynamic characteristics, load characteristics and expected disturbances can rarely be defined. Hence, in order for industry to capitalize on advanced control strategies, emphasis must be put on the ability to obtain specific system parameters or characteristic dynamic properties such as natural frequencies, damping ratio and system gain based on sensors generally available in industry, i.e. piston- and valve spool positions- and load pressure measurements. By successfully obtaining such parameters previous to motion control commissioning- and on the fly would greatly promote the successful application of more advanced control strategies in industry.

A. Identification of Electro-Hydraulic Actuator (EHA) Systems

Identification of EHA systems is typically applied as a part of (indirect) adaptive control schemes. Various approaches have been reported in literature, including various hydraulic system types and EA types span from being based on neural networks, differential evolution theory, supervised learning etc., to various recursive and least squares approaches and identification based on MATLAB functionalities. In general many papers fail to provide information or guidelines on how- and under which conditions the identification process is carried out, whether time variant parameters are accounted for etc. In the following a brief status on hydraulic system identification is given to provide an overall picture on the topic.

The authors of [1], [2], and [3] applied neural networks for the generation of regression models of nonlinear semi-active hydraulic dampers, resulting in fairly precise models when considering transient performance. The contributions [4], [5] and [6] all concerned the identification (and for [4] and [6] also the control) of electro-hydraulic systems by use of neural

networks. In [4] a so-called *optimal tracker* employing neural networks as its identifying structure and controller was developed, and shows to poses good adaptability and robustness, concluded from transient responses, but shows poor steady state performance. Also [5] presents good transient and steady state model performance, whereas [6] lacks information on the actual performance of the identification process.

Regarding supervised learning, [7] presented a so-called Self-Adaptive Controller based on the least square support vector machine. The controller termed LSVM-PID has the main features of a LSVM identification- and self-adaptive control networks. The scheme has been implemented as an electro-hydraulic force servo, and results on the performance of the identification process are limited, but an identified constant parameter transfer function is presented, which is known to fit hydraulic actuators only for specific operating points, due to time variant dynamics.

System identification based on differential evolution theory was first proposed by [8]. In [9] this method was applied for the parameter estimation of an electro-hydraulic system with a flexible load, and promising results on transient- and steady state performance were presented. However, [9] lacks information on the actual implementation, and the ability of the algorithm to track time variant parameters.

In [10] and [11] an approach for identification and control of electro-hydraulic position- and pressure servo systems are presented, applying Matlab Toolbox functionalities. In both cases model and parameter estimates of a symmetric EHA system loaded by a spring-damper system are made - the presentation of the hydraulic systems are limited. The identification procedures are carried out previous to a control design process, and the results are in both cases models that contained constant parameter values - this will, as mentioned previously, only depict the system at a specific operating point. A similar approach was presented in [12], that concerned the modeling of a hydraulic circuit for off-highway vehicles, with the parameter identification carried out off-line applying a nonlinear least squares approach in Matlab.

B. Problem Statement & Contribution

This paper has the purpose of providing a review of contributions reported in literature regarding recursive identification/estimation of EHA systems - more specifically with the application of the recursive least squares (RLS) algorithm. This review is mainly focused on strategies for the control of the RLS update gain. During the review of contributions emphasis is put on the EHA system types on which RLS is applied, the regression model applied, the parameter tracking ability and the boundedness of the algorithm. Many contributions focus mainly on the related control design and little on the parameter estimation algorithm, and lack information on how the implementation is carried out, performance of the algorithms regarding the ability to actually estimate the true parameters, track time variant parameters etc. Regarding the latter, due to the inherent nonlinear dynamics of EHA systems, some level of parameter variation will be present (depending on the components), even if physical properties such as inertia load, supply pressure, friction coefficients etc. remain constant. This is due to volume chamber variation, nonlinear flow characteristics of valves etc. Furthermore, parameter variations will result from perturbations in the physical parameters. Hence the ability of the EAs to capture such variations is crucial. The nature of parameter variations depend naturally on operating environment, available states and parametric information and the approach to regression modeling.

Hence this review provide mains focus on the following criteria, in order to draw some level of comparison between the different contributions:

System type: The type of hydraulic system used, emphasizing main component properties as well as the load system and available feedbacks.

Regression model: The regression model used for parameter estimation, including the level of model simplification etc.

Parameter variations: Whether the EAs are able to track time variant parameters (henceforward designated parameter variations) resulting from unmodeled dynamics, variations in the system states and/or resulting from variations in physical parameters.

Algorithm boundedness: Whether the EAs, from the information presented in the papers, may be considered bounded at all times, and especially in periods of insufficient PE.

To maintain some structure in the exposition of the contributions, these are divided into five main sections defined by the type of update gain control approach applied. These are:

Exponential forgetting factor (EFF-RLS): Modifications to RLS algorithms containing exponential forgetting factors of constant values.

Variable forgetting factor (VFF-RLS): Modifications to RLS algorithms containing variable forgetting factors.

Variable forgetting factor with dead zone (VFDZ-RLS): Modifications to RLS algorithms containing some kind of dead zone in relation to the parameter updates.

Regularization of the covariance matrix (CR-RLS): Modifications to RLS algorithms containing so-called regularization of the covariance matrices.

Controlled covariance trace (CT-RLS): Modifications to RLS algorithms applying control of the covariance matrices.

Although it turns out that most papers in which RLS type of algorithms are applied, are concerned with indirect adaptive control schemes, focus is put on the EA part of the algorithms.

III. Exponential Forgetting Factor (EFF)

In the area of RLS gain update modifications, the application of EFF (with constant values) to RLS algorithms seems the most common when investigating the general literature, and in relation to EHA systems different contributions have been reported.

In [13] a so-called adaptive high bandwidth controller is proposed, constituted by an adaptive feed forward combined with a feedback control scheme. Here an EFF-RLS algorithm is used for parameter estimation. The system for which the controller is developed is a horizontally mounted, servo valve controlled asymmetric cylinder with a constant inertia load. Full state feedback is available in terms of piston velocity- and position, and the actuator force. The system is modeled in state space with the coulomb friction and stiction considered unknown and the individual equations of the state space representation are established as regression models. For parameter estimation an EFF-RLS algorithm is applied as proposed in [14], but with no discussion on the choice of EFF. No discussion on algorithm boundedness is presented, even though it is a well known property of EFF-RLS algorithms, that the update gain may grow unbounded in periods with insufficient PE. The tracking performance of the developed controller is experimentally validated with sinusoidal reference trajectories of different frequencies in the range $0.5 - 11.0$ $[Hz]$ and amplitudes of ~ 0.4 $\%$ of the actuator range. Due to the limited trajectory, and that no parameter perturbations are made, the tracking ability of the EA may not be concluded from the results.

In [15], a continuous EFF-RLS algorithm is applied as a part of an indirect adaptive control scheme for a hydraulic asymmetric cylinder, actuating the rotary movement of a robot arm. The cylinder is controlled by a servo valve, with full state feedback available in terms filtered angular acceleration, velocity and position of the swing motion, as well as the actuator pressures. The system is modeled as a linear-in-parameters (LP) regression model, and the EFF-RLS proposed in [16] is applied for parameter estimation, not discussing size of forgetting factor, EA boundedness etc. The tracking ability of the controller is experimentally verified via a rectangular-like cyclic reference position with a frequency of approximately 1.5 $[Hz]$. Off-line parameter estimates are obtained to represent the *true* system parameters (used to evaluate the on-line parameter estimates), through a method not further specified. Due to the regression model applied, the assumption of constant parameters is considered reasonable. Only estimates on the inertia load, coulomb friction and oil bulk modulus are presented, showing convergence to the off-line estimates. Furthermore, no information on the EA performance after parameter convergence is shown, and no perturbations to physical parameters are made. This together with the somewhat constant parameters estimated, the ability of the EA to track varying parameters can not be concluded.

Another but similar approach to parameter estimation is proposed in [17], where an EFF-RLS algorithm is applied in an indirect adaptive backstepping control scheme for an EHA system. The system is constituted by a servo valve controlled, fixed displacement motor with a constant inertia load, and an external load not further specified. Full state feedback in terms of velocity-, position and actuator load pressure is available. A state space representation of the system is established, assuming the load to be zero, and the regression model for parameter estimation is established as a LP model, i.e. with the regression vector containing known nonlinearities and remaining parameters obtainable through data sheet information and feedbacks. The EA is operating on-line, with the continuous EFF-RLS algorithm proposed by [18]. However, no discussion on the choice of EFF, nor the algorithm boundedness is presented. The proposed controller is validated through simulations, using a sinusoidal position reference as input, with an amplitude of $\sim 2\pi$ $[rad]$ and a frequency of 1 $[Hz]$. The parameter tracking ability of the EA is verified through a step-like perturbation to the viscous damping coefficient of roughly 25 $\%$ of the initial value. Whether the parameters converge to their true values is not presented, however the control scheme shows adaptability to the parameter variation.

In [19] an EFF-RLS algorithm is implemented as a part of an iterative learning control scheme for an EHA system. The system is constituted by a horizontally mounted symmetric cylinder, controlled by a flapper nozzle type servo valve. A time discrete linear regression model is applied, with the load constituted by inertia-, damping and an additional force containing disturbances and friction and full state feedback are available in terms of piston velocity- and position. The EFF-RLS method applied is similar to that of [20], but is operating with respect to the number of operation cycles, and not the number of samples. With the application of a 2 $[Hz]$ sinusoidal position trajectory with an amplitude of 5 $\%$ of the cylinder range, the proposed controller is evaluated. The parameter tracking ability of the EA is evaluated by reducing the supply pressure to half of its initial value on-line, and it is shown that the controller regained its tracking performance after six iterations.

In [21] a self-tuning controller is designed for a passive electro-hydraulic loading system, employing an EFF-RLS algorithm. The hydraulic system is a servo valve controlled, fixed displacement motor, apparently with a constant inertia load, and position feedback. A discrete linear regression model is used to represent the system in an EA, similar to that of [22]. For controller validation experiments are carried out by feeding a rectangular periodic reference to controller. The parameter tracking ability of the EA is not presented, however, the self-tuning controller utilizing the EA demonstrates improved performance compared to a similar but non-self-tuning type.

In [23] an adaptive state controller is designed for a servo valve controlled asymmetric cylinder drive, with a constant inertia load. Available feedbacks used in the parameter estimation are the valve spool position, piston position-, velocity- and acceleration. The model used in the EA is based on a continuous linear transfer function containing the feedbacks in the regression vector. The EA applied is

similar to that of [22]. Apparently some kind of switch is also applied in order to turn off the EA in periods of insufficient PE - however no discussion this is given, nor is a discussion on whether the algorithm will remain bounded. The reference trajectory is not presented, nor are the parameter estimation results, hence the parameter tracking ability of the EA may not be evaluated.

In [24] a self-tuning controller is designed for a servo valve controlled fixed displacement motor with a constant inertia load, with the motor speed fed back. The system is modeled as a linear time discrete model as proposed in fx [22]. The EA applied is similar to that of [22]. A rectangular periodic reference trajectory is applied for the evaluation of the combined EA- and control scheme. The resulting parameter estimates demonstrated convergence to constant parameters. Furthermore, the tracking ability of the EA is evaluated toward perturbations in the supply pressure and the shaft load. The EA proves to respond to these perturbations, however whether true parameter values are tracked is not presented. Note; perturbations are applied shortly after initiation of the EA, and in the case of a *large* initial covariance matrix the parameter update gain might have been sufficiently high to track these variations - hence the effect of an ill-chosen forgetting factor may not be clear.

In [25] a self-tuning controller containing an EFF-RLS algorithm is applied to a servo-hydraulic materials testing machine. The system is constituted by a servo valve controlled symmetric cylinder with a constant mass-spring-damper type of load. Feedback available are the piston position, load force and specimen strain. The system is modeled as a linear regression model, and the EA applied is the EFF-RLS type of algorithm proposed in [26]. In the results shown, sinusoidal load- and strain references are fed to the controller with a frequency of approximately $0.5\ [Hz]$. Estimated parameters respond to some level of parameter variation, however, convergence of parameters to their true values is not discussed.

In [27] a self-tuning pole placement controller is proposed for a hydraulic positioning system. The system is a servo valve controlled symmetric cylinder with a constant inertia load and spring like load, with the spring attached to a fixture, having the position fed back. The system as modeled as a linear regression model and the EFF-RLS approach proposed by [18] is used for parameter estimation. Further discussion on the EFF is not presented. The controller and EA are evaluated by feeding a rectangular periodic input to the controller for which the frequency and amplitude are not clear. The EA demonstrated its tracking ability when parameters are abruptly changed, however with a significant transient stage.

A. Summary on EFF-RLS

It may be summarized that in general only few contributions have been made with EFF-RLS algorithms applied to EHA systems, and the ones made provide only limited information on parameter convergence to true parameters, and generally lack information on ability to track parameter variations. Furthermore, it is noted that applying an EFF of constant value will cause old data to be discarded exponentially in time, meaning that the weighting of old data compared to new data is constant. Hence in periods with insufficient PE, noise may become the dominant variation in the regressors, and may lead to erroneous parameter estimates.

IV. Variable Forgetting Factor (VFF)

Having considered contributions utilizing the (constant valued) EFF modification of the RLS algorithm for parameter estimation, attention is put on contributions applying the obvious modification of a variable forgetting factor. This has been investigated thoroughly in the general literature on the subject, and regarding VFF approaches related to EHA systems in literature, various approaches have been presented - from being dependent on time only, to being dependent on the internal states of the EA, etc.

A. Time Dependent VFF

In [28], the application of a VFF-RLS algorithm for identification of an EHA system is discussed. The system used is a horizontally mounted asymmetric cylinder with a constant load, controlled by a two stage overlab valve, with the piston position used as feedback. The system is modeled as a linear discrete time model, based on the assumptions that the piston areas are equal to each other, and that the valve dynamics can be approximated by first order dynamics - following from this, parameter variations must be expected, however no discussion on this is presented. The VFF-RLS algorithm proposed in [22] is applied, with the VFF being variable according to [29], with no further discussion of this topic. The VFF has the ability to vary from some predefined initial value (below one), up to one, as the number of samples evolves, i.e. the value of the VFF is completely independent on the remainder of the algorithm, and will eventually converge to one, and the update gain to zero. For experimental verification of the EA, a sum of sinusoidal type of input is applied, but no indication on the input signal range, nor the resulting output position range is presented. The model order is determined through off-line experiments, and it is concluded that a third order model is sufficient to represent the system. For comparison with on-line estimated parameters, the model obtained in the off-line experiment is used to represent the *true* system model, even though some level parameter variation must occur, unless small in- and output ranges are used. In the results presented, the parameters converge to constant values - this can, however, only be the case in a limited piston range (where parameter variations must be considered small), or due to the fact that the VFF converges to one, causing the parameter update gain to tend to zero. This type of VFF modification will cause the algorithm to eventually be bounded as the VFF tends to one as the number of samples evolves. However, if insufficient

PE is merging with a low value forgetting factor, the update gain may grow unbounded similar to the EFF.

Another contribution by the same authors is presented in [30], which discusses the application of a similar VFF-RLS algorithm as in [28] - however, here the aspect of open-loop versus closed-loop identification is taken into account in the discussion. The system used is similar to that of [28], with the same assumptions and regression model. However, for the experimental results, a direct (open loop) approach is used, making the estimation procedure somewhat similar to that of [28].

In [31] a VFF-RLS algorithm similar to those presented in [28] and [30] is applied as a part of an adaptive nonlinear backstepping control scheme for an EHA system. Here the system and regression model (LP approach) are similar to those of [32] and [17], but with a VFF being dependent only on time, but here being a continuous version. For experimental validation, a sinusoidal angular position reference with an amplitude of approximately $2\pi[rad]$ and a frequency of $1\ [Hz]$ is applied. The parameter tracking ability of the EA is verified by application of an external load torque of ten times the nominal load. The EA responds to this variation, and the performance of the adaptive backstepping controller is maintained, opposite to a similar but non-adaptive version in which the increased load torque clearly affects the performance of the controller. As the VFF will eventually tend to one, this parameter adaption may be less effective if applied after a larger period of time. It is found that the VFF approaches of [28], [30] and [31] are somewhat similar in the sense that they depend only on time (or the number of samples).

B. Model Error Dependent VFF

An alternative to a purely time dependent VFF, is to make it dependent on the model estimation error. Such an approach is made in [33], where a VFF-RLS algorithm is employed for the parameter estimation related to an indirect adaptive control scheme for hydraulically actuated materials testing machines. The testing machine used has the possibility to control load, position- and strain. The hydraulic actuation system is a vertically mounted symmetric cylinder, attached to a test specimen from below - hence it has a fairly constant inertia load and a spring-like load produced by the test specimen. The cylinder is controlled by a servo valve, not further specified. Furthermore, the filtered- actuator force and piston position are available from measurements. Regarding the parameter estimation only an on-line estimate of the spring stiffness is considered, as additional parameters are known, resulting in a single parameter model (relating the displacement to the force). An RLS approach similar to the one proposed in fx. [22] is applied, modified with a VFF inversely proportional to the squared model error within a predefined lower bound, and an upper bound of one. Furthermore an upper bound on the covariance trace is applied in order to avoid covariance blow-up. Experiments are carried out on three different machines, with the force range for the three machines as $10\ \% - 100\ \%$ of the maximum rated force, the stroke range as $37.5\ \% - 100\ \%$ of the maximum stroke, and the piston area range as $10\ \% - 100\ \%$ of the maximum piston area. Results show a fluctuation in the VFF within its bounds, the covariance trace bounded, and a varying estimated stiffness. However, no discussion on parametric convergence is presented, but the adaptive controller shows improved performance in comparison with a similar, but non-adaptive type.

C. Covariance Trace Based VFF

Opposite to the VFF approaches given in the above subsections, a rather thorough documented approach to apply a VFF is reported in [34]. Here a VFF-RLS algorithm is applied as a part of an indirect adaptive controller for hydraulic crane axes. Here the individual links of the crane are actuated by (mobile) valve controlled asymmetric cylinders. The filtered- piston position and actuator load pressure are used as feedbacks. Through the filtering of feedback signals, the derivatives of the signals are obtained, in order to carry out the parameter estimation on continuous time transfer functions representing the system (with a discrete VFF-RLS algorithm). It is recommended that filters should be one order higher than these transfer functions. A covariance trace based VFF and an additional parameter- and covariance update control variable is implemented, leaving only the covariance trace upper bound and the VFF lower bound as variable EA parameters. For the control of these parameters the VFF lower bound is calculated based on the sampling time of the controller hardware, and an identification time constant based on the approximate time constant of the system. The upper bound of the covariance trace is based on the average of the information matrix (the inverse of the covariance matrix). Furthermore, to handle component saturation, an override control of the parameter- and covariance update terms is introduced. In order to verify the proposed controller and EA, an input signal to the valve is applied as a pulse like input with exponential decay and of different amplitude and occurrence in time. The range of the actuator is not defined. Through simulation studies, the parameter tracking ability of the EA is evaluated by, at some point in time, suddenly increasing the resonance frequency by $1/3$, in a period with limited PE. Due to appropriate design of the VFF control and the additional control variable, limited response of the EA occurs - however, as some level of PE is restored, the parameter change is quickly adapted by the EA.

D. Eigenvalue *Based VFF*

In [35] an adaptive speed controller used for constant load pressure control is designed for a variable displacement motor, with the swash plate angle controlled by a servo valve. The regression model is based on the continuous time model, and available feedbacks are the motor speed and the torque. In periods of poor excitation, the forgetting factor is set to one (no guidelines given), and in periods of excitation, the VFF is operated in a range below one, dependent on the level

of excitation. The VFF control is based on the *eigenvalue* of the estimator, with the VFF proportional to this. In the results shown, the parameters tend to constant values, and no parameter variations are applied in order to evaluate the ability to track parameter variations. Furthermore, algorithm boundedness is not discussed.

E. Summary on VFF-RLS

Considering the VFF-approaches discussed in this section, it is found that those presented in [28], [30] and [31] are not applicable to EHA systems in general, as the VFF tends to one, as time (or the number of samples) evolves. This causes the VFF-RLS to approach the basic RLS, for which it is known that the update gain will tend to zero in the presence of sufficient PE, and the RLS will eventually loose its ability to update the parameters (for a thorough discussion on this, see [36]). Regarding the VFF-approach applied in [33], the parameter estimates will be updated based on more recent measurements, as the model error is increased. The contribution reported in [34] seems generally applicable as all system parameters here are considered unknown. The regression models are based on filtered states and the parameters of continuous time transfer functions are identified directly. Furthermore, during tests the update gain varies with the level of PE, and the algorithm shows boundedness at all times, and has the ability to track parameter variations. Also the eigenvalue updated VFF presented in [35] may be suitable, however this paper suffers from lack of information on how to deactivate the EA in periods with limited PE. Furthermore the stability and boundedness of the algorithm can not be concluded directly from the paper.

V. Dead Zone based RLS (DZ)

Another approach is to update the algorithm based on a dead zone for the model estimation error.

Such an algorithm is proposed in [37] as part of an indirect adaptive control scheme for an EHA system. The EHA system used is not completely defined, and information on the load is limited - however it is periodic. Whether this is in terms of inertia, gravity, external load force etc. is not presented. It is stated that the system contains a two-stage flapper nozzle type servo valve, and the actuator type appears to be an asymmetric cylinder. Actuator load pressure- and piston position are used as feedbacks. The system is modeled as an 8^{th} order discrete time linear model in order to include some level of higher order dynamics from disturbances, and in this way make the identified model somewhat more accurate in the presence of unmodeled dynamics (however this increases the requirement for PE). The basic algorithm in this paper is somewhat different from the type usually seen (e.g. [22]). The model prediction error at the k^{th} sample is based on the estimated parameter of the k^{th} sample, which is numerically impossible - furthermore the update terms are based on the regression vector and the covariance matrix at the $(k-1)^{th}$ sample, which differs from update terms usually seen for RLS algorithms. The covariance matrix is updated based on the sum of covariance matrices from previous samples, and not the gradient as normally seen, which implies that the EA may not be stated correctly. The forgetting factor is controlled based on a model error dead band, causing the forgetting factor to attain values between zero and one. In case the model error is within the dead band, the parameter- and covariance updates are turned off. This provides no information on the boundedness of the EA - if e.g. the model error increases in a period of insufficient PE, the forgetting factor is reduced, causing the parameter estimates to based on more recent information - however, as PE is insufficient, the covariance trace, hence the update gain may grow unbounded. For experimental validation a cyclic trajectory is applied, with an amplitude of approximately $25\ \%$ of the actuator range and a frequency of $10\ [Hz]$. No results on the actual parameter estimates are presented, hence only verified through the performance of the proposed controller. It is shown that the adaptive controller maintain stability, and exhibits a small tracking error compared to a non-adaptive version, indicating parameter tracking performance of the EA. The parameter tracking ability of the combined EA and control scheme is verified through an on-line perturbation in the supply pressure to $2/3$ of its nominal value. Results for the controllers are shown for the situation in which the supply pressure has settled, not showing the transient stage even though of great importance.

A similar approach is applied in [38], in which an adaptive and repetitive controller are applied to a hydraulic system for non-circular machining. The system is constituted by a servo valve (two stage) controlled, symmetric cylinder with a carriage constituting the load, with the piston position applied as feedback. The system is modeled as a third order discrete time model. The DZ-RLS algorithm in this paper is rather similar to that of [37]. However, the covariance matrix is updated based on the gradient between covariance matrices from previous samples, and not the sum as in [37] - further implying that the EA of [37] may be stated incorrectly. Again the boundedness of the EA is not discussed, but poses similar properties as that of [37]. No results on the actual parameter estimates are presented, hence only verified through the performance of the proposed adaptive controller, for which the impact of the parameter estimation is not clear. In the paper [39], by the same authors, the same DZ-RLS as in [38] is applied for parameter estimation for an adaptive feed-forward controller. Also here there is no discussion on algorithm boundedness, and the risk of the update gain growing unbounded in periods of insufficient PE. However, parameters show convergence to constant parameters.

In [40] a VFDZ-RLS algorithm is applied together with a nonlinear adaptive controller for an EHA system. The system used is a horizontally mounted cylinder with a constant inertia load, controlled by a low-cost proportional valve with nonlinear flow characteristics and dead band, and with the

piston position fed back. The system is modeled as a linear time discrete system, extended to a Hammerstein model with a polynomial term to account for the static nonlinear flow characteristics. For parameter estimation, the RLS algorithm for systems with bounded noise proposed in [26] is applied. This proposes an additional control variable in the parameter- and covariance update terms, including a dead band related to whether or not a measure of the model error is exceeded. Furthermore, a constant EFF is implemented (this approach is also applied in [41]), and it is stressed that the EA is stable. However, it is apparent from the EA that the covariance and parameter update terms are switched off if the squared model error is within some predefined bound - hence in periods of insufficient PE, the covariance matrix may grow unbounded due to the constant EFF. Hence in order for this algorithm to work properly, some upper covariance bound must be applied. The proposed controller and EA are verified experimentally by applying a rectangular cyclic position reference with a frequency of $1/8\ [Hz]$, and a stroke of $50\ \%$ of the maximum stroke. To validate the ability of the EA to track parameter variations, the load is increased to 6.25 times its initial value (the system is here at rest), to which the EA responds well. Furthermore the supply pressure is increased on-line by $250\ \%$, and the controller and estimated parameters respond rapidly to this, without the controller becoming unstable.

A. Summary on DZ-RLS

In this section two different RLS algorithms are discussed. In [40] the activation/deactivation of the parameter- and covariance update terms based on the dead zone on the model estimation error is presented. The EA in [37] is considered incorrectly stated, and rather limited results on the actual parameter estimation are presented. However, in [40] the actual performance of the parameter estimation is well documented through perturbations in inertia load and supply pressure, to which the EA adapted well. Boundedness of the dead zone based algorithm in [37] may not be concluded - however, a proof of stability of the algorithm proposed in [40], is provided in [42].

VI. Variable Forgetting with Covariance Resetting (VFCR)

An alternative to control the update gain, i.e. the covariance trace through a VFF, is by covariance resetting, as done in [43] and [44]. In [44] a VFCR-RLS algorithm is applied as a part of an direct/indirect adaptive control scheme for a hydraulic asymmetric actuator. The system used is similar to that of [15], with full state feedback. Two types of system configurations are considered - one with a nullap servo valve, and one with a proportional directional overlap valve. The regression model applied is similar to that of [15], based on physical system parameters, but also taking into account the dead band of the valve. Furthermore, the regression model is established in a LP type of way, such that the parameter vector is nearly constant. The EA is similar to that used [15] (with EFF), but with an additional modification in terms of covariance resetting (CR), as proposed by [45]. The CR is constructed as such, that when the lowest valued eigenvalue of the covariance matrix reaches a predefined minimum, the covariance matrix is reset to a diagonal matrix with predefined values in the diagonal. For validation of the EA and the controller, a rectangular like cyclic trajectory is applied with a frequency of approximately $1/4\ [Hz]$. Parameter convergence is achieved within few motion cycles for both the servo valve-, and proportional valve configurations. The EA performance in the presence of parameter variations is not presented.

Another, but similar approach (regarding parameter estimation) is presented in [43]. Here an indirect robust adaptive controller for hydraulic actuators is proposed, applying a continuous VFCR-RLS type of algorithm for on-line parameter estimation. The system used is similar to those of [15], [44] and [46]. State feedback is available through filtered position-, velocity and chamber pressure measurements, and a LP type of regression model similar to [15], [32], [17] and [31], is used. A VFCR-RLS similar to that of [44] is applied, with an additional upper bound on the covariance matrix. Furthermore, regarding the VFCR-RLS implementation, a parameter update restriction is applied in order to avoid parameter updates in periods with insufficient PE - as a result of this, the parameter update is turned off if the velocity and acceleration are below some predefined values. The validation of the controller and EA is carried out under similar conditions as in [44]. In the results shown, parameters are only nearly converging, not showing the behavior of the EA after convergence. Furthermore, as for [44], the parameter tracking ability EA is not evaluated.

Another contribution reported in [47] also applies a CR-RLS algorithm for parameter estimation. The system used is a servo valve-controlled, horizontally mounted asymmetric cylinder with a fixed inertia load, and piston position feedback. The system is modeled as a third order regression model. The EA applied is the EFF-RLS type similar to that of [18]. The CR modification is not explicitly presented, but it is stated that the covariance is reset when a directional change in the reference position is applied, which seems reasonable due to asymmetric volume variation and flow gain. The EA responds to parameter variations - however, whether convergence to true parameters is achieved is not discussed. As the CR-RLS apparently had an EFF of one, the EA must be considered bounded.

A. Summary on VFCR-RLS

Application of VFCR-RLS algorithms in relation to EHA systems appears limited. Similar systems are used [44] and [43], and the EAs are in both cases based on the state space formulation for the system. The actual performance of the CR is not evaluated in either of the papers, neither is the parameter tracking ability of the EAs. Furthermore, only the EA presented in [43] and [47] may be considered bounded.

VII. Regularization of the Covariance Matrix (RC)

Another approach which may be applied in order to prevent the update gain from tending to zero and at the same time maintaining the update gain bounded, is the so-called covariance regularization approach.

This approach is reported in [48], and discusses the relations between the covariance modification and regularization of the RLS algorithm, and presents an analysis of the effect of implementing such modifications with the main focus on how to obtain regularization as proposed in [49], through covariance modification. The achievements are implemented on a hydraulic crane, not further presented. As mentioned, the main focus is on how to obtain regularization via covariance modification i.e. adding an additional matrix term in the covariance update algorithm. The regularization part of the paper is based on the so-called Levenberg-Marquardt regularization discussed in [20]. The focus is on deriving an algorithm that possesses both tracking and regularization properties. Through different approximations the algorithm proposed in [49] is obtained, and it is stated that the eigenvalues of the covariance matrix remains bounded, i.e. the trace of the covariance matrix remain bounded. Simulation results show the covariance trace being bounded during periods of poor excitation. Whether the EA is able to track parameter variations is not presented.

VIII. Controlled Covariance Trace - CCT-RLS

Another approach to control the parameter update gain is through so-called controlled trace modification. Contributions containing such modifications when applied to EHA systems is presented in the following, and the section is divided into two parts - one containing contributions related to constant covariance trace control, and one containing a contribution related to variable covariance trace control.

A. Constant Covariance Trace Control

In [50] a simplified adaptive control scheme for EHA systems is presented using RLS for estimation of parameter variations. The system used is a servo valve controlled, horizontally mounted symmetric cylinder, apparently with a constant inertia load and piston position feedback. The system is modeled as a pure integrator and a gain in the discrete time domain, neglecting remaining dynamics and disturbances. Due to the simplified model, only the system gain is unknown, and is estimated on-line via a CCT-RLS - however, the CCT algorithm is not presented, as well as no references are given regarding the origin of the algorithm in literature. For experimental validation of the proposed controller, a rectangular periodic reference with a frequency of $0.4\ [Hz]$ is applied. The parameter tracking ability of the EA is evaluated by a change in the system gain to $2/3$ of its initial value both in simulation studies and experimentally, and proved effective in tracking this variation.

In [51] an CCT-RLS algorithm is applied in the adaptive control of a water hydraulic servo system. The system used is an overlap servo valve controlled symmetric cylinder with a constant sliding load, with the piston position fed back. The regression model used for parameter estimation is a linear discrete type of model. The method applied for parameter estimation a RLS algorithm with two different forgetting factors, controlled in order to achieve controlled trace of the covariance matrix as proposed in [26], with no further discussion on the controlled trace approach. For validation of the controller, a rectangular periodic reference with maximum stroke of $1/6$ of the stroke range, at a frequency of $1/10\ [Hz]$ is applied. The ability for the EA to track parameter variations is evaluated through load- and no-load situations, and at two different supply pressures. No specific results on the parameter estimation are presented.

In [32] a continuous CCT-RLS algorithm is applied for parameter estimation, previous to parametrization of a nonlinear backstepping controller for an EHA system. The system and regression model are similar to those used in [17] and [31], and the parameter estimation is carried out by use of the continuous RLS algorithm with controlled trace proposed by [18]. The parameter estimation is carried out prior to the control operation, in open loop, and with an input signal being a sinusoidal input of $3\ [Hz]$ frequency and an amplitude of $10\ \%$ of the input range. It is stated that parameter convergence is achieved, but parameter estimates are not presented. Parameter convergence to true values is not considered.

B. Variable Covariance Trace Control

Another and well-documented CCT-RLS approach is reported in [52], in which a CCT-RLS is implemented as a part of an indirect adaptive pole assignment position control scheme for an EHA system. The system used is a servo valve (overlap) controlled, horizontally mounted asymmetric cylinder with a constant inertia load. The filtered (third order filter) piston position is used as feedback, and the regression model used is a third order discrete time model. The EA applied is similar to the ones in [22] and [20] with EFF, and with a CCT providing an upper bound on the covariance trace, and the ability to turn off the parameter adaption if the upper covariance trace bound is reached. The scheme is experimentally validated by applying a rectangular periodic reference with an amplitude of $\sim\ 3\ \%$ of the actuator range, and a frequency of $\sim 0.60\ [Hz]$. For verification of parameter tracking, the supply pressure is reduced to $20\ \%$-, and increased by $300\ \%$, and the volumes between valve and cylinder chambers are in- and decreased. The changes are made abruptly during operation, and the parameter estimates as well as the controller adapts well to these changes. A similar contribution is reported in [53], by the same authors.

C. Summary on CCT-RLS

In [50], [51] and [32] controlled covariance trace algorithms with the object of maintaining the covariance trace constant, are presented. The boundedness of the EAs is not discussed,

hence this property can not be concluded - however, if functioning properly, such a modification will render the update gain bounded. The ability of EAs to track parameter variations is evaluated in [50], [51], but not in [32]. In [52] a CCT-RLS algorithm, with object of controlling the trace dependent on the level of PE is presented. The covariance trace is shown to be bounded, and the ability of the EA to track parameter variations through perturbations is shown.

IX. Summary

In general the application of RLS type algorithms applied to EHA systems appears rather fragmented regarding the modification to fit the specific purpose, regression models etc. Furthermore the evaluation of the EA performance also varies significantly, both regarding the actuator range, and regarding the parameter tracking ability, and no common approach on how to design, nor validate EAs in relation to EHA systems is demonstrated. Furthermore the general impression on this topic is that only limited attention has been given to the EAs when applied to EHA systems, an on how to compensate for the drawbacks of RLS algorithm. The main attention are in general given to the control schemes which are usually are the main topics of papers containing EAs. Also the evaluation of the EA performance is often given little attention, although being crucial for the controller performance. In the following a summary relating to the criteria of evaluation is given.

A. System Types

The most common system types used as target for the EA- and controller design are horizontally mounted asymmetric/symmetric cylinders controlled by servo valves, subjected to nearly constant loads. This is the case in [13], [23], [25], [27], [19], [28], [30], [47], [38], [39], [40], [50], [51], [52], [53] and to some extend [15], [44], [43]. In [33], the cylinder is vertically mounted, and in [37] the system information does not allow the reader to consider the system at hand. Only in [34], [48], due to the crane applications, parameter variations are inherently present. The only significantly different systems used are in [32], [17], [31], [24] and [21] in which valve controlled fixed displacement motors are used, and in [35] in which a variable displacement motor is used.

B. Regression models

The regression models applied in the contributions reviewed, can be summarized to primarily LP-models, linear time discrete models and continuous transfer function models. In [13], [15], [44], [43], [32], [17] and [31] the regression models applied are LP models based on space space system models.

In [21], [24], [25], [27], [19], [28], [30], [33], [37], [40], [47], [51], [50], [52] and [53] linear time discrete (and in [35] continuous time) models of different orders and simplifications/extensions are applied - e.g. in [37] an eighth order model is applied, assuming that all unmodeled dynamics and disturbances are represented in this, and in [50] the system is modeled as a discrete integrator and a gain. Also in [40] also the system is modeled by a time discrete model, but with a Hammerstein like extension incorporating a static polynomial like nonlinearity to account for nonlinear spool-flow characteristics.

In [23] and [34], continuous transfer functions are used as regression models.

From the above it is found that mainly two approaches are applied when considering the regression models - namely LP models based on state space system representations, when full state feedback is available, and linear time discrete models, when a limited number of states are available.

C. Parameter Variations

Regarding the ability of the EAs to track parameter variations, this is not presented in several papers, even though this is a rather crucial property when considering EHA systems.

In [13], [15], [21], [23], [25], [17], [28], [30], [47], [38], [39], [35] [33], [44], [43], [48] and [32] no parameter perturbations are made in the system parameters in order to evaluate the tracking ability. In [19], [24], [37], [40], [51], [52] and [53] the supply pressure is changed online, and in [24] and [40] also by changing the load, and in [52] and [53] also by changing the volumes between valve and cylinder chambers. In [17] the viscous damping is perturbed, and in [31] and [51] different load situations are considered. In [34] the resonance frequency is perturbed, and in [50] and [27] model parameters are perturbed.

It is found that many papers lack information on the ability to track parameter variations, and in papers where this is discussed, various parameter perturbations have been made, not indicating any common approach for evaluation of EA tracking ability.

D. Boundedness of Estimation Algorithms

None of the contributions utilizing EFF-RLS algorithms, consider the boundedness of the EAs, even though this type of RLS modification has the property that the update gain may grow unbounded in periods of insufficient PE.

Regarding the VFF-RLS approaches made in [28], [30], [31], these depend only on time, or on the number of samples in the sense that as time evolves, the VFF will tend to one, which eventually will cause the covariance trace, hence the update gain tending to zero, and eventually to be bounded - however, until this stage, if insufficient PE is merging with a low valued forgetting factor, the update gain may grow unbounded similar to the EFF-RLS. The VFF proposed in [33] is inversely proportional to the squared model error within a predefined lower bound, and an upper bound of one. Furthermore an upper bound on the covariance trace is applied in order to avoid covariance blow-up, rendering the algorithm bounded.

Also the VFF-RLS proposed in [34] will remain bounded through a covariance trace based VFF and an additional parameter- and covariance update control variable. Furthermore, to handle component saturation, an override control of the parameter and covariance update terms is implemented.

This renders the overall EA bounded, and provides the ability to control the parameter update taking into account the level of PE.

Regarding the DZ-RLS algorithms, no discussion on whether or not the EAs remain upper bounded is given. However, a lower level of the covariance trace is obtained based on the on model error dead band. For the DZ-RLS algorithms discussed in [37], [38] and [39] in case of the model error exceeding the dead band in a period of insufficient PE, the VFF will decrease, and the covariance trace may grow unbounded. In the algorithm proposed in [40], in periods of insufficient PE, the update gain may grow unbounded.

In the VFCR-RLS algorithm proposed in [44], the covariance trace will remain above some lower bound different from zero, depending on the CR design, but no upper bound is defined. In [43] on the other hand, an upper bound is provided on the covariance trace also, and an override variable is defined, disabling the update ability in periods of insufficient PE. The EA presented in [47] must be considered bounded as an EFF of one is apparently applied.

The RC-RLS algorithms presented will, due the nature of the RC, cause the covariance trace to be globally bounded, reducing the update gain in periods of insufficient PE.

Discussions on the boundedness of the CCT-RLS algorithms in [50], [35] and [51] are not presented, and as limited information is presented on the CCT modifications, no conclusions can be made on EA boundedness. The algorithm proposed in [32] can be considered bounded according to [18], and the CCT applied in [52] and [53] provide an upper bound on the covariance trace, and the ability to turn off the parameter adaption if the upper covariance trace is reached - this renders the EA bounded making the update robust towards periods with insufficient PE.

It is found that boundedness of the EA algorithms reported in many contributions are most often not discussed, and in many cases boundedness of the algorithms can not be concluded from the algorithms. This seems rather strange, as this is a crucial and fundamental property, when applying EAs to continuously operating systems, and especially EHA systems.

E. Overview on Results

To provide a concluding overview on the (rather fragmented) findings obtained from the discussion of this paper, these are summarized in table I, regarding two important properties - the ability of tracking *parameter variations* and whether algorithm *boundedness* may be concluded.

Evaluation Criteria	Parameter variations	Algorithm boundedness
[13]	No	No
[15]	No	No
[17]	Yes	No
[19]	Yes	No
[21]	No	No
[23]	No	No
[24]	Yes	No
[25]	No	No
[27]	Yes	No
[28]	No	No
[30]	No	No
[31]	Yes	No
[33]	No	Yes
[34]	Yes	Yes
[37]	Yes	No
[38]	Yes	No
[39]	Yes	No
[35]	No	No
[40]	Yes	No
[44]	No	No
[43]	No	Yes
[48]	No	Yes
[50]	Yes	No
[51]	Yes	No
[32]	No	Yes
[52]	Yes	Yes
[53]	Yes	Yes

TABLE I
OVERVIEW OF FINDINGS REGARDING THE EA BOUNDEDNESS AND PARAMETER TRACKING ABILITY. "YES" INDICATES THAT THE PROPERTY CAN BE CONCLUDED, AND "NO" MEANS THAT IT CAN NOT BE CONCLUDED FROM THE INFORMATION PROVIDED BY CORRESPONDING PAPER.

X. CONCLUSION

In this paper a review on the application of RLS-type algorithms to EHA systems has been presented. The focus was placed on the control of the parameter adaption gain, and approaches reported in literature appear rather fragmented, but may be divided into five overall approaches; the *exponential forgetting factor* approach, the *variable forgetting factor* approach, the *variable forgetting factor approach with dead zone*, the *covariance matrix regularization* approach and the *controlled covariance trace* approach.

This main purpose of the review was investigation of existing research contributions within RLS approaches to parameter estimation, and to evaluate their applicability in relation to continuously operating EHA systems. Here crucially important properties are the parameter tracking ability of the algorithm, and the algorithm boundedness. From the review, it is found that two of the proposed approaches posses these properties and may be applicable to continuously operating EHA systems - these are presented in [34], [52] (and [53]). The remaining papers reviewed may not be considered directly applicable without further analysis and testing.

REFERENCES

[1] M. Witters and J. Swevers, *Black-box identification of a continuously variable semi-active damper*. 17th IEEE International Conference on Control Applications, 2008.

[2] M. Witters and J.Swevers, *Black-box model identification for a continuously variable, electro-hydraulic semi-activedamper*. Mechanical Systems and Signal Processing 24, 2009.

[3] F. Codec, S. M. Savaresi, C. Spelta, M. Montiglio, and M. Ieluzzi, *Identification of an electro-hydraulic controllable shock absorber using black-block non-linear models*. 17th IEEE International Conference on Control Applications, 2008.

[4] H. Anyi, R. Yiming, Z. Zhongfu, and H. Jianjun, *Identification and adaptive control for electro-hydraulic servo system using neural networks*, volume 1 ed. ICIPS '97. 1997 IEEE International Conference on Intelligent Processing Systems, 1997, digital Object Identifier:

10.1109/ICIPS.1997.672874. Publication Year: 1997 , Page(s): 688 - 692 vol.1.

[5] S. He and N. Sepehri, *Modeling and Prediction of Hydraulic Servo Actuators with Neural Networks*. Proceedings of the American Control Conference San Diego, California, 1999.

[6] H. Yuanfeng and Z. Youwang, *Identification and Control of Eltro-Hydraulic Servo System Based on Direct Dynamic Recurrent Fuzzy Neural Network*. Proceedings of 2009 4th International Conference on Computer Science and Education, 2009.

[7] Y. Wan, C. Wu, and Y. Zhang, *Electro-hydraulic Proportional Self-adaptive ControllerBased on LSVM Intelligent Algorithm*, volume 3 ed. ICNC08 - Fourth Internation Conference on Natural Computation, 2008, digital Object Identifier: 10.1109/ICNC.2008.312. Publication Year: 2008 , Page(s): 175 179.

[8] R. Storn and K. Price, *Differential evolution a simple and efficient adaptive scheme for global optimization over continuous spaces*. Technical report, TR-95-012, 1995.

[9] H. Yousefi, H. Handroos, and A. Soleymani, *Application of Differential Evolution in system identification of a servo-hydraulic system with a flexible load*. www.elsevier.com/ locate/mechatronics, 2008.

[10] J. Shao, Z. Wang, J. Lin, and G. Han, *Model Identification and Control of Electro-hydraulic Position servo system*. 2009 International Conference on Intelligent Human-Machine Systems and Cybernetics, 2009.

[11] J. Shao, G. Han, Y. Dong, and Z. Wang, *Model Identification and Control Method Study on Electro-hydraulic Pressure Servo System*. 2009 Fourth International Conference on Innovative Computing, Information and Control, 2009.

[12] W. Acuna-Bravo, E. Canuto, S. Malan, D. Colombo, M. Forestello, and R. Morselli, *Fine and simplified dynamic modelling of complex hydraulic systems*. 2009 American Control Conference, Hyatt Regency Riverfront, St. Louis, MO, USA, 2009.

[13] J. E. Bobrow and K. Lum, *Adaptive, High Bandwidth Control of a Hydraulic Actuator*. Proceedings of the American Control Conference. Seattle, Washington, June 1995, 1995.

[14] J. E. Bobrow and W. Murray, *An Algorithm for RLS Identification of Parameters that Vary Quickly With Time*. IEEE Transactions on Automatic Control, Vol. 38, No. 2, Feb 1993, pp. 351-354., 1993.

[15] S. Liu and B. Yao, *Indirect Adaptive Robust Control of Electro-Hydraulic Systems Driven by Single-Rod Hydraulic Actuator*. Proceedings 01 the 2003 IEEE/ASME International Conference on Advanced Intelligent Mechalronics (AIM 2003), 2003.

[16] I. Landau, *Adaptive Control*. Springer, 1998.

[17] C. Kaddissi, J.-P. Kenn'e, and M. Saad, *Indirect Adaptive Control of an Electro-Hydraulic Servo System Based on Nonlinear Backstepping*. IEEE ISIE 2006, July 9-12, 2006, Montreal, Quebec, Canada, 2006.

[18] K. J. Astrom and B. Wittenmark, *Adaptive Control*. Reading, MA, Addison-Wesley, 1989.

[19] H. J. Park and H. S. Cho, *On the Realization of an Accurate Hydraulic Servo Through an Iterative Learning Control*. Mechatronics Vol. 2, No. 1, pp. 75-88, 1992, 1992.

[20] L. Ljung and T. Sderstrm, *Theory and Practice of Recursive Identification*. MIT Press, Cambridge, MA, 1983.

[21] Y. Bin, W. Bo, and H. Qingchao, *The Study of Self-Tuning Control of a Passive Electro-Hydraulic Servo Loading System*. Proc. 2nd Int. Conf. on Fluid Power Transmission and Control, China., 1989.

[22] L. Ljung, *System Identification, Theory for the User*. Prentice Hall, Englewood Cliffs, New Jersey 07632, 1987.

[23] C. Boes, *Adaptive Zustandsregelung fr Hydraulische Zylinderantriebe*. lhydraulik und Pneumatik, 36(6), 386-396., 1992.

[24] S. A. Daley, *Application of a Fast Self-Tuning Control Algorithm to a Hydraulic Test Rig*. Proc. Instn. Mech. Engrs., 201(C4), 285-295, 1987., 1987.

[25] K. Lee, *Dynamisches Verhalten der Steuerkette Servoventil-Motor-Last (Diss)*. Technical Universuty of Aachen, Germany, 1977.

[26] G. Goodwin and K. Sin, *Adaptive filtering Prediction and Control*. Prentice-Hall, 1984.

[27] S. LeQuoc, Y. F. Xiong, and R. M. H. Cheng, *Realixation of a Pole-Placement Adaptive Control in a Hydraulic Position System*. Flucome, Fourth Triennial International Symposium, Toulouse, France, 1, 119-124., 1994.

[28] R. Ghazali, Y. M. Sam, M. F. Rahmat, and Zulfatman, *On-line Identification of an Electro-hydraulic System using Recursive Least Square*. IEEE Student Conference on Research and Development (SCOReD 2009), 2009.

[29] T. Soderstrom and P. Stoica, *System Identification*. Prentice Hall International (UK) Ltd, Hertfordshire, 1989, 1989.

[30] R. Ghazali, Y. M. Sam, M. F. Rahmat, and Zulfatman, *Open-loop and Closed-loop Recursive Identification of an Electro-hydraulic Actuator System*. IEEE Conference on Robotics, Automation and Mechatronics, 2010.

[31] C. Kaddissi, J.-P. Kenne, and M. Saad, *Indirect Adaptive Control of an Electrohydraulic Servo System Based on Nonlinear Backstepping*. IEEE/ASME Transactions on Mechatronics, VOL. 16, NO. 6, December 2011., 2011.

[32] C. Kaddissi, J.-P. Kenn'e, and M. Saad, *Identification and Real-Time Control of an Electrohydraulic Servo System Based on Nonlinear Backstepping*, vol. 12, no. 1 ed. IEEE/ASME Transactions on Mechatronics, 2007.

[33] D. W. Clarke, *Adaptive Control of Servohydraulic Materials-Testing Machines: A Comparison Between Black- and Grey-Box Models*. Annual Reviews in Control 25 (2001) 77-88, 2001.

[34] P. Krus and S. Gunnarsson, *Adaptive Control of a Hydraulic Crane Uning On-line Identification*. LiTH-ISY-R-1520, Linkbing University, S-58183, Sweden, 1993.

[35] J. Glotzbach and R. Isermann, *Adaptive Speed Control of Hydraulic Rotary Drives*. Proceedings of the American Control Conference, 1(WA1), 16-20., 1992.

[36] J. E. Parkum, *Recursive Identification of Time Varying Systems*. DTH, Lyngby, 1992.

[37] Z. Sun and T.-C. Tsao, *Adaptive Control With Asymptotic Tracking Performance and Its Application to an Electro-Hydraulic Servo System*. Transactions of the ASME, 188 / Vol. 122, MARCH 2000, 2000.

[38] T.-C. Tsao and M. Tomizuka, *Robust Adaptive and Repetitive Digital Tracking Control And Application to a Hydraulic Servo for Nincircular Machining*. ASME Journal of Dynamic Systems, Measurement and Control, 116(), 24-32., 1994.

[39] ——, *Indirect Adaptive Feed-Forward Tracking Controllers*. Proceedings of the American Control Conference, 1(WA4), 115-120., 1988.

[40] K. Ziaei and N. Sepehri, *Design of a Nonlinear Adaptive Controller for an Electrohydraulic Actuator*, vol. 123. ed. Transactions of the ASME, 2001.

[41] K. Ziaei, *Development of a Nonlinear Adaptive Control Scheme for Hydraulic Actuators*. M.Sc. thesis, Department of Mechanical and Industrial Engineering. The University of Manitoba, Winnipeg, Manitoba, Canada., 1998.

[42] P. A. Iannou and J. Sun, *Robust Adaptive Control*. Prentice-Hall, Upper Saddle River, NJ., 1996.

[43] A. Mohanty and B. Yao, *Indirect Adaptive Robust Control of Hydraulic Manipulators With Accurate Parameter Estimates*. IEEE Transactions in Control Systems Technology, VOL. 19, NO. 3, May 2011, 2011.

[44] ——, *Integrated Direct/Indirect Adaptive Robust Control of Hydraulic Manipulators With Valve Deadband*. IEEE/ASME Transactions on Mechatronics, VOL. 16, NO. 4, August 2011, 2011.

[45] I. D. Landau, R. Lozano, and M. MSaad, *Adaptive Control*. Springer-Verlag, 1998.

[46] P. Garimella and B. Yao, *Nonlinear Adaptive Robust Observer for Velocity Estimation of Hydraulic Cylinders using Pressure Measurent only*. SKRIV konference, 2002.

[47] R. R. Fullmer and S. Ananthakrishnan, *Experimental Adaptive Controllers for a Class of Electrohydraulic Systems*. International Journal of Adaptive Control and Signal Processing, Vol. 7, 151-162., 1993.

[48] S. Gunnarsson, *On Covariance Modification and Regularization in Recursive Least Squares Identification*.

[49] M. Salgado, G. Goodwin, and R. Middleton, *Modified least squares algorithm incorporating exponential resetting and forgetting*. International Journal of Control, 47: 477-491., 1988.

[50] N. Hori, P. Ukrainetz, P. Nikiforuk, and D. Bitner, *Simplified adaptive control of an electrohydraulic servosystem*. IEEE Proceedings, Vol. 137, Pt. D, No. 2, March 1990, 1990.

[51] H. Takahashi, K. Ito, and S. Ikeo, *Application of Adaptive Controller to Water Hydraulic Servo Cylinder*. Proceedings of the 6th JFPS International Symposium on Fluid Power, 2005.

[52] A. R. Plummer and N. D. Vaughan, *Robust Adaptive Control for Hydraulic Servosystems*. Journal of Dynamic Systems, Measurement and Control, June 1996, Volume 118, Issue 2, 1996.

[53] N. D. Vaughan and A. R. Plummer, *Robust Adaptive Control for Hydraulic Servosystems*. ASME Winter Annual Meeting, Dallas, Texas, 1990.

Bibliography

[al Shammari, 2006] al Shammari, K. (2006). *Filippov's operator and Discontinuous Differential Equations*. PhD Dissertation, Louisiana State University.

[Andersen, 1993] Andersen, T. O. (1993). Kompendium i robotmekanismens dynamik - newton-euler metoden. Danmarks Tekniske Universitet.

[Andersen, 1996] Andersen, T. O. (1996). *Adaptive Control of Hydraulic Actuators and Multivariable Hydraulic Systems*. PhD thesis, Department of Control and Engineering Design, Technical University of Denmark.

[Andersen and Hansen, 2003] Andersen, T. O. and Hansen, M. R. (2003). *Fluid Power Systems - Modelling and Analysis*. Aalborg University, Denmark, 2nd Edition.

[Angue-Mintsa et al., 2011] Angue-Mintsa, H., Venugopal, R., Kennet', J.-P., and Belleau, C. (2011). Adaptive position control of an electrohydraulic servo system with load disturbance rejection and friction compensation. *Journal of Dynamic Systems, Measurement, and Control*, 133.

[Anosov, 1959] Anosov, D. V. (1959). On stability of equilibrium points of relay systems. *Automatica i telemechanica (Autom. Remote Control)*, 2:135–149.

[Astrom and Wittenmark, 1989] Astrom, K. J. and Wittenmark, B. (1989). *Adaptive Control*. Reading, MA, Addison-Wesley.

[Bacciotti and Rosier, 2005] Bacciotti, A. and Rosier, L. (2005). *Liapunov Functions and Stability in Control Theory*. Springer Verlag, London.

[Bartolini et al., 2007] Bartolini, G., Pisano, A., and Usai, E. (2007). On the finite-time stabilization of uncertain nonlinear systems with relative degree three. *IEEE Transactions on Automatic Control*, 52(11):2134–2141.

[Batur and Zhang, 2003] Batur, C. and Zhang, L. (2003). Sliding mode observer and controller design for a hydraulic motion control system. In *Proceedings of the American Control Conference*, pages 1721–1726.

[Bhat and Bernstein, 1997] Bhat, S. P. and Bernstein, D. S. (1997). Finite-time stability of homogeneous systems. In *Proceedings of the American Control Conference*, pages 2513–2514.

[Bonchis et al., 2001] Bonchis, A., Corke, P. I., Rye, D. C., and Ha., Q. P. (2001). Variable structure methods in hydraulic servo systems control. *Automatica*, 37:pp. 589–595.

[Bu and Yao, 1999] Bu, F. and Yao, B. (1999). *Adaptive robust precision motion control of singal-rod hydraulic actuatorswith timevaring unknown inertia: A case study*. ASME International Mechanical Engineering Congress and Exposition (IMECE97), vol. fpst-6, pp. 131-138, 1999. edition.

[Cetinkunt, 2006] Cetinkunt, S. (2006). *Mechatronics*. Wiley, 1 edition.

[Chen et al., 2005] Chen, H.-M., Renn, J.-C., and Su, J.-P. (2005). Sliding mode control with varying boundary layers for an electro-hydraulic position servo system. *International Journal of Advanced Manufacturing Technology*, 26:117–123.

[Chern and c. wu, 1991] Chern, T.-L. and c. wu, Y. (1991). Design of integral variable structure controller and application to electrohydraulic velocity servosystems. In *IEE Proceedings-D*, volume 138.

[Chiang, 2011] Chiang, M.-H. (2011). A novel pitch control system for a wind turbine driven by a variable-speed pump-controlled hydraulic servo system. *Mechatronics*, 21:753–761.

[Chin-Wen Chuang, 2005] Chin-Wen Chuang, C.-L. H. (2005). Applying discrete dynamic integral sliding surface control to hydraulic position control. In *IEEE International Conference on Industrial Technology (ICIT 2005)*.

[Craig, 2005] Craig, J. J. (2005). *Introduction to Robotics - Mechanics and Control*. Prentice Hall, third edition. ISBN: 0-13-123629-6.

[Davila et al., 2005] Davila, J., Fridman, L., and Levant, A. (2005). Second-order sliding-mode observer for mechanical systems. *IEEE Transactions on Automatic Control*, 50(11):1785 – 1789.

[Emelyanov et al., 1986a] Emelyanov, S., Korovin, S., and Levantovsky, L. (1986a). Higher order sliding modes in binary control systems algorithms, in russian. *Soviet Physics, Doklady*, 31(4):pp. 291–293.

[Emelyanov et al., 1986b] Emelyanov, S., Korovin, S., and Levantovsky, L. (1986b). Second order sliding modes in controlling uncertain systems, in russian. *Soviet Journal of Computing and Systems Science*, 24(4):63–68.

[Emelyanov et al., 1990] Emelyanov, S., Korovin, S., and Levantovsky, L. (1990). New class of second order sliding algorithms. *Mathematical Modelling*, 2(3):89–100.

[Filippov, 1960] Filippov, A. (1960). Differential equations with discontinuous right-hand side. *Matematicheskii, in Russian*.

[Filippov, 1988] Filippov, A. (1988). *Differential Equations with Discontinuous Righthand Sides*. Kluwer Academic Publishers Academic Publishers, Dordrecht, the Netherlands.

[Fridman et al., 2012] Fridman, L., Moreno, J., and Iriarte, R. (2012). *Sliding Modes after the first Decade of the 21st Century*, volume 412 of *Lecture Notes in Control and Information Sciences*. Springer-Verlag Berlin Heidelberg.

[Fung et al., 1997] Fung, R.-F., Wang, Y.-C., Yang, R.-T., and Huang, H.-H. (1997). A variable structure control with proportional and integral compensators for electrohydraulic position servo control system. *Mechatronics*, 7(1):67–81.

[Fung and Yang, 1998] Fung, R.-F. and Yang, R.-T. (1998). Application of vsc in position control of a nonlinear electrohydraulic servo system. 66(4):365–372.

[Ghazali et al., 2010] Ghazali, R., Sam, Y. M., Rahmat, M. F., Hashim, A. W. I. M., and Zulfatman (2010). Position tracking control of an electro-hydraulic servo system using sliding mode control. In *Proceedings of 2010 IEEE Student Conference on Research and Development (SCOReD 2010)*.

[Ghazy, 2001] Ghazy, M. A. (2001). Variable structure control for electrohydraulic position servo system. pages 2194–2198.

[Goodwin and Sin, 2009] Goodwin, G. and Sin, K. (2009). *Adaptive filtering Prediction and Control*. New York: Dover Publications.

[Guan and Pan, 2008] Guan, C. and Pan, S. (2008). Adaptive sliding mode control of electro-hydraulic system with nonlinear unknown parameters.

[Guo et al., 2008] Guo, H., Liu, Y., Liu, G., and Lic, H. (2008). Cascade control of a hydraulically driven 6-dof parallel robot manipulator based on a sliding mode. *Control Engineering Practice*, 16:1055–1068.

[Habibi, 1995] Habibi, S. R. (1995). Sliding mode control of a hydraulic industrial robot. In *Proceedings of the American Control Conference*, pages 1523–1527.

[Hansen et al., 2005] Hansen, M. R., Andersen, T. O., and Pedersen, H. C. (2005). Robust control of a hydraulically actuated manipulator using sliding mode control. In *Proceedings of The 6th International Conference on Fluid Power Transmission and Control*.

[Hansen, 1997] Hansen, P. E. (1997). *Autonomous and Adaptive Control of Hydraulic Actuator Systems*. PhD thesis, Department of Control and Engineering Design, Technical University of Denmark.

[Hisseine, 2005] Hisseine, D. (2005). Robust tracking control for a hydraulic actuation system. In *Proceedings of the 2005 IEEE Conference on Control Applications*.

[Hwang and Lan, 1994] Hwang, C. and Lan, C. (1994). The position control of electrohydraulic servomechanism via a novel variable structure control. *Mechatronics*, 4(4):369–391.

[Jerouane et al., 2004a] Jerouane, M., Sepehri, N., and Lamnabhi-Lagarrigue, F. (2004a). Dynamic analysis of variable structure force control of hydraulic actuators via the reaching law approach. *International Journal of Control*, 77(14):1260–1268.

[Jerouane et al., 2004b] Jerouane, M., Sepehri, N., Lamnabhi-Lagarrigue, F., and Abou, S. C. (2004b). Design and experimental evaluation of robust variable structure control for hydraulic actuators. In *5th Asian Control Conference*. 5th Asian Control Conference.

[Komsta et al., 2010a] Komsta, J., Adamy, J., and Antoszkiewicz, P. (2010a). Input-output linearization and integral sliding mode disturbance compensation for electro-hydraulic drives. *11th International Workshop on Variable Structure Systems, Mexico City, Mexico*.

[Komsta et al., 2010b] Komsta, J., Antoszkiewicz, P., Heeg, T., and Adamy, J. (2010b). New nonlinear robust control concept for electro-hydraulic drives. In *Proceedings of the 7th International Fluid Power Conference*.

[Krus and Gunnarsson, 1993] Krus, P. and Gunnarsson, S. (1993). *Adaptive Control of a Hydraulic Crane Uning On-line Identification*. LiTH-ISY-R-1520, Linköbing University, S-58183, Sweden.

[Kryachkov et al., 2010] Kryachkov, M., Polyakov, A., and Strygin, V. (2010). Finite-time stabilization of an integrator chain using only signs of the state variables. In *2010 11th International Workshop on Variable Structure Systems*, Mexico City, Mexico.

[Landau, 1980] Landau, Y. (1980). *Adaptive Control*. Marcel Dekker, Inc.

[Levant, 1993] Levant, A. (1993). Sliding order and sliding accuracy in sliding mode control. *International Journal of Control*, 58(6):1247–1263.

[Levant, 1996] Levant, A. (1996). Higher order sliding modes as a natural phenomenon in control theory. In Garofalo, F. and Glielmo, L., editors, *Robust Control via Variable Structure and Lyapunov Techniques*, volume 217 of *Lecture Notes in Control and Information Sciences*, pages 107–133. Springer Berlin Heidelberg.

[Levant, 1998a] Levant, A. (1998a). Arbitrary-order sliding modes with finite-time convergence. In *Proceedings of the 6th IEEE Mediterranean Conference on Control and Systems*.

[Levant, 1998b] Levant, A. (1998b). Robust exact differentiation via sliding mode technique. *Automatica*, 34(3):379–384.

[Levant, 2001a] Levant, A. (2001a). Higher order sliding modes and arbitrary-order exact robust differentiation. *Proceedings of the European Control Conference, Porto, Portugal*, pages 996–1001.

[Levant, 2001b] Levant, A. (2001b). Universal siso sliding-mode controllers with finite-time convergence. *IEEE Transactions on Automatic Control*, 46(9):1447–1451.

[Levant, 2003] Levant, A. (2003). Higher-order sliding modes, differentiation and output-feedback control. *International Journal of Control*, 76(9/10):924–941.

[Levantovsky, 1985] Levantovsky, L. (1985). Second order sliding algorithms: Their realization, in russian. *Dynamics of Heterogeneuos Systems. Material of the Seminar (Moscow: The Institute for System Studies), in Russian*, pages 32–43.

[Liu and Yao, 2003] Liu, S. and Yao, B. (2003). *Indirect Adaptive Robust Control of Electro-Hydraulic Systems Driven by Single-Rod Hydraulic Actuator*. Proceedings 01 the 2003 IEEE/ASME International Conference on Advanced Intelligent Mechalronics (AIM 2003).

[Liu and Handroos, 1999] Liu, Y. and Handroos, H. (1999). Sliding mode control for a class of hydraulic position servo. *Mechatronics*, 9:111–123.

[Lizalde et al., 2005] Lizalde, C., Loukianov, A., and Sanchez, E. (2005). Force tracking neural control for an electro-hydraulic actuator via second order sliding mode. In *Proceedings of the 2005 IEEE lnternational Symposium on lntelligent Control*.

[Ljung, 1987] Ljung, L. (1987). *System Identification, Theory for the User*. Prentice Hall, Englewood Cliffs, New Jersey 07632.

[Ljung and Söderström, 1983] Ljung, L. and Söderström, T. (1983). *Theory and Practice of Recursive Identification*. MIT Press, Cambridge, MA.

[Loukianov et al., 2008] Loukianov, A., Sanchez, E., and Lizalde, C. (2008). Force tracking neural block control for an electrohydraulic actuator via second-order sliding mode. *International Journal of Robust Nonlinear Control*, 18:319–332.

[Loukianov et al., 2009] Loukianov, A. G., Rivera, J., Orlov, Y. V., and Teraoka, E. Y. M. (2009). Robust trajectory tracking for an electrohydraulic actuator. *IEEE Transactions on Industrial Electronics*, 56(9):3523–3531.

[Merritt, 1967] Merritt, H. E. (1967). *Hydraulic Control Systems*. New York: Wiley.

[Mohieddine Jelali, 2004] Mohieddine Jelali, A. K. (2004). *Hydraulic servo systems*. Springer. ISBN: 1-85233-692-7.

[Nguyen et al., 2000] Nguyen, Q., Ha, Q., Rye, D., and Durrant-Whyte, H. (2000). Force/position tracking for electrohydraulic systems of a robotic excavator. In *Proceedings of the 39th IEEE Conference on Decision and Control*.

[Parkum, 1992] Parkum, J. E. (1992). *Recursive Identification of Time Varying Systems*. PhD thesis, Danmarks Tekniske Universitet.

[Pi and Wang, 2011] Pi, Y. and Wang, X. (2011). Trajectory tracking control of a 6-dof hydraulic parallel robot manipulator with uncertain load disturbances. *Control Engineering Practice*, 19(2):185–193.

[Plummer and Vaughan, 1996] Plummer, A. R. and Vaughan, N. D. (1996). *Robust Adaptive Control for Hydraulic Servosystems*. Journal of Dynamic Systems, Measurement and Control, June 1996, Volume 118, Issue 2.

[Rexroth, 2004] Rexroth, B. (2004). *Datasheet RE29075/08.04, Proportional directional valve, pilot operated with electrical position feedback and integrated electronics (OBE) Type 4WRKE.*

[Rexroth, 2005] Rexroth, B. (2005). *Datasheet RE29061/10.05, 4/2 and 4/3 proportional directional valves direct operated, with electrical position feedback, without/with integrated electronics (OBE), Types 4WRE and 4WREE.*

[Rexroth, 2006] Rexroth, B. (2006). *Datasheet RE29083/09.06, 4/3-way high response valve pilot operated with electrical position feedback and integrated electronics (OBE), Type 4WRTE.*

[Rexroth, 2008] Rexroth, B. (2008). *R911324661, Rexroth IndraControl L45/L65*, 01 edition.

[Sam et al., 2004] Sam, Y. M., Osman, J. H., and Ghani, M. R. A. (2004). A class of proportional-integral sliding mode control with application to active suspension system. *Systems and Control Letters*, 51:217–223.

[Schmidt et al., 2013] Schmidt, L., Andersen, T. O., and Pedersen, H. C. (2013). Second order sliding control with state dependent gain & its application to a hydraulic drive. In *Proceedings of ASME/Bath 2013 Symposium on Fluid Power & Motion Control, Sarasota, Florida, USA*.

[Schmidt and Nielsen, 2008] Schmidt, L. and Nielsen, K. H. (2008). Comparison of advanced control schemes implemented on hydraulic actuated robot manipulator. Master's thesis, Institute for Energy Technology, Aalborg University, Denmark.

[Slotine and Li, 1991] Slotine, J. J. E. and Li, W. (1991). *Applied Nonlinear Control*. Englewood Cliffs, NJ: Prentice-Hall.

[Spong et al., 2004] Spong, M. W., Hutchinson, S., and Vidyasagar, M. (2004). *Robot Dynamics and Control*. Wiley, second edition.

[Utkin et al., 2009] Utkin, V., Guldner, J., and Shi, J. (2009). *Sliding Mode Control in Electro-Mechanical Systems*. Taylor & Francis Group, LLC, second edition.

[Wang et al., 2011] Wang, S., Burton, R., and Habibi, S. (2011). Sliding mode controller and filter applied to an electrohydraulic actuator system. *Journal of Dynamic Systems, Measurement, and Control*, 133.

[Wang and Su, 2007] Wang, X. and Su, X. (2007). Modeling and sliding mode control of the upper arm of a shotcrete robot with hydraulic actuator. In *Proceedings of the 2007 IEEE International Conference on Integration Technology*.

[Yoon and Manurung, 2010] Yoon, J. and Manurung, A. (2010). Development of an intuitive user interface for a hydraulic backhoe. *Automation in Construction*, 19:pp. 779–790.

[Zulfatman et al., 2011] Zulfatman, Rahmat, M. F., Husain, A. R., Ghazali, R., and Rozali, S. M. (2011). Smooth control action of sliding mode for a class of electro-hydraulic actuator. *4th International Conference on Mechatronics (ICOM11), Kuala Lumpur, Malaysia.*